Hover-bike

Group 12

Y. Chen | E. Dedding | M. Elbertse | A. T. Genç | J. Laffita van den Hove | E. Lodder | T. Suys | A. Tork | W. Vellema | G. H. R. Vos

E. van Kampen | H. Ma | T. Mkhoyan

Final report

TU Delft Design Synthesis Exercise 2018

Scorpeon Hover-bike

Hover-bike

Final Report - Version 1.2
AE3200 Design Synthesis 2018

by

Group 12

Tutor:	van Kampen, Erik-Jan	
Coaches:	Ma, Hao	
	Mkhoyan, Tigran	
Members:	Chen, Yuze	4466527
	Dedding, Erik	4485092
	Elbertse, Mitchel	4393724
	Genç, Alp	4213920
	Laffita van den Hove, Jonathas	4431693
	Lodder, Erwin	4300548
	Suys, Tom	4464036
	Tork, Ahmed	4436121
	Vellema, Wieger	4443438
	Vos, Gerrit Hermanus Ruben	1378988

Executive overview

Tutor
van Kampen, Erik-Jan

Coaches
Ma, Hao
Mkhoyan, Tigran

Students
Chen, Yuze
Dedding, Erik
Elbertse, Mitchell
Genç, Alp
Laffita van den Hove, Jonathas
Lodder, Erwin
Suys, Tom
Tork, Ahmed
Vellema, Wieger
Vos, Gerrit Hermanus Ruben

"If you surrendered to the air, you could ride it." -Toni Morrison

Ever since we were kids, we all had this dream to roam freely. With the development of technology motorbikes came, which allowed us to freely wander the land and jetskis to roam the oceans, but there is an aerial equivalent missing. Therefore, the goal of this project is to develop an aerial equivalent of a high-performance motorbike, capable of vertical take-off and landing.

The design has a few requirements attached to it. One of these, as just mentioned, is that the vehicle should be capable of vertical take-off and land (VTOL). Apart from VTOL, the hover-bike should sustain flight for 1 hour and fly over 100 km, both at an airspeed of at least 100 km/h. At the same time, the hover-bike should provide high levels of thrill and fun, which comes in terms of quick turns and high loads. In terms of safety, there should be a system that allows for a safe descent and landing from 3000 ft in case of emergency. All of these requirements should be met within a total mass constraint of 500 kg, of which 100 kg is reserved for the pilot with gear.

The Scorpeon The answer to this dream is the Scorpeon , which is a vehicle in a tri-copter layout with three ducted contra-rotating propellers with wings attached to the ducts. This vehicle can be used in two different configurations, one focusing on transportation with high range and endurance, which can be seen in Figure 16.2a. The other configuration aiming at providing high thrill levels and high manoeuvrability, which is shown in Figure 16.2b. In order to provide the best of both modes, being able to transport it in a regular size and making the vehicle appealing it was decided to attach the wings to detachable ducts around the rotors. As the wings will only aid in providing lift and are not used for manoeuvrability, these will be fixed in their most efficient position for cruise-flight.

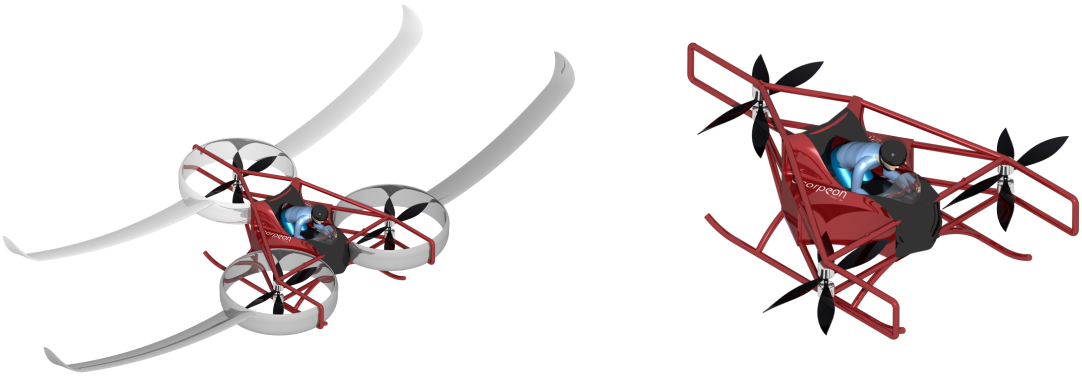

(a) (b)

Figure 1: Isometric views of the Scorpeon in (a) transportation mode and (b) thrill mode.

Market analysis Before the detailed analysis a market analysis for Scorpeon was performed. Its purpose is to predict the best way to enter the market and to make sure the product will bridge the gap in the hover-bike market. First the market needs were analysed to see where this gap is. Nowadays there is no small, relatively cheap personal vehicle that can take-off/land anywhere, that can achieve high velocities and is easy to fly. This is where the Scorpeon steps in.
Several target audiences were defined, those include young people who seek for adrenaline who will buy the hover-bike for the thrills and experience. This group will bring credibility to the machine and safety concerns to rest. Then we have the rich middle-aged adult, this audience will prefer to use the transportation mode over the high acceleration in thrill mode. After

the Scorpeon has gained some more confidence in the market the everyday person looking for faster transport will become a target audience as well.
Furthermore, a quick look into the market volume has been performed. Existing markets that were used to give an estimate of the market volume are: expensive luxury cars, motorcycles and light and single engine helicopters.
Lastly, the competition is been addressed, Scorpeon does not have many competitors which are made for thrills and experience. The closest competitors are mainly designed for transportation, therefore the hover-bike will add something new to the table.

Trade-off summary Before Scorpeon was born an extensive concept design was performed. Four totally different concepts were chosen and analysed to see which concept would have the best performance, and meet the most requirements. When all aspects were analysed a trade-off has been performed, then these separate trade-offs were brought together and put in one large trade-off table. This trade-off table gives a nice overview which concept has the best overall performance. The colours of the trade-off table are explained in the colour scheme. As can be seen concept 4 outperforms the other concepts, because it performs really well on performance and the fun factor. Concept 4 performs satisfactory on safety, cost, transport and sustainability. Concept 2 scores the least, because it scores poor or satisfactory on most categories except airspeed and user friendliness. Concept 1 and 3 score in between concept 2 and 4.

Table 1: Colour scores

Score	0	1	2	3	4
Colour	Does not meet requirements	Poor	Satisfactory	Good	Excellent

Table 2: Trade-off summary table

	Performance			Fun Factor		Safety	Cost	Transport	Sustainability		Total
	Air Speed	Longitudinal Acceleration	Control	User Friendliness	Appearance				Carbon Footprint	Noise	
Weight	8%	16%	16%	16%	5%	10%	10%	5%	7%	7%	100%
Concept 1	2	3	3	3	2	3	3	4	1	2	2.71
Concept 2	3	1	2	4	2	2	1	1	1	1	1.95
Concept 3	2	2	3	2	2	4	2	3	3	1	2.41
Concept 4	4	3	4	4	4	2	2	2	3	2	3.13

Hover-bike concept development In previous phases of designing the hover-bike a trade-off has been performed. In this trade-off four totally different concepts were analysed and compared to each other. From this analysis a winning concept resulted which made use of a blended wing body and three tilt-able propellers. With this concept the preliminary design phase began, where this design was analysed and iterated. There have been a few design iteration before Scorpeon was born, first instead of using tilt-able rotors the wings were made tilt-able and the propellers fixed. Tilt-able rotors were wiped of the table because it would drive the structural mass high so the weight requirement could never be met.

With the new design which has tilt-able wings, a new problem was found. The advantage of the wings was not sufficient enough to meet the range and endurance requirements. This could be solved by using bigger batteries but then the weight requirement can never be met. A solution to this problem was found by making the wings fixed and attaching them on the ducts. However this design change greatly increases the weight and moments of inertia of the hover-bike, which decreases the manoeuvrability of the hover-bike. This is against the definition of the hover-bike, which was all about the thrills and experience. To solve this problem the wings together with the ducts were made detachable, therefore the hover-bike has two configurations which were already mentioned before, the thrill mode and the transportation mode. This design was chosen as the final preliminary design on which all further analysis is focused.

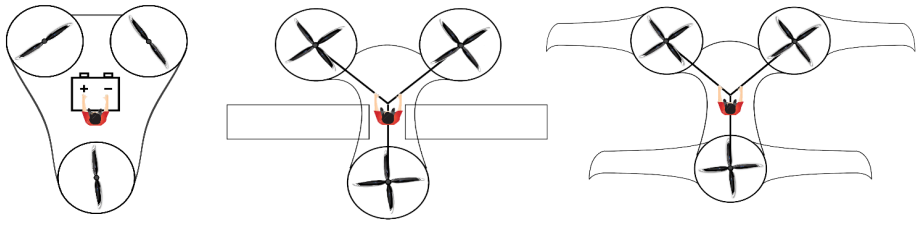

Figure 2: Visualisation of the iterations made

Design preparation The relationships between subsystems and subgroups have to be specified to make the design progress smoothly. For this purpose, the N2 chart is made to specify the inputs and outputs between subgroups. On the other hand, relationships between subsystems are clarified in hardware and software block diagram. Moreover, the data flow will be shown in data handling block diagram and communication flow diagram.

An N2 chart has been made in the third phase. In the fourth phase, a specific concept is chosen so the N2 chart can be made more concept specific. The subgroups in N2 chart include aerodynamics, power & propulsion, control & human machine interface (HMI), structure, and safety system.
In addition to an N2 chart, figures of system communication are made. In hardware block diagram, power system and control system are two central systems. Power system transmits electrical power to all other systems, while control system either gives out control signals to carry out instructions or sends data to HMI or for communication. As input, the control system takes data from sensors, pilot control and communication system. Similar to hardware block diagram, the software block diagram shows data flow at a top level. The data flow is split into three stages, which are input, process and output. Another diagram is the data handling block diagram, which is also similar to hardware block diagram. The most straightforward difference is that power system and communication system are removed in data handling block diagram. The central module consists only control system but control system is introduced in more detail. The lift device and safety blocks are also simplified. The last one is the communication flow diagram, which shows in more detail the interaction between pilot, hover-bike and the environment.

Aerodynamic design The design of the wing starts with selecting the airfoil. Several airfoils are compared in a trade-off table. Finally, the airfoil chosen is Selig S406 due to its high lift-to-drag ratio and low minimum drag coefficient. After the airfoil is chosen, a series of wing parameters will be identified. The span is constraint by the length of trailer and the half span is determined to be 3.0m. For the aspect ratio, the iteration method is used, where aspect ratio is set at first and root chord is adjusted to approach the cruise speed. After iteration, the cruise speed is determined to be 105 km/h, which will also lead to a portion of 60% of lift that is provided by wing. A taper ratio of 0.45 is chosen to approximate an elliptical lift distribution in order to reduce the induced drag. Dihedral is decided to be zero due to it will make the vehicle too stable and even produce Dutch roll. The incidence angle is set according to the pitch of hover-bike so that when the hover-bike pitches during cruise, the wing is at the right angle of attack. Since the drag depends on the incidence angle and the incidence angle depends on the thrust needed which is equivalent to drag, an iterative process will be used to determine the incidence angle. Lastly, miscellaneous wing devices will be determined. High-lift devices will not be used because of the VTOL feature. Turbulators can increase the applicable angle of attack, but this is not helpful so turbulators will also be discarded. Finally, only the aft-swept wing tip will be applied to reduce induced drag.
The rotor size and operation state are estimated and determined by the power subgroup. More details of rotors will be analysed by aerodynamics. First the airfoils for rotor are selected. The criteria include the maximum lift coefficient $C_{L_{max}}$ to generate sufficient lift, lift-to-drag ratio C_L/C_D to be efficient, drag divergence number M_{DD} to postpone or avoid shock wave and wave drag, moment coefficient C_m to decrease load on control system and twist in blade. Since JAVAprop is planned to be used, all airfoils in JAVAprop will be looked at. Besides, some other airfoils in literature of modern design will also be included. Finally, the MH series airfoils are chosen for most of the blade for lift and efficiency, and ILH308 is applied at tip in order to have a high drag divergence number.
Afterwards, the blade element method is introduced and used directly. BEM assumes the blade to consist of multiple small elements that can be treated as airfoil to calculate lift and drag. BEM shall be applied under the conditions that the disk loading is not too high, and the 3D effects are small, and the number of blades are small, and Compressible flow effects are small and mostly two-dimensional. The calculation using blade element method gives a power that is four times larger than what is estimated before, and is verified to be inaccurate.
Afterwards, more analysis is done through JAVAprop. The power required is estimated to be a few percent larger than the power available when the designed maximum thrust is generated. JAVAprop is verified and validated to be quite accurate, but the estimated power can be larger than the actual value, probably because a much lower lift-to-drag ratio is used. The power that is available will remain constant, but it should be noticed that the power available is at a margin, which may need further power estimation.
As to geometry parameters, the rotation speed is iterated to obtain the most efficient point with a constant thrust that needs to be generated. The blade angle is decided from the optimum point to be 20° at 75% of blade. An average chord length of 0.1m will be sufficient. The spinner diameter is decided to be 0.05m, although the analysis shows it does not have large influence on the result as long as it is small enough. From the JAVAprop analysis, the duct can have a positive result, but the influence is not large. Since the aerodynamics effect is limited, the size can be determined by other subgroups that will have more insight into duct design.
After the wing and rotor are designed, their interference will be discussed. First the duct effect will be introduced. In the case of no duct, the high pressure on the bottom of the wing counteracts the pressure of the rotor and the flow next to the wing root will be disturbed. In addition, the flow on the top of the wing will also be disturbed by the low pressure above the rotor. If a duct is installed, the flow over the wing will be blocked from the rotor and disturbance will be reduced. Apart from the block effect, a duct also has stabilising effect. Afterwards, the wing twist will be discussed. Due to the downwash effect of rotor at the wing root, the wing twist can be applied so that wing is at the designed angle of attack. The distributions of induced velocity and pressure by the rotor can be used to determined the wing twist. The vehicle aerodynamic characteristics will also be discussed, which mainly covers the total drag. The total drag consists of body drag, wing drag and rotor drag, which will be calculated with a set of equations.

Power and propulsive design In the power and propulsive design three things had to be designed. The department had the responsibility to give the propeller diameter, the electric engine choice and the battery design. Next to these designs an

analysis was performed on the use of ducted and contra rotating propellers on the final design.
First the analyses on the effects of uses ducts and contra rotating propellers were analysed, since this would influence the rotor diameter. In the analysis for ducted propellers it was found that the propellers could have efficiency gains of 29%. This would be beneficial for the energy usage of the hover-bike and, therefore, would increase the range and endurance. This efficiency increase, however, only implies when the air stream is orthogonal to the rotor area. The efficiency increase decreases when the flow becomes more and more parallel to rotor area. Next to ducts contra rotating propellers have been analysed to find the efficiency increase. It was found that the efficiency can improve up to 17%.
After, these analyses the rotor size was to be determined. To be able to come with the most optimum size for the rotor area, the influence of the rotor size on the total mass was evaluated. Changing the rotor size would influence the weight of the propeller, the engine, the battery, the structure, the duct and the miscellaneous. The most optimum propeller diameter was found at the place of minimum mass. This resulted in a propeller diameter of 1.6 m.

From the propeller diameter the required power required to fly the hover-bike was calculated. For this the actuator disk theory was applied. After the calculations were performed the max power that should be provided to the propellers form the engine is 282 kW, divided over six engines. This means that a single electrical engine should be capable to provide at maximum 47 kW. The engines that will be used for the hover-bike are brushless engines, they will be capable providing a maximum power output of 50 kW. The total weight of both the engines and the electronic speed control (ESC) will be 42.6 kg.
After the engines have been determined, the a power and energy requirement for the battery pack could be determined. With the power requirement a initial design for the layout of the battery pack could be determined. After this initial design was made the battery size was increase such that it would made the energy requirement. This resulted in a final design which makes use of 2920 *Panasonic B 20700* battery cells. Which will be arranged such that 40 cells will be in string (in series) and it will have 73 strings placed in parallel. The battery pack will consist out of two battery packs both weighting about 92 kg.

Structural design The first step when designing the structure of the hover-bike is to identify the size and mass constraints. With a normal drivers license one is allowed to tow a trailer with a total mass of 750 kilograms, this includes the payload on the trailer. Because the hover-bike has to be transported over public roads, the maximal allowable width is determined by the width of car lanes, which is around 2.6 meter. Finally the maximum allowable length for the hover-bike is determined by the maximum length of the trailer, which is 4.2 meters. After the designing was done the maximum width without the wings became 2.42 meters, with the wing attached the width became 10.41 meters
Next the materials were selected for the structure. Materials were selected based on a few criteria. The criteria were strength, stiffness, mass and cost. Several materials were ruled out immediately due to there poor stiffness or high cost. Therefore only metals and composites were considered as a potential material for the structure. Eventually an aluminium alloy 6061T6 was chosen as the material for the structure. Aluminium was chosen due to its low density and high strength. Furthermore aluminium 6061T6 has superior weldablity capability. The material chosen for the landing gear is aluminium 7075, because this alloy has better stiffness.
When the constraints and materials are chosen the structure can be designed. It was chosen to use finite element method (FEM) to analyse the structure. FEM allows for faster iterations and more accurate results, because hand calculations iterate much slower and are less accurate. When high stress concentrations are found in the structure then these stress concentrations will be mitigated either by increasing the beam thickness or by adding trusses. Finally it is important to optimise the design for the lightest weight possible. There are several load cases that were considered when calculating the stresses in the structure:

- Maximum lift caused by the propellers
- Maximum lift caused by the wing during cruise
- Maximum impact during hard landing
- Maximum stress when parachute is being deployed

After the structure has been designed the centre of gravity and moment of inertia of the structure were determined. Because the two parameters greatly influence the performance of the hover-bike. The moment of inertia was calculated using CAD software, due to the high complexity of the structure.
Several iterations took place during the design of the structure.

- The first reorganised the frame into an upper frame and lower frame.
- The second iteration changed the position of the rear rotor and the beams were changed to thinner hollow beams.
- The third iteration added a landing gear, curved rotor guard beams and the inner diameter of the beams were varied.
- The fourth iteration implemented bent beams, brackets for corners and optimise the inner diameter of the beams.

After these iterations the weight for the structure became 58.8 kilograms.

Control and Manoeuvrability design The hover-bike will have two different mission profiles. These profiles are the transportation profile and the thrill profile. As the name of the profiles already suggest, the transportation profile will mainly be used for efficient transportation between point A and B. Therefore, the transportation profile will be characterised by low accelerations and efficient use of subsystems, in order to meet the range an endurance requirements. Furthermore the ease

in control of the hover-bike be increased by assisted altitude control. The second profile is the thrill profile. In the thrill profile all the limits of the hover-bike will be neared. Flight in the thrill profile consists out of high load manoeuvres in addition to full control by the pilot of the hover-bike. In Figure 3 and Figure 4 the mission profiles are visualised.

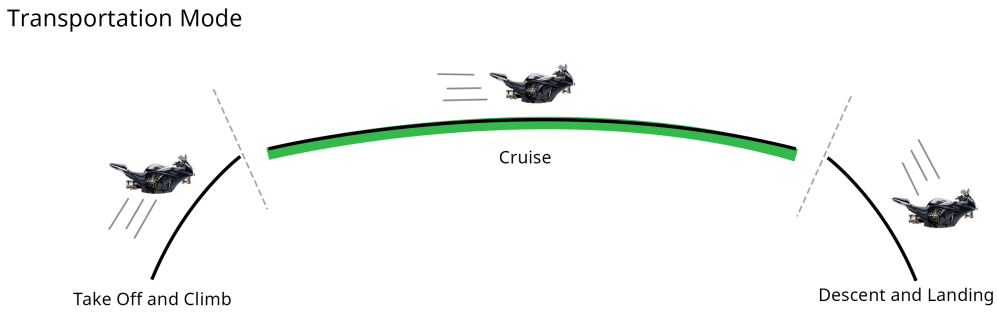

Figure 3: Transportation mission profile, the green phase indicates eco-modus is enabled.

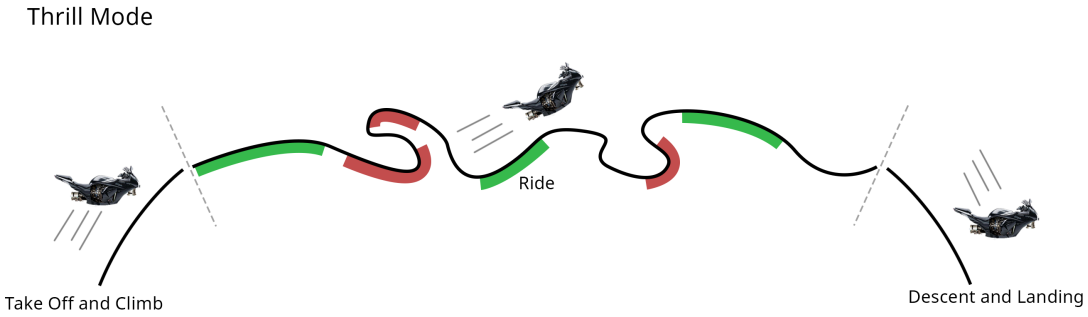

Figure 4: Thrill mission profile, the red phases indicate sport-modus is enabled.

Before control design could begin first the equations of motions (EOM) had to be derived. First the EOM have been rewritten for calculating the accelerations. Also the EOM for calculating the angular accelerations have been derived. Using $Matlab$ a simulation of the hover-bike was generated. In the control layout a number of proportional integrated derivative controllers (PID) were used. The PID loop is a control feedback loop mechanism which restores the actual state to the desired reference state in a optimum manner.
An exemplary flight case is given in figure 5 which shows data divided over multiple graphs. This particular flight simulation from the beginning starts accelerating to an altitude of 5 m. After 6 seconds the maximum pitch angle is applied resulting in a longitudinal acceleration. The graphs in the first row demonstrate the response delay of the electric motors. The first graph 5a demonstrates the real response for total thrust in blue while the second graph indicates the delay in pitch torque. The maximum thrust that is applicable is as previously mentioned 7500 N, which can be observed at about 7.5 s where to thrust is maximised. Another aspect worth noting is the initial decrease in altitude after the pitch angle is maximised. Due to a torque the total thrust generated is not enough to keep the hover-bike at the same altitude resulting in an altitude decrease of a meter. The final graph shows the pitch angle which is set at 0.78 rad at 6 seconds.

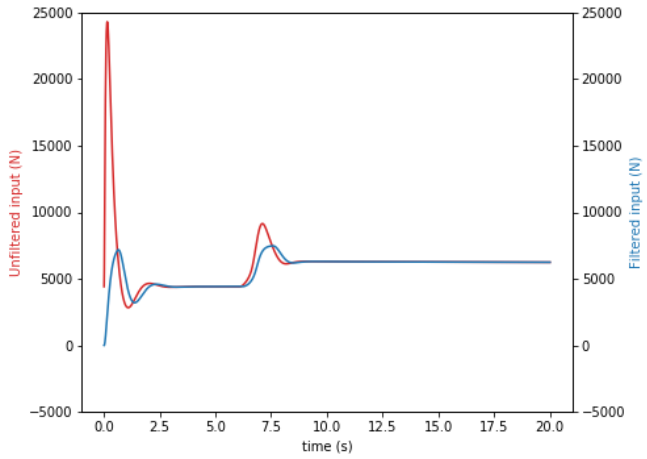

(a) Total thrust.

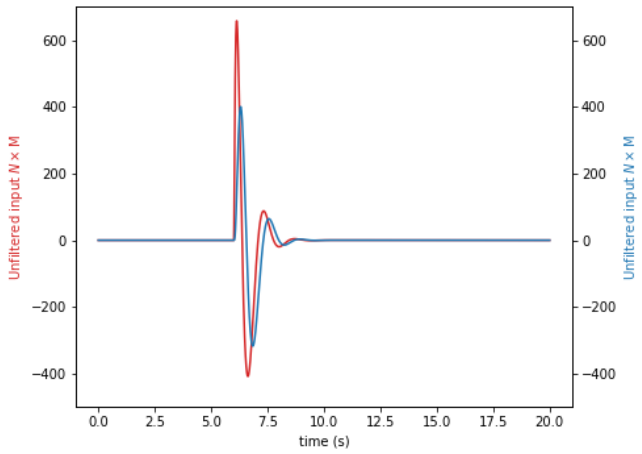

(b) Pitch torque.

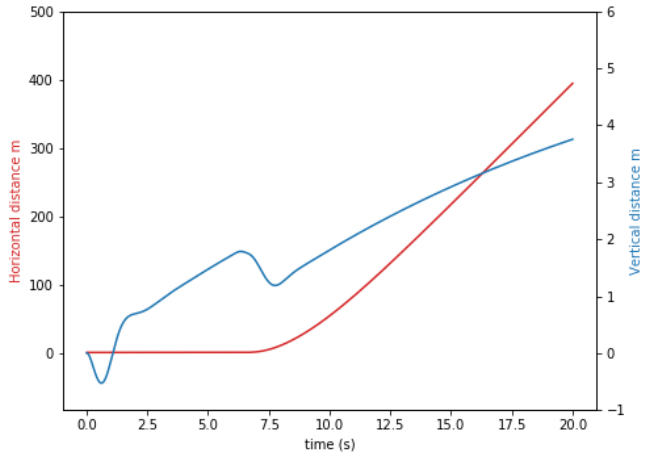

(c) Distance covered for x and z

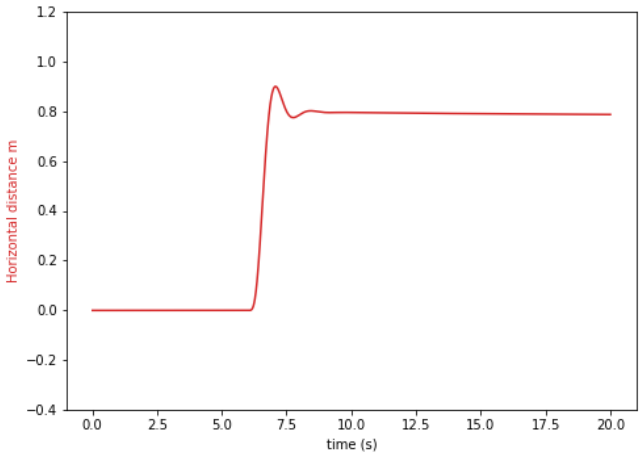

(d) Pitch angle.

Figure 5: Sample test simulation

Human-machine interface

The human machine interface was divided into "Fundamental controls", "In-flight information", "Secondary controls", and finally "Vehicle options interface and customisation". The control of the bike is achieved solely through differential thrust, which means that analogous to a drone there are only four possible forces that can be exerted on the vehicle: τ_x,τ_y, τ_z and Z. Note that a body reference frame is used,where τ_x,τ_y, τ_z are angular accelerations around x, y, z respectively and Z is a linear acceleration along z. Through these four forces, position, velocity, acceleration and attitude are achieved. There are therefore four possible "fundamental" inputs for the main control of the Hover-bike. Since the pilot needs to be able to support the accelerations on his body without creating bio-dynamic feed-through, the controls must support him in x, y and z. The joybar does this very effectively by using newly designed ball and socket joint joysticks.

In-flight information is important to supply the pilot with information about the system. The data that he is given in-flight is divided into two categories: "crucial information" and "optional information". While the crucial information must be displayed at all times, the pilot can choose from a bank of optional information to be displayed next to the crucial information. There is some data that must still be accessible to the pilot despite the screen failing. Battery status, km available on battery, and vertical height are redundantly displayed above the main (and only) screen.

Secondary controls are used to choose options on the screen, or access fast function on the bike. There is a mechanical handle to deploy parachute, which allows for rapid deployment that is not affected by any software issue. There are also two toggle switches and two three-position switches used to activate, autopilot, immediate self-land and two customised inputs respectively. To interact with the options in the screen, there is a knob that can be pushed sideways and forward/backwards and has a button on top. This knob is the equivalent of a mouse or track-pad for a computer. The full system setting can be accessed before or after flight to customise Scorpeon to the user's taste. A big variety of things can be changed ranging from maximum bank/pitch angles or acceleration to the way the data is displayed in the cockpit. The Human machine interface can be seen in Figure 10.4.

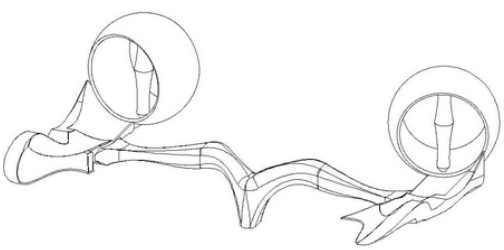

(a) Isometric view of the joybar

(b) Cockpit as seen from the pilot

RAM RAM is an acronym that stands for reliability, availability and maintainability which is an analysis that has been performed in order to predict failure modes and their consequences on the hover-bike and pilot. Moreover, these analysis are done to check the functionality of the hover-bike under certain conditions.
Reliability is defined as the probability of the hover-bike to perform a certain function under given conditions within a specific time. Due to the Scorpeon being in an early stage of design, real-life numbers are not available. Therefore, reference from other vehicles have been used in the analysis. Using reliability values of study done by NASA over small aircraft, a reliability of 98% has been found. This represents a six hour mission reliability. However, in the case of the hover-bike it will be an innovative form of flying with risks that might not be accounted for which might lowers the reliability for the hover-bike. Availability is a measure of how much time the system can be operational assuming optimum performance. It is found that the availability for transportation mode is 0.25 and for thrill mode is 0.1 using transportation time of 45 minutes as an average value.

Safety To estimate the safety of the hover-bike several aspects were looked into. The redundancy of the design, the safety aspects of the parachute, safety aspect of human error and the passive safety. Redundancy means that if on part fails, the other parts can quickly take over and allow the pilot to get to safety. For example if one of the engines fail the other five have to produce all the thrust and keep the hover-bike controllable. Then in the main time the pilot can land and get to safety. The parachute can only be deployed when the hover-bike is high enough above the ground. That is because the parachute needs time to fully open and deploy before the hover-bike hits the ground. Human error is another concern for safety. Human error can be reduced by building in safety nets into the design, such as a FLARM system. An airborne collision avoidance system warns the pilot when other vehicles in the air are getting too close to the hover-bike. This way collisions in mid-air can be reduced. Passive safety systems are there to reduce the impact when something goes wrong. For example the battery has a shell to shield the pilot, If the battery catches fire or explodes then the pilot is protected from harmful material.

Risk During the design process of the hover-bike the risks have been assessed and mitigated. To do so a fault tree analysis (FTA) has been performed. A FTA is a top-down approach for analysing reliability from systems level into component level, organising the component in terms of failure relationships. Moreover, the fault tree is structured by starting on the top cell with the final event that can occur, then going down the tree the cells will represent system failure that must occur to result into the higher event to occur. After all the risks at the the lowest level were analysed, they have been mitigated to reduce the overall risk of the hover-bike.

Sustainability Sustainability is rapidly gaining more and more attention from companies. Sustainability covers three main aspects; social, environmental and economic sustainability. Despite a hover-bike not being a the most sustainable transport vehicle, sustainability methods have been implemented to improve its sustainability. First the social sustainability has been analysed. In the analysis the following aspects have been taken into account; employment rate, employee satisfactions, customer satisfaction, legislation, noise an maintenance. These aspects can have big impact on society and, therefore, are of great importance to be analysed.
Concerning environmental sustainability, four main things have been taken into account in the design of the Scorpeon. The first thing is recyclability. One of the requirements for the design of the hover-bike was that at least 50% should be recyclable. Expecting batteries to be recyclable in the near future and taking into account that the aluminium frame is recyclable, this requirement is met. Secondly is the production pollution. In order to limit the production pollution, a lean manufacturing production is used in order to decrease the amount of wast material. As third is the carbon footprint. Despite the production of batteries having a penalty in terms of CO_2 emission, on the long term the carbon footprint is less comparable to combustion engines. As last the noise pollution is analysed. To reduce the noise pollution, designated flying zones will be assigned in rural areas at least 700 m from building and civilians in order to be able to take-off and land without disturbing the civilians.
The last aspect of sustainability is the economic sustainability. Economical sustainability is crucial to ensure a longer lifespan for the company's survival in the market. As mentioned before lean manufacturing will be used. This will not only be beneficial for the environmental sustainability, but it will also reduce the production cost. Next to lean manufacturing also other aspects have been evaluated. These aspects are the investors, maintenance en the end of life disposal.

Scorpeon design outline Now that all analyses are done a complete picture of Scorpeon will be given, which includes characteristics, operations, production plan and recommendations.

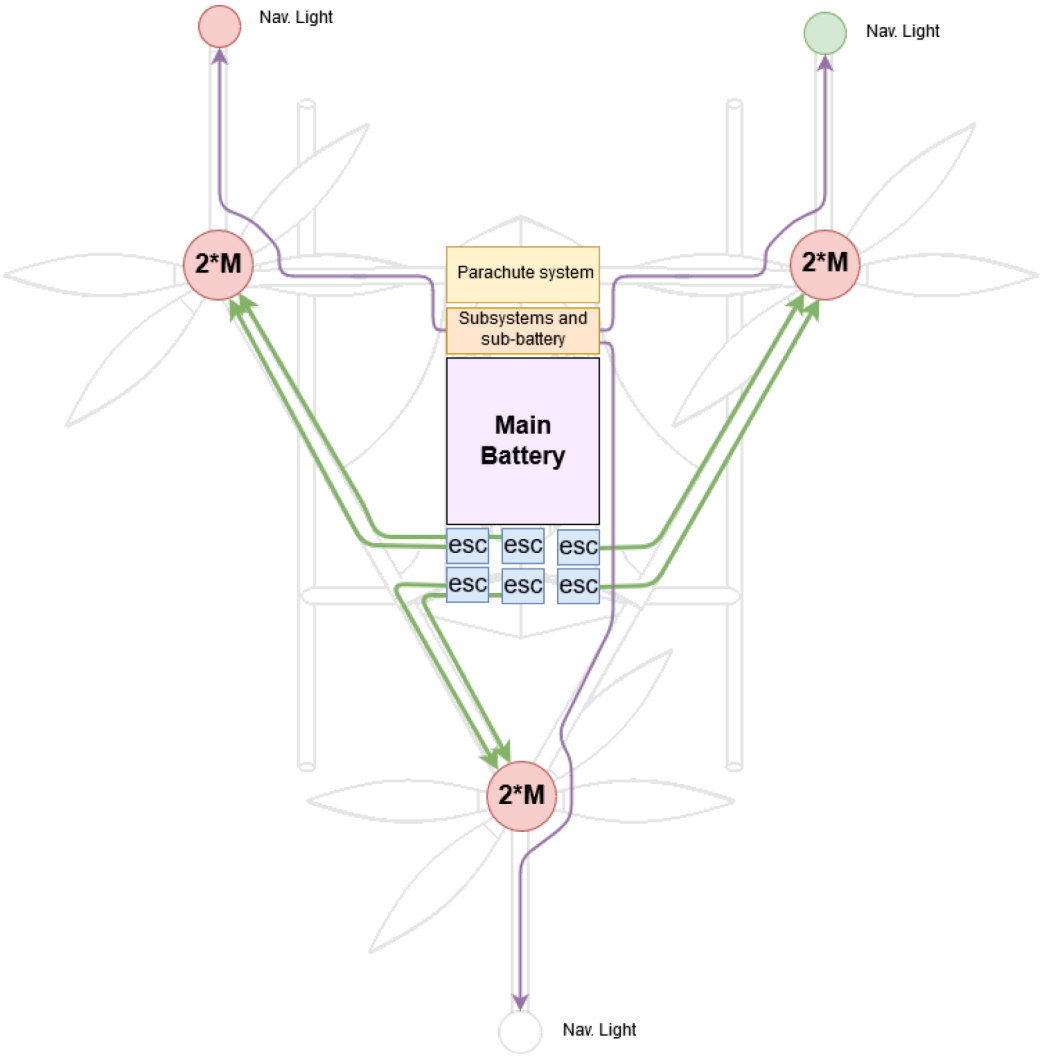

Figure 7: Electrical layout of the hover-bike (Green line = power from ESC to electric motors, purple line = power from subsystem-battery to lights)

In this figure the electrical layout of the hover-bike is given. All the subsystems are in the front together with the parachute. The electric motors are fed from the main battery via the electronic speed controllers (ESC).

In the table below Table 3 you can find all subsystems characteristics of Scorpeon.

Table 3: Overview of subsystem details of the hover-bike concept.

Subsystem	Aspect	Value	Subsystem	Aspect	Value
Wing	Half wing span	3.2 m	Rotor	Diameter	1.6 m
	Aspect ratio	10.4		Contra-rotor gap	0.16 m
	Total surface area	8.7 m^2		Airfoil distribution (root-to-chord)	MH126-MH112-MH114-MH120
	Quarter chord sweep	0°	Power	Number of engines	6
	Taper ratio	0.45		Maximum power output	300 kW
	Root-tip twist	28° (washin)		Battery voltage	148 V
	Geometric angle	37°	Body structure	Width	2.4 m
	Airfoil	Selig S4061		Length	3.4 m
				Height	0.6 m

There are three design budgets made for the hover-bike. There is the cost budget, the mass budget and the power budget. In Figure 8a the cost budget is given and in Figure 8b the mass budget is given. The mass budget summarises the weight of each component into one chart. The mass budget is given for the transportation mode

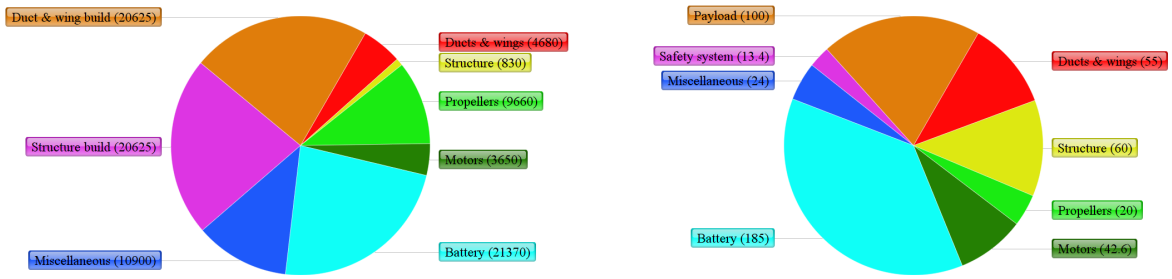

Figure 8: Pie charts displaying (a) the cost distribution in euros and (b) the mass distribution in kilograms. In both charts, the value of each component is given in the brackets after the component name.

In Table 4 a power budget is given. This mainly consist out of the power for the miscellaneous. It can be seen that the power for the miscellaneous is negligible compared power required for the engines. Also, since lower voltage levels are needed for the miscellaneous a separate battery pack will be used.

Table 4: Subsystem power distribution.

Subsystem	Power [W]
LCD screen	4.5
Lights	35.0
Flight data recorder (black box)	5.0
Safety ecu	5.0
FLARM	0.72
Joystick	4.5
Flight controller	8.0
Transmitter/receiver	5.9
Total miscellaneous	68.6
Electric engines	282,000

In Table 5 the cost budget is presented. As can be seen the cost budget is build up out of material cost, manufacturing cost, operational cost and the selling price. The material cost and manufacturing cost together form the cost of the prototype at a combined price of €80000. The selling price is determined by a profit margin of 12.5%. The operational cost is the cost of ownership for 1 year and is pretty low compared with the other costs.

Table 5: Overview of the cost analysis

	Price
Material cost	€51610
Manufacturing cost	€28180
Selling price	€90000

All these subsystems combined determine the performance of Scorpeon, performance parameters in both the transportation mode and thrill mode are shown in the corresponding table below (Table 6).

Aspect	Transportation mode	Thrill mode
Speed	29.7 m/s	55 m/s
Acceleration	8 m/s^2	12 m/s^2
Range	105 km	32 km
Endurance	60 min	9.8 min

Table 6: Performance characteristics transportation mode

Operations and logistics Before the user of Scorpeon can fly the hover-bike it needs to be properly checked first. The first check is a general visual one. The pilot shall see if the hover-bike does not have any obvious damage, such as dents and cracks. The second check is denoted as a "pre-operational checklist". This is comparable to a pre-check before driving a car. The pilot will check if there are any warning lights/signs active, if there is enough power left and if the sensors are working properly. If there are any issues that the driver can not fix by him/herself, he/she is directed to the maintenance section. If everything is working properly Scorpeon is ready to fly.

The maintenance starts when the customer calls the maintenance centre to describe what problems he is facing. The maintenance centre will try to assist the customer if the problem can be fixed without the need of professional help. However, in case of a critical failure or a problem that needs to be checked by a professional, the customer will have to transport the hover-bike to the maintenance centre to perform the maintenance procedures.
For manufacturing of the structural tubes the drawn tube process is used in order to form metal tubes from aluminium T6061 metal rods. Aluminium T6061 can be manufactured using the mentioned process due to its high formability property. For the duct and wing assembly, composite materials were chosen. The reason for this is the high strength to weight ratio for these materials. This allows the wing and duct assembly to be made very lightweight. For the production process of the ducts and wings, the hand lay up technique was chosen. Hand lay up allows for the manufacturing of complex shapes and curves with higher dimensions.
The assembly will be analysed during the mass production phase as at that time is were assembly is the most crucial. After analysing it was found that line production is more optimal for the hover-bike due to its benefits: simple planning, minimal transport, good progress indicator as delays would be clear in the line and lastly maximum routine work per crew.
Quality control and assurance is a main step and measure that needs to be considered for the hover-bike. During this process, every part is checked before and after each stage to make sure that every part is within the high standards and expectations set by the company. In addition, for quality control every hover-bike presented will be tested for performance and tested for critical situations.
Scorpeon will have a headquarters which is defined as the group of 10 engineers that designed the hover-bike. The aspects that are provided by the headquarters:

- Software updates to hover-bikes.
- Training for aviation service centres in order to become licensed hover-bike mechanics.
- Manuals to the aviation service centre.
- Training to get the the hover-bike licence. This is done by a weekend training in which the basics will be taught to operate the hover-bike.
- Warranty of 1000 flight hours or 5 years (which one expires first).

Furthermore, hover-bikes must undergo a yearly mandatory check, similar to cars, which will be done at aviation service centres.

Contents

List of symbols

Quantity	Description	Unit
a	Lift-curve slope	[-]
A	Collective rotor disk area	[m^2]
b	Wing span	[m]
c	Chord length	[]
c_{blade}	Blade chord length	[m]
c_{wing}	Wing chord length	[m]
C_{Cell}	Battery cell capacity	[Ah]
C_D	Drag coefficient	[-]
$C_{D,0}$	Zero-lift drag coefficient	[-]
$(C_D S)_S$	Equivalent flat plate area	[m^2]
C_L	Lift coefficient	[-]
$C_{58L,\text{b}}$	Body lift coefficient	[-]
$C_{L,\text{max}}$	Maximum lift coefficient	[-]
C_m	Moment coefficient	[-]
$C_{m,0}$	Zero lift pitch moment coefficient	[-]
c_{mac}	Moment coefficient about aerodynamic centre	[-]
d	Distance between centre of gravity and centre of twist	[m]
d_{cg}	Distance to centre of gravity	[m]
dr	Blade element width	[m]
dT	Thrust of one blade element	[N]
dQ	Torque of one blade element	[N]
D	Aerodynamic drag	[N]
D.L.	Disk loading	[kg/m^2]
D_{Prop}	Propeller diameter	[m]
e	Distance between centre of lift and centre of twist	[m]
e_{eff}	Effective oswald efficiency factor	[-]
E	Young's modulus	[Pa]
E_{Batt}	Total available battery energy	[Wh]
f_{Usable}	Permissible battery pack depth of discharge	[-]
F.M.	Figure of merit	[-]
g	Gravitational acceleration	[m/s^2]
$\bar{GJ}$	Effective polar moment of inertia	[kg·m^2]
I_{cm}	Moment of inertia of component i about own centre of mass	[kg·m^2]
$I_{\text{Max,Batt}}$	Maximum current the battery can supply	[A]
$I_{\text{Max,Cell}}$	Maximum current a cell can supply	[A]
$I_{\text{Max,Eng}}$	Maximum current drawn by engines	[A]
I_{xx}	Moment of inertia about x-axis	[kg·m^2]
I_{yy}	Moment of inertia about y-axis	[kg·m^2]
I_{zz}	Moment of inertia about z-axis	[kg·m^2]
k_r	Induced drag power factor	[-]
k	ratio between induced velocity downflow and upflow	[-]
k_ω	Estimation rate for rotational speed scaling	[-]
K	Factor for M_{DD}	[-]
K_p	Factor for lift of a flat plate	[-]
L	Aerodynamic lift	[N]
L_1	Noise level at location 1	[dB]
L_2	Noise level at location 2	[dB]
m	Mass of the hover-bike	[kg]
m_i	Mass of component i	[kg]
m_{Batt}	Mass of the battery	[kg]
M	Mach number	[-]
M_{DD}	Drag divergence mach number	[-]
MTBF	Mean time between failures	[hr]
MTTF	Mean time to failure	[hr]
MTTR	Mean time to repair	[hr]
N	Maximum load factor	[-]
N_{Cells}	Total number of cells	[-]
N_{Series}	Number of cells in series	[-]

N_{Strings}	Number of strings in battery	[-]
$\bar{o}_z$	Height vector	[m]
p	Pressure	[Pa]
p_x	Probability distribution	[-]
p_∞	Free stream pressure	[Pa]
P_{actual}	Actual rotor power	[W]
P_{ideal}	Ideal rotor power	[W]
P_{total}	Total power	[W]
q	Dynamic pressure	[Pa]
Q	Torque at rotor hub	[N·m]
R	Reliability	[-]
R_{rotor}	Rotor radius	[m]
Re	Reynolds number	[-]
r_1	Distance to location 1	[m]
r_{v0}	Distance long blade from rotational axis where relative velocity is zero at cruise	[m]
t	Airfoil thickness	[m]
S	Surface area	[m^2]
S_b	Equivalent body surface area	[m^2]
S_{wing}	Wing surface area	[m^2]
t_{hover}	Time in hover	[min]
t_{op}	Operational time	[hr]
T_{design}	Designed thrust	[N]
T_{estimate}	Estimated thrust	[N]
u	Velocity in longitudinal direction	[m/s]
u_{Batt}	Battery energy density	[Wh/kg]
U_{Batt}	Battery voltage	[V]
U_{Cell}	Battery cell voltage	[V]
U_{eng}	Operational voltage of engines	[V]
v	Velocity in lateral direction	[m/s]
v_1	Induced axial velocity at location 1	[m/s]
$\bar{v}_i$	Normalised induced velocity	[-]
V_{cruise}	Airspeed at cruise	[m/s]
V_{element}	Velocity at one blade element	[m/s]
V_i	Induced velocity	[m/s]
$V_{\text{resultant}}$	Resultant velocity at one blade element	[m/s]
V_∞	Free stream velocity	[m/s]
w	Velocity in vertical direction	[m/s]
W	Weight of vehicle	[N]
X	Force in x-direction	[N]
y	Distance from wing root	[m]
Y	Force in y-direction	[N]
Z	Force in z-direction	[N]
α	Angle of attack	[rad]
α_{Body}	Body flight angle of attack	[rad]
α_r	Angle of attack for rigid body	[rad]
$\overline{\alpha}_r$	Constant additional rigid angle of attack	[rad]
β	Blade pitch angle	[rad]
Γ	Linearised input torque	[N·m]
η_{Batt}	Battery efficiency	%
η_{Batt}	Contra rotating propeller gain	%
η_{Batt}	Efficiency gain duct	%
η_{Batt}	Electric motor efficiency	%
θ	Pitch angle	[rad]
θ_b	Angle of rotor disk in longitudinal direction	[rad]
θ_{el}	Elastic twist deformation	[rad]
λ	Aeroelastic eigenvalue	[-]
λ_f	Failure rate	failure/hr
μ	Dynamic viscosity	[kg/(m/s)]
ν	Poisson ratio	[-]
ρ	Air density	kg/m^3
τ_B	Input torque	N·m
τ_θ	Torque about pitch axis	N·m
τ_ϕ	Torque about roll axis	N·m
τ_ψ	Torque about yaw axis	N·m
ϕ	Roll angle	[rad]
ψ	Yaw angle	[rad]
ω	Rotational speed of rotor	[rad/s]
ω_{max}	Maximum rotational speed	[rad/s]

List of abbreviations

Abbreviation	Description
CAD	Computer aided design
cg	Centre of gravity
cm	Centre of mass
ESC	Electronic speed controller
EOM	Equations of motion
FEM	Finite element method
FIT	Failure in time
HTOL	High temperature operational life
MOI	Moment of inertia
NAFEMS	National agency for finite element methods and standards
PID	Proportional integral derivative
VTOL	Vertical take-off and landing

1
Introduction

There are three modes of transportation, namely water, land and air transport. Over water, cargo ships are used for freight transport, ferries are used for public transport, boats are used for regular multi-person transport and jet skis are used for a single/double-seated thrill ride. Over land, trucks are used for freight transport, busses are used for public transport, cars are used for regular multi-person transport and motorcycle are used for a single/double-seated thrill ride. Through air, cargo aircraft are used for freight transport, commercial aircraft are used for public transport, private jets and helicopters are used for regular multi-person aircraft, but nothing concrete exists for a single/double-seated aerial thrill ride yet. In other words: A hover-bike, a motorcycle for the air, that can deliver at least similar performance, thrills and freedom as a high performance motorcycle, must be designed to outperform existing designs. This gives rise to the need for *a motorcycle for the air, that can deliver at least similar performance, thrills and freedom as a high performance motorcycle, must be designed to outperform existing designs.*
This need is filled by the design of a hover-bike, capable of vertical take-off and landing. A hover-bike is defined as *an aerial vehicle with six degrees of freedom that is engine powered, capable of vertical take-off and landing and providing non-enclosed seating for up to two people.* Although this specific hover-bike need described above is focused on providing thrills, other hover-bike designs could theoretically be used for different purposes, similar to how motorcycles are used by the police and jet skis can be used for on-sea rescue operations. Therefore, this project also paves the road for future companies or starters to design their own hover-bike concept driven by different needs, such as rescue operations.

By using system engineering tools and the engineering knowledge gained during the bachelor of Aerospace Engineering at TU delft, a group of ten students has been working for ten weeks to design a hover-bike. The purpose of this report is to document the result of the preliminary design solution that satisfies the need of a motorcycle for the air. The design solution is a vehicle in a tilt-copter layout with three ducted contra-rotating rotors with wings attached to the ducts, dubbed the Scorpeon.

This report starts of with the market analysis in chapter 2, which has been performed to see where the hover-bike could enter the market. Then a mission analysis is done in chapter 3 where the mission profile, functional analysis and requirements and constrains are discussed. After that the hover-bike concept development is done in chapter 4, here it is explained how the Scorpeon has come to life. Before the engineering could start some preparation activities has been done and are shown in chapter 5. Next the analyses of the final iterated concept is performed which includes aerodynamics (Equation 7.1.1), power and propulsion (chapter 7), structures (**??**) and control (chapter 9) which also includes the human machine interface in chapter 10. Furthermore the reliability, availability and maintainability is discussed in chapter 11, additionally safety and risk analysis can be seen in chapter 12 and chapter 13 correspondingly. As last the cost and sustainability of the design are assessed in chapter 14 and chapter 15. To end the report the complete picture of Scorpeon is shown in chapter 16, where characteristics, operations and logistics, a production plan, requirements compliance and recommendations are shown.
This report is the final version of the final report. The final report describes the progress during the fourth phase of this DSE project: Design of a hover-bike. This fourth phase focuses on the analysis of the preliminary design, following up on the chosen concept during the conceptual concept. The change record of this report is depicted in Table 1.1.

Table 1.1: Change record of final report.

Version	Date	Affected pages	Brief description of changes of final report
1.2	29th June 2018	all	

2
Market analysis

The main purpose of this chapter is to know what is expected of Scorpeon , and predict as accurately as possible the best way to successfully enter the market. This includes understanding the main interests of the customers and their concerns, which will not only shape the requirements, but also point towards the best marketing methods. Scorpeon attempts to be the jet-ski or motor-bike equivalent of the air, and to make sure it is able to bridges this gap, a closer analysis of the market has to be made. The hover-bike team must therefore analyse the current market, and predict how its product (Scorpeon) will perform. To do this, the market need will first be clarified, the target market will then be identified and the market value will be calculated. Later on, the product will be compared to that of competitors before finishing by discussing some barriers to entry that the team might encounter. Given that the start up is in the Netherlands, the market analysed will be within the Netherlands.

2.1. Market needs

Throughout time, most people have at least once in their life wished they could fly, and around 160 years ago, we achieved what was thought to be impossible. Nowadays anybody can buy a plane ticket and "fly", but it is not them who control the craft through the air; the freedom of flying is only accessible to a small amount of people. To begin, a pilot's licence is needed, which requires years of training, and even after this is achieved, a conventional ultralight-aircraft is too big to feel like the flying that we had dreamed off. This is where a hover-bike steps in: a small, relatively cheap personal vehicle that can take-off/land anywhere, that can achieve high velocities, and is easy to fly. The market needs a machine that lets people achieve their dream of flight without going though too much of a hassle. In the same sector, there is also a need for a small VTOL aircraft which can not only be used to remove the congestion in the ever-increasing road traffic, but also for operation like rescue missions. However, even-though Scorpeon can be used as a mean of transport, the design of Scorpeon will stay focused on the "fun aspect" and freedom of flying.

2.2. Target market

Knowing the target market is crucial for the design and marketing of the hover-bike. Three types of potential customers have been identified:

Thrill seekers

These thrill seeking customers are generally young adults and they are the ones who will push the Scorpeon to its technical limits. The first group of buyers will most likely be in this category, as they have less safety concerns and will hesitate less before hopping on the vehicle. It is them who will bring credibility to the machine and safety concerns to rest.

Less adventurous curious adults

After watching social media posts of the aforementioned thrill seekers, Curious adults who enjoy adventure (but are not too courageous) will start gaining confidence in the safety of Scorpeon and will likely be the second group to start buying hover-bikes. While the previous group are expected to use the thrill mode a lot more than the transportation mode, this group is expected to start using this bike for transportation more and more as they don't use the full extent of what the thrill mode can bring. This second group will give a lot more confidence to the everyday person of the functionality of the hover-bike as means of transport as well.

The everyday person looking for faster congestion-free transport

By the time the everyday person starts buying this hover-bike, its production price will likely have gone down and its safety concerns put to rest. This group is harder to attract and since they are so far into the future, they will not be used as extensively as the first two groups to design the hover-bike.

From this three main groups, the Scorpeon team has decided that it is acceptable if the vehicle does not target the everyday person as it would make the Hover-bike's design to focus more on transportation and less in thrills. There are enough customers in the first two groups and not everybody can be satisfied.

2.3. Market volume

To have a good idea of the demand that the product will have, it is important to estimate the market volume. This is normally done by simply looking at the already established market. However, there is no true existing market for such vehicle so it must be estimated by looking at vehicles that share functions/price with the Scorpeon . The potential market size will be estimated using a top down approach which consist in starting with a global number and reducing it pro-rata. The markets that are analysed in this estimation are:

Expensive luxury/sports cars as as they share the adrenaline pumping objectives while still not being indispensable. Addi-

tionally,people who can afford these expensive cars can also afford a hover-bike.
Motorcycles, especially sports bikes, as they tend to be owned by moto enthusiasts who are in for a thrill, and would not loose a chance to experience the Scorpeon . This group is also more likely to buy a hover-bike than any other kind of VTOL aircraft.
Light & Single engine helicopters, as their pilots have in some way, affinity with flying, so a part of this group will also be interested in buying a hover-bike.
In table 2.1 an estimate of the market value of the three different markets is given. Aiming to have a significant percentage of the market as a start-up is not realistic, as expensive cars or helicopters can easily exceed 1million euros, which is already ten times the allowed prototype price of the Hover-bike. However, the Scorpeon team should aim to supply at least 50% of all the personal aerial vehicles in the Netherlands.

Table 2.1: Market value overview

Market	Global Market value [$\times 10^9$ €] [1]
Expensive luxury/sports cars	408 [2]
Motorcycles	75.6 [3]
Light & Single engine helicopters	62.9[4]

In the first years that the hover-bikes are produced and sold, the market still has to grow to its full extend as the machine gains credibility. This growth can take a couple of years before it stabilises and is strongly affected by government regulations. Any estimation of such market would therefore be very unrealistic. This is why the best option for the team is to pre-sell a set number of prototypes before producing them which not only gives funding for further development, but also guarantees that the vehicle is sold before it is even produced.

2.4. Competition

Taking a closer look at the competition is helpful to assess their product's advantages and disadvantages over ours. Simply put, if our hover-bike brings nothing special to the table compared to the competitors, it will not strive in the market. All vertical takeoff and landing (VTOL) aircraft that are in development or already in the market will be considered competition because the customers have these as substitutes to fly in the air. In Table 2.2 different competitors are shown with their corresponding performances.
The first visible aspect is that most of these competitors focus on personal transport and not on entertainment. There are therefore generally more seats, on a more comfortable control-less cabin. These designs are aimed at the customer being a passenger, not a pilot. This is one of the areas where the Scorpeon can stand out, as it is designed for the passenger to be the pilot, and enjoy handling this vehicle through the skies.
Most of the performance parameters are bested by other vehicles in terms of range, which further highlights that there is a gap in the market; there is no VTOL aircraft designed to feel the adrenaline pumping through the veins. This might explain why information about accelerations on different axes are not gievn for any other competitor, which makes it hard to compare how the Scorpeon 's aggressive manoeuvres. This further reaffirms that the Scorpeon team must aim at designing a fun vehicle.
The team participated in a Lunch lecture given by the Lilium jet company, which aims to provide fast, affordable and hassle-free transport. Despite having a different target market, there are a lot of engineering challenges that Scorpeon might also experience like transitioning to cruise from hovering flight or optimising the body to create the best lift to drag ratio. All engineering divisions took note of the different design approaches used. One of the most important aspects the team learned is how flying regulations kill the functionality and even whole concept of some designs. For instance, nowadays, a helicopter, or any other craft of relatively the same size have big restrictions on where they can take-off and land, mainly due to noise. This would make a craft like Lilium useless. Having a company like this before Scorpeon is very beneficial as we will not have to spend time and money to make the authorities adjust to the new electric aircraft era.

2.5. Barriers to entry

The potential problems that could prevent the Scorpeon to succeed in the market should be identified to find solutions. This task is specially challenging for new products as there is no example of past mistakes to learn on and predicting something that has never happened is more complicated. The main two clear problems that may affect the demand of the vehicle are different government regulation and aspects that may affect consumer trust. All these will be discussed individually.

[1] URL: https://www.statista.com/statistics/412794/euro-to-u-s-dollar-annual-average-exchange-rate/ [cited 1 May 2018]
[2] URL: https://www.statista.com/statistics/281574/size-of-the-luxury-car-market/ [cited 1 May 2018]
[3] URL: https://www.persistencemarketresearch.com/market-research/motorcycle-market.asp [cited 1 May 2018]
[4] URL:http://www.airbus.com/content/dam/corporate-topics/publications/backgrounders/Global-Helicopter-Forecast-2017.pdf [cited 9 May 2018]
[5] URL:http://aerofex.com/ [cited 1 May 2018]
[6] URL: http://www.ehang.com/ehang184 [cited 9 May 2018]
[7] URL: https://lilium.com/ [cited 9 May 2018]

Table 2.2: Performance properties of different personal aerial vehicles

Competitor		range [km]	endurance [min]	Seats	Top Speed [km/h]
	Scorpeon	100	60	1	100
	Aerofex[5]	90	75	1-2	72
	Vahana	80-120	21	1	225
	Cora	100	33	2	180
	Joby Aviation	240	48	4	300
	Ehang 184[6]	41.7	25	2	100
	Lilium[7]	300	60	5	300
	City Airbus	30-50	24	4-6	100
	Volocopter	27	16	2	100

2.5.1. Government regulation

Noise regulations could be a potential harm for practicality. If the hover-bike emits a lot of noise, there will be regulations that state where you can fly it, which would make it's use purely recreational. For instance, going to work on a motorcycle might be the reason to wake up in the morning (the only fun thing in the day). However, if the hover-bike can not be flown in the city, then it must first be transported to a site where it's use is allowed, which might demotivate anyone to even buy the product. Additionally, moving to a noise friendly area implies transporting the machine, which takes us to the next point.
Transportation regulations should be closely monitored as it might constraint the design. For instance, a person with a normal car Driver's licence should be able to transport the flying bike or else the number of potential customers could decrease even further. The previous constraint means you can only use single-joint trailers where the combined mass of the car + trailer should not exceed 3500kg and should be less than 2.40m wide [8], which again gives constraints to the design.
Privacy regulations are naturally not in place for hover-bikes yet. However, given how easy it would be to spy on your neighbours with this machine, regulations similar to that of drones could be expected. These include minimum time under a specific altitude, or even a ban on flying in populated areas.
Safety regulations could also discourage the potential customers. If this technology becomes widely implemented governments might demand for lower top speeds, lower manoeuvrability or limit thrilling performance in any way. That would again mean that to seek more thrills you have to go to a special area just like a race track for road illegal sports cars.
Piloting regulations could be one of the biggest demand killer. If a government finds the hover-bike potentially dangerous to fly around other people, it might impose a certain age requirement accompanied by a license or a mandatory training. Once again, this would make customers need to move the hover-bike to an area with no bystanders. Clearly the main consequence of various regulations would be the need to transport the bike to safer areas. The design for an efficient method of transportation should therefore be considered.

2.5.2. Public trust

safest concerns are rational. It is not reasonable to expect the public to trust a fast machine soaring to the air while being between very fast moving propellers. It is therefore recommended to do public tests of failures that the public might be scared of. For instance, show that if a propeller brakes mid-flight, it will not reach the pilot's compartment and the Scorpeon will land safely.
Practicality might be the deciding factor of potential customers who do not have money to spare. If they do such considerable investment, they must be confident that they will actually use it. A solution to this, could be events in which demonstration of the different operational aspects including flying, to reaffirm the user-friendliness of Scorpeon .

[8] URL:https://auto-en-vervoer.infonu.nl/transport/10162-verkeer-auto-afmetingen-lading-aanhangwagen.html [cited 09 may 2018]

2.6. Overall overview

This analysis has helped the team to know with certitude that it is the exciting thrills that will set Scorpeon apart from the other competitors. It is therefore acceptable if some endurance or range characteristics are sacrificed at the expense of a more enjoyable, agile Hover-bike. It has also been clear that such vehicle will have a sceptical public at first, but by offering demonstration and test flights, people will start getting enticed by the vehicle. The team must not think that all is lost if demand for such bike is not as high as expected. Finally, it has been clear that there are a lot of regulations that would highly restrict the use of the vehicle. Thankfully, Lilium will pave the way to a future more comprehensible of new generation electric aircraft and do so without being competition as they have a different target market.

3
Mission analysis

In order to generate a hover-bike design which will comply with all the requirements and constraints, a missions analysis has to be performed. First is the flight profiles of the hover-bike are given. This is done in section 3.1 Next a functional analysis is performed. For the functional analysis, a functional flow diagram and a functional breakdown are used. These can be found in section 3.2. After that, the requirements and the constraints are given in section 3.3

3.1. Mission Profile

The mission profile gives an overview of the flight profiles of the Scorpeon. For the Scorpeon, two different mission profiles can be distinguished, namely a transportation profile and thrill profile. The transportation mission profile is characterised by low accelerations and efficient use of subsystems in order to fly as far and long as possible. For this reason, the Scorpeon will use ducts with wings attached to increase range and endurance characteristics. Further properties of the transportation profile include assisted manoeuvring and control by the flight controller and autopilot as well as direct altitude selection instead of full control of descent and ascent rates. The transportation is especially linked to the Eco-mode as shown in figure 16.4 and displayed in green in figure 3.1. The thrill mission profile is defined by a flight phase operating at the near limits of the hover-bike. Proportionally high-performance manoeuvres will be practised, meaning the limits at subsystem level will be near. In this condition, the wings and ducts are taken off from the hover-bike, making the vehicle more manoeuvrable. Flight in the thrill profile contains high load manoeuvres in addition to full control of the pilot of the hover-bike. As a result of full controllability by the pilot, a certain skill level is necessary. This flight profile can be linked to the sports mode as shown in Figure 16.4. The colour linked to sports mode is red as shown in Figure 3.2. Apart from the sports mode, the hover-bike also have a standard mode that can be used in the thrill profile, which is characterised by the pilot controlling the direct attitude angles, simplifying pilot controls.

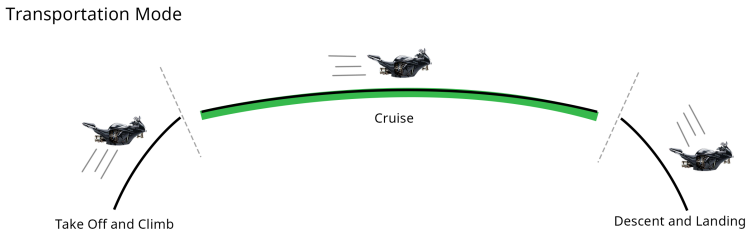

Figure 3.1: Transportation mission profile, the green phase indicates Eco-mode is enabled.

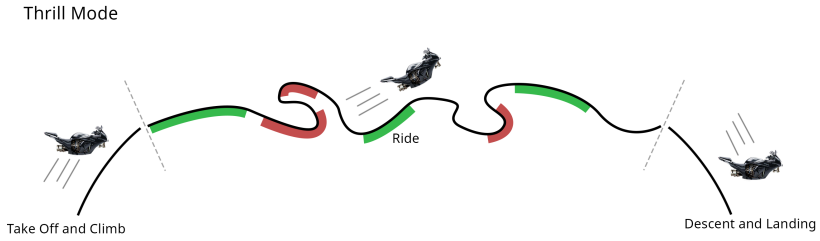

Figure 3.2: Thrill mission profile, the red phases indicate sport-mode is enabled.

3.2. Functional analysis

Before it is possible to design the hover-bike, it is necessary to determine what it should actually do. Or in more professional terms, the functions that the hover-bike must execute should be worked out. In this case, two tools will be used to accomplish this, a functional flow diagram (FFD) and a functional breakdown structure (FBS). The FFD focuses more on the relations between each function, while the FBS is more focused on the hierarchical structure of the functions.
The FFD for the hover-bike is depicted in subsection 3.2.1. In this section, extra information is also provided about the flow diagram in general and some functions are more clearly explained in words. Then, in subsection 3.2.2, the functional

breakdown structure is provided. This structure contains the same elements as the FFD and they only differ in structure. Therefore, there is no extra information provided on some functions as is done for the FFD.

3.2.1. Functional flow diagram of hover-bike

The FFD for the hover-bike is given in Figure 3.3. This diagram starts with the five highest level of operations functions that can be identified. These consist of start-up procedure, flying off the hover-bike, checking for failure, initiating safety modes and end-of-flight procedure of the hover-bike. These main functions are then broken down into another sub-level. At this stage of the design, most focus lies on the operational functions of the hover-bike. In the next couple of lines, some of the functions are explained in more detail.

Operate the hover-bike The operation of the hover-bike is the most important function at this stage of the design. These functions actually determine most of the characteristics of the vehicle. The operations are split into 5 main components. First the start-up procedure where the hover-bike functions are provided to support the pilot , authorisation method, etc. Secondly comes the main operation phase of the hover-bike which is flying it in hover and cruise situation which includes the transition phase which is going from hovering into cruise. After that comes the failure checking part which is a passive monitoring system that checks for failures and warns pilot in case of failure. Following that, its the initiating safety modes in case of critical failures where the pilot initiates the safety mode to start landing. Finally comes the end-of-flight procedure which is a procedure that is valid for an electric vehicle.

As a final comment on the FFD, it is already decided that the hover-bike will allow for an automated or manual take-off and landing. It is up to the driver to choose how he/she will take-off or land. The modes during manoeuvre will influence the handling of the vehicle. Possible mode options can be found in subsection 16.2.1.

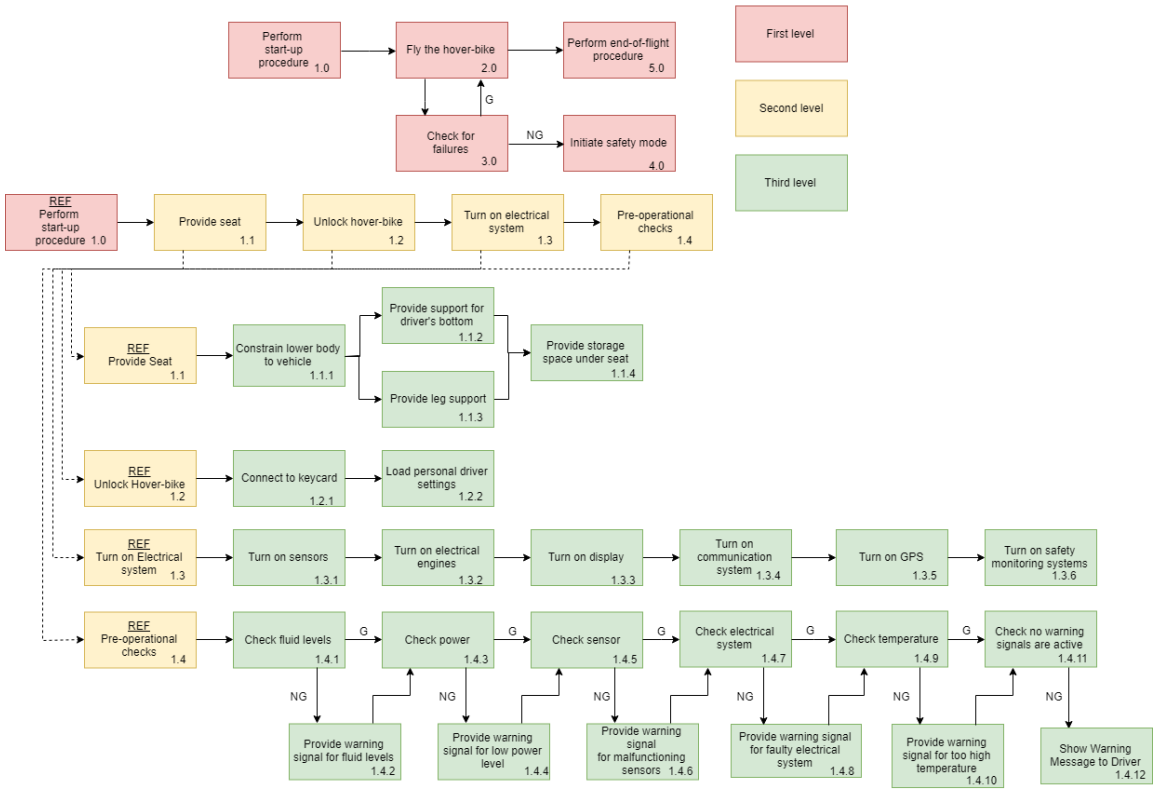

Figure 3.3: Part 1 of the functional flow diagram for the hover-bike. In this diagram red = 1st level, yellow = 2nd level, 3rd = green

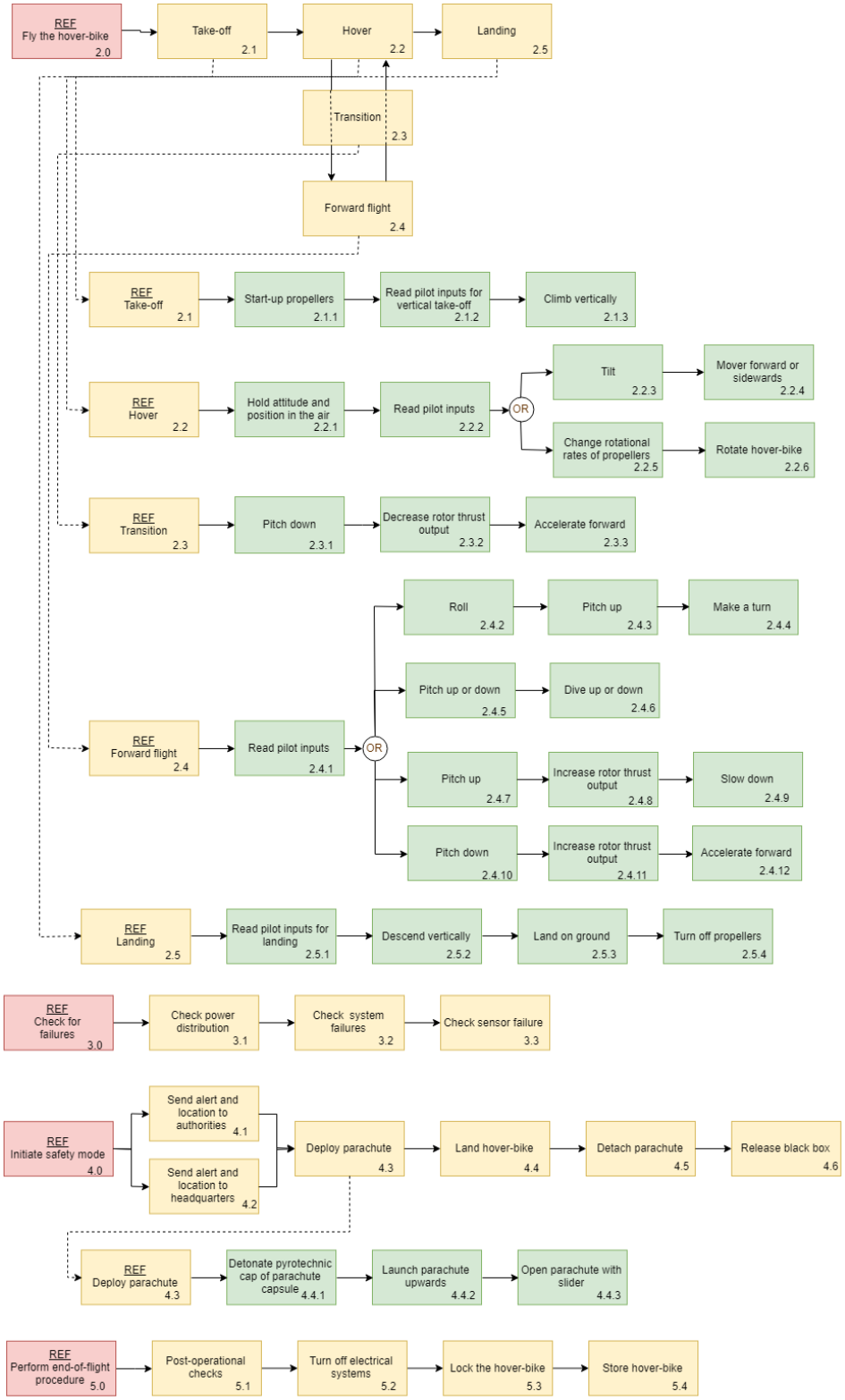

Figure 3.4: Part 2 of the functional flow diagram for the hover-bike. In this diagram red = 1st level, yellow = 2nd level, 3rd = green

3.2.2. Functional breakdown structure

The FBS diagrams are given in Figure 3.5 & 3.6 it represents the functions that the hover-bike must achieve in a form of an AND tree. The FBS is mainly inspired by the generated FFD given in subsection 3.2.1 with the main focus given to the operational functions of the hover-bike presented in a hierarchical order.

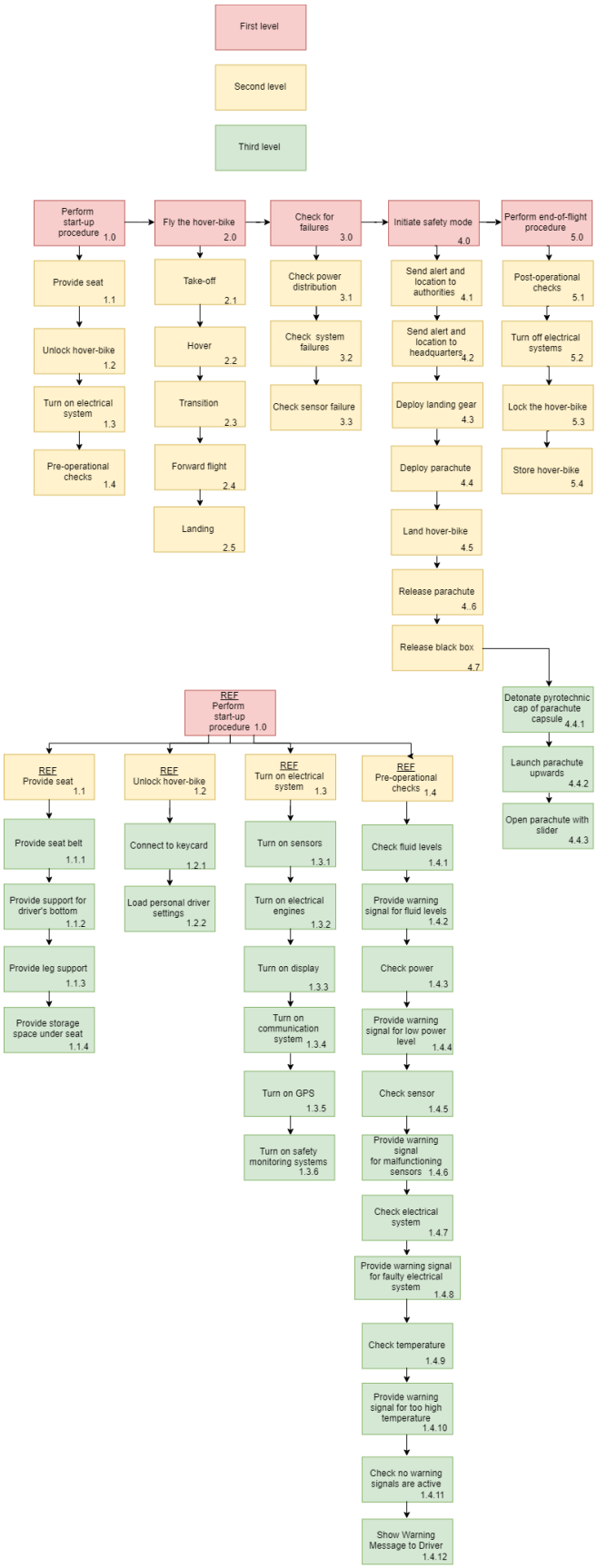

Figure 3.5: Part 1 of the functional Breakdown Structure for the hover-bike. In this diagram red = 1st level, yellow = 2nd level, 3rd = green

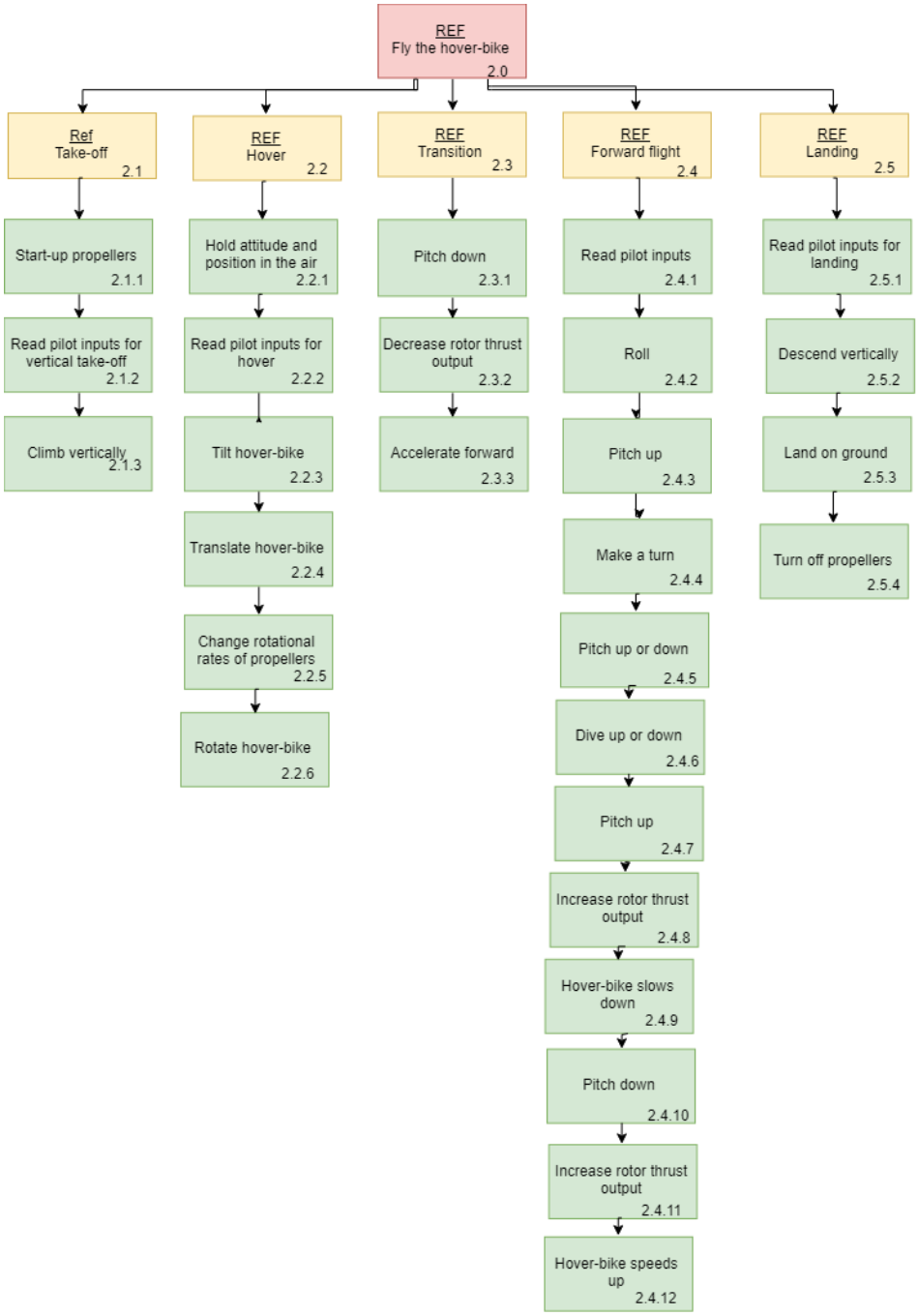

Figure 3.6: Part 2 of the functional Breakdown Structure for the hover-bike. In this diagram red = 1st level, yellow = 2nd level, 3rd = green

3.3. Requirements and Constraints

In this section, the functional requirements and the constraint for the hover-bike are given. First, an overview of the functional requirements and constrains are given.
The functional requirements are broken down into performance requirements and operational requirements. Performance requirements can be split up into several measures like: the performance measures contributing to the thrill and experience of riding a bike and general technical performance standards regarding common mechanical aspects of comparable vehicles. Requirements expressing the fun and excitement of piloting the hover-bike initially are the maximum speed, acceleration and turning rates in the longitudinal, lateral and vertical direction as can be seen in Table 3.1.
While the functional requirements describe what the system shall do, constraints are real-world limits or boundaries which will limit the design of the hover-bike. These constraints are mainly derived from stakeholders such as the government, environmental agencies or general public. The constraints are broken down into several sections; engineering constraints, cost constraints, law and regulation, safety constraints, schedule constraints and sustainability constraints. An overview of the constraints are given in Table 3.2.
Driving requirements are displayed in orange in Table 3.1 and Table 3.2. A driving requirement is defined as a requirement which is either user-defined or derived, which will drive the design of the hover-bike more than other requirements. Potential killer requirements are displayed in red in Table 3.1 and Table 3.2. A killer requirement is defined as a requirement which will drive the design of the hover-bike to an unacceptable extent.

Table 3.1: Functional Requirements

ID	Requirements
	Technical Performance
HB-FR-ST-01	The hover-bike shall be movable in 6 degrees of freedom.
HB-FR-ST-02	The hover-bike shall have a minimum range of 100 km while maintaining a 100 km/h speed.
HB-FR-ST-03	The service ceiling shall be at least 3000 ft above sea-level
HB-FR–ST-04	The hover-bike shall be able to fly for at least 1 hour while maintaining a 100 km/h speed.
HB-FR-ST-05	The hover-bike shall be able to vertically take-off and land.
HB-FR-S-06	The hover-bike shall be statically stable and dynamically damped.
HB-FR-S-07	The hover-bike shall have a maximum pitch angle of 45 degrees.
HB-FR-S-08	The hover-bike shall be able to operate in an atmospheric temperature range of 0 to 40 degrees Celsius.
	Experience
HB-FR-S-09	The longitudinal acceleration shall be at least 8.3 m/s^2.
HB-FR-S-10	The vertical acceleration shall be at least 1.7 m/s^2.
HB-FR-S-11	The longitudinal speed shall be at least 150 m/s.
HB-FR-S-12	The Hover-bike shall be able to take turns with at least 1.7 G.
	Operational Requirements
HB-FR-ST-13	The hover-bike shall be able to safely bring down the pilot from FL030 in case of emergency.
HB-FR-ST-14	The hover-bike shall transmit its position with a transponder.
HB-FR-ST-15	The hover-bike shall be able to be handled by a single person at any time.
HB-FR-ST-16	The hover-bike shall possess a radio for communication.
HB-FR-S-17	The hover-bike shall be equipped with a system that monitors the operational state of the hover-bike.
HB-FR-ST-18	Handling qualities shall be such that 6 hours of training is sufficient to safely operate the hover-bike.
HB-FR-ST-19	The hover-bike shall be equipped with instruments showing the operational state of the hover-bike.
HB-FR-ST-20	The turn around time of the hover-bike shall be less than 30 hours.
HB-FR-ST-21	The start-up procedure of the hover-bike shall take less than 3 minutes.

Table 3.2: Constraints

ID	Constraints
	Engineering Constraints
HB-CS-ST-01	The maximum take-off weight of the hover-bike shall be 500 kg.
HB-CS-ST-02	The maximum payload weight of the hover-bike shall be 100 kg.
HB-CS-ST-03a	The hover-bike shall fit in a trailer of width 2.6 m.
HB-CS-ST-03b	The hover-bike shall fit in a trailer of height 4 m.
HB-CS-ST-03c	The hover-bike shall fit in a trailer of length 4.2 M.
HB-CS-ST-04	The hover-bike shall have a front vertical viewing angle of at least 15 degrees.
HB-CS-ST-05	The hover-bike shall have a side vertical viewing angle of at least 45 degrees.
HB-CS-ST-06	The hover-bike shall be able to take off from a site with diameter or length and width of 12 m[16].
	Cost Constraints
HB-CS-ST-07	The production costs of a prototype shall be at most €100,000.
	Law and Regulation Constraints
HB-CS-ST-08	The pilot has should have a *Recreational Pilot License*.
	Safety Constraints
HB-CS-S-09a	The hover-bike shall be able to withstand bird strikes.
HB-CS-S-09b	The driver shall be shielded against hazardous components.
HB-CS-S-10	The hover-bike shall have a safety rate of at most 1 fatality for every 200.000 flight hours.
HB-CS-S-11	Vital components of the hover-bike shall be "safe-life" for the operational life of the vehicle.
HB-CS-S-12	The hover-bike shall be equipped with a black-box.
HB-CS-ST-13	The pilot shall have a clear 360 degrees view.
HB-CS-ST-14	The hover-bike shall be equipped with navigation lights.
HB-CS-ST-15	The pilot shall be warned when approaching restricted airspace.
HB-CS-ST-16	The pilot shall be able to safely exit the hover-bike in case of emergency.
	Schedule Constrains
HB-CS-ST-17	The first prototype of the hover-bike shall be build before 2022.
HB-CS-ST-18	The design phase of the hover-bike shall be finished before 2020.
	Sustainability Constraints
HB-CS-ST-19	At least 50% of the materials used for the production of the hover-bike shall be recyclable.
HB-CS-ST-20	At the end of life 50% of the operative empty mass of the hover-bike shall be able to be disassembled, disposed of and recycled.
HB-CS-ST-21	The hover-bike shall have a minimum operational life of 3000 flight cycles.

4

Hover-bike concept development

This chapter shows the progress of how the final concept of the hover-bike, the Scorpeon , came to its final design. The hover-bike concept development started with generating a variety of concepts. After that a trade-off was made where a winner came out of the generated concepts. Next the trade-off criteria where the "losing" concepts scored higher than the winning concept were looked at, too analyse if these strong point could be implemented in the winning concept in order to improve it. Finally, the process of how the improved winning concept of the trade-off became the Scorpeon is explained followed by a render of the final design.

4.1. Design concept generation

The generation of the concepts was such that the concepts covered a wide variety of design options. The design of the concepts started by looking at the aspects in which the concepts would differ from each other. These criteria were the thrust, power, control, handling, structure, landing gear and safety system. Looking at these criteria, four concepts were generated which looked as shown in Figure 4.1 and a summary of the concepts can be seen in Table 4.1.

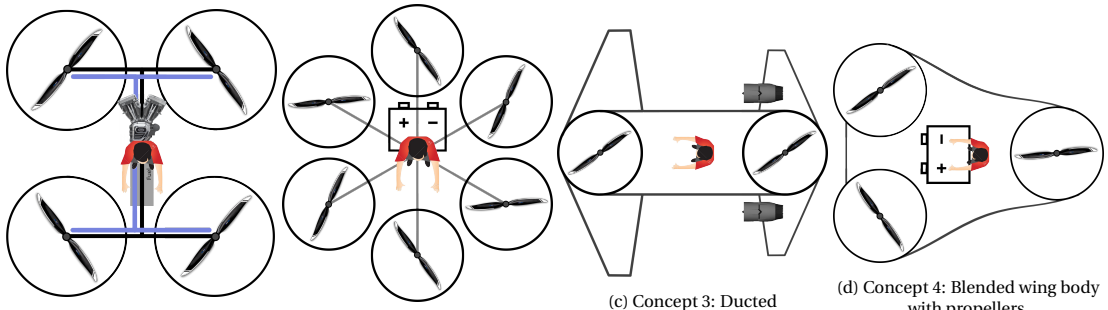

(a) Concept 1: Four propellers driven by a single engine.

(b) Concept 2: Jets, propellers and wings.

(c) Concept 3: Ducted counter-rotating fans.

(d) Concept 4: Blended wing body with propellers.

Figure 4.1: The four subfigures each show a sketch of a concept for a hover-bike design.

Table 4.1: Design concepts overview

	Concept 1	**Concept 2**	**Concept 3**	**Concept 4**
Thrust	Propellers	Propellers, Wings, Jet engine	Propellers	Propellers, Wings
Power	Chemical	Hybrid	Electric	Electric
Control	Pitch control	MDOF control surface, Vanes	Differential thrust	Control surface, Differential thrust, thrust vectoring
Handling	Wheel and buttons	Handlebar	Joysticks	Handlebar, Pedals
Structure	Truss, Metal	Monocoque	Truss, Composite	Monocoque
Landing gear	Floaters	Retractable pylons	Skids	Retractable wheels
Failure	Autorotation, Airbags	Gliding, Parachute	Redundancy	Gliding Parachute

4.2. Trade-off

To make an unbiased decision which concept has the best hover-bike characteristics and will be further worked out in the the detailed design, a trade-off has been performed. The trade-off was done by first determining the trade-off criteria. After the trade-off criteria were determined each were assigned a certain weight which showed the importance of each trade-off criteria. The trade-off criteria and their assigned weights can be seen in Table 4.2.

Table 4.2: Trade-off table

	Performance			Fun factor		Safety	Costs	Transport	Sustainability	
Criteria	Air speed	Acceleration	Control	User friendliness	Appearance				Carbon footprint	Noise
Weight	8%	16%	16%	16%	5%	10%	10%	5%	7%	7%

The trade-off was performed by each department analysing their assigned trade-off criteria for each concept. For example, the control department did the control analysis on all four concepts, and the performance department analysed all the performance characteristics (air speed, acceleration). Based on these analyses every concept is ranked in each trade-off criteria as shown in Table 4.3.

Table 4.3: Colour scores

Score	0	1	2	3	4
Colour	Does not meet requirements	Poor	Satisfactory	Good	Excellent

And eventually the trade-off was performed as objectively as possible. The only exception to this was the "appearance" criteria, which is subjective on its own. So the way this was ranked was by letting every team member rate each concept again from 1 to 4 and then averaging out the scores. The results of the entire trade-off are summed up in Table 4.4.

Table 4.4: Trade-off summary table

	Performance			Fun Factor		Safety	Cost	Transport	Sustainability		Total
	Air Speed	Longitudinal Acceleration	Control	User Friendliness	Appearance				Carbon Footprint	Noise	
Weight	8%	16%	16%	16%	5%	10%	10%	5%	7%	7%	100%
Concept 1	2	3	3	3	2	3	3	4	1	2	2.71
Concept 2	3	1	2	4	2	2	1	1	1	1	1.95
Concept 3	2	2	3	2	2	4	2	3	3	1	2.41
Concept 4	4	3	4	4	4	2	2	2	3	2	3.13

As can be seen the Table 4.4, the concept with the highest total score is concept 4 (Figure 4.1d). Concept 4 outperformed the other concepts in airspeed, control and appearance criteria. Furthermore, concept 4 scored below average in safety, cost, transport and noise criteria.

4.3. Improved winning concept

The next step was to dive deeper in concept 4 and see if the design could be improved by re-evaluating all of the trade-off criteria. This meant that even tough concept 4 scored excellent on a criteria, this did not imply that there wouldn't be changes made that will affect, or even lower that criteria. For example, if the safety could increased from a 2 to a 4 (on a scale from 1 to 4), but if that specific change would lower the airspeed to a 3, this design change would be possible and favourable to apply. Changes to concept 4 are mainly done by looking at the design choices which stood out in the trade-off from the other concepts, and implementing these into concept 4, in order to design the preliminary final design. The following changes were implemented in the design in order to improve concept 4.

- **The rotors are fixed instead of tilt-able**
  Having a tilt-able rotor means that the structure has to be strong enough to move the rotors during flight. This stronger structure automatically makes the structure heavier. Analysing the concepts, it was calculated that the forward thrust provided by the concepts with fixed rotors was sufficient without pitching the hover-bike into too large and uncomfortable angles. Due to this, eventually it is decided that the fixed rotors are preferred over a tilt-able rotors.

- **Separate wings are used instead of a blended wing body**

  In concept 4, other than for providing thrust when flying, the tilt-able rotors were also used for stability using thrust-vectoring. Fixing the propellers creates a new problem in the stability analysis which was previously solved by thrust-vectoring. This problem arises from the fact that during forward flight, the wings start generating lift, and because the wings are not located in the centre of gravity, a moment is created by this lift. Also, observing the wings in concept 4 it is expected that the effective wing area between the 2 front propellers is less than expected due to the pilot's position behind the wing disturbing the flow. Furthermore, the 2 smaller wings on the side of the pilot are not contributing as preferred due to its geometry as the airflow bends due to the pressure difference above and below the wing, which can be seen in Figure 4.2.

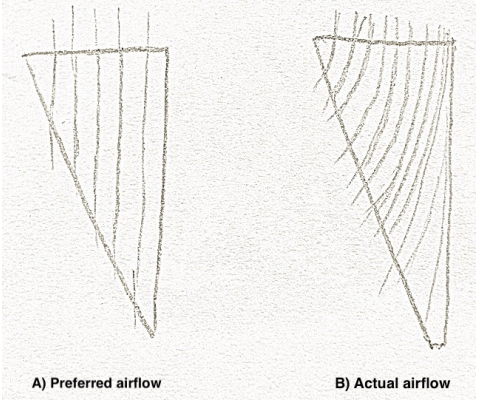

Figure 4.2: Wingflow underneath the side wing in concept 4

Taking into account these disadvantages of the wing shape and position of concept 4, and the new stability problem when fixing the propellers, eventually it is chosen to replace the main front wing by 2 larger wings between the propellers, as can be seen in Figure 4.3. This design change mitigates the moment that the front wing of concept 4 created and makes more use of the available wing area between the front and the back propellers. To ensure that the wing will be at an optimal angle of attack during all flight phases, it is assumed that the updated wings contain a movable mechanism (further wing properties and dimensions shall be determined in the next phase in more detail).

- **Motor redundancy and a parachute are used as safety system**
  In the safety analysis, it was analysed that gliding for concept 4 was not feasible. Since the design uses 6 independent electric motors, redundancy is an important safety system. In case of a single motor failure, the hover bike will still be able to provide enough thrust to land safely with the remaining motors. Furthermore a parachute safety system is incorporated. This will be the primary safety feature when flying at altitudes of 400 feet and above.

After implementing these changes the final design looked as shown in Figure 4.3, where the wing is located in between the front and back rotors.

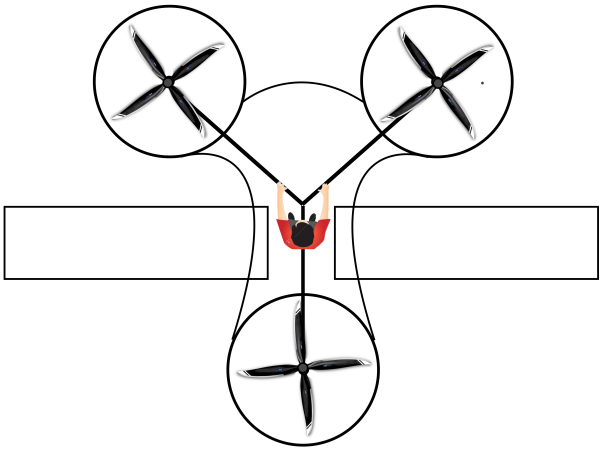

Figure 4.3: Preliminary Final Design

4.4. Final design iteration

After the midterm the final concept was looked into further detail and the subsystems were sized and designed. During this process all members communicated using the N2 chart and continued to iterate the hover-bike. During the iteration it was soon found out that the current design became too heavy if the range and endurance requirements wanted to be met. The maximum take-off weight was 500 kg and the mass budget was as follows:

Table 4.5: Mass budget after first iteration.

Part	Propeller	Structure	Duct	Motor & Controller	Miscellaneous	Wing	Safety System	Battery	**Total**
Mass (kg)	25	80	25	35	30	65	25	140	**500**

The battery weight was determined by subtracting the weight of every part except the battery from the maximum take-off weight (500kg) and the remaining mass was assigned for the battery. By doing this, it was observed that the battery was too small to reach the range and endurance requirements. After facing this problem and discussing the possible solution, first it was decided to see how much the hover-bike mass (except battery) could be lowered in order to carry a larger battery. Every group member was assigned to a part of the hover-bike and tried to iterate more, to analyse if the weight of that particular part could be lowered. After this intensive analysis and iteration a new mass budget was created:

Table 4.6: Mass budget after second iteration.

Part	Propeller	Structure	Duct	Motor & Controller	Miscellaneous	Wing	Safety System	Battery	**Total**
Mass (kg)	20	70	20	42.6	26	30	14.4	178	**500**

Comparing Table 4.5 and Table 4.6 one can see that most parts decreased in mass. The only part that turned out to be higher than the first iteration was the "motor + controller" mass. The mass left for the battery in the second iteration was 178 kg which was sufficient to meet the range and endurance requirements. Although the range and endurance requirements were met, in the second iteration this was done at the expense of the manoeuvrability of the hover-bike. The wings had a high aspect ratio and the structure could handle lessened loads.

4.5. Versatile Scorpeon concept

Eventually it was decided that in order to meet both range and endurance requirements, yet maintaining good manoeuvrability performance, the wing were decided to be made detachable and fixed and due to the hover-bike's shape it is called "Scorpeon". Depending on the flight profile (transportation mode or thrill mode) one can choose to to use the hover-bike with or without wings. Due to the wings, the loads on the structure are higher so the hover-bike is designed for the "with wing" configuration. This way the hover-bike will be able to be used in both flight profiles and the hover-bike will be slightly over-designed in for the "no wings" manoeuvring flight profile.
Making the wings fixed also created another freedom, namely the location of the wings. The wings were in the previous iteration located between the front and back propellers. Further analysis on the wings showed that the disturbance of the propellers on the wing was quite significant, which led to reduced lift production from the wing, and more wing location options were considered and compared. Consulting with the power and propulsion department of the aerospace faculty of the TU Delft[1], it was determined that wings on the ducts are preferable over wings between the propellers, due to cleaner airflow over the wings Equation 7.1.1. Additionally, the wings are fixed to an angle where it has the highest lift over drag at cruise speed.

Figure 4.4: Artist impression of the Scorpeon concept.

[1]For privacy reasons the names of the professors are not included.

5
Preparation

Before the design process starts, subsystems and subgroups shall be identified and allocated to ensure a smooth design progress. The relations between subsystems and subgroups have to be specified to simplify and improve the communication with in each group. In order to ensure this smooth progress, certain tools were used for design preparation discussed in the sections below.

5.1. Subsystem interactions

In the design phase of the Hover-bike , an interference chart was made to identify the links between subsystems, and facilitate the crucial communication between the different designing parties. Now that a specific concept was chosen, a more concept specific N chart is made. Since this subsystem interactions chart's purpose is to help the group enforce a proper communication, the division of its functional blocks matches the different engineering divisions in the hover-bike design group, which are shown in Figure 6.16.

Aerodynamics	• Aerodynamic characteristics	• Aerodynamic characteristics	• Aerodynamic characteristics		• Wing size • Body size	
	P&P **Power**				• Battery weight and size	
• Rotor size • Propeller rpm • Cruise flight angle		**Propulsion**	• Thrust response time		• Motor weight • Propeller size and weight	
			Vehicle control **Control**		• Acceleration rates • Load factors	
			• Handling mechanism output	**Human-machine interface**		
• Structural constraints • Total weight	• Structural constraints • Total weight	• Structural constraints • Total weight	• Structural dimensions • Moment of Inertia's		**Structures**	• Total weight
					• Safety system weight • Parachute anchor points • Parashute loads	**Safety System**

Figure 5.1: Subsystem interaction chart of the hover-bike.

Aerodynamics encompasses the wing and body design. The team in charge of this group (the aerodynamics team) will investigate the propeller-wing interaction. The aerodynamic characteristics which are forwarded to the power and propulsion and control group are lift, drag and thrust coefficients.
Power & propulsion treats the power supply (batteries), power distribution and propulsion. For propulsion, the team will choose an adequate electric motor and propeller to deliver the required thrust magnitude and response.
Vehicle control has two crucial subgroups which were joined together and can now be seen as one big group with all their respective outputs and inputs. These two functional blocks were put together because they interact very closely with eachother, which makes it more efficient if only one team works on them. The two subgroups are flight control and human-machine interface. The flight control section is about all the electronics (sensors included) and software used for the stabilisation and control of the vehicle. The human-machine interface is about all the pilot displays and controls.
Structures Structure is the backbone of hover-bike. It supports the other subsystems and makes sure all possible load cases are supported. The landing gear is also included in this functional block. The structure subsystem is designed by the structures group.
Safety system The safety system encircles the safety monitoring software/hardware, safety harness/seat belt, parachute and anything else of which the purpose is solely assuring safety.

5.2. System communication

In this chapter the hover-bike systems will be explained by means of hardware and software diagrams, data handling block diagram and the communication flow diagram. All these diagrams are meant to help understand the vehicle better and to show how different subsystems are related.

5.2.1. Hardware block diagram

Hardware block diagram shows the general subsystems included in the hover-bike. It is a good overview of the total system. In Figure 5.2 subsystems are shown in blocks which are connected with arrows which show the relations between them. The hardware is divided into several groups: human-machine interface, communication, power, control, safety, lift devices and operational sensors. In Figure 3.3 power system and control system are two central systems. Power system transmits electrical power to all other systems, while control system either gives out control signals to carry out instructions or sends data to user interface or for communication. As input, the control system takes data from sensors and communication system and pilot control. The reason that control system takes sensor data is to help to transform the pilot inputs to subsystem-level commands.

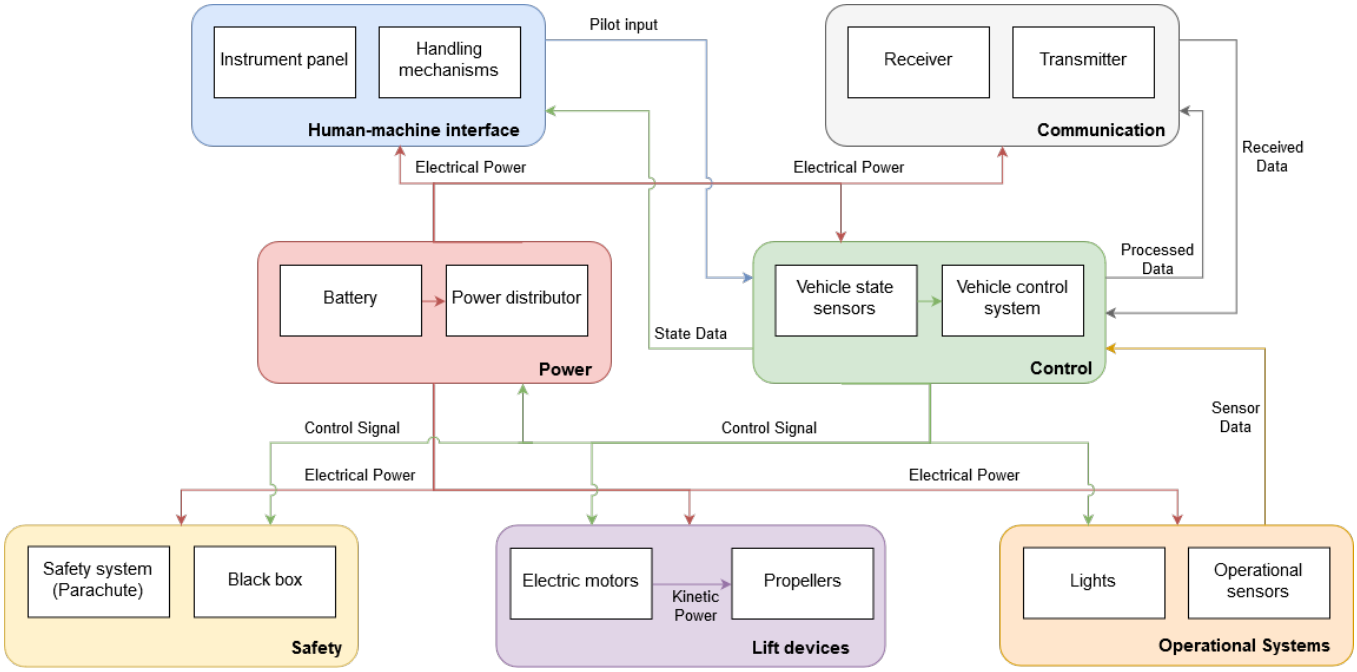

Figure 5.2: Hardware block diagram

5.2.2. Software block diagram

Just as the hardware block diagram, the software block diagram gives a general overview of the software included in the system. This software is needed to let the the hardware properly function. It is a top level diagram still, since the software details is not yet developed and identified. The diagram is split into inputs, processes and outputs to show the interaction between the different subsystems.

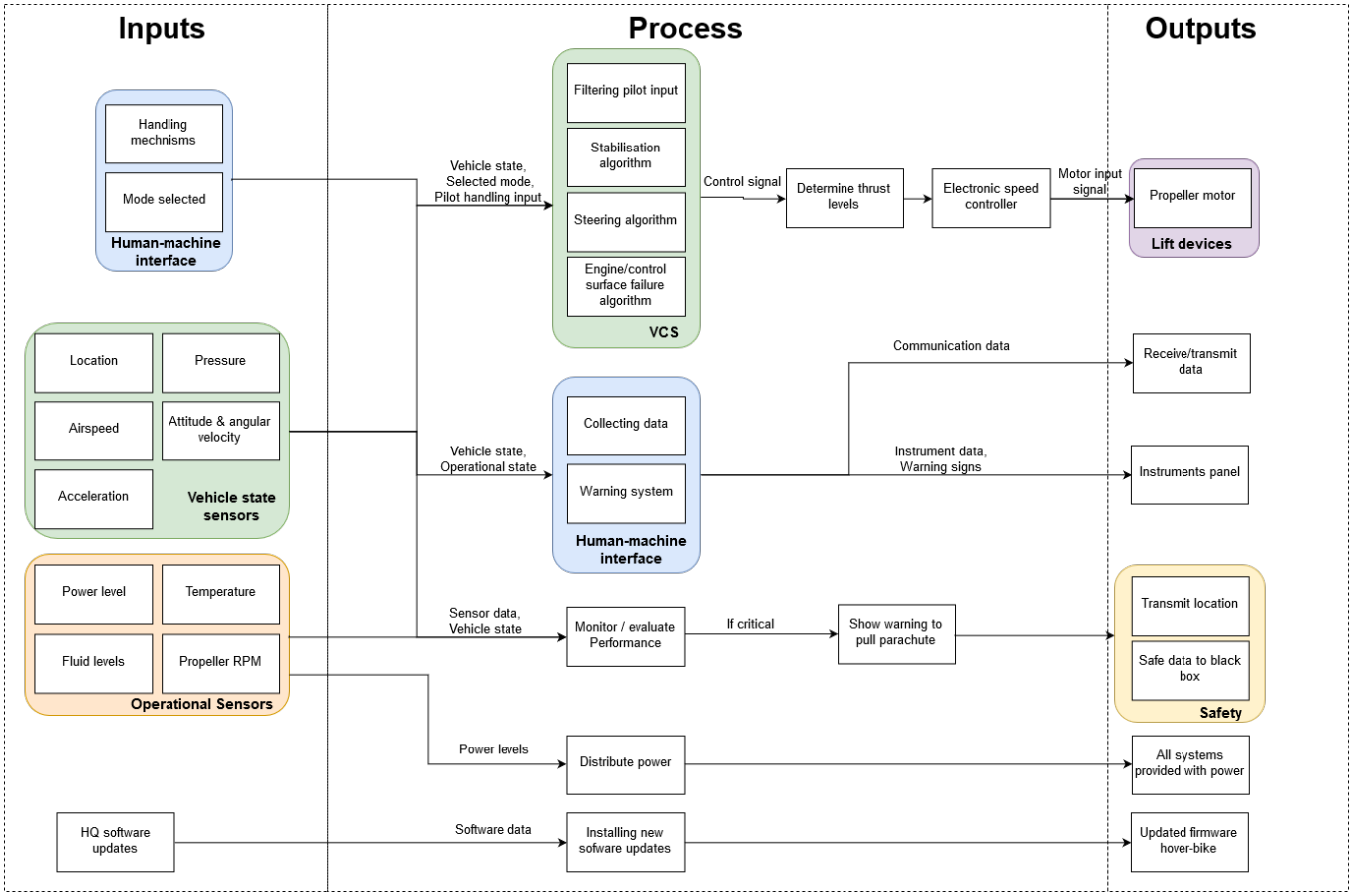

Figure 5.3: Software block diagram

5.2.3. Data handling block diagram

The data handling block diagram is similar to hardware block diagram, shown in Figure 5.4. The central module is still the control system, but power system and communication system have been removed. Due to no power system in data handling block diagram, there are no arrows of electrical power transmission and only data flow, which is consistent with the content of data handling. On the aspect of detail, the human-machine interface block does not change, but safety and lift device blocks are simplified and control and operational systems are detailed. To be more specific about operational block, there are only sensors in the operational system block so no input goes into the operational system. As to the control block, the main structure remains the same, with both data from various sensors and control from pilot the input and control instructions or vehicle state the output, but it is introduced in more detail.

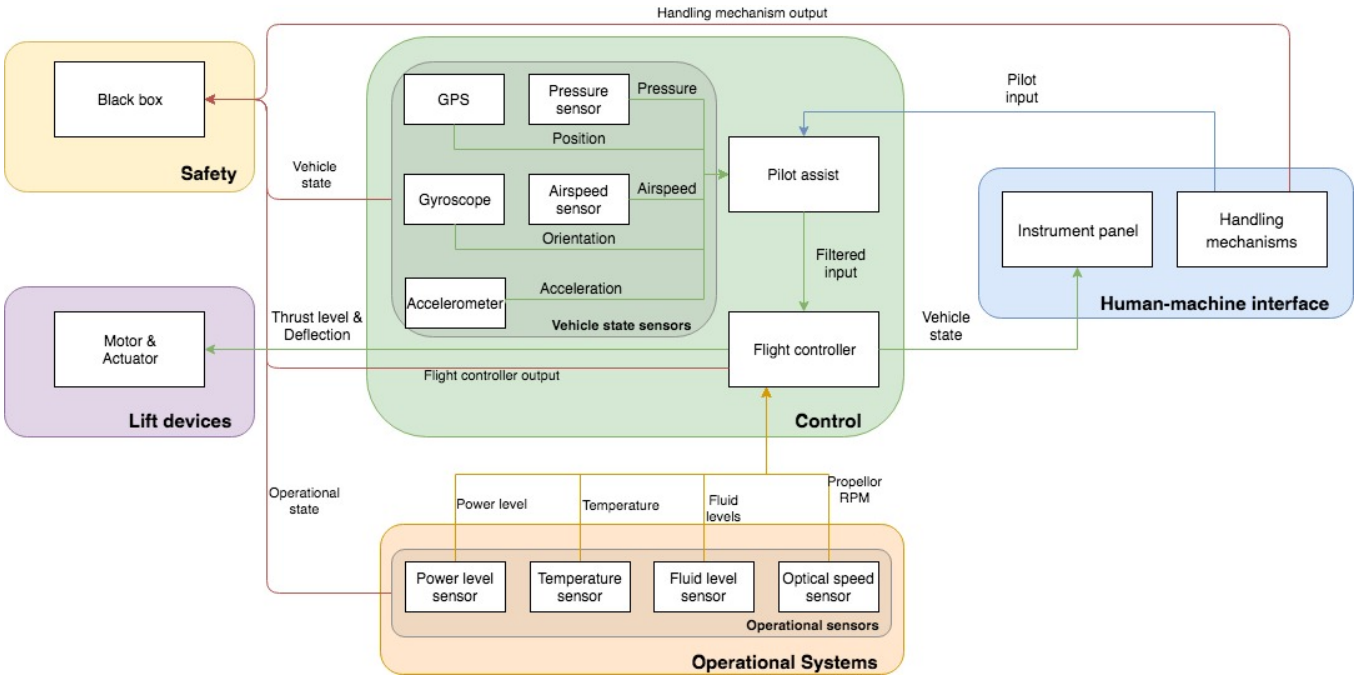

Figure 5.4: Data handling block diagram

5.2.4. Communication flow diagram

The communication flow diagram shows the interaction between the pilot, the hover-bike and the outside world. Via human-machine interface the pilot can control the hover-bike and give specific inputs. Feedback to the pilot is given by the machine human interface. Furthermore, sensory input will determine the pilot's actions since he will experience roll rates, accelerations and changing scenery while operating the vehicle. The hover-bike will regularly receive software updates and updated maps from the Scorpeon headquarters. The pilot can also contact the headquarters to send status reports and resolve any problem quickly and effectively, should they arise. Furthermore the pilot has the ability to contact air traffic control or other aircraft via the on-board very-high-frequency antenna and radio.

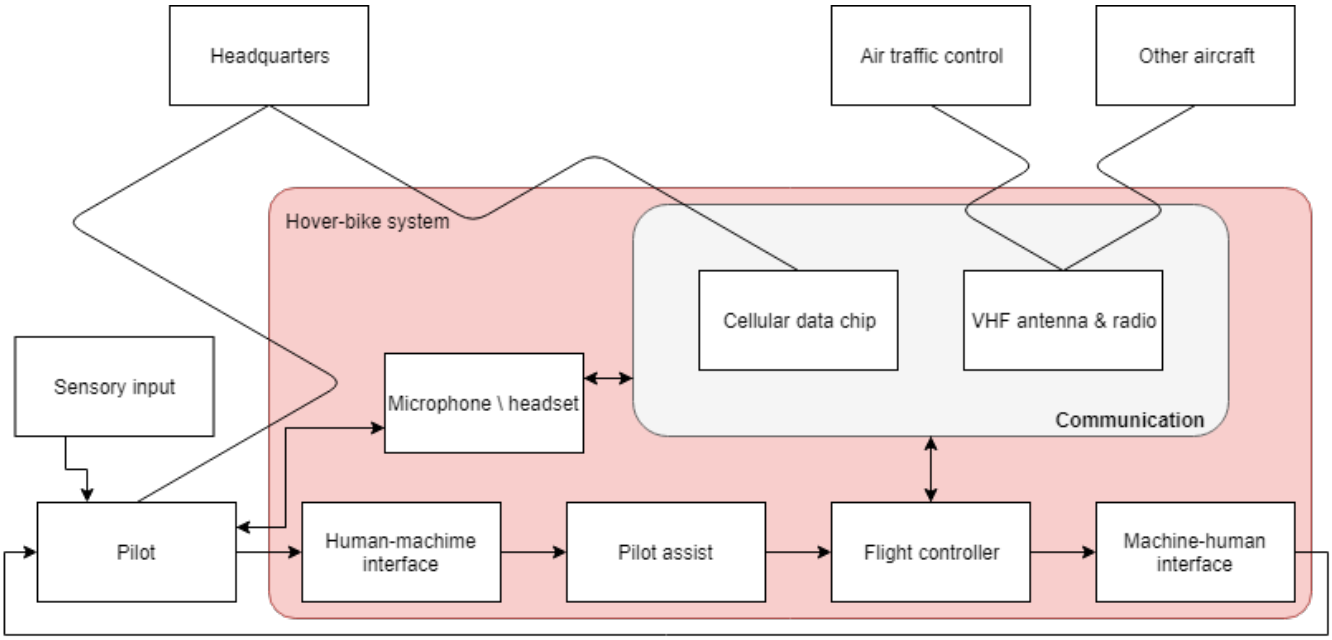

Figure 5.5: Communication flow diagram

6
Aerodynamics analysis

Considering that the Scorpeon will be flying, the aerodynamics of the design are of vital importance. The design will have two different layouts, one for the economic mode with wings attached and one for the thrill mode without wings. As this is the only difference between the two vehicle arrangements, the body and propellers must be designed to be most efficient in both scenarios. The first step in the aerodynamic design is to analyse the wings and rotors separately. The next step is to determine the interference between the wing and the rotor,. Then, the analysis on the aerodynamics of the body is modelled and lastly, the aerodynamic characteristics of the complete hover-bike are determined.
Like the other technical analysis chapters, this chapter starts of by outlining the methods in section 6.1, after which the iterations of the design and how these affect aerodynamics are delineated in section 6.2. The results are then summarised in section 6.3. In section 6.4 the verification & validation of the software and calculations are provided. Lastly, an analysis on the sensitivity of the outcome is performed and the results are shown in section 6.5.

6.1. Method

6.1.1. Wing Design

The first step in the design of the wings was to determine the driving parameters of the wing. A wing for a commercial transport aircraft which flies around mach of 0.8, such as the Boeing 747[1], has a wing with sweep, high aspect ratio and an airfoil that minimises drag. On the other hand, an aerobatic aircraft, such as the Extra 300L.[2], uses a wing with no sweep, a moderate aspect ratio and an airfoil with a high stall angle to delay separation The main purpose of the wing on the hover-bike is to extend its range and endurance. Therefore, the key parameter of the wing is that the drag should be minimised, while the lift should be maximised.
When designing the wing, the airfoil was selected first. From there on, the 3-dimensional planform of the wing was determined which includes other devices, such as wingtips or turbulators. Lastly, the results of the aerodynamic characteristics are delineated in section 6.3. The wing analysis is mainly performed with the software XFLR5 version 6.42, of which the applied theory and assumptions are summarised at the end of this section subsection 6.1.5.

Wing airfoil design method

As said above, the driving wing parameter is to minimise drag and maximise lift. In other words, this means that the chosen airfoil should have a high lift-to-drag ratio. However, this is not the only parameter that drives the airfoil choice. Preferably, the airfoil also has a low minimum drag coefficient, a small moment and a higher thickness-to-chord ratio to decrease wing weight. As the wing is fixed during flight and is only designed to aid in the lift production, the stall characteristics were deemed irrelevant for this wing.
Extensive studies exist that present accurate methods and techniques to manually design airfoils for the most optimal conditions.[66] However, these methods are rather extensive and due to time constraints, such design approach is not suitable. A better approach was to use an already existing, well-known airfoil. For this approach, a selection of airfoils has been made, namely:

- Selig S3024
- Selig S4061
- NACA 63-012A
- NACA 63-412
- Eppler E392
- Wortmann FX63-137

These airfoils have mostly been chosen based on their high lift-to-drag ratio. The Selig series have been applied to small model sailplane and are, therefore, designed to operate at low Reynolds numbers, namely below 500 000. [57] The NACA 6-series has been designed with the purpose of maximising laminar flow over the airfoil. [60] Of these, the NACA 63-412 was chosen for its high lift-to-drag ratio, while the second one was picked for its symmetry. Lastly, the Eppler E392 was chosen, as it is a well-known sailpane airfoil [57] and the Wortmann FX63-137 was included for its high maximum lift coefficient, combined with its high lift-to-drag ratio. The coordinates of these airfoils were obtained from airfoiltools.com.
In the next paragraphs, the analysis of the driving parameters for the airfoils are outlined in more detail. This is mainly done using the XFLR5 software.
Lift-to-drag ratio As the wings for the hover-bike should be as efficient as possible, the lift-to-drag ratio is considered as the key parameter for the design of the wing and, therefore, of the airfoil too. The graph depicting the lift-to-drag ratios of the six airfoils is shown in Figure 6.1a.

[1] URL:https://www.boeing.com/resources/boeingdotcom/commercial/airports/acaps/747_123sp.pdf [cited 27 June 2018]
[2] URL:https://www.extraaircraft.com/docs/tech-manuals/MM300L/300L_MM_20090631.pdf [cited 27 June 2018]

Aerodynamic moment Secondly, a zero aerodynamic moment to is most preferable in this case. The front and rear wing will be roughly equal in size and, as such, the centre of lift, which is then in the middle of the two wings, is located near the centre of gravity. An aerodynamic moment will then require more power from the rotors to keep the hover-bike level. The aerodynamic moments of the six airfoils can be seen in Figure 6.1b.
Drag bucket size Then, the size of the drag bucket is also taken into consideration. The wing will not be at the exact same angle of attack during cruise flight, as the hover-bike will shake slightly due to small disturbances. If the airfoil has a bigger drag bucket, the oscillations will not significantly affect the drag on the airfoil, which is desirable. The drag bucket can be best observed in the lift coefficient versus drag coefficient graph, Figure 6.1c.
Thickness-to-chord ratio Another factor that can be of big importance is the thickness-to-chord ratio. Since there is only 30 kg assigned to the wings, minimising the wing weight is of high importance. A thicker airfoil can aid in this, so thicker airfoils were favoured. The thicknesses of each airfoil is summarised in Table 6.1, along with other airfoil characteristics.
Lastly, for the sake of completeness, the lift slope of the airfoils is also provided in Figure 6.1d. This curve depicts the general trend and it could be used to determine the lift slope, the maximum lift coefficient and the stall angle of attack.

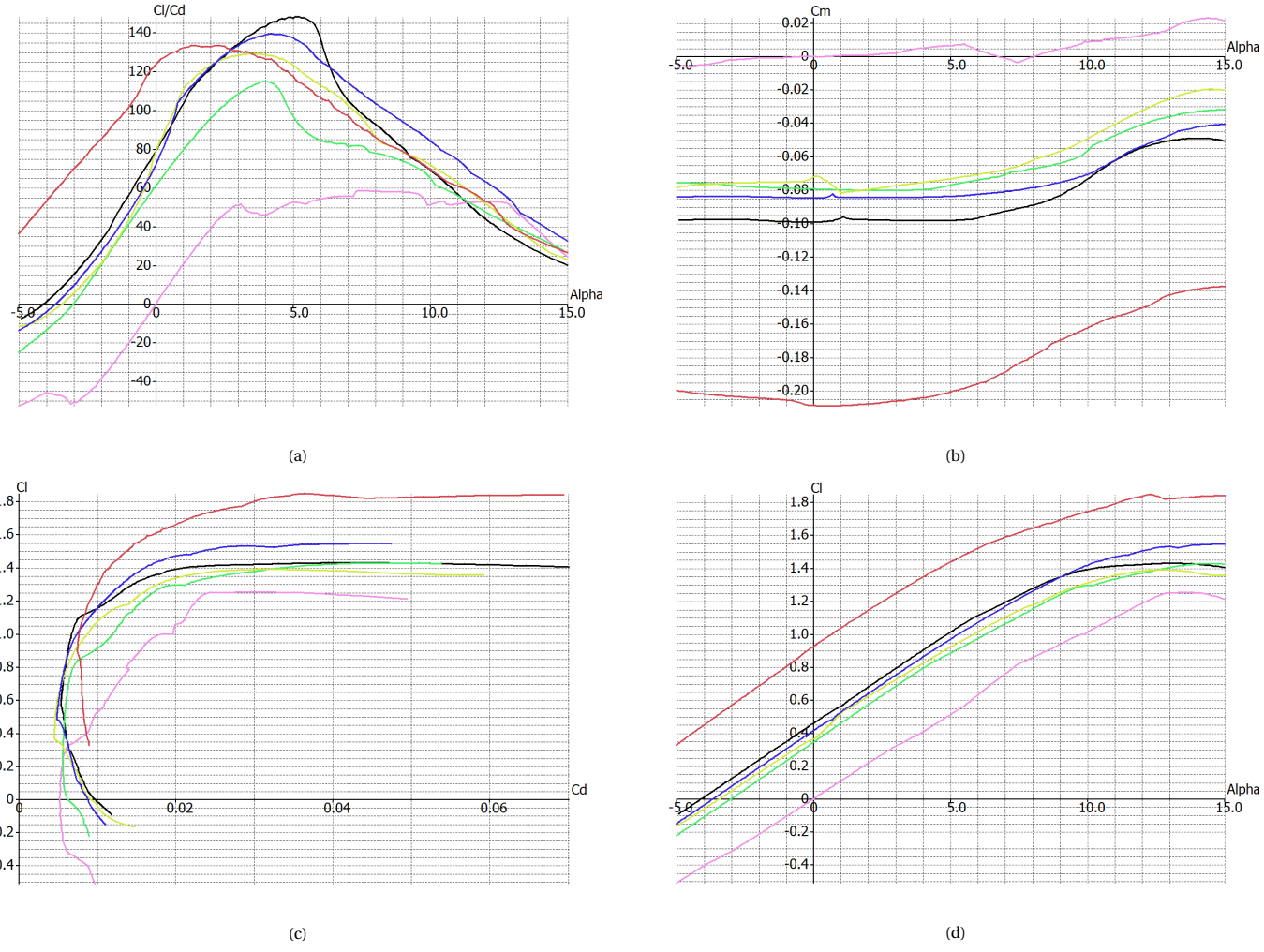

Figure 6.1: These four subfigures contain the polars (a) C_l/C_d versus α, (b) C_m versus α, (c) C_l versus C_d and (d) C_l versus α. The S3024 is depicted in yellow, the S4061 in blue, the NACA 63-012A in pink, the NACA 63412 in green, the E392 in black and, lastly, the FX63-137 is shown in red.

Table 6.1: Geometric characteristics of the six investigated airfoils.

	S3024	S4061	NACA 63-012A	NACA 63-412	E392	FX63-137
Max thickness-to-chord % (at chord %)	9.85 (31.32)	9.63 (29.29)	11.99 (35.36)	12.00 (34.33)	10.15 (32.33)	13.72 (30.28)
Max camber % (at chord %)	3.52 (42.43)	3.91 (43.43)	0 (NAP)	2.2 (50.50)	3.84 (42.43)	5.97 (54.53)

3D Wing design
After the airfoil was chosen, the wing planform could be established. The wing planform was as described above, designed to minimise drag in cruise flight. 3D wing characteristics that can be altered for this purpose are for instance the aspect and taper ratio. Furthermore, wing twist is generally added to control the stalling behaviour of the wings, something taper

can also be used for. Finally, other devices, such as winglets and turbulators are also considered. This analysis is performed mainly with the use of the 3D wing design and analysis tool of XFLR5.
The characteristics that were first identified are the wing span and the aspect ratio. From there, the wing surface area was determined. Further analysis was done on the sweep and taper of the wings. After that, a twist was added and wing dihedral was also considered.

Wing Span The span of the wing can be directly determined from the constraints. The hover-bike should be able to be transported in a regular sized trailer. For this purpose, it was decided to make the ducts with the wings detachable. The maximum combined length of the wing with the duct is then constrained to the maximum length of a trailer. This length is 4.2 m, and including 10 cm of margin on both size and the length of half a duct (where the wing is attached to), which is 0.8 m, 3.2 m is left for the wings. To include some margins for the wingtips too, a half span of 3.0 m was chosen. A schematic of this wing-duct configuration is depicted in Figure 6.2.

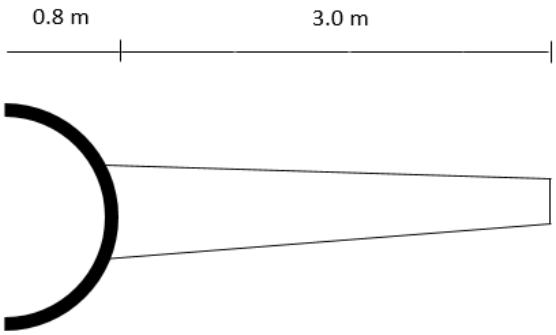

Figure 6.2: Schematic of the half-duct wing combination with length dimensions.

Aspect ratio Next, the aspect ratio of the wing is determined. Increasing the aspect ratio lowers the induced drag, but it has a significant impact on the wing weight. To find the aspect ratio, an iterative process was used. As the drag decreases with increasing aspect ratio, the cruise speed will increase. From the requirements it can be seen that the cruise speed (speed at maximum endurance and maximum range) should be at least 100 $\frac{\text{km}}{\text{h}}$. Using XFLR5, a 3D wing model was created with a certain starting aspect ratio and, therefore, root chord too. After that, the sweep, taper, twist and dihedral, as will be explained later, were applied. Then, the drag-velocity curve was created with XFLR5, from which the minimum drag and the corresponding airspeed were determined. If the corresponding airspeed was below 100 $\frac{\text{km}}{\text{h}}$, the root chord was increased. If it was deemed too high, the root chord was decreased, thereby changing the aspect ratio. After the root chord/aspect ratio was changed, the sweep, taper, twist and dihedral were readjusted and the new drag-velocity curve was created. This iterative process is visualised in a flowchart in Figure 6.3.

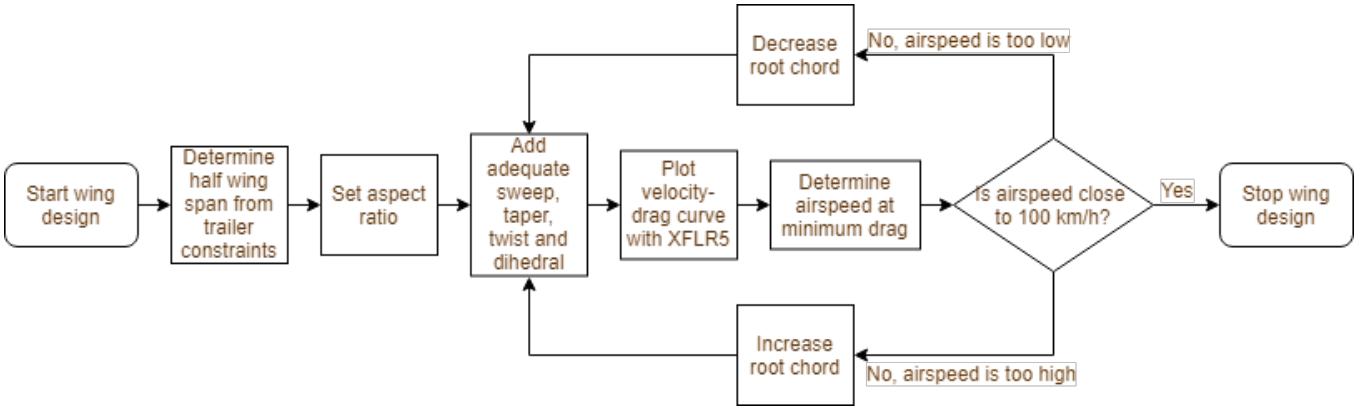

Figure 6.3: Flowchart depicting the iterative design process for the wing design.

Sweep Wing sweep affects many performance characteristics. Firstly, wing sweep is applied to decrease the local velocity over an airfoil to avoid formation of shock waves, yet this is only necessary when the vehicle would fly at airspeeds close to Mach 1. As the hover-bike will fly at maximum airspeeds between Mach 0.1 and 0.2, adding wing sweep is needless. A second effect of wing sweep is on the stability, as a swept wing has a natural dihedral effect. This stability can also be obtained with adding dihedral, which is about 10 times more effective, according to Raymer[30]. Finally, sweep can also be added to move the aerodynamic centre either backwards or forwards. Considering that the hover-bike uses a double wing configuration, and the centre of gravity of the vehicle is closer to the front, the centre of lift will be behind this, therefore ensuring longitudinal stability. Adding wing sweep to move the aerodynamic centre more back is thus needless.

Taper Wing taper affects the distribution of lift along the span of the wing. As proven by the Prandtl wing theory, an elliptical lift distribution minimises the induced drag. However, building an elliptical wing is difficult and costly. Another option to obtain an elliptical lift distribution is by adding taper to the wings. Another benefit of adding taper is, the local lift coefficient on the outboard wing is decreased. By having a higher lift coefficient on the inboard wing, stall will occur there first. This is preferred over outboard stall, as outboard stall on one wing creates a large rolling moment. According to Raymer (2012) [30], "a taper ratio of 0.45 completely eliminates those effects for an unswept wing, and produces a lift distribution very close to the elliptical ideal. This results in an drag due to lift that is only 1% higher than the ideal, elliptical wing." The spanwise lift distributions for different taper ratios and for an elliptical wing is shown in Figure 6.4. Because of these reasons, a taper ratio of 0.45 was chosen for this wing.

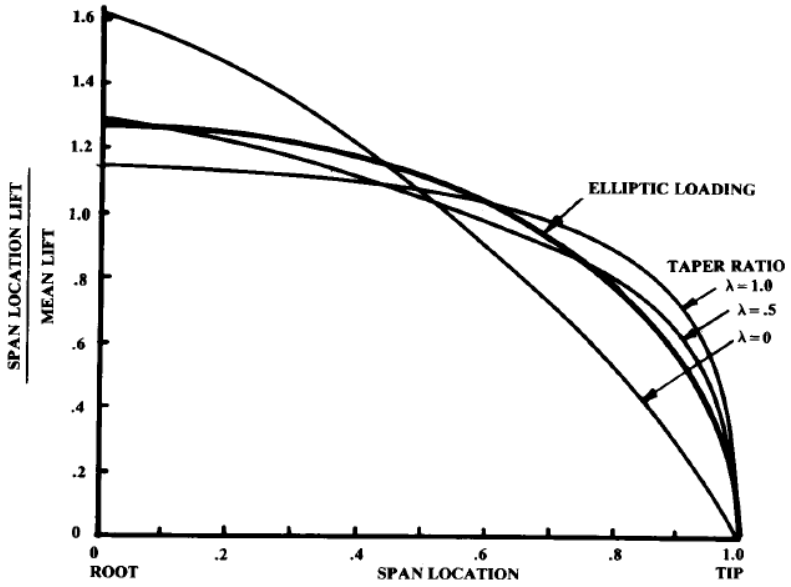

Figure 6.4: Effect of taper on lift distribution over the span of the wing.[30]

Twist Wing twist is normally added to control the stalling behaviour of the wings. By adding a small degree of washout, the tips of the wings are put at a lower angle preventing tip stall. This is a similar design solution to why taper is added to prevent tip stall [30]. As is described in subsection 6.1.3, there will be more twisted added to account for the induced velocity generated by the rotor. As this twist is relatively large, it was decided not to add more twist to prevent tip stall.
Additionally, aeroelasticity can pose difficulties in the design of the wing twist. Due to aerodynamic loads the wing can twist more during flight, lowering the drag performances as the wing does not fly at the optimal angle. In the worst case, it is even possible for the wing twist to keep growing during flight, which eventually leads to failing of the wing. This is an example phenomenon of static aeroelastic instability also known as "divergence" [21]. Explicit models exist that determine the dynamic pressure for uniform unswept wings at which divergence occurs. The divergence pressure and torsional distribution are given by Equation 6.1 & 6.2, respectively. In these equations, $\overline{\alpha}_r$ is determined from Equation 6.3, while λ is calculated with Equation 6.4. The dimensions of the wing are defined as shown in Figure 6.5.

$$q_D = \left(\frac{\pi}{2b}\right)^2 \frac{\overline{GJ}}{ec_{\text{wing}}a} \tag{6.1}$$

$$\theta_{\text{el}} = \left(\alpha_r + \overline{\alpha}_r\right)\left[\tan(\lambda b)\sin(\lambda y) + \cos(\lambda y) - 1\right] \tag{6.2}$$

$$\overline{\alpha}_r = \frac{c_{\text{wing}}c_{\text{mac}}}{ae} - \frac{Nmgd}{qcae} \tag{6.3}$$

$$\lambda = \sqrt{\frac{qcae}{\overline{GJ}}} \tag{6.4}$$

Dihedral By adding dihedral to a wing, it will tend to roll the vehicle level when banked. This disturbance to roll is artificially restored by changing the thrust output from the rotors. Adding too much dihedral can then even be unwanted, as the vehicle becomes too stable and the hover-bike becomes difficult to roll. Excessive dihedral effect even produces Dutch roll [30]. For these reasons, it was decided to not add dihedral to the wings.

Incidence angle Lastly, wings can also be put at a certain incidence angle. The incidence angle is chosen such that when the hover-bike flies in cruise, the wing is at the correct angle of attack. Since the hover-bike pitches as a whole, the wings will also pitch with it. The actual magnitude of pitch is determined by the ratio of the forward thrust and the upward thrust that the rotors need to deliver. The upward thrust depends on the ratio of the lift produced by the wings versus the lift provided by the rotors. The forward thrust is dependent on the drag of the hover-bike at cruise. As this drag also depends on the wing geometry and thus the incidence angle, the optimal incidence angle is determined by means of an iterative process.

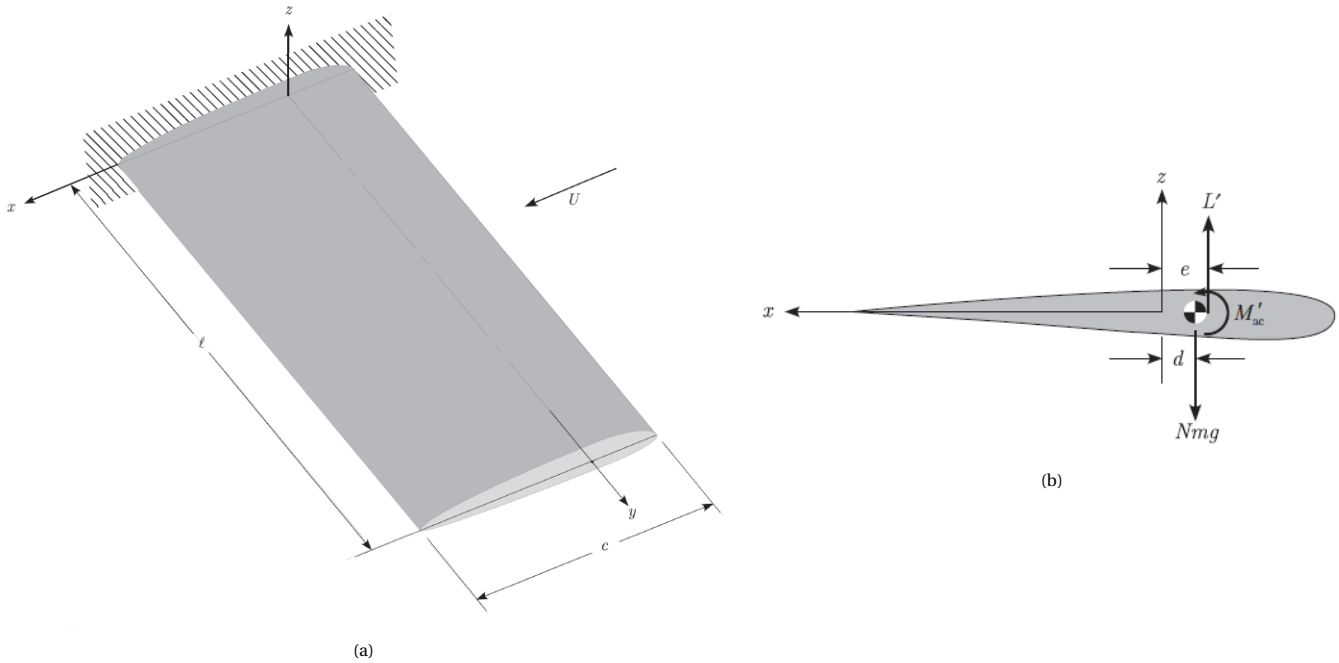

Figure 6.5: Schematics depicting (a) the uniform unswept clamped-free lifting surface model and (b) the cross section of the spanwise uniform lift surface model with dimensions.[21]

Firstly, an incidence angle is assumed from the values obtained in the conceptual design phase. Secondly, the drag at cruise speed is determined and from this, the pitch of the hover-bike at cruise is determined. The incidence angle is then updated accordingly and the drag is redetermined. This is then continued until the two values converge.

Miscellaneous wing devices Lastly, extra wing devices are also considered to improve the wing's performance characteristics. An example is high-lift devices in the forms of slats and flaps. These devices increase the maximum lift coefficient of the wing by increasing camber and wing surface area. Yet devices are only helpful when the wing needs to produce more lift at lower velocities than generally required during cruise, which is mainly during the take-off and landing phases. The hover-bike will not operate in such flight conditions, as it takes off and lands vertically with the use of its rotors. Therefore, flaps and slats are not considered to be helpful for this wing.
Secondly, wing tip devices can be very beneficial in decreasing the induced drag of the wing. Many types of wing tips are already analysed in great detail, which leaves a wide range of options to choose from. Apart from the wing tip shape, the level of forward or aft-sweep, also influences the decrease in induced drag. According to Raymer [30], an aft-swept wing tip tends to have a lower drag, at the cost of increased wing torsional loads. A trade-off between desired drag gains and wing weight is required to determine the most suitable wing tip.
Lastly, turbulators were also analysed for their usefulness. However, these were quickly discarded. Turbulators induces transition, turning laminar flow into turbulent flow. This delays separation of the flow, which reduces the separation drag of the airfoil, but, on the other hand, turbulent flow has a higher skin friction drag. Turbulators are also used to increase the stall angle of attack, since turbulent flow is less prone to separation than laminar flow, yet this is not a need for the wings on the hover-bike. The effect of turbulators on the lift performance was analysed using XFLR5, but there was no increase in performance observed and as such turbulators were not added to the wings.

6.1.2. Rotor design

The rotor size has been estimated by assuming a thrust coefficient and using the designed thrust. Afterwards, more details will be designed so that more accurate thrust and power can be obtained. If necessary, some iterations will be made. First, the airfoil for the rotor will be chosen. Afterwards, power will be estimated from the thrust input. Other geometry parameters will be determined by adjusting rotational speed.
Airfoil Requirements To start the design of rotors, the airfoils have to be chosen. To introduce the design process of blade airfoil of hover-bike, the history of blade airfoil will be introduced. Before 1960s, the old practice was just to use NACA0012 airfoil or its improved types for blades. The reason is that old helicopters were not so fast. As a result, the airfoil aerodynamics are not as important as structure or control. Not until the helicopter speed reached a high level, did aerodynamics pushes forward new requirements for blade design, resulting that the update for blade airfoil design was attached sufficient significance. On the other hand, the material used for blade was aluminium in the past, which is difficult to adapt to a complicated blade design. When the material evolved into composite at a later stage, it becomes possible that several different airfoils are adjusted to one single blade.
It can be concluded by researching that the helicopters in the 1950s had reached a cruise speed of more than 100 km/h, which is one requirement for hover-bike. This means that hover-bike can also just use the NACA0012 airfoil due to a even lower cruise speed. However, the rotational speed and tip speed of rotors of hover-bike is much higher than normal aircraft

rotors. It can be estimated that the tip speed of hover-bike rotor is about 280 m/s which is almost a Mach number of 0.82. On the other hand, typical Mach number for the tip speed of a rotor is between 0.5 and 0.6. As a result, despite of a low cruise number, the tip speed of hover-bike rotor can still reach transonic region and drag divergence requirement has to be taken into account. More modern airfoils instead of the old airfoil NACA0012 have to be considered.
Before the comparison, the criteria for airfoil of rotor have to be specified. The following criteria can be found in Wojciech [64]:

1. High value of maximum lift coefficient $C_{L_{max}}$ at Mach number $M = 0.4$. The reason is to delay stall on the blade going backward, as well as to reduce vibrations at high speed.

2. High lift-to-drag ratio C_L/C_D at Mach number $M = 0.6$ and at lift coefficient $C_L = 0.6 \sim 0.7$. The goal is to decrease power required.

3. High drag divergence number M_{DD} at zero lift coefficient and low drag coefficient in transonic range. This is aimed at decreasing power and reducing the high speed impulsive noise HSL at high tip speed.

4. Very low pitching moment coefficient C_{m0} ($C_{m0} \geqslant -0.01$) at zero lift coefficient and low Mach number, in order to decrease loads in the control system and to reduce the blade twist. The Mach number used will be 0.4 according to Wojciech [64]. The moment is also more favourable to be negative than positive, because a negative moment coefficient is stable.

It has been introduced that the airfoil can change along the span in contemporary practice. Generally the blade can be divided into three sections, namely from root to 80% of span, from 80% to 90%, and from 90% to tip. The root airfoil can also be different from the middle part. For the inner part of blade, the most important criterion is a high $C_{L_{max}}$. For the outer part, the crucial criteria are the first three. For the tip, the key requirement would be a high drag divergence number M_{DD}. The fourth criterion of pitching moment coefficient C_{m0} applies for all cases [64].
Airfoil Selection Some types of airfoil are specifically used for propeller or rotor blades, which can be found and chosen from. In the design of the rotor, one programme called JAVAprop is used. Unfortunately, there are only a few airfoils available for estimation in JAVAprop. Although it is possible to load other airfoils into JAVAprop, it is quite troublesome and takes quite some time. Furthermore, it has not been known how the airfoils that are mentioned in literature perform compared to the airfoils available in JAVAprop. Thus, the airfoils available in JAVAprop will all be compared, and the next step will be to also compare with other airfoils.
Most airfoils that are available in JAVAfoil can be found in Airfoil Tools[3], except for MH-126. Apart from the airfoils mentioned above, some other airfoils in Wojciech [64] can also be found in Airfoil Tools 3. The airfoils that cannot be found for details will be left out. For analysis, airfoil profiles can be downloaded from Airfoil Tools and then loaded into XFLR5 to analyse the performance with respect to the criteria. The only criterion that cannot be analysed in XFLR5 is the drag divergence number M_{DD}. The data of other three criteria obtained from XFLR5 are shown in Table 6.2.

Table 6.2: Trade-off table for blade airfoil. Each α column corresponds with the column just left to it, indicating the angle of attack at which the corresponding values are taken. Green boxes means the values of good performance. The three values with brackets in the α_4 column means the corresponding airfoils can not reach a value of $C_L = 0$.

	$C_{L_{max}}$ (M=0.4, Re=9.2×10^5)	α_1 [°]	C_L/C_D ($C_L = 0.7$, M=0.6, Re=1.4×10^6)	α_2 [°]	$(C_L/C_D)_{max}$ (M=0.6, Re=1.4×10^6)	α_3 [°]	$\alpha_1 - \alpha_3$ [°]	C_m [10^{-2}] ($C_L = 0$, M=0.4, Re=9.2×10^5)	α_4 [°]
Clark Y	1.437	13.5	99.466	1.7826	109.712	3	10.5	-9.93	-3.844
E 193	1.2482	10	124.013	1.462	154.282	4	6	-8.67	-3.409
ARA D	1.6679	10	96.088	-0.602	121.216	1	9	-11	-4.72
MH 126	1.583	29.5	22.26	2.916	22.1	2	27.5	-21.56	(-10)
MH 112	1.8173	14.5	65.744	-2.481	96.58	1	13.5	-20.42	(-6.5)
MH 114	1.8304	13	78.773	-2.513	128.764	1	12	-15.5	(-8.5)
MH 116	1.3685	9.5	113.894	0.271	162.3	2.5	7	-13.23	-4.6924
MH 120	1.1169	10	112.262	2.0768	126.077	3.5	6.5	-7.2	-2.8965
VR 12	1.4829	13	75.738	2.953	90.75	5	8	5.8	-1.3344
VR 13	1.4146	12	79.87	3.035	94.83	5.5	6.5	-0.62	-1.1624
VR 14	1.304	10.5	85.846	3.256	97.855	5.5	5	-0.447	-0.9495
VR 15	1.1658	10	83.478	3.606	93.063	5	5	0.82	-0.3818
OA213	1.5282	11.5	74.21	2.774	79.81	4.5	7	0.05	-1.4584
OA209	1.3482	10.5	81.544	3.715	93.051	6	4.5	-0.025	-0.7328

Each column of α corresponds to the column just left to it. For example, the column of α_1 means the angle of attack at which the $C_{L_{max}}$ is reached. The green box means favourable values. The $C_{L_{max}}$ and C_m criteria are straightforward, while the lift-to-drag criterion needs some explanation. The column of $\alpha_1 - \alpha_3$ indicates how far the maximum lift coefficient is

[3] url: http://airfoiltools.com/ Cited: 20th June, 2018

from the maximum lift-to-drag point. The larger this difference is, the closer to maximum lift-to-drag ratio point that the operational point will be. When there is sufficient margin, the optimum point which is the maximum lift-to-drag point can be taken. Thus, it is favourable to have columns of $(C_L/C_D)_{max}$ and $\alpha_1 - \alpha_3$ with large values, which is the case for Clark Y, ARA D, and MH-114. E193 and MH-116 also perform well in lift-to-drag ratio, but E193 may not generate enough thrust due to a relatively low $C_{L_{max}}$. As to the moment coefficient C_m, most of the airfoils are not so small. In particular, the MH series have a quite large C_m, which can be a drawback. However, considering the performance in generating thrust and being efficient as well as simplicity, the MH series will be used.
Afterwards, the criterion of drag divergence will be examined. The Reynolds number that will be used at airfoil analysis can be estimated as

$$Re = \frac{\rho V_{element} c}{\mu} \tag{6.5}$$

where c is chord length of one blade and will be taken as 0.1 m, which value can be referenced to subsection 6.2.2. $V_{element}$ is relative velocity on blade, either at Mach number of 0.4 or 0.6 according to the criteria. μ is dynamic viscosity of the fluid, which will be 1.81×10^{-5} (kg/(m/s)) for air. The resulting Reynolds number will be about 9.2×10^5 for $M = 0.4$, and 1.4×10^6 for $M = 0.6$.
The results indicate that the MH series are good at generating lift. The maximum lift coefficients $C_{L_{max}}$ and maximum lift-to-drag ratios $(C_L/C_D)_{max}$ of three MH-series airfoils are at the highest level. The maximum lift-to-drag ratio of MH airfoil makes sense because the maximum lift coefficient is also large for MH airfoil and there is sufficient margin if the airfoil operates at the optimum lift-to-drag ratio. The only drawback of MH airfoils is the relatively large moment coefficient C_m. At a later stage where the airfoils are used in JAVAprop, the power is estimated to be quite large, so at this stage the most efficient airfoils MH series will be chosen for lower power requirement. The fact that the power is estimated to be high can be seen from Figure 6.7. As to the drag divergence number, MH-120 is only suitable for Mach numbers no more than 0.8 according to the airfoil introduction of JAVAprop website[4], while MH-116 is only suitable when the tip does not exceed a Mach number of 0.6 as introduced by the airfoil introduction page by JAVAprop[5], which does not meet the requirement. Therefore, MH airfoils do not fulfil the M_{DD} requirement and another airfoil will be chosen for tip.
The tip airfoil can be chosen from Figure 6.6 from Wojciech [64], which shows drag divergence Mach number and $C_{L_{max}}$ of different airfoils. According to one table in the same report, the difference in Mach number between two vertical lines is 0.2, and VR-14 is at Ma=0.84. Assuming maximum speed to be $150km/h$, the maximum tip speed can reach a Mach number of $(\frac{150}{3.6} + 280)/340 = 0.95$, which means the airfoil with maximum drag divergence number that is available in the figure shall be used, which is ILH308 with $M_{DD} = 0.865$.

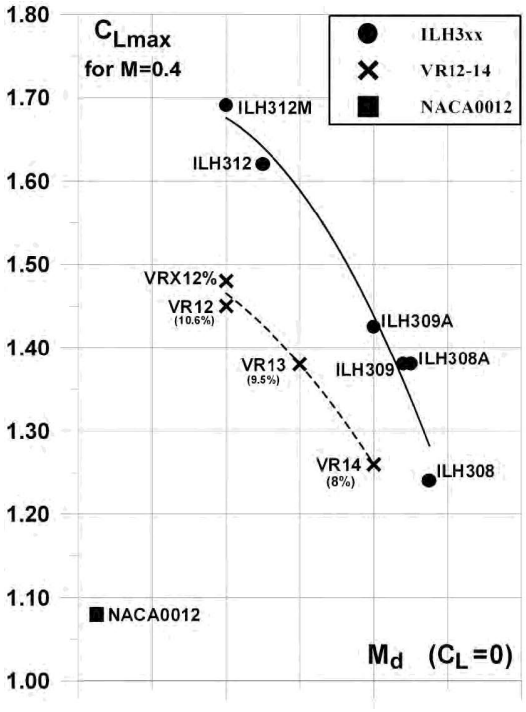

Figure 6.6: Comparison between several modern blade airfoils for drag divergence Mach number M_{DD} (x axis) and maximum lift coefficient $C_{L_{max}}$ (y axis). Difference between two vertical lines is 0.2 and VR-14 is at Ma=0.84 [64].

The functions of MH series airfoils are listed in the online user's manual of JAVAprop[5]. For the root part, the MH-126 airfoil will be used. This airfoil is said to cover a wide range of angle of attack to avoid flow separation. Besides, its large thickness can withstand the structural load at the root, but it can only be used very close to the hub[6]. For the inboard region that is

[4]url: https://www.mh-aerotools.de/airfoils/mh120koo.htm Cited: 22th June, 2018
[5]url: https://www.mh-aerotools.de/airfoils/javaprop.htm Cited: 21th June, 2018
[6]url: https://www.mh-aerotools.de/airfoils/mh126koo.htm Cited: 21th June, 2018

just outward from the root, MH-112 can be used, which covers the typical range of C_L. Furthermore, it is introduced that MH-114 is suitable for the middle. Finally, ILH308 airfoil will be used for tip.

Airfoil Distribution The four airfoils will be arranged in the following way. The root airfoil MH-126 will be applied from the root to the point where relative flow velocity to the blade is zero during cruise in order to adapt to the reverse flow region. The distance from the root can be estimated with cruise speed of 100 km/h and maximum rotational speed of 3345 rpm:

$$r_{v0} = \frac{V_{cruise}}{\omega_{max}} = \frac{100/3.6 m/s}{3345 * 2\pi/60 s^{-1}} = 0.079 m \tag{6.6}$$

Dividing this value by the radius of 0.8m gives a percentage of about 10%. Since the rotational speed used is a maximum, the real distance from the centre can be larger than this value. Nonetheless, the MH-126 airfoil is not aerodynamically efficient, still a 10% from the root will be taken for MH-126. Afterwards, the sections for MH-112 and MH-114 are determined. MH-114 has a higher maximum lift-to-drag ratio, which means a larger portion of MH-114 is more favourable for a higher efficiency. Finally, MH-112 is determined to be from 10% to 30%, and MH-114 will be from 30% until tip airfoil. Estimation about Mach number shall be made to check whether shock wave appears at the boundary between the middle airfoil MH-114 and tip airfoil MH-120.

The Mach number is estimated to be 0.70 at 85% blade length and 0.66 at 80% blade length, with rotational speed 3350 rpm and acoustic velocity 340 m/s. The rotational speed used is a maximum, so the actual rotational speed and Mach number are mostly lower than this value. The drag divergence number of MH-114 can be estimated using the Korn's equation in Peckham [18]:

$$M_{DD} + \frac{C_L}{10} + t/c = K \tag{6.7}$$

where M_{DD} is the drag divergence number for the airfoil to be estimated; C_L is lift coefficient; t/c is thickness-chord ratio; K is a factor which is 0.87 for conventional airfoils and 0.95 for supercritical airfoils. Assuming the operational angle of attack to be $-2°$, C_L is about 0.80. Thickness t/c can be found on Airfoil Tools[7] to be 13.02%. As to the factor K, a value of 0.87 will be used. Thus, the drag divergence Mach number M_{DD} can be estimated to be 0.66, which is equal to the Mach number at 80% blade length. The Mach number estimated at this 80% blade length does not consider the horizontal inflow velocity, which will increase the Mach number at this point of a forward blade. On the other hand, the rotational speed can also be lower than what is used for estimation. In short, the Mach number at 80% blade length can be either larger or smaller than 0.66. Finally, the upper limit for airfoil MH-114 is designed to be 80% blade length from the root, and MH-120 will be from 80% to the tip.

Airfoil Aerodynamic Characteristics After the section proportions of the airfoils are determined, the aerodynamic characteristics have to be known to design the twist angle and to estimate characteristics of the blade. The centre of each section will be used to estimate the average Mach number and Reynolds number for this section, which will be further used as an input for airfoil analysis. The aerodynamic characteristics can be estimated in xlfr5. Afterwards, the thrust and power required for blade and rotor will be estimated using blade element method.

Blade Element Method and Calculation Blade element method is a fundamental method that is used to estimate propeller or rotor thrust and power and efficiency, apart from actuator disk theory using momentum theory. This theory has four requirements for application. First, it does not take into account the 3D effects so the 3D effects have to be small. Second, this model works well for relatively small thrust loading, but it will become increasingly inaccurate when the loading goes up. Third, the number of blades shall be small to avoid strong interaction due to overlap and thickness. Last, the compressible effects are minor and the flow is mostly 2D [69]. The assumptions that this theory uses are:

1. The blade is composed of narrow strips or elements that are aerodynamically independent [73].
2. A differential blade element of chord c and width dr, located at a radius r from the rotor axis is considered as an airfoil section [73], which means the forces on blade elements are only determined by lift and drag coefficients [71].

The lift and drag that an element is subject to will be analysed as airfoil as below. The velocity is assumed to be composed of tangential rotational velocity ωr and axial velocity at disk V_1. Thus, the thrust and torque about the rotation axis of an element can be expressed as

$$dT = \frac{1}{2}\rho V_{resultant}^2 c_{blade}(C_L cos\beta - C_D sin\beta)dr \tag{6.8}$$

$$dQ = \frac{1}{2}\rho V_{resultant}^2 c_{blade}(C_D cos\beta + C_L sin\beta)rdr \tag{6.9}$$

where C_L, C_D are lift coefficient and drag coefficient respectively, α is the angle of attack of the element, c is chord length equal to 0.1 m. $V_{resultant}$ is the resultant inflow velocity, which can be expressed as a quadratic sum of the total axial velocity at disk V_1 and rotational speed ωr. The total axial velocity at disk V_1 can be expressed as a sum of upstream velocity V_∞ and induced velocity upstream of rotor v_1. The upstream induced velocity v_1 can be derived from the thrust equation in momentum theory [31]:

[7] url: http://airfoiltools.com/airfoil/details?airfoil=mh114-il Cited: 23th June, 2018

Table 6.3: Lift and drag coefficients of four airfoils used for estimation, assuming a constant angle of attack of −2°.

	MH-126	MH-112	MH-114	MH-110
C_L	0.71	0.96	1.1	0.37
C_D [$\cdot 10^{-3}$]	9.6	6.8	6.2	7.7

$$T = \rho(V_\infty + v_1)\pi R^2 v_2 \tag{6.10}$$

where T is thrust of the rotor disk, ρ is air density, R is radius of rotor, v_2 is induced velocity downstream of rotor. The maximum thrust will be used for T, which is 1.7 times a weight of 500 kg. The hover status will be used so $V_\infty = 0$. ρ is 1.229 kg/m^3 and R is 0.8 m. v_2 is k times v_1 . k is 2 in inviscid flow, but in reality $k = 1.6$ where viscosity is taken into account. Substituting the values into Equation 6.10 gives

$$v_1 = \frac{-V_\infty + \sqrt{V_\infty^2 + \frac{4T}{\rho\pi R^2 k}}}{2} = 19.76 m/s \tag{6.11}$$

The inflow velocity at disk V_1 can then be known to be about 20 m/s. The angle of attack will be determined based on this inflow velocity. Set the angle between the element chord line and rotation plane to be β, then the angle of attack at radius r can be expressed as

$$\alpha = \beta - arctan\frac{V_1}{\omega r} \tag{6.12}$$

α will be assumed to be constant along the blade. By assuming $\alpha = -2°$, C_L, C_D will be constant in each airfoil section and their values can be obtained from XFLR5. Details of ILH308 airfoils cannot be found, so for the tip airfoil the MH-120 will be used for estimation. The coefficients of the four airfoils used are listed in Table 6.3

Afterwards, the thrust and torque will be calculated by integrating Equation 6.8 and Equation 6.9 from root to tip, and multiply the integration with the number of blades in order to get the thrust and torque of the whole rotor. The thrust from integration is only of one rotor. Assuming the thrust of one set of rotors is 1.8 times that of one single rotor, the total thrust is about $1.8 \cdot 3 = 5.4$ times thrust of one single rotor. Finally, the power required can be calculated with

$$P = Q\omega \tag{6.13}$$

Q is torque from Equation 6.9 equal to 1030 N·m, ω is the rotational velocity of rotor. The thrust of each rotor is estimated to be 1900 N, and the power required is estimated to be 360 kW, which is unreasonably high compared to the output power by one single motor to be 50 kW. Multiplying the thrust of single rotor by 5.4, a total thrust of about 10.2×10^3 N can be obtained. Using a total weight of 500 kg, an acceleration of 2.1 g can be obtained. This acceleration is higher than designed but it is still within a reasonable range.

JAVAprop

JAVAprop is a basic software that is used to estimate propeller and rotor thrust, power, efficiency and sizes. JAVAprop also uses blade element method which has been introduced. The power of one rotor can be estimated by giving inputs as shown in

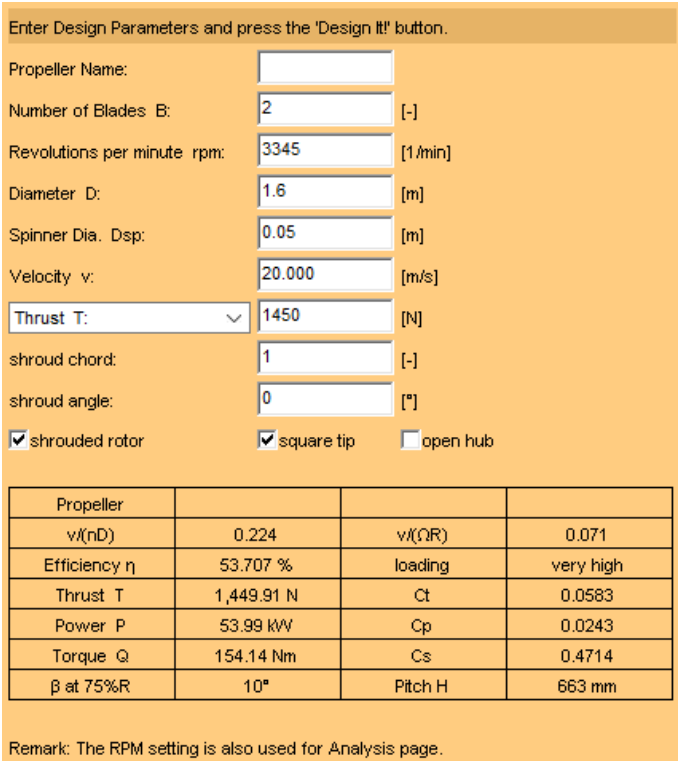

Figure 6.7: Inputs and estimated power of hover-bike in JAVAprop. The airfoil is chosen to be MH-126 at root, MH-112 at 1/3 blade length from root, MH-114 at 2/3 blade length, MH-120 at tip. The intermediate airfoil will be transition airfoil between the airfoils that are set at specific points.

Four sections of airfoil are defined at equal spacing, at 0, 1/3, 2/3 and 1 of the blade length from root respectively. The power is the most important output. In the validation part, the power estimated is larger than the actual power, so the actual power can also be lower than estimated by JAVAprop and be lower than the power estimated by basic power estimation. However, it should be also be noted that the power required tends to exceed the power available. If the "shrouded rotor" box is ticked, the output power would be lower, but the decrease is not so much, only a few kW. In addition, the airfoil selected are operating near the optimum lift-to-drag point, so if the operation points deviates, the thrust available will be smaller with limited power. Also to mention the diameter of spinner, the influence is so small that changes within a moderate range are not visible in the outputs.

6.1.3. Interference between wing and rotor

The effect of propellers applying thrust parallel to the airflow on the wing flow has been analysed in great detail. However, there is no proper research done on the effect of a rotor on a wing next to it. This makes the engineering analysis of the interference between the wing and rotor for the Scorpeon much more difficult. Therefore, the analysis mainly concerns with determining solutions to minimise the effects that the rotor and wing have on each other. Two design solutions were considered to minimise the severity of these effects. Firstly, ducts around the rotors are considered to be helpful in separating the flow over the wing from the flow through the rotors and, secondly, the wings will have extra twist to account for the induced velocity from the rotors.

Ducts around rotors Placing the wing next to the rotor creates some interference effects. As there is a high pressure on the bottom of the wing and a low pressure on the top, the air will naturally want to flow from bottom to top. With the propeller next to it, it is possible for part of the air on the bottom of the wing to travel through the airflow into the propeller towards the top of the wing. This distorts the airflow that is sucked in through the rotor. Conversely, the rotor will suck in air from the sides of the rotor as well, including the air that would otherwise flow over the wing. The distorted velocity field also affects the performances of the wing. This effect is schematically depicted in Figure 6.8. In Figure 6.8a the effect of the flow travelling from the bottom of the wing to the top through the rotor disk is depicted, while in Figure 6.8b the effect of the rotor sucking in airflow from the wings is visualised. Finally, it should also be mentioned that there is both a pressure distributions over the rotor as well as over the wings. Placing these two objects with differing pressure distributions next to each other will affect the combined distribution. This may cause a pressure gradient affecting performance of both the rotor and the wing.

By placing ducts around the rotors, the air inflow into the rotors can be separated from the airflow over the wings. This separation of airflow can help alleviate the effects depicted in Figure 6.8. With a duct present around the rotors, the effects can possible be allayed, as is schematically depicted in Figure 6.9. By blocking air which flows from the bottom of the wing to the top, the influence on the airflow through the rotor, while the duct also stops the air over the wing from flowing through the rotor.

A downside of a duct, however, is its stabilising effect. When hovering, the duct lips will improve the thrust output from the rotors as is shown in Figure 6.10a. The airflow over the lips is accelerated and, according to Bernoulli's principle, this

Figure 6.8: Interference effect between rotor and wing without ducts shown in (a) a rear view of the propeller-wing combination and (b) a top view.

Figure 6.9: Estimated interference effect between rotor and wing if ducts are present shown in (a) a rear view of the propeller-wing combination and (b) a top view.

corresponds to a lower pressure over the duct lips. Due to this lower pressure region over the duct, two forces F on the lips pull the duct up, increasing the lifting capabilities of the rotor. If the same ducted rotor now flies forward, the airflow will want to level the rotors, visualised in Figure 6.10b. The airflow over the bottom duct lip merges with the incoming free stream. This combined flow increases the velocity over the bottom lip, which decreases the pressure more than in hover and also increases the region of low pressure. Contrarily, the flow over the top duct lip collides with the incoming free stream. This decreases the velocity over the top lip and, thereby, the region of low pressure is decreased. This will create a higher lifting force on the bottom lip than on the top lip, which creates a moment M that levels the rotor. To counteract this effect, a solution is needed that negates the differences in these low pressure regions over the lips during forward flight.

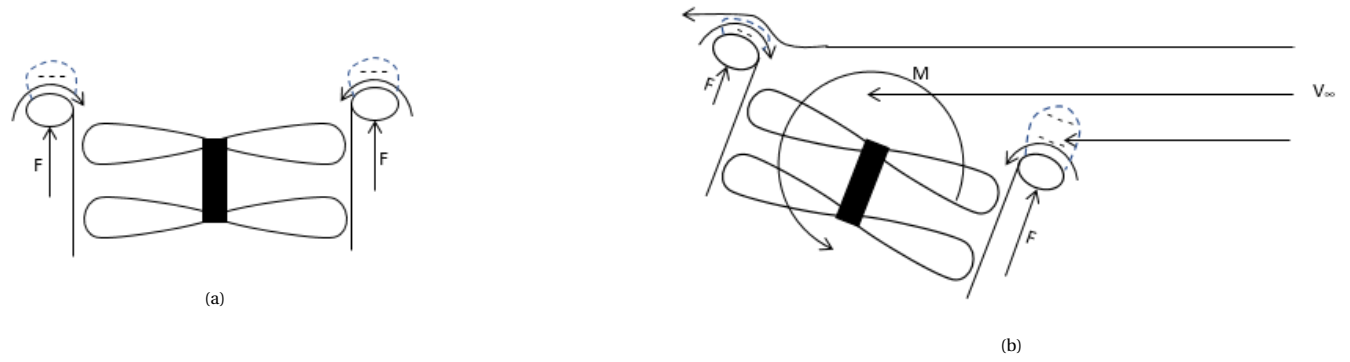

Figure 6.10: Schematics of the induced forces and moments from the duct during (a) hovering flight and (b) forward flight. The dashed lines with the minus signs depict regions of lower pressure.

Wing twist The rotors at the wing roots will induce a downward flow velocity. This decreases the angle of attack quite significantly and as a result the wings may even generate a downward lift. This decrease in angle of attack is visualised in the schematic of Figure 6.11. To account for this induced velocity, washin is added, since the induced velocity gets smaller, moving away from the rotor. By increasing the geometric angle of attack of the wing at the root and slowly decreasing this, the wing was trimmed to have every wing section experiencing airflow at the design angle of attack, which is the angle of attack corresponding to the highest lift-to-drag ratio. Contrarily, the effect of high twists on a wing have not been examined in detail yet and according to Raymer (2012) [30], large amounts of twist should be avoided, because "The more twist required

to produce a good lift distribution at the design lift coefficient, the worse the wing will perform at other lift coefficients". However, this statement holds for conventional aircraft, while the hover-bike has rotors located at the wing roots, adding a downward velocity component to the airflow. Something which has not been analysed in detail yet for other designs and it was, therefore, considered as a promising solution to account for the induced velocity.

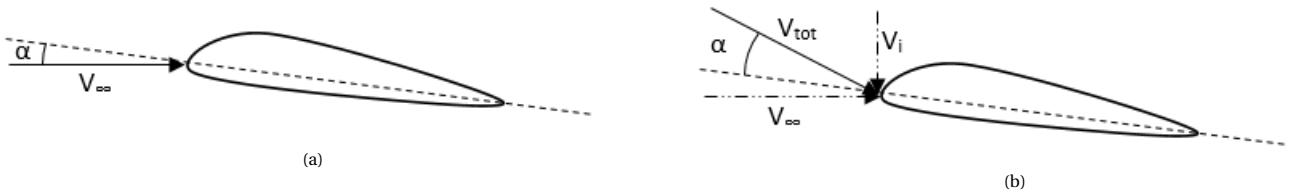

Figure 6.11: Schematic depicting the effect of induced velocity on the angle of attack experienced by the wing. (a) shows a wing in free stream flow, (b) shows a wing that experiences an additional downward induced velocity.

The optimal angle of twist at each wing section is thus dependent on the induced velocity, as seen in Figure 6.11b. So to determine the wing twist, the induced velocity as a function of distance from the rotor had to be determined. This induced velocity outside the wake of the rotor is found by Mangler and Squire (1953) as shown by Equation 6.14, where the pressure distribution outside the rotor wake is found with Equation 6.15.[53] In these equations, the rotor is assumed to have an infinite number of blades or in other words, it's modelled as a solid disk. Furthermore, the thrust is everywhere normal to the disk and the small forces in the plane, corresponding to the torque distribution are neglected. Lastly, the induced velocities are assumed to be small compared to the stream velocity V_∞. Lastly, the induced velocity effect of the rotors that are not attached to the wing section are neglected.

$$\frac{V_i}{V_\infty} = \frac{p - p_\infty}{\rho V_\infty^2} \tag{6.14}$$

$$\nabla p = \frac{\partial^2 p}{\partial x^2} + \frac{\partial^2 p}{\partial y^2} = \frac{\partial^2 p}{\partial r^2} + \frac{1}{r}\frac{\partial p}{\partial r} + \frac{1}{r^2}\frac{\partial^2 p}{\partial \theta_b^2} = 0 \tag{6.15}$$

The Laplace equation for the pressure distribution is then solved in two dimensions using a separation of variables and for the following conditions, which describe the pressure field outside the rotor disk, but limited to the wing on either side only:

$$r >= R_{\text{rotor}} \tag{6.16}$$

$$\theta_b = \frac{\pi}{2} \quad \cup \quad \theta_b = \frac{3\pi}{2} \tag{6.17}$$

$$V_i(R_{\text{rotor}}, \theta_b) = u_0 \tag{6.18}$$

$$p(\infty, \theta_b) = p_\infty \tag{6.19}$$

This leads to an induced velocity distribution over the span of the wing, from which the change in angle of attack can be derived. Based on this distribution, washout is added to the wing.

6.1.4. Body design and vehicle aerodynamic characteristics

Lastly, a skin around the Scorpeon is designed and the aerodynamic characteristics of the complete vehicle need to be determined. This also includes estimating the drag of the body structure as a function of its angle of attack.
This is accounted for in the parasitic drag, which increases quadratically with the airspeed. The drag of the body had to be determined for all three flight directions: longitudinal, lateral and vertical. As a first order estimate, this was done by modelling the structure as a simplified flat plate of a certain shape. The simplified shapes for all three flight directions are shown in Figure 6.12.

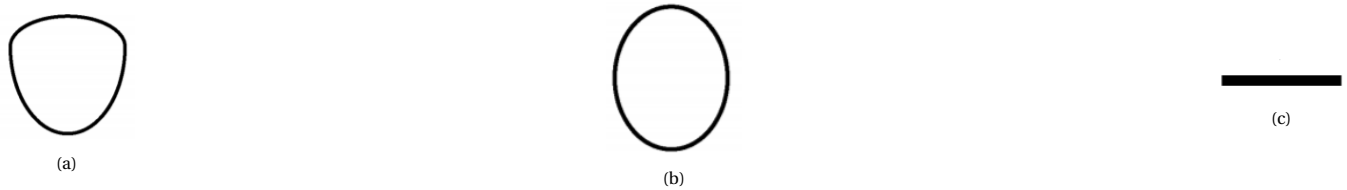

Figure 6.12: The simplified body shapes for (a) longitudinal flight, (b) lateral flight and (c) vertical flight. In this view, the free stream flow approaches from the top of the images.

From [0], it was found that the lift and drag coefficients for the shapes of Figure 6.12a & 6.12b are given by Equation 6.20 & 6.21, respectively.

$$C_L = (\sin(\alpha_b)\cos(\alpha_b))\left(K_p \cos(\alpha_b) + \pi \sin(\alpha_b)\right) \tag{6.20}$$

$$C_D = C_{D,0} + K_d C_L^2 \tag{6.21}$$

The values for K_b & K_p are provided by [0] as a function of the aspect ratio. The value of $C_{D,0}$ is also provided by Torres & Mueller, and it is approximately 0.015 for both shapes. The drag coefficient C_D of the flat plate shown in Figure 6.12c is obtained from NASA to be around 1.28[8]. Then using the standard equation for drag, Equation 6.22, the drag of the body as a function of angle of attakc and airspeed was determined.

$$D = C_D \frac{1}{2} \rho V^2 S \tag{6.22}$$

These drag values were, as said above, a first order estimate, given to the other departments to work with. Next follows the method describing the design of the skin around the body of the vehicle and the method that was adopted to determine the drag characteristics of the Scorpeon as a whole.

Skin design Apart from the hover-bike structure which takes all the loads, a skin for the hover-bike is necessary to keep the equipment inside the hover-bike in place, to provide protection and to guide the airflow smoothly over the skin. The protective skin is between the propellers and the pilot and between the structure bars. The aerodynamic skin is the skin over the structure that guides the air over the frame.

To determine the drag characteristics of the complete vehicle, the drag of the wing and rotors should be added to the body drag. The drag of the wing and body were already determined during the mid-term and, as this method was already validated, the same methodology is applied. The difference now is that the vehicle has a drag built up of both rotor and wing drag, whereas the drag four concepts in the mid-term was either fully rotor or fully wing drag.

The drag is assumed to be built up of a parasitic drag and an induced drag. For the rotors, the induced drag coefficient was given as the equivalent flat plate area $\sum (C_D S)_S$. This equivalent flat plate area is then derived from reference aircraft with the use of Figure 6.13, by assuming a clean helicopter. The induced drag power is determined from Equation 6.23, where the normalised induced velocity is approximated using Equation 6.24.

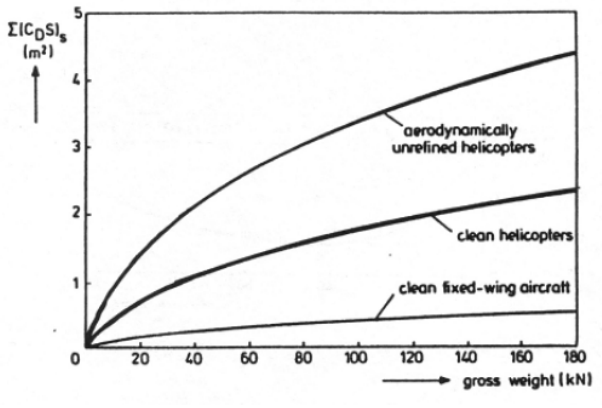

Figure 6.13: Equivalent flat plate area as a function of gross weight.

$$P_{i,\text{rotor}} = k_r W \bar{v}_i \sqrt{\frac{W}{2\rho\pi R_{\text{rotor}}^2}} \tag{6.23}$$

$$\bar{v}_i = \frac{\sqrt{\frac{C_T}{2}}\omega R_{\text{rotor}}}{V_\infty} \tag{6.24}$$

The drag coefficient corresponding to the parasitic drag of the wings $C_{D,0,\text{wing}}$ is determined from the C_L versus C_D graph of the wing, generated by XFLR5. The induced drag is obtained through the lift-drag polar given by Equation 6.25. Next, the lift coefficient C_L of the wing is not simply dependent on the vehicle weight, but also on the negative lift generated by the body of the Scorpeon. The resulting relation for the wing lift coefficient is given by Equation 6.26, where the body lift coefficient is dependent on α_b as shown in Equation 6.20.

$$C_{D,\text{wing}} = C_{D,0,\text{wing}} + \frac{C_{L,\text{wing}}^2}{\pi A e_{\text{eff}}} \tag{6.25}$$

$$C_{L,\text{wing}} = \frac{W}{0.5\rho V_\infty^2 S_{\text{wing}}} + C_{L,\text{b}} \frac{S_\text{b}}{S_{\text{wing}}} \tag{6.26}$$

The oswald efficiency factor is determined based on how close the lift distribution is to the ideal elliptic distribution, which depends on a number of characteristics, such as the taper ratio. The weight W in Equation 6.23 & 6.26 depends on the amount of lift generated by the rotors and by the wings. The drag of the body, rotors and wings are then added together to obtain the drag versus airspeed for the Scorpeon in eco-mode for a certain cruise angle of attack. The drag of the hover-bike without wings is then obtained by leaving out the drag contribution from the wing, and setting the weight W, such that the rotors carry all of the take-off weight minus the weight of the wings with duct. The maximum velocity can then be determined from the drag versus velocity curve of the hover-bike without wings, by taking an angle of attack of 45°, which is the maximum allowable angle as described in section 12.2.

[8]URL:https://www.grc.nasa.gov/www/K-12/airplane/shaped.html [cited on 25 June 2018]

6.1.5. Theory and assumptions by XFLR5

XFLR 5 is a wing analysis tool, which has been freely distributed. There are two main applications that have been used for this analysis and will, therefore, be explained in detail. Firstly, there is the direct airfoil analysis and, secondly, there is the wing, plane and body design and analysis application.
For the 2D wing analysis, XFLR5 uses code from XFOIL. These are split into viscous and inviscid analyses. As the hoverbike operates at relatively low velocities, it experiences low Reynolds numbers, which means that the viscosity can not be neglected, especially near the airfoil itself where the boundary layer is located. Therefore, all analyses that have been done in XFLR5 were including viscous flow. For the inviscid flow analysis, a general two-dimensional inviscid airfoil flowfield is constructed by superposing a freestream flow, a vortex sheet on the airfoil surface and a source sheet on the airfoil surface and wake. The contours of the airfoil and wake trajectory are discretized into flat panels, where each airfoil panel has a linear vorticity distribution and the airfoil and wake panels all have a constant source strength. To incorporate the upper and lower flow airflow meeting at the sharp trailing edge, a Kutta condition is used. Then, in the calculations for inviscid flow, the source strengths on the airfoil are set to zero.
For the viscous analysis, the source strengths on the airfoil are nonzero. This adds an extra unknown to the system of equations, which is solved using the boundary layer equations. To determine the location of transition, the growth of the amplite of the most-amplified Tollmien-Schlichting wave is determined and when this value exceeds e^9, transition occurs. The governing equations are then discretised using two-point central differences with the boundary layer variables located at the panel node. For more information regarding the 2D wing analysis theory, the reader is directed to [35].

The 3D wing analysis can be performed using the lifting line theory, a vortex lattice or a 3D panel method. Since only the VLM was used for this analysis, this approach will be explained in more detail. According to the XFLR5 manual: "The principle of the VLM is to model the perturbation generated by the wing by a sum of vortices distributed of the planform. The strength of each vortex is calculated to meet the appropriate boundary conditions, i.e. the non penetration conditions on the surface of the panels." Furthermore, according to [32], "The resolution of the VLM problem requires the inversion of a square matrix of the size of the number of panels. This inversion is performed by Gauss' partial pivot method."
The main limitations of the VLM are as follows:

1. VLM results should not be considered around angle of attack values close to stall angles.
2. The VLM assume a small angle of attack. As a consequence, the trailing vortices are not aligned with the free stream velocity.

6.2. Iterations

Before the final design is obtained, some iteration steps were taken for optimisation. These are spread out over the different aerodynamic components, namely the wings, rotors and body of the Scorpeon. In subsection 6.2.1, the iterations in the wing design are described. The iterations on the duct are given in subsection 6.2.3.

6.2.1. Wing design

To design the aspect ratio such that the minimum drag is reached at about a velocity of 100 $\frac{\text{km}}{\text{h}}$, the wing planform was iterated as depicted in the flowchart of Figure 6.3. As the wing span was constrained, the aspect ratio could only be increased at the cost of surface area, which only increased the flight velocity. The chord was the only parameter that could be increased, which increases the surface area and thereby lowering the flight velocity. The initial result was a flight velocity of around 105 $\frac{\text{km}}{\text{h}}$.
After that, it was decided to increase the lift contribution of the wings from 50% to 60% to improve the endurance of the Scorpeon. The result was that the wing area increased thereby shifting the airspeed corresponding to minimum drag to the right. This means that the cruise airspeed will be slightly higher than initially designed for, which is considered acceptable. The cruise airspeed can only be lowered by increasing the chord length, but this only increases the minimum drag at this point. Furthermore, the wing will be connected to the duct at the root and because of that, the root chord should not become larger than the duct.

6.2.2. Rotor design

In the calculation of applying blade element method directly and the verification of the calculation, the rotational speed is always adjusted until the thrust estimated is close to the designed thrust. The power at this rotational speed will be the power estimated.
To have a more reliable result, JAVAprop is also used for thrust and power estimation. The variable that can be changed in the inputs is the rotational speed. The diameter of rotor will have a large influence, but it will also influence the geometry and weight of Scorpeon so the diameter will stay constant. The JAVAprop itself uses iteration method and no redundant inputs are given so the user will just give inputs and get outputs. The geometry details are output and will change according to performance input. On the other hand, the changing rotational speed will not influence the thrust input. When the rotational speed is lowered, the blade angle (angle between chord and rotational plane [69]) β increases, which will lead to a larger lift coefficient to compensate for the decreasing rotational speed, as well as a lift-to-drag ratio that will increase first and decrease after the blade angle reaches a certain value. A lower rotational speed will also lead to a higher thrust coefficient and solidity, leading to an increased length of blade chord length. Although it is also possible that blades with

constant chord can also provide enough lift with a lower rotational speed if the blade angle increases, the increase may be due to an optimisation in the blade design of JAVAprop.
By taking smaller rotational speed, the point at which power estimated reaches its minimum can be found. This point can be considered to be the optimum blade design. For both maximum thrust and cruise situations, this point is figured out. At this optimum point of maximum thrust, angle β at 75% blade is equal to 18.7° occurring at 1700rpm. At cruise, the optimum occurs at 1100rpm and at 75% blade $\beta = 21.7°$. The values are quite close, indicating a good compatibility. Thus, at 75% blade a blade angle of 20° can be used. On the other hand, the chord length given can be as long as 0.34m, which is too stout for air blades. Furthermore, in the process of decreasing rotational speed from estimated value to the optimum point, the power required does not change much. Thus, the estimated high rotational speed will be used. At the maximum thrust and the high estimated rotational speed, the maximum chord length is about 0.2m. However, this is at a low blade angle thus low thrust coefficient and low lift-to-drag ratio, the chord length can be further reduced if the blade angle at optimum is used.
To estimate the blade chord length in case the blade angle of 20° is used, the thrust is considered to be proportional to chord length and a linear function of ω^2. With the thrust constant, the product of chord length c and ω^2 is assumed constant for estimation. Thus, the chord length can be estimated as $0.34 \cdot (\frac{1700}{3345})^2 \text{m} = 0.088\,\text{m}$. This estimation shows that an average of 0.1m will be sufficient.

6.2.3. Interference between wing and rotor

As explained in subsection 6.1.3, ducts were chosen as a partial solution to the interference effects between the wing and rotor. The ducts, however, had the disadvantage of stabilising themselves when tilted. To account for this levelling, it was first thought that angling the duct of the hover-bike such that the ducts will favour a certain angle to fly at. This angle would then be the angle of attack of the Scorpeon during cruise flight. Such a tilted duct would decrease the hover performances, however, the vehicle is not designed for hover during the eco-mode. Later, it was determined by the Power & Propulsion and the Structures department that tilting the rotors would be an unfeasible solution, both structurally and in rotor-effectiveness. This concept was for that reason omitted and a new design solution was thought of, outlined in subsection 6.3.3.

6.2.4. Body design and vehicle aerodynamic characteristics

In the design of the body and the iterations to obtain the optimal cruise flight parameters, the main iterations consisted of determining the flight angle from the drag at cruise conditions. As can be seen from the N^2 chart in section 5.1, the cruise flight angle is obtained from the Power & Propulsion department. This department requires the minimum drag value at cruise speed to determine the cruise flight angle, which is an iterative process. The design was started at a flight angle of 20° and with a wing that generates 60% of the lift. After iterations between the Power & Propulsion department, it was found that the endurance requirement would not be met in these conditions. As a result, the wing effectiveness was increased to generate 62% of lift. Then another set of iterations let to a cruise flight angle of 33.1° at which the endurance requirement was met.

6.3. Results

The results of the aerodynamics analysis are summarised in this section. The results comprise of both design solutions and performance characteristics. Firstly, the results of the wing design analysis are outlined. Then, the rotor analysis results are summarised. Then, the solution to the duct design to account for the wing-rotor interference is provided, while lastly, the aerodynamic characteristics of the Scorpeon are denoted.

6.3.1. Wing design

The airfoils were all ranked from 1 to 6 for certain characteristics. This ranking is shown in Table 6.1. The two airfoils with the highest lift-to-drag ratio are the Eppler E392 and the Selig S4061. In the end, it was opted to go for the Selig S4061 for its low minimum drag coefficient.

Table 6.4: Airfoil ranking for different performance characteristics.

	S3024	S4061	NACA 63-012A	NACA 63-412	E392	FX63-137
Lift-to-drag ratio	4	2	6	5	1	3
Minimum drag coefficient	1	2	3	5	4	6
Drag bucket size	5	4	2	1	3	6
Thickness-to-chord-ratio	5	6	3	2	4	1
Maximum Lift coefficient	5	2	6	4	3	1
Moment coefficient	2	4	1	3	5	6

Then, to determine the necessary twist over the span, Equation 6.14 & 6.15 were solved for the region outside the wake of the rotor. The resulting induced angle of attack distribution over the span is shown in Figure 6.14a. The twisting of the

wing due to aerodynamic loading was obtained from Equation 6.2 and the result is plotted in Figure 6.14b. It can be seen that the angle is very insignificant which can be attributed to the small span of the wing and the small loads that act on it. Therefore, there was no extra twist added to account for such aeroelastic angular deflections. Furthermore, the velocity at which divergence of the wings occurs was obtained from Equation 6.1 and this is around 150 $\frac{m}{s}$, which is well outside the flight envelope of the Scorpeon.

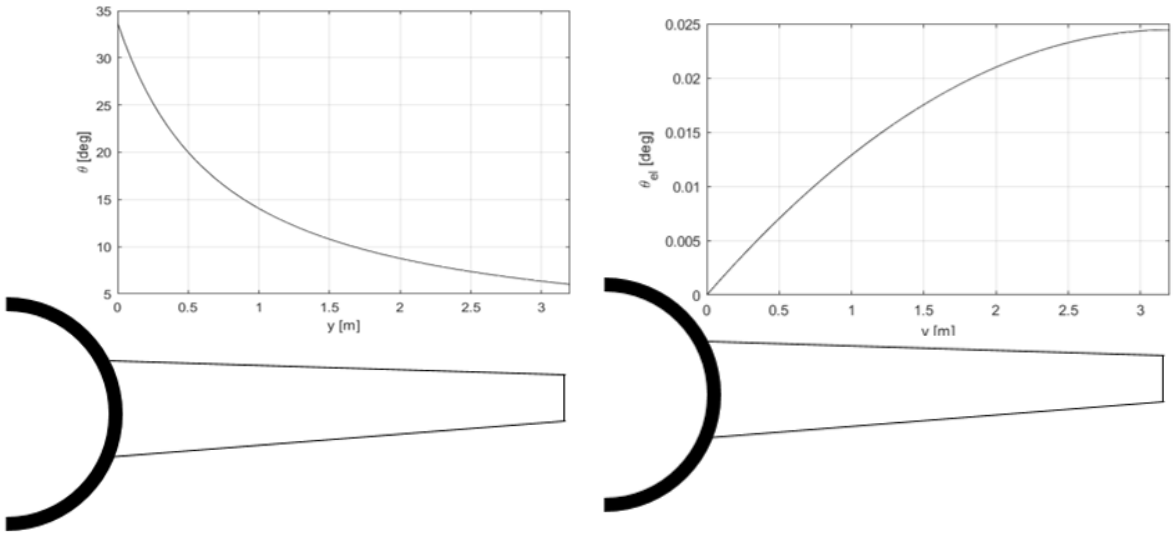

(a) (b)

Figure 6.14: Twist distributions (a) to account for induced velocity of the rotor and (b) due to the aeroelastic behaviour of the wings.

The resulting wing is shown in Figure 6.15. The geometric dimensions of the wing are summarised in Table 6.5. As can be seen from the design, a winglet is added as a wing tip device. As there is a limitation on the span, it was decided to use a winglet to increase the effective span, as described in [30]. Also, as the design must have an appealing look, wing tips will improve the Scorpeon appearance, giving it a "faster" look, although this is a rather subjective statement.

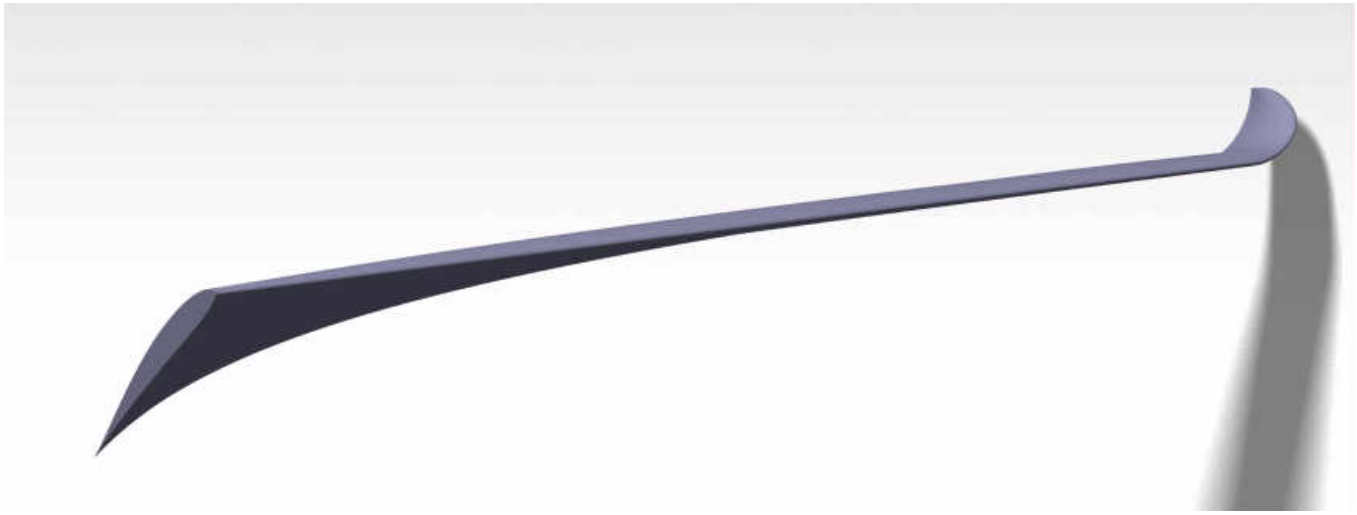

Figure 6.15: CATIA render of final half wing

Wing half span	Aspect Ratio	Half wing surface area	Root chord	Tip chord	Geometric angle	Twist (root to chord)	Winglet height
3.2 m	10.3	2.18 m^2	0.9 m	0.405 m	37°	0.15 m	

Table 6.5: Summary of the geometry of the final wing

6.3.2. Rotor design

First the airfoils for rotor are selected. The MH series are used for most of the blade for high thrust and lift-to-drag ratio. For the tip blade, the ILH308 airfoil is applied in order to have a high drag divergence number on this part. Afterwards, more analysis is done through JAVAprop. The power required is estimated to be $\frac{54-50}{50} = 8\%$ larger than the power available when the designed maximum thrust is generated. JAVAprop is verified and validated to be quite accurate, but the estimated power can be larger than the actual value probably because a much lower lift-to-drag ratio is used. As to geometry parameters, the

rotation speed is iterated to obtain the most efficient point with a constant thrust that needs to be generated. The blade angle is decided from the optimum point to be 20° at 75% of blade. An average chord length of 0.1m will be sufficient. The spinner diameter is decided to be 0.05m, although the analysis shows it does not have large influence on the result as long as it is small enough. From the JAVAprop analysis, the duct can have a positive result, but the influence is not large. Since the aerodynamics effect is limited, the size can be determined by other subgroups that will have more insight into duct design.

6.3.3. Wing-propeller interference

As was explained in subsection 6.1.3, ducts around the rotor can help separate the airflow through the rotor and the airflow over the wing. The disadvantage of ducts, however, is their stabilising effect, which is caused by a bigger region of low pressure on the bottom lip of the duct that is turned into the flow and a smaller region of low pressure on the top lip of the duct. So a proper solution had to be sought to decrease the difference in size of these pressure regions. The simplest solution was to decrease the radius of the lips. This decreases the effectiveness of the duct, however, a smaller radius means there is less extra inflow into the duct that will add to the region of low pressure. This decreases the absolute difference in size of the two low pressure regions. At the same time, the duct will still be effective in splitting the airflow of the rotor and wing. Furthermore, the ducts minimise the wing tip losses nonetheless, which still improves the ducted rotor performances.

6.3.4. Skin design

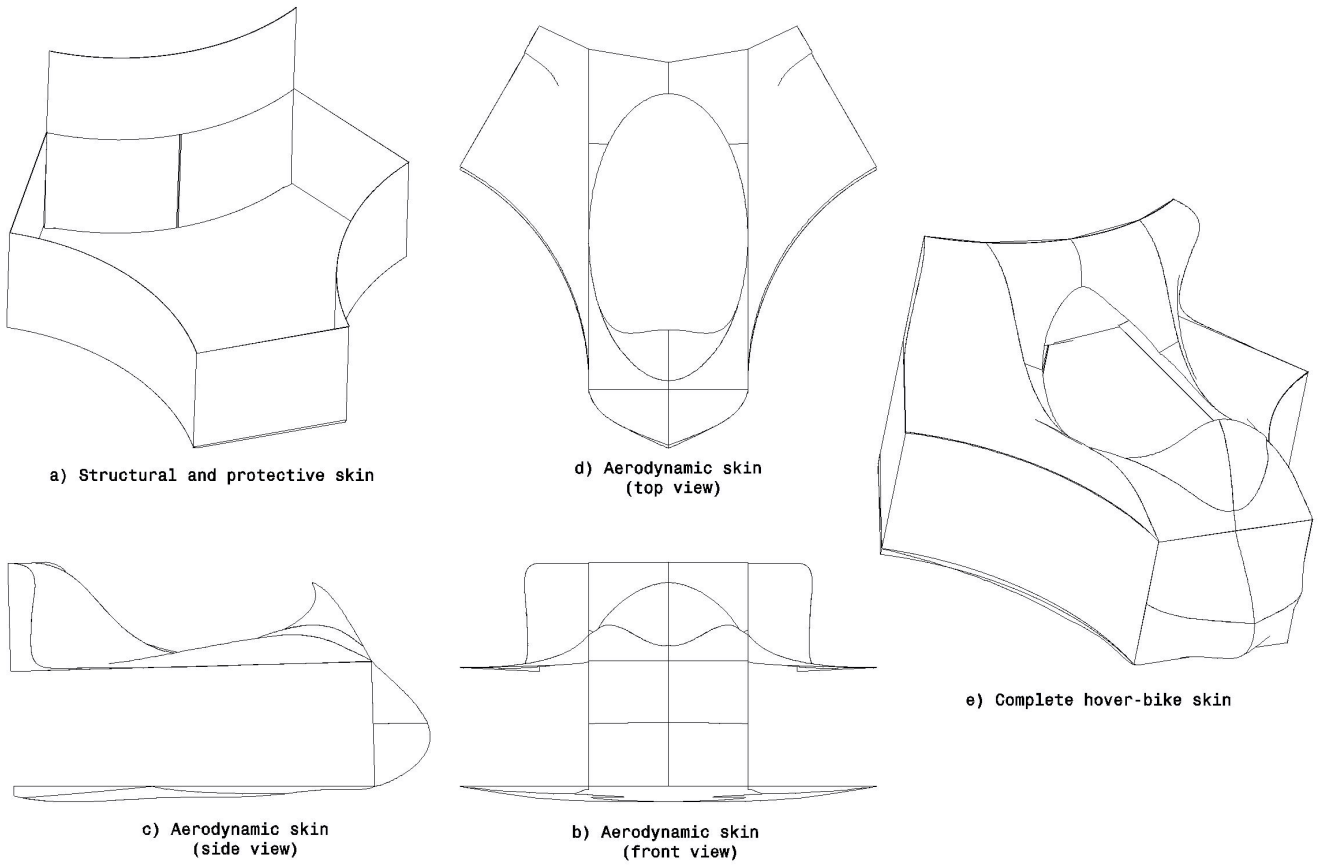

Figure 6.16: Skin-design of the hover-bike

6.3.5. Complete vehicle characteristics

The resulting drag of the Scorpeon with wings is plotted versus the airspeed in Figure 6.17a, while the drag polar is depicted in Figure 6.17b. The drag of the whole vehicle was evaluated with the hover-bike at a body angle of attack of 33.1° (vehicle pitched downwards), as this is also the cruise speed angle of attack of the body. As can be seen from the graph, the cruise speed is then about 105 $\frac{\text{km}}{\text{h}}$.
Furthermore, the drag of the Scorpeon in thrill mode is shown in Figure 6.18. This figure contains the drag-velocity curve in both longitudinal direction and in lateral direction. As can be seen, the drag in both directions is as good as equal, which is expected as the only difference between the two directions lies in the evaluation of the body drag, which depends on the planform shape depicted in Figure 6.12. As the difference in body drag between longitudinal and lateral flight small, the resulting total drag in both directions is approximately the same. This drag was evaluated at a body angle of attack of 10° (vehicle pitched downwards). From evaluating the drag curve at a body angle of attack of 45°, it was found that the maximum speed of the hover-bike is around 200 km/h.

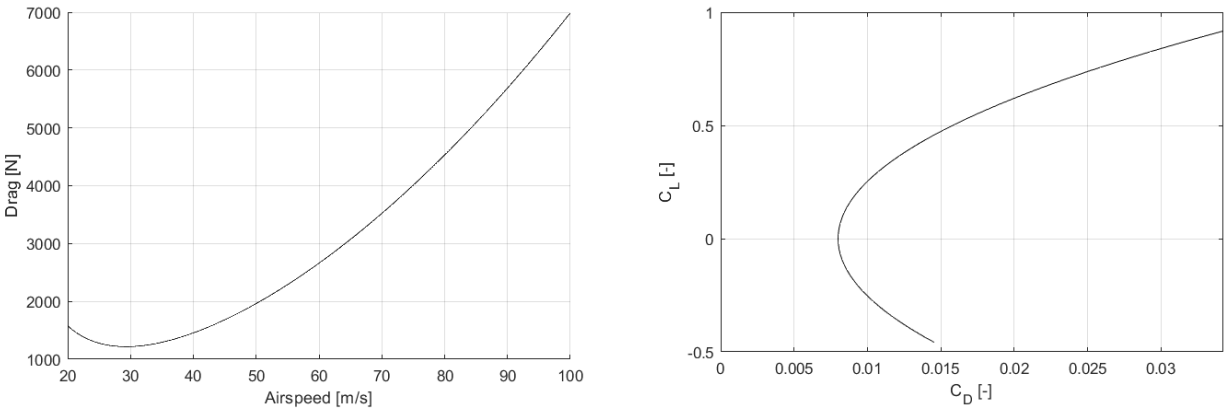

(a) (b)

Figure 6.17: Drag characteristics of the hover-bike with wings in forward flight. The drag curve is shown in (a), while the drag polar of the wing can be seen from (b).

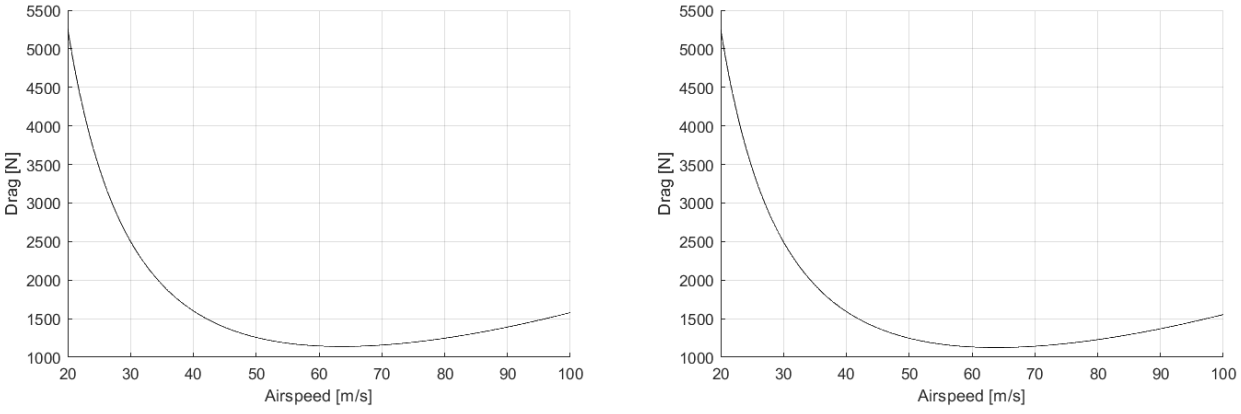

(a) (b)

Figure 6.18: The drag versus velocity of the hover-bike in sport mode for (a) longitudinal velocity and (b) lateral velocity.

6.4. Verification & Validation of aerodynamic analysis tools

To ensure that the calculations model reality with sufficient accuracy, the calculations should be verified and validated. As the XFLR5 software has been provided by third parties, after thorough checks that the program works properly. Therefore, XFLR5 is only validated.

Velocity-drag curve The velocity-drag curve is, however, verified. The verification is performed in terms of unit tests.

Action	Expected effect on drag	Actual effect on drag
Increase altitude	Decrease	Decrease
Increase wing area	Increase	Increase
Increase mass	Increase	Increase
Increase body zero-lift drag	Increase	Increase

Table 6.6: Effects of changing certain input parameters on the minimum drag.

As can be seen from Table 6.6, all unit tests give the expected results. Next, the tool must be validated too, this is performed in a similar manner as was done in the mid-term report [42]. The drag of the Fokker 50[9] and McDonel Douglas Helicopter[63] were determined with the program, of which the result is shown in Table 6.7. As the program combines a helicopter and aircraft design, and there is not a well-known existing combi-vehicle, it is seen as sufficient that the program gives sufficiently accurate results for separate aircraft and helicopters.

	Simulated result	Actual result	Error
Fokker 50	0.024	0.028	16%
McDonel Douglas Helicopter	0.064	0.076	19%

Table 6.7: Validation of method on drag coefficient calculation for aircraft and helicopter.

XFLR5 The validation of XFLR5 is done by looking at previous research. As XFLR5 is designed for sailplanes, it was also validated with a sailplane. The result is shown in Figure 6.19. As can be seen from the graphs, the zero-lift angle correctly predicts the zero-lift angle and the VLM method approximates the lift polar as a linear function, which means it is not valid near stall conditions. Then, the VLM method tends to underestimate the drag, which may be due to the viscosity and can most likely be attributed to a wrong value for N_{crit}, to predict transition. In conclusion, it can be said that XFLR5 represents the software with enough accuracy and the model is validated.

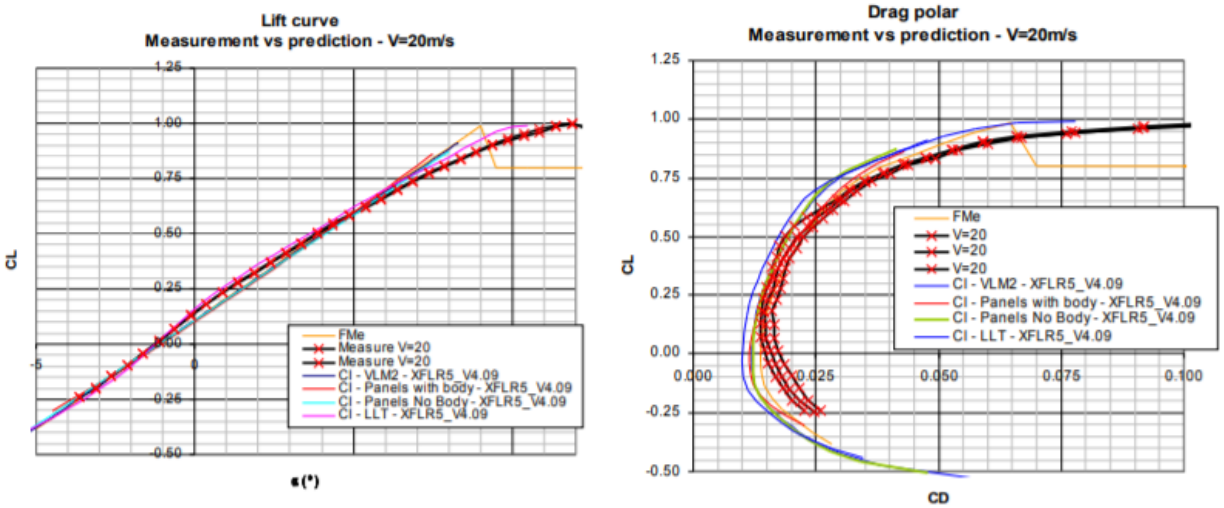

(a) (b)

Figure 6.19: Plots of (a) lift polar and (b) drag polar from XFLR5 plotted against measurement points for a sailplane [67]

.

Direct calculation using blade element method Using the VA115 helicopter for verification[10], the power estimated is also much higher than the actual value. Website of VA-115 provides more information than what can be found about most other helicopters, including the airfoil, rotor diameter, and power, which is helpful for verification. The weight of VA-115 is also quite light instead of being too heavy comparing to hover-bike. This similar weight level can help to avoid possible discrepancies due to a different weight level.

For the airfoil, it is assumed that the airfoil always operate at an angle of attack 5°, resulting C_L of 0.7 and C_D of 6.5×10^{-3} The angular velocity is derived from the tip speed of 150 m/s and rotor radius of 2.25 m. The inflow velocity is taken at

[9] URL: `http://www.flugzeuginfo.net` [cited 31 May 2018]

[10] url: https://www.rotorschmiede.de/va-115/ Cited: 25th June, 2018

Table 6.8: Lift and drag coefficients of four airfoils used for estimation, assuming a constant angle of attack of 2°.

	MH-126	MH-112	MH-114	MH-120
C_L	0.87	1.2	1.3	0.63
C_D 10^{-3}]	11	7.2	7.0	6.5

hover state and an induced velocity of 9 m/s is calculated using Equation 6.10. A total chord length of 0.375 m is adjusted in according to the thrust, so that the thrust can be estimated to a reasonable value. Finally, the thrust can be estimated to be be about the maximum thrust, but the power required would be as high as 305 kW. On the other hand, the power at maximum performance is 35 kW. The power estimated is more than eight times the actual power, indicating a wrong estimation for power. To approach a lower power value, another estimation where the airfoil operates at the maximum lift-to-drag ratio 1.1 and C_D of 8.8×10^{-3} To obtain a comparable thrust level, the total chord length is adjusted to be 0.24 m. The power is estimated to be 300 kW, which almost does not change compared to the previous estimation using the other airfoil operation point. Thus, the too high power is not caused by a relatively low lift-to-drag ratio, but due to the problem in the method.

The same adjustment of choosing the operation point near maximum lift-to-drag ratio point can also be applied to the hover-bike rotor estimation. The angle of attack is assumed to be constantly 2°, where the lift-to-drag ratio reaches the maximum for MH-114 which takes half of the blade. The angle of attack is also near the optimum point of other airfoils that are applied. The lift and drag coefficients are listed in Table 6.8. Finally, the total thrust is estimated to be 14 kN, providing an acceleration of about 2.8 g using a total weight of 500 kg. The power is 495 kW, which is even larger due to a higher drag. Thrust is a linear function of ω^2, while power is a linear function of ω^3 according to Equation 6.8, Equation 6.9, and Equation 6.13. Thus, by multiplying ω by a factor smaller than one, both thrust and power will be lowered. This factor is denoted as k_ω and can be estimated as

$$k_\omega = \sqrt{\frac{T_{design}}{T_{estimate}}} = \sqrt{\frac{1.7}{2.8}} = 0.78 \tag{6.27}$$

Using this factor and making adjustments, a thrust that is more reasonable can be obtained. Using a rotational velocity of 2500 rev/min, the thrust of one rotor is estimated to be 1450 N, which can provide about 1.7 times the weight, using the mass 445 kg without wings. The power for this thrust is about 210 kW, which is much lower than previous estimations, but still much higher than a fundamental estimation of power. In conclusion, the method used is inaccurate. This direct calculation will be discarded and JAVAprop will be used instead.

Validation of JAVAprop The validation of JAVAprop will also use the helicopter VA-115[10]. The hover state at MTOW is used as input, with a rotational of 650 rev/min and thrust of 1350 N for one rotor. This state is judged by JAVAprop to be high loading, which can be inaccurate due to the characteristics of blade element method introduced in the blade element method introduction part. The total thrust is considered to be two times the thrust of one single rotor. The reason that factor two is used is to have a lower power output, due to a high power output in case of a factor of 1.8. Finally, the power output is 21.5kW for one rotor so 43 kW in total, which is still 6.3 kW larger than the power given and is about 17% off.

Something that needs to be noted is that the VA-115 uses NACA23012 on blade, which is an improved version of the traditional airfoil NACA0012. On the other hand, the airfoil that is used in JAVAprop is MH-114 and the angle of attack is always 1°. One fact that needs to be noticed is that in JAVAprop the lift-to-drag ratio of airfoil is much lower than what is given in XFLR5 and Airfoil Tools[3]. One example for this difference can be the MH-114 airfoil at $Re = 5 \times 10^5$ shown in Figure 6.20. The results in XFLR5 show that at angle of attack of 1° and low Mach number, the lift-to-drag ratio is between 112 and 116. On the other hand, the lift-to-drag ratio at 1° given by JAVAprop is only 30., times smaller than the result of the airfoil. On the other hand, even if the lift-to-drag ratio that is used as operation point in JAVAprop of one airfoil is several times larger or smaller than another airfoil, the resulting power is only a few kW off for some reason. Thus, although the lift-to-drag ratios of airfoil NACA23012 and MH-114 differ a lot at 1°, the output power can still be only a few kW off. However, at the same time this also indicates a even larger power if airfoil NACA23012 instead of MH-114 is used, increasing the error. Despite the error, JAVAprop can still said to be competent for estimation.

It has been mentioned that the power estimated tends to be larger than reality. The reason can be that the airfoil lift-to-drag ratios in JAVAprop are lower than airfoil aerodynamics characteristics for some reason. Besides, the high loading situation is also inaccurate in blade element method, which can also be one reason. The influence of this error on power estimation of Scorpeon is that the real power can be smaller than estimated. Therefore, the real power can be smaller than what is estimated to be available, but the excessive power will not be that much.

6.5. Sensitivity analysis

Lastly, a sensitivity analysis was performed to test the robustness of the design solution and establish the degree of feasibility of the preliminary design. The effect of a change in major system parameters is documented and investigated. From the aerodynamic analysis, the following outputs are determined and the sensitivity of these outputs is investigated as an effect of changing major system inputs given below.

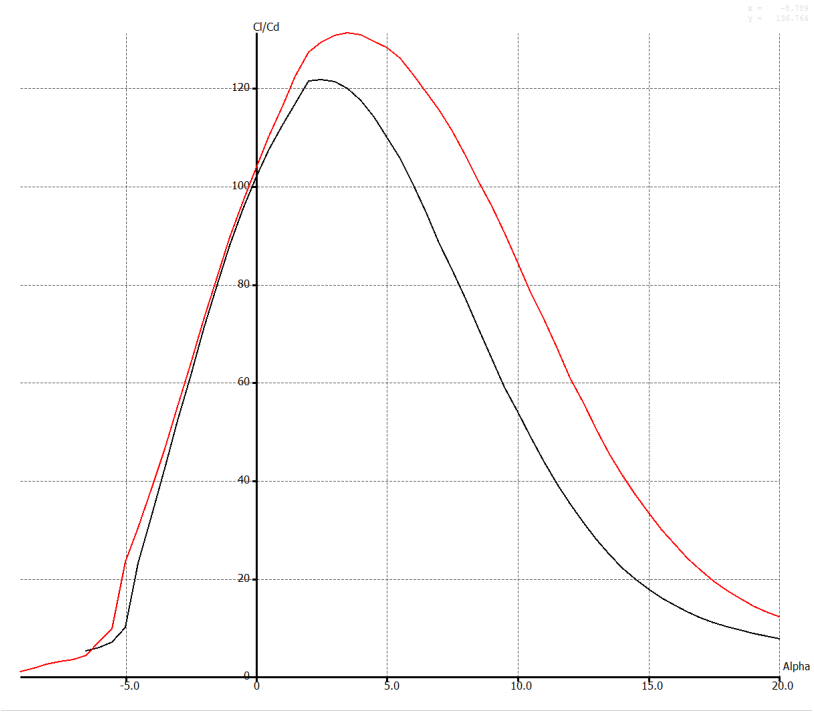

(a)

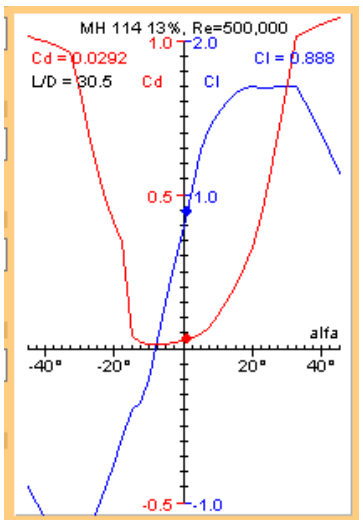

(b)

Figure 6.20: MH-114 airfoil lift-to-drag ratio at Re=5 × 10^5. (a) shows curves from XFLR5, where the red and black curves are at M = 0 and 0.4, respectively. (b) shows the lift and drag curves as well as lift-to-drag ratio at angle of attack 1° at Re=5 × 10^5

Inputs

- Hover-bike mass m
- Lift generated by the wing L_{wing}.
- Half wing surface area S
- Wing aspect ratio A

Outputs

- Minimum drag at cruise D_{min}
- Airspeed at cruise in transportation mode V_{cruise}
- Maximum flight speed in thrill modeV_{max}

Change of the system parameters is investigated one by one in the following paragraphs.
Change in m The change of the hover-bike mass on the drag versus velocity curve is shown in Figure 6.21. From the curve of Figure 6.21a, it can be seen that the cruise airspeed ranges from 21 $\frac{\text{m}}{\text{s}}$ at a mass of 200 kg to 35 $\frac{\text{m}}{\text{s}}$ at a mass of 800 kg. Similarly at the same respective masses, the cruise drag ranges from 595 N to 1764 N. The maximum airspeed can be determined from Figure 6.21b, with a maximum forward thrust of 4900 N. This V_{max} ranges from 65 m/s at 200 kg to 55 m/s at 500 kg. The lines corresponding to heavier hover-bikes have too much drag to reach a maximum velocity at an angle of attack of 45°.

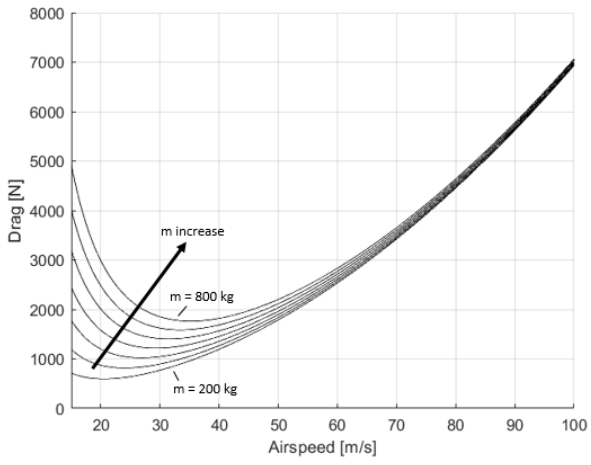

(a)

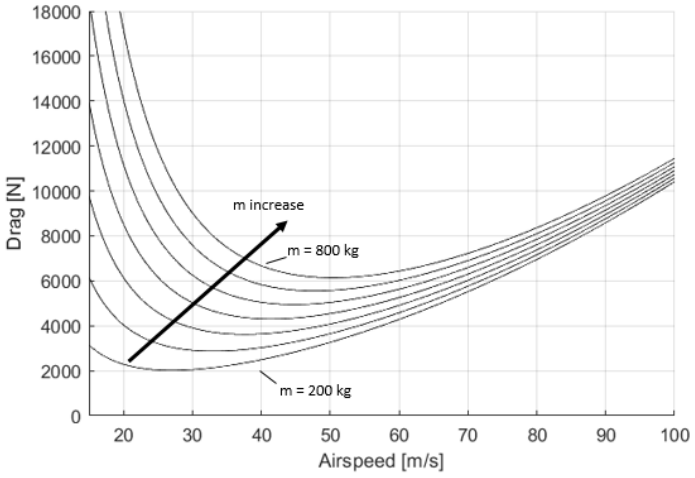

(b)

Figure 6.21: Effect of increasing mass on the drag versus velocity curve of the hover-bike in (a) transportation mode at α_b = 33.1° and (b) in thrill mode at α_b = 45°.

Change in L_{wing} Changing the amount lift that must be generated by the wing will only affect the parameters in transportation mode, as the thrill mode has no wings. This means that the maximum airspeed stays unchanged. The change in the cruise parameters, however, is determined from Figure 6.22. As can be seen from the graph, the minimum drag ranges from

2300 N at $L_{\text{wing}} = 0.4$ to 1185 N at $L_{\text{wing}} = 0.9$. Similarly the cruise airspeed decreases from 40 $\frac{\text{m}}{\text{s}}$ to 28 $\frac{\text{m}}{\text{s}}$ at the same respective values of L_{wing}.

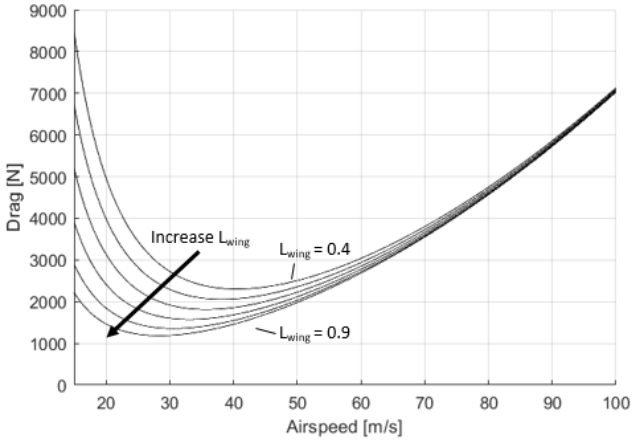

Figure 6.22: Effect of increasing percentage of lift generated by the wing on the drag versus velocity curve of the hover-bike in transportation mode at α_b = 33.1°

Changes in S **and** A As the aspect ratio and the wing surface area are related to each through the wing span and only effect the parameters corresponding to the transportation mode, these are summarised together. Firstly, the effect of a change in the wing surface area (with aspect ratio kept constant) is depicted in Figure 6.23a. The effect of changing the aspect ratio (with surface area kept constant) is shown in Figure 6.23b. As can be seen from the two graphs, they have a similar effect. Changes in the aspect ratio do not heavily affect the cruise speed, which is 30 $\frac{\text{m}}{\text{s}}$ for an aspect ratio of 5 and 29 $\frac{\text{m}}{\text{s}}$ for an aspect ratio of 20. The drag on the other hand ranges from 1330 N to 1165 N at the same respective aspect ratios. Similarly, changes in the wing surface area do not affect significantly affect the cruise speed, which ranges from 31 $\frac{\text{m}}{\text{s}}$ to 29 $\frac{\text{m}}{\text{s}}$ at a half-surface area of 1 m^2 and 3.4 m^2, respectively. At these half-wing surface areas, the minimum drag ranges from 1320 N to 1200 N.

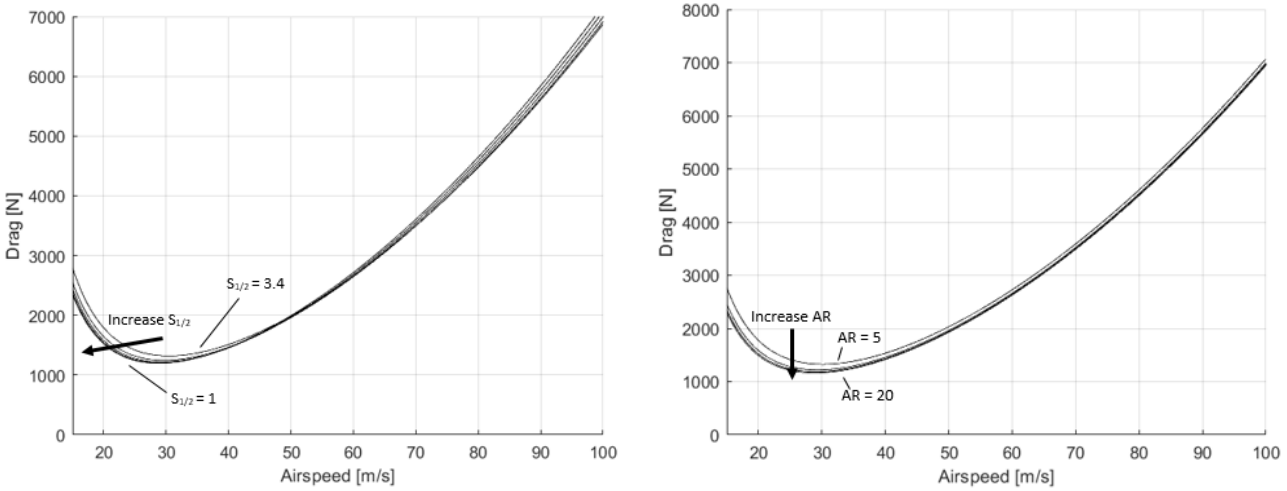

(a) (b)

Figure 6.23: Effect of increasing (a) wing surface area and (b) aspect ratio on the versus velocity curve of the hover-bike in transportation mode at α_b=33.1°

From the sensitivity analysis, it can be concluded that a change in the hover-bike mass has a significant impact on the minimum drag, cruise airspeed and maximum airspeed in both the transportation and thrill mode. Furthermore, increasing the percentage of lift that must be generated by the wing, greatly lowers the minimum drag and cruise velocity. This means that the aerodynamic parameters are very sensitive to the initial mass estimate of the hover-bike and the percentage of lift that the wings are required to produce. Care must therefore be taken that later changes of these parameters may require significant design alterations to meet the requirements.

7
Power and propulsion

Power and propulsion is one of the main departments which worked on the final design of the hover-bike. Power and propulsion analyses the propeller size by determining the diameter and the speed. Next to that the electric engines are chosen and the battery is sized by determining the power required to meet the requirements.

7.1. Method

In this section the methods that were used in the power and propulsion analysis are shown. The methods are split into the different subsystems.

7.1.1. Propeller sizing

The hover-bikes primary method of providing lift is with the rotors. The first important consideration is the size of these rotors as it will have a very large influence on the total vehicle and its mass. Six subsystems were determined to have the largest influence on the total mass. A relation between the mass of these components as a function of rotor size was established.

- **Propeller weight.** A larger rotor diameter means that the propeller becomes heavier.
- **Engine weight.** A larger rotor has a lower disk loading for the same amount of thrust. Therefore the power required goes down and lighter engines are can be used.
- **Battery weight.** A less powerful engine needs less energy. Therefore a larger rotor will lead to less battery mass due to a less powerful engine required.
- **Structure weight.** A larger rotor will cause the structure weight to go up, because of higher loads introduced in the structure of the hover-bike.
- **Duct weight.** Larger propellers will need larger ducts, and larger ducts obviously lead to more weight.
- **Miscellaneous weight.** Miscellaneous weight consists out of components like sensors, cabling, seat, control input devices, pilot screen and lights. The payload weight is also included in this category. The weight of these components is assumed to be constant with varying propeller diameter.

The relation between propeller weight and rotor size was found from reference data. A similar approach was used for the motor weight. The reference data and trend lines following from this data can be found in Appendix A. For the battery weight estimation, a relation between the rotor size and required power was needed. The required power (P_{req}) was calculated using momentum theory with Equation 7.1

$$P_{req} = \sqrt{\frac{L^3}{2\rho A}} \frac{1}{(F.M.)} \tag{7.1}$$

The lift (L) is assumed to be 500·9.81 = 4905[N], which is the thrust necessary to keep hovering in the air. The Figure of merit (FM) is assumed to be 0.6. The momentum theory and figure of merit are further explained in subsection 7.1.3. Total rotor area (A) will vary with rotor diameter. Following from the required power, the battery mass can be calculated. A specific energy for Li Ion batteries of 240 [Wh/kg][1] is used. In this specific analysis the wing lift was not accounted for. To be able to estimate the necessary battery mass, an endurance of 0.4 [h] was taken for hovering performance. A first weight estimation for the battery pack can be made using the following relationship:

$$m_{battery} = \frac{P \cdot 0.4}{240}$$

For the duct and wing weight, the wing weight was set 20 [kg] for a wing that has to produce 300 [kg] of lift, regardless of the rotor diameter. The circumference of the rotors increases linearly with increasing rotor diameter. Therefore the duct weight was also set to increase linearly for an increasing rotor diameter. The structure weight is estimated by calculating the required moment of inertia for a cantilever beam.

$$\delta_{max} = \frac{FL^3}{3EI} \tag{7.2}$$

$$\theta = \frac{FL^2}{2EI} \tag{7.3}$$

Longer beams will require a larger moment of inertia for a given deflection and will therefore get proportionally heavier for a larger structure. Then the weights of these sub-components were added up. The optimal rotor size is found at the minimum total weight.

[1] URL: https://voltaplex.com/panasonic-b-20700-battery-ncr20700b [Cited 17 June 2018]

Contra rotating propellers After the trade-off was performed it was decided that the hover-bike shall have contra rotating propellers. Contra rotating propellers have several advantages and disadvantages over traditional single propellers. Single propellers create quite a bit of tangential and rotational airflow, which is wasted energy because these air flows are not in the same direction as the thrust. Contra rotating propellers reduce the tangential and rotational airflow, making them more efficient than single propellers. J.S. Vanderover and K.D. Visser showed efficiency improvements of 9% to 17% when contra rotating propellers are implemented on a commercial passenger aircraft [61]. The disadvantage of contra rotating propellers is that they produce more noise than single propellers. In axial direction the noise level increase by as much as 30 dB and 10 dB in tangential direction [61].

Ducts The effects of ducts on the design of the hover-bike have been studied in chapter . A lot of studies have been done on ducted propellers and it was shown that ducted propellers have a lot of potential. Efficiency gains of 29% are achievable for ducted propellers where the duct has constant diameter over open propellers. However in this case the duct propeller combination is perpendicular to the airflow [55]. When the duct propeller combination is parallel to the airflow the efficiency gain goes down to 0%. Therefore the relation between the duct efficiency and flight angle becomes.

$$\eta_{duct} = sin(\alpha_{body}) \cdot 29\% \tag{7.4}$$

In this equation the positive angle α_{body} points down. The flight angle is calculated by taking the tangent of F_x over F_y, which is easily visualised by looking at Figure 7.1b. Then Equation 7.4 becomes:

$$\eta_{duct} = sin\left(arctan\left(\frac{F_x}{F_y}\right)\right) \cdot 29\% \tag{7.5}$$

7.1.2. Motors

The final concept was chosen to have electric engines. Nowadays two main engines exist for the purpose of a hover-bike. These are brushed motors and brushless motors. Both of these engines require a direct current which is what the battery pack will deliver. The main difference is the rotor, the part which is rotating. In brushed motors a coil is used as a rotor which is spinning in a magnetic field; the current in the coil is mechanically switched. This makes up for an easy design, hence inexpensive, but more maintenance is required. In brushless motors the magnets and coils are reversed, therefore the magnets are now rotating. With these motors less maintenance is required, and the lifetime is longer and the efficiency is higher. Only the cost is increased due to the higher complexity and the controller needed to operate the engines. [2]
Brushless motors are used in UAV's, para gliders and RC aircraft, for this reason and the above mentioned benefits the hover-bike is chosen to have brushless motors to drive the propellers. Six engines are required since we have 3 counter rotating pairs of propellers.

7.1.3. Power estimation

The power that will be consumed by the engines has to be estimated for the two different configurations of the hover-bike. The hover-bike can be configured with the wing and ducts installed for better range and endurance, and the wing and ducts can be removed for better manoeuvrability. The range and endurance are estimated by calculating the thrust that is required to overcome the drag and the weight. The total thrust required by the engines is determined by the sum of forces during flight. The drag is in the horizontal direction and the force in vertical direction is necessary to keep the hover-bike in the air, as can be seen in Figure 7.1b. Then the total thrust is calculated by using the Pythagorean theorem. Where T is the total thrust required.

$$T = \sqrt{F_x^2 + F_y^2} \tag{7.6}$$

Furthermore the maximum endurance is achieved when the drag is minimal and maximum range is achieved when the drag over speed is minimal, as can be seen in Figure 7.1a. The drag values and the respective speeds for the endurance and range were derived in the aerodynamics analysis Equation 7.1.1. When the hover-bike is configured for maximum performance the total thrust required is determined by the mass of the hover-bike times the thrust to weight ratio. The thrust to weight ratio is a unit-less factor that was determined in the midterm report [42]. Then the total thrust becomes

$$T = m \cdot g \cdot \left[\frac{T}{W}\right] \tag{7.7}$$

[2] URL: http://www.quantumdev.com/brushless-motors-vs-brush-motors-whats-the-difference/ [cited on 18-6-2018]

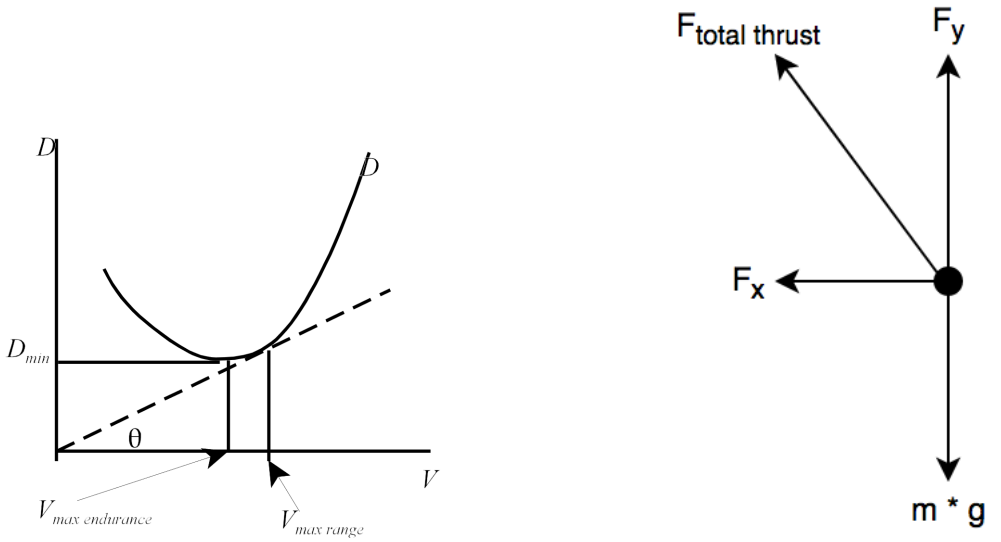

(a) (b)

Figure 7.1: Schematics for determining maximum endurance, where (a) shows the drag versus velocity graph with optimal velocities for endurance and range [3] and (b) the force equilibrium during flight.

Power required The power required is estimated by using the disk actuator theory. The disk actuator theory is a mathematical model of an ideal actuator disk. This theory is extensively used to determine the required power for helicopters. The momentum theory uses the following assumptions in order to model the rotor disk:

- The total area is modelled as a single actuator disk adding momentum to the flow.
- The flow is steady, inviscid, incompressible and unrotational.
- The flow is one dimensional and uniform through the rotor disk.
- The rotor disk is modelled as an infinitely thin disk
- The disk loading of the rotor is uniform

The ideal power is related to the thrust and disk area through Equation 7.8 [24]. In this equation T is the thrust that is required, ρ is the air density and A is the disk area. Equation 7.9 is an equivalent form of Equation 7.8, by substituting the disk loading into the equation. The disk loading is defined as the amount of kilograms per square metre of disk area, $D.L. = \frac{m}{A}$. The thrust is then rewritten as $T = m \cdot g$, and this leads to the equivalent form of Equation 7.8. A uniform disk loading means that the power required will scale linearly with increasing the area of the rotors. The thrust is defined as $T = m \cdot g$.

$$P_{ideal} = \sqrt{\frac{T^3}{2 \cdot \rho \cdot A}} \tag{7.8}$$

$$P_{ideal} = T \cdot \sqrt{g} \cdot \sqrt{\frac{D.L.}{2 \cdot \rho}} \tag{7.9}$$

Figure of merit The disk actuator theory calculates the ideal power that is required for a certain amount of thrust and disk area. In real life there are losses when a rotor disk accelerates air. The losses include:

- Rotor tip losses
- Viscous effects of the flow
- The inner part of the rotor is less effective

The figure of merit (F.M.) is defined as the ideal power over the actual power. The figure of merit is an efficiency factor that encompasses the losses that occur when a rotor accelerates air. With the figure of merit the actual power can be calculated from the ideal power. The figure of merit can be at most 1, in case of an ideal rotor. An inefficient rotor would have a figure of merit of 0.5, and a well designed rotor a figure of merit of 0.8 [24]. Therefore a design figure of merit of 0.6 was chosen. The figure of merit is dependent on many aspects of the rotor design, such as blade taper, blade twist, lift coefficient of the blades, number of blades and pitch of the blades. To find the figure of merit via analytic methods is beyond the scope of the of the project, therefore [24] was used as a reference for the figure of merit.

$$F.M. = \frac{P_{ideal}}{P_{propeller}} \tag{7.10}$$

Substituting Equation 7.8 into Equation 7.10 gives the following equation for the actual power:

$$P_{propeller} = \sqrt{\frac{T^3}{2 \cdot \rho \cdot A}} \cdot \frac{1}{F.M.} \tag{7.11}$$

[3] URL:http://www.dept.aoe.vt.edu/~lutze/AOE3104/range&endurance.pdf [cited 24 may 2018]

Flight time The flight time is dependent on the available battery mass, the energy density (u) of the batteries and the actual. Then the flight time is given by the following formula:

$$t_{flight} = \frac{m_{battery} \cdot u_{batt}}{P_{propeller}}$$
$$t_{flight} = m_{battery} \cdot u_{batt} \cdot F.M. \cdot \sqrt{\frac{T^3}{2 \cdot \rho \cdot A}}^{(-1)} \tag{7.12}$$

The flight time is calculated by adding battery mass in steps of 10 kg to the hover-bike without any batteries. Additional batteries make hover-bike heavier, but they also provide more energy for the engines and systems, increasing the flight time. At some point the penalty of adding weight will surpass the benefit of providing more energy. Under such circumstance, adding batteries will only reduce the flight time.

7.1.4. Power distribution

Next to the electric engines, there are several other subsystems which will need power. These are identified in subsection 5.2.1 where the hardware block diagram is shown. Here it can be seen that the human machine interface, communication system, control system, safety system and operational system also need power. For determining the power required by these subsystems, some reference systems has been looked up. The cable losses were estimated by an online tool[4], and came out to be 0.58%. Because 0.58% is very low the cable losses were ignored in the method to calculate the power.

7.1.5. Battery pack

During mid-term a first weight estimation of the battery package was made. The battery weight was solely based on energy density of a battery cell. After an estimation was made on how much energy was needed in total during flight, a first battery weight estimation could be made. Using a energy density of 500 W/kg and an approximation for the total energy to be 100 kWh, the mass of the battery pack was estimated to be around 200 kg[42].
In this first weight estimation a number of things were not taken into account. The battery should not only be capable of storing enough energy, but it should also be capable to provide enough power, i.e. it should be able to discharge fast enough. Secondly the battery cells used in the weight estimate, the Licerion[5], is not available for the market yet. The first cells can be expected to reach the market in late 2018. However, those cells are then just provided to a select group of partners first[6]. This means that the cells are not yet been flight proven and that the long term performance is not yet known. Thirdly the total amount of energy used during flight, used to determine the battery size, is a rough estimate. For a more detailed design a more accurate value is needed.

Battery cells The battery pack should be as lightweight as possible but still be capable of providing enough power and store enough energy. Therefore, to come up with the most optimum design it is important to look at the cell mass, the cell capacity and the maximum current that can be drawn from the cell. Next to having good technical performance the battery cell should preferably currently be available and have proven itself. Firstly, due to the constraint **HB-CS-ST-19**, which states that the design should be finished before 2020, the design of the hover-bike is on a tight schedule. Therefore, already proven technology is preferred for the design of the battery pack. Secondly, looking at the cost constraint, **HB-CS-ST-07**, the production cost for the prototype shall not exceed €100,000.-. Therefore, when using already available battery cells the total price of the battery pack can be reduced.
Table 7.1 gives a overview of all different battery cells that were considered in the design process are given. It shows all the the technical performance of the cells.

Table 7.1: Battery cells that were taken into account during the design process.

Battery cell:	Capacity [Ah]:	Max. continuous discharge current [A]:	Peak discharge current [A]:	Energy density [Wh/kg]:	Cell mass [g]:
LG M42 20650[7]	4.20	15.0	26	263	58
Panasonic-Sanyo 18650 (NCR18650GA)[8]	3.50	10.0	*Not avialable*	278	46
Samsung 30Q 18650[9]	3.00	15.0	20	228	48
Panasonic B 20700[10]	4.25	20.0	35	242	63
Samsung INR 21700 30T[11]	3.00	10.0	35	159	68
Samsung 25R 18650[12]	2.5	20.0	*Not avialable*	200	45
LG HB6 18650[13]	1.5	30.0	*Not avialable*	126	43
LG HG2 18650[14]	3.0	20	*Not avialable*	228	48

[4]URL:https://photovoltaic-software.com/DC_AC_drop_voltage_energy_losses_calculator.php[cited 24-06-2018]
[5]URL: https://sionpower.com/products/ [Cited 15 June 2018]
[6]URL:https://sionpower.com/2018/sion-power-announces-launch-of-its-groundbreaking-licerion-rechargeable-lithium-battery/ [Cited 15 June 2018]
[7]URL: https://voltaplex.com/lg-m42-20650-battery-20650m42 [Cited 13 June 2018]
[8]URL: https://www.orbtronic.com/18650-battery-3500mah-li-ion-high-drain-panasonic-sanyo [Cited 13 June 2018]
[9]URL: https://www.orbtronic.com/samsung-18650-30Q-3000mah-15a-high-drain-battery-flat-top [Cited 13 June 2018]
[10]URL: https://voltaplex.com/panasonic-b-20700-battery-ncr20700b [Cited 13 June 2018]
[11]URL: https://lygte-info.dk/review/batteries2012/Samsung%20INR21700-30T%203000mAh%20%28Gray%29%20UK.html [Cited 13 June 2018]

Battery pack layout A battery package is a set of battery cells arranged in such a way that it can provide enough power and store enough energy. The cells can be arranged in series or in parallel. Placing the cell in series increases the voltage of the battery pack, while placing the cells in parallel increases the maximum current of the battery pack. These relationships can be found in equations 7.13 and 7.14 [20].

$$U_{Batt} = N_{Series} \cdot U_{Cell} \tag{7.13}$$

$$I_{Max,Batt} = N_{Strings} \cdot I_{Max,Cell} \tag{7.14}$$

In these relationships N_{Series} and $N_{Strings}$ are the number of battery cells in series and parallel, respectively, U_{Batt} the battery voltage, U_{Cell} the voltage of a individual cell, $I_{Max,Batt}$ the max current output of the battery and $I_{Max,Cell}$ the maximum current output of a individual cell.
Using these relationship a first design of the battery layout can be made. For this initial layout only the power requirement has been taken into account. Therefore, after the initial layout is set up, the battery pack energy has to be compared to the required energy for flight. For the energy analysis of the battery pack equation 7.15 is used, where $E_{battery}$ is the total battery energy in Wh, N_{Cells} the number of cells, C_{Cell} the cell capacity, U_{Cell} the nominal cell voltage, η_{Batt} the battery efficiency and f_{Usable} the maximum depth of discharge. The theoretical maximum performance of the battery is achieved if the depth of discharge is 100%. This, however, using the full capacity of the battery will reduce the lifespan of the battery drastically[45].

$$E_{battery} = N_{Cells} \cdot C_{Cell} \cdot U_{Cell} \cdot \eta_{Batt} \cdot f_{Usable} \tag{7.15}$$

[12] URL: https://www.imrbatteries.com/samsung-25r-18650-rechargeable-battery/ [Cited 13 June 2018]
[13] URL: https://www.imrbatteries.com/lg-hb6-18650-1500mah-30a-flat-top-battery/ [Cited 13 June 2018]
[14] URL: https://batterybro.com/blogs/18650-wholesale-battery-reviews/57179459-lg-hg2-review-20a-3000mah [Cited 13 June 2018]

7.2. Iterations

Iterations in the design occur due to the fact that there is a lot of interference between each components. When a different battery technology is used, a larger battery pack is needed, which means that the maximum take-off weight will increase or that other components have to become lighter.

7.2.1. Rotor sizing

Following from the results outlined in subsection 7.3.1, iterations on the rotor size were not deemed necessary. The 3 main reasons for this are given below.

- **No major changes in overall mass budget**
  Since no major changes in the overall mass budget occurred during the design phase, the individual effect of changing subsystem masses on the rotor size is not significant.
- **Broad range of optimal rotor size for minimum mass**
  According to the analysis, the total mass of the vehicle is not very sensitive to changes in the rotor diameter. A rotor diameter 20 cm below or above the optimal diameter, will result in a total mass increase of only 7kg. This is visually shown in Figure 7.2.
- **Geometrical constraints**
  Next to optimising rotor size for minimal mass, geometrical constraints also need to be taken into account. The obtained rotor size in the analysis gives a small enough structure for easy transportability, while maintaining enough space inside the structure to accommodate all subsystems and the pilot. Changing the rotor size significantly might interfere with these constraints. The vehicle size is further explored in chapter 8

7.2.2. Power estimation

The estimated power required depends heavily on the weight of the hover-bike, because the wings only provide partial lift. When the power required changes, the need for battery energy changes and this will affect the battery mass. A different battery size will affect the total mass of the hover-bike and a different total mass will affect the battery size again. This interaction between battery mass and total mass of the vehicle causes a loop in the calculations of the required power. Several iterations were performed to test the effect of making the hover-bike lighter or by changing the lift production of the wing. It can be seen in Table 7.2 that the hover-bike mass in the second column is affected by the change in battery mass in the third column. Eight or nine iterations are necessary to find the new battery mass, when the base weight of the hover-bike has changed.

Table 7.2: Iterations of hover-bike mass by changing total weight

Hover-bike weight decreases by 15 kg		
# iteration	Hover-bike mass [kg]	Battery mass [kg]
0	500.0	187.7
1	485.0	180.3
2	477.6	176.6
3	473.9	174.8
4	472.1	174.0
5	471.3	173.4
6	470.7	173.3
7	470.6	173.2
8	470.5	173.2
	470.5	

Hover-bike weight increased by 15 kg		
# iteration	Hover-bike mass [kg]	Battery mass [kg]
0	500.0	187.7
1	515.0	195.3
2	522.6	199.2
3	526.5	201.3
4	528.6	202.3
5	529.6	202.9
6	530.2	203.2
7	530.5	203.3
8	530.6	203.4
9	530.7	203.4
	530.7	

The above table shows how sensitive the required battery mass is when the mass of other components grow. During the design of hover-bike at first a wing lift of 50% was chosen. At 50% the wing does not have to produce a lot of lift, making it smaller and lighter. However during the sizing of the battery it turned out that the range and endurance requirements would not be met. Therefore an major iteration was done to increase the wing lift to 62%. In subsection 7.3.3 the results for the range and endurance are presented for a wing lift of 62%.
The drag, wing lift and lift from the propeller determine the flight angle of the hover-bike. The flight angle of the hover-bike influences the aerodynamic drag of the hover-bike. Therefore an iteration took place between the aerodynamics group and the power and propulsion group. The interaction between the aerodynamics group and power and propulsion group is visisble in the N2 chart. The power and propulsion group gave a new flight angle and necessary wing lift, and the aerodynamics group gave an aerodynamic drag in return. This iteration gave an flight angle of 33.1° and an necessary wing lift of 62%. Together with the aerodynamic drag the flight time became 60.2 minutes.

7.2.3. Battery

During the design process of the battery a number of small iterations were performed. The first (minor) iteration that was performed in the the design process was on the battery layout. Before the first iteration was performed, a first design was generated to meet the power requirement given from the engine choice.

Using the relationship between maximum power use of the engine ($P_{max,eng}$), the operational voltage (U_{eng}) and the maximum current ($I_{max,eng}$) given by equation 7.16 the maximum current that would be drawn from the batteries can be calculated. Using the equations 7.13 and 7.14 a first layout was designed to meet the power requirement. After a first design was made, the battery layout was checked if it would meet the energy requirement. If it did not meet the energy requirement another string of cell was added to the battery pack. In this way the minimum amount of cells was used in the design which would meet both the power and the energy requirement. If the energy requirement was met with the first design it would mean that the battery could not optimised for the energy requirement.

$$P_{max,eng} = U_{eng} \cdot I_{max,eng} \tag{7.16}$$

For the first design the cell with the highest energy density (*Panasonic-Sanyo 18650*) was used. This resulted in a battery mass of 203 kg. This was too heavy for the hover-bike. Therefore, different cells were considered as well. A list of battery cells is given in table 7.1. From this the cells with best numbers on capacity, energy density and cell mass were considered. After this iteration it was found that the *Panasonic B 20700* battery cell gave the most optimal battery mass.

7.3. Results

The results of the methods explained in section 7.1 are shown in this section. Results are included of the propeller sizing, engines, power estimation, power distribution and the battery pack.

7.3.1. Propeller sizing

The results of the propeller sizing analysis are shown in Figure 7.2 with further elaboration given below.

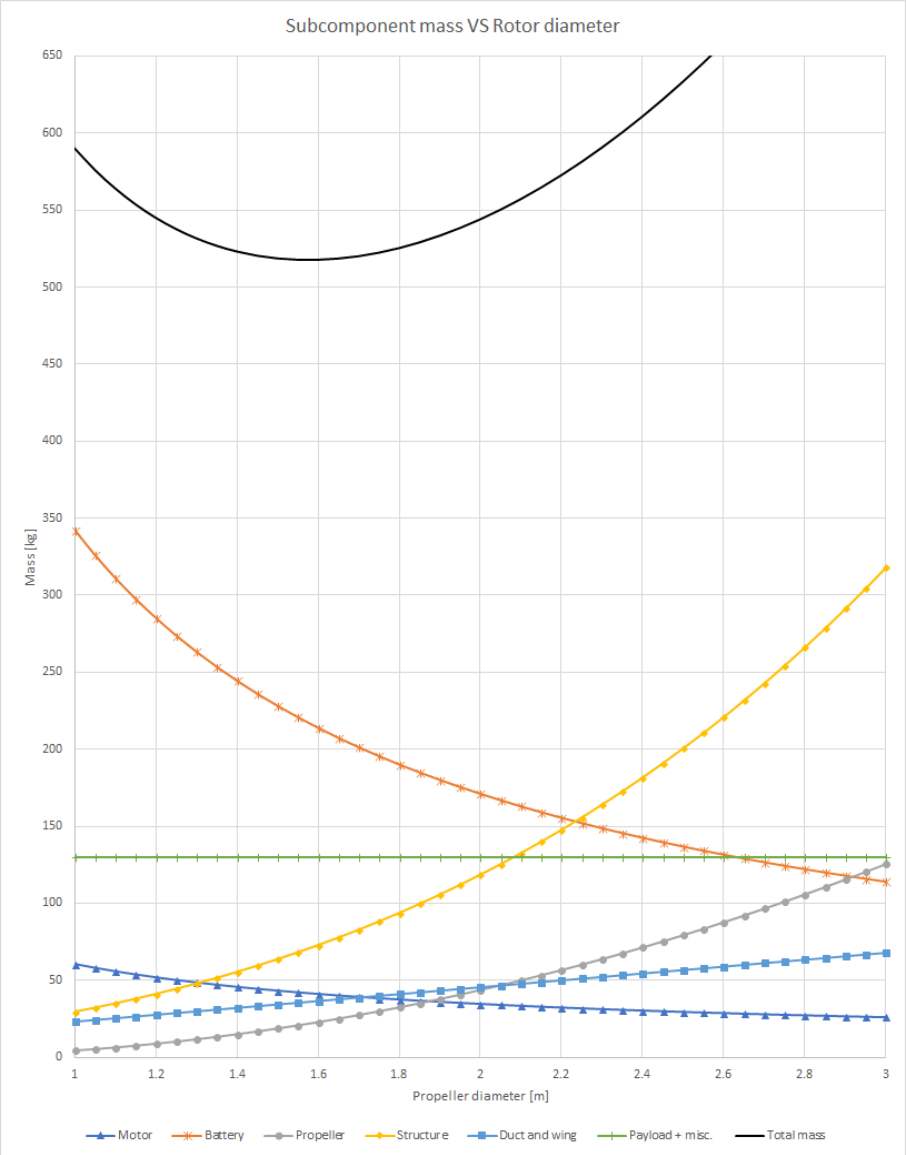

Figure 7.2: Weight vs propeller diameter

Figure 7.2 shows the behaviour of the weight when the propeller sized is changed. When the weight of the different aspects

are added a minimum mass was found for a propeller diameter of 1.6 m. It can be seen that the battery mass and structure mass have the biggest influence on the weight. The mass of the all the components added together follow a parabolic trend, where the minimum of the parabola is very broad. Meaning that when a slightly larger or smaller propeller size is necessary, the weight in not much affected. The reference data for the propeller weight and engine weight with respect to the diameter of the propeller are given in Appendix A.

7.3.2. Motors

As explained in the method, the hover-bike was chosen to have electrical DC brushless motors. Due to time constraints an off-the-shelf electrical engine has been chosen. In Table 7.7 the required output power for all engines combined was calculated and came out to be 253.7 kW. This means that each engine has to deliver 42.3 kW. So an engine which is capable of meeting this requirement has been chosen. This engine is normally used for paragliding and its specifications can be found in the table below. The power output of this motor is rated at 50 kW which is more than 42.3 kW. This brings an safety factor into the design, because this way one can be sure that enough power can be delivered.

Table 7.3: Electrical engine specifications [15]

Parameter	Value
P_{max}	50 kW
I_{max}	500 A
R	140 mΩ
Radius	154 mm
Height	115.54 mm
Weight	5.9 kg

Furthermore to calculate the power required, the input power of the motors should be known, which is dependent on the efficiency. Electric motor efficiencies are relatively high, especially brushless motors do not waste a lot of energy (comparing it to brushed engines). The efficiency of brushless motors is around 90%, this value will be used in the power calculation[16]. Since six engines will be used for the hover-bike the total weight for the engines will be $6 \cdot 5.9 = 35.4$ kg. Brushless engines do need a controller, one is required for each engine. An electronic speed controller has been chosen which is capable of delivering the power required to the engines[17]. These controllers will weigh about 1.2 kg each, so 7.2 kg in total.
The total weight of the motors and controllers will be 35.4 + 7.2 =42.6 kg.

7.3.3. Power estimation

The drag has a large influence on the range and endurance of the hover-bike, because the drag has to be overcome by the propellers and engines. The data for the drag of the hover-bike is given in Table 7.4, which was determined in the aerodynamics analysis in Equation 7.1.1. The method described in subsection 7.1.3 applies to aircraft, where the maximum range is equal to $(D/V)_{min}$. In the case of the hover-bike this is not true, because the wings are fixed at an angle. When the speed is increased the flight angle becomes bigger, because the propellers have to produce more thrust by tilting forward. This decreases the angle of attack of the wings, which lowers the produced lift, and lower lift from the wings means that the propellers have to produce more lift. This increases the power consumption and the range will actually reduce. Therefore the range is defined at the maximum endurance. This gives a minimum range that can be achieved by the hover-bike.

Table 7.4: Drag values for endurance

	Drag [N]	Speed [m/s]
Endurance	1217	29.3

Table 7.5 shows the data that is input for the thrust and power that have to be calculated. The rotor diameter is determined in subsection 7.3.1, the thrust to weight ratio was determined in the midterm report [42] and the figure of merit was determined by using literature in subsection 7.1.3.

Table 7.5: Input data

mass	500 [kg]
Air density	1.225 [kg/m^3]
Gravitational acceleration	9.81 [m/s^2]
Rotor diameter	1.6 [m]
Thrust to weight ratio	1.7
Figure of merit	0.6

[15] URL: www.reacherbrushless.com/product/45KW-motor.html [Cited 19-06-2018]
[16] URL: http://www.quantumdev.com/brushless-motors-vs-brush-motors-whats-the-difference/ [Cited 18-6-2018]
[17] URL:https://www.alibaba.com/product-detail/2018-MP15470-35KW-Outrunner-Brushless-Motor_60764122235.html?spm=a2700.7735674.35.11.M9QVwk [Cited 19-06-2018]

Substituting the numbers from Table 7.4 and Table 7.5, the total thrust and the actual power can be calculated by using Equation 7.6, Equation 7.7 and Equation 7.11. The results are shown in Table 7.6, where it can be seen that the thrill mode of the hover-bike requires considerably more thrust and power. Which is to be expected because in this mode the hover-bike is configured for maximum accelerations. The maximum take-off weight in thrill mode is lighter than eco mode, because the wing and ducts are removed.

Table 7.6: Propeller power

	Thrust [N]	$P_{propeller}$ [kW]
Endurance	2226.0	45.5
Thrill mode	7504.7	281.7

Power calculations When the efficiencies of the contra rotating propellers (CRP), ducts, engines and battery are included then the power required and battery power become less. The power required is defined as the power that the engines need to deliver. The battery power is defined as the power output of the batteries. The efficiencies of the ducts and contra rotating propeller have a positive influence and the efficiencies of the motor and batteries have a negative influence.
The efficiency of the duct is dependent on the flight angle. Using Equation 7.5 the duct efficiency for the endurance becomes 15.85% respectively. In the mode for maximum performance the ducts are removed and therefore the efficiency gain is 0%.
The efficiency of contra rotating propeller over single propellers can vary from 9% to 17%. Because the exact gain could not be estimated analytically an improved efficiency of 10% was chosen, to keep the calculations conservative.
The efficiency of the motors is around 90% which is shown in subsection 7.3.2. The same can be said for the batteries, because the discharge efficiency of batteries is relatively high. The charge/discharge cycle efficiency of lithium-ion batteries is around 90% [18]. Therefore it is assumed that the discharge efficiency is 95%. When all the efficiencies are combined the battery power is calculated via the following relation and the results are shown in Table 7.7.

$$P_{battery} = \frac{(1-\eta_{crp})\cdot(1-\eta_{duct})}{\eta_{motor}\cdot\eta_{battery}} \cdot P_{propeller} \tag{7.17}$$

Table 7.7: Power required

	$P_{propeller}$ [kW]	η_{duct}	η_{crp}	P_{motor} [kW]	η_{motor}	$\eta_{battery}$	$P_{battery}$ [kW]
Endurance	45.5	15.85%	10%	34.5	90%	95%	40.3
Thrill mode	281.7	0%	10%	253.7	90%	95%	296.7

Flight time When the required battery power is known the flight time can be calculated by dividing the available battery energy over the battery power. It can be seen from the power numbers that the maximum performance case will have very little flight time due to the high power consumption. The weight of the hover-bike without the battery is 315 kg, which is deduced from the mass breakdown chapter 8. Then adding batteries in steps of 10 kg gives the following flight times for endurance. The batteries provide energy but also add weight, which means that there will be an optimum for the battery weight. It turned out that the flight time for endurance is 60.2 minutes. This excludes 2 minutes of vertical take-off and landing (VTOL) flying procedures, meaning that there are 62.2 minutes of flying in total. The endurance is called transportation mode, because the wing and ducts are attached to the hover-bike. The mode for maximum performance is called thrill mode. Both these modes are more thoroughly explained in section 3.1.
To calculate the time for the thrill mode, the weight of the hover-bike becomes less. The weight without the ducts, wings and batteries becomes 260 kg. The weight reduction is also visible in Figure 7.3. Then the flight time for thrill mode becomes 9.8 minutes. Also in this case the 2 minute flight time of VTOL is not included, meaning that the total flying time will be 11.8 minutes.

[18] URL: http://large.stanford.edu/courses/2010/ph240/sun1/ [Cited 19-6-2018]

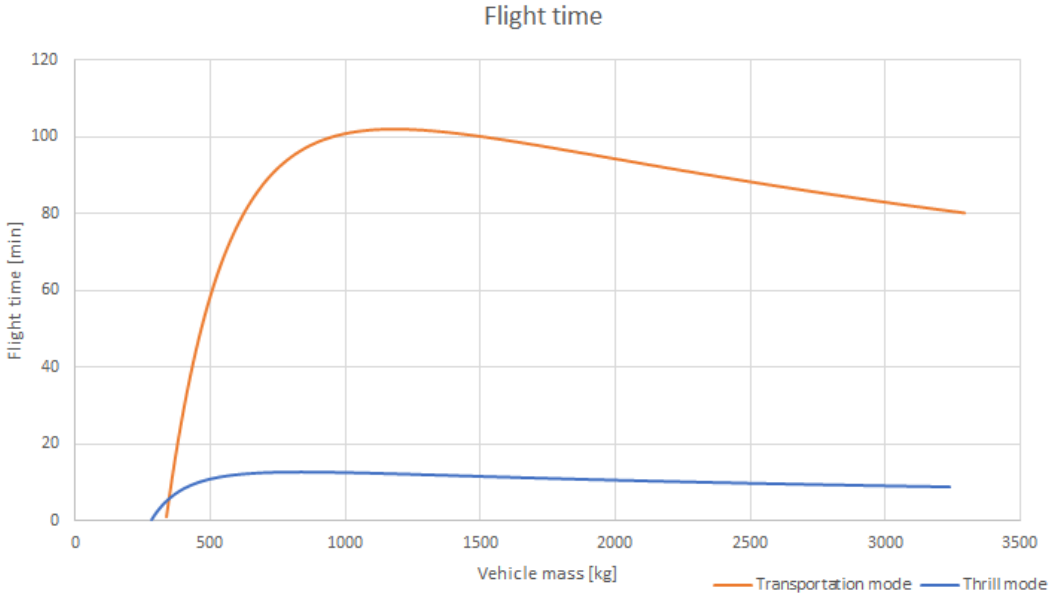

Figure 7.3: Flight time for transportation mode and thrill mode

It has to be noted that the hover-bike could potentially have more flight time, especially when the hover-bike is in transportation mode. But then the hover-bike will become considerably heavier, because the weight would become 1175 kg. Which means that the hover-bike would not meet the weight requirement. Furthermore it would hamper the accelerations, due to the higher mass and moments of inertia.
Finally the range is calculated by multiplying the flight time for endurance with the speed. This means that the range is equal to $R = 60.2 \cdot 60 \cdot 29.3 = 105 km$. The top speed was determined in Equation 7.1.1 and was 55 m/s, with a flight time of 9.8 minutes the range is equal to $55 \cdot 9.8 \cdot = 32 km$

7.3.4. Power distribution

As explained in the method there are more subsystems than the engines which require power, these systems can be found below with the power consumption. Similar systems were looked up as a reference to come up with estimated about the power consumption.

Table 7.8: Subsystem power distribution.

Subsystem	Power [W]	Voltage [V]
LCD screen [19,20]	4.5	5.5
Lights [21]	35.0	14.8
Flight data recorder (black box)[22]	5.0	28
Safety ecu [23]	5.0	5.0
FLARM [24]	0.7	16.0
Joybar [25]	4.5	5.0
Flight controller [26]	8.0	5.0
Transmitter/receiver [27]	5.9	13.8
Total	68.6	93.1

As can be seen the total required power by all the subsystems is 68.6 W. This is relatively low compared to what the engines require 253.7 kW as can be seen in Table 7.7. Therefore the subsystems will not greatly influence the battery size of the hover-bike. For this reason the power required of these subsystems is insignificant and therefore is neglected with respect to the total power requirement.
The subsystems are powered via a power distribution system and a separate battery, as can be seen in Figure 7.4. The power distribution system has multiple transformers that change the voltage for each subsystem. It was found in literature that

[19] URL:https://www.rtings.com/tv/learn/led-oled-power-consumption-and-electricity-cost [Cited 18 June 2018]
[20] URL:https://focuslcds.com/journals/lcd-voltage-inputs-for-lcd-displays-explained/ [Cited 25 June 2018]
[21] URL:http://aviolights.com/navigator-ultra-360.html [Cited 25 June 2018]
[22] URL: http://l3comm.us/products-services/docoutput.aspx?id=1650 [Cited 18 June 2018]
[23] URL: http://www.efitechnology.com/R4_ECU.html [Cited 18 June 2018]
[24] URL: http://lxnavigation.com/downloads/manuals/Flarm/Flarm-red-Box-SD-IGC-26-6-2013.pdf [Cited 25 June 2018]
[25] URL: https://en.wikipedia.org/wiki/USB#cite_note-70 [Cited 18 June 2018]
[26] URL: http://www.efitechnology.com/X3_ECU.html [Cited 18 June 2018]
[27] URL: http://www.xcom-usa.com/manuals/XCOM-Users-Manual-2.3.pdf [Cited 18 June 2018]

DC/DC converters have an efficiency of around 90% [28]. These DC/DC converters transform the voltage from the battery to the required voltage of each subsystem. The separate battery will have a back-up battery to make sure that the subsystems of the hover-bike are operable. Then the combined subsystem batteries will have a capacity of $\frac{2 \cdot 68.6}{0.9} = 152.4 Wh$. The following figure show the wiring diagram for the electrical system of the hover-bike. The voltages are included and flow direction of the current are included.

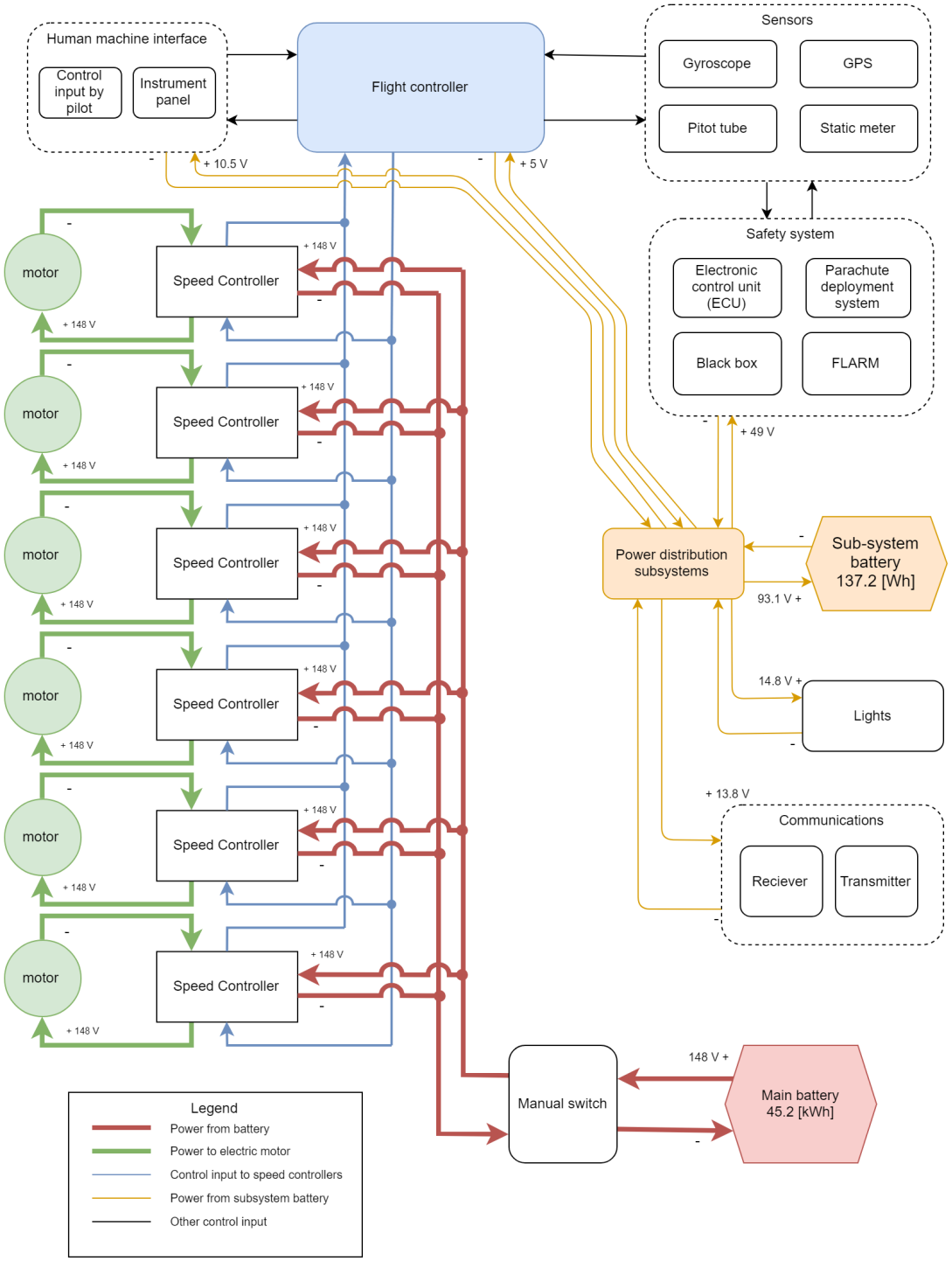

Figure 7.4: Wiring diagram

7.3.5. Battery pack

After the different cells, mentioned in Table 7.1, have been compared a final design is found. In the final design for the battery pack the *Panasonic B 20700* battery cell will be used. To be able to provide enough power and store enough energy, the total battery pack will need a total of 2920 cells. The cells will be arranged such that it consist of 73 strings which consist of 40 battery cells. The maximum power output of the batteries is 371 kW and the battery energy is 45.2 kWh. This meets both the power requirement and the energy requirement.

The battery pack will be divided in two separate battery packs. This will increase the ease of handling and the maintainability. Each battery pack will weight 92 kg and the battery will be cubical shaped with the sides being 35 cm. The operational

[28] URL:`https://www.maximintegrated.com/en/app-notes/index.mvp/id/3166` [cited 28 june 2018]

temperature range on which the battery pack can operate is determined by the minimum and maximum temperature on which the cells can operate. The operational temperature range is between −20.00 °C and 60.00 °C.

Battery charging After the hover-bike is used for flight, the battery has to be recharged. To increase the ease of use of the hover-bike it is important to make it as universal as possible. Therefore, the hover-bike makes use of the *Type 2 connector* to connect the hover-bike to the charger. This connector type is one of the most used connector types for electric vehicles in Europe[29]. This connector is capable of providing a maximum power output 43 kW.
The battery pack will be able to store 45.2 kWh. This battery size is comparable to the battery size of a *Renault Zoé*, which has a battery size of 41.0 kWh[30]. The time to charge this cars is about two hours, when a fast-charger, which has a power output of 22 kW, is used. Therefore, when using the *Renault Zoé* as reference vehicle, the hover-bike will have an estimated charging time of about two hours. However, this is only possible if the charger can to charge the hover-bike in about two hours if a 22 kW is available. Most charging points at houses will be rated at 3 kW, which increases the charging time with more than 7 times.

7.4. Verification and Validation

In this section the verification and validation of the methods used are performed. Verification and validation is needed to make sure the right tools or equations are used for the analysis.

7.4.1. Method verification

To calculate the thrust, power and battery mass excel sheets were used. Using excel sheets allows to quickly recalculate output variables when one of the input variables changes. Mistakes easily occur when typing in formulas into excel, because of the interface of excel. Therefore each calculation is tested by changing the input values.

- By increasing the figure of merit to 1.2, the real power becomes lower than the ideal power. This is physically not possible, but it shows that the calculation is correct.
- Increasing the battery energy density shows an linear decrease in battery mass.
- Increasing the required thrust shows an linear increase in power required.
- Doubling the rotor area decreases the power required with a factor of $\sqrt{2}$.
- Doubling the rotor diameter divides the power required by 2.

From the outcomes of these tests it can be concluded that the formulae were correctly implemented by comparing the test results with formulae from the momentum theory.

7.4.2. Method validation

Assumptions that were made in the methods used were the following.

- The range and endurance calculations do not include the effects of gusts or other external forces
- The power consumption of other subsystems next to the engines is negligible
- Cable losses are ignored
- The total area is modelled as a single actuator disk adding momentum to the flow
- The flow is steady, inviscid, incompressible and irrational
- The rotor disk is modelled as an infinitely thin disk
- The disk loading of the rotor is uniform

The method used to calculate the thrust, power and battery size does not include the effects of gust. Gust has a negative influence on the energy consumption, and because it is not estimated it would mean that the range and endurance would diminish. Therefore the flight time of 60.2 minutes for transportation mode is only reached on days without wind.
The power consumed by other subsystems such as lights, radio, flight controller, etc.... is very low compared to the power consumption of the engines. The power consumption of the subsystems is only $\frac{68.6}{253700} \cdot 100 = 0.027\%$
The cable losses that were estimated with the online tool were very low subsection 7.1.4. Therefore hand calculations were used to validate the tool.

Table 7.9: Cable data

Cable length	10 [m]
Cable cross-sectional area	185 $[mm^2]$
Resistivity aluminium	2.65×10^{-8} $[\Omega/m]$
Current	305 [A]
Voltage	148 [V]

[29] URL: `https://www.zap-map.com/charge-points/connectors-speeds/` [Cited 18 June 2018]
[30] URL: `https://ev-database.uk/car/1128/Renault-Zoe-R110-ZE40` [Cited 18 June 2018]

Using this data the power loss was calculated via the following method:

$$\begin{aligned} R &= \rho \cdot \frac{l}{A} = 2.65 \times 10^{-8} \cdot \frac{10}{185 \times 10^{-6}} = 0.0014 \quad [\Omega] \\ V_{drop} &= I \cdot R = 305 \cdot 0.0014 = 0.427 \quad [V] \\ P_{final} &= (V - V_{drop}) \cdot I = (148 - 0.427) \cdot 305 = 45009.8 \quad [W] \\ P_{loss} &= 1 - \frac{P_{final}}{P} = 1 - \frac{45009.8}{148 \cdot 305} = 0.3\% \end{aligned} \tag{7.18}$$

According to the hand calculations the power loss is very low in the cables, confirming the earlier result from the online tool that calculated that the power loss will be 0.58%.
The last 4 assumption were made in the momentum theory. These assumptions cause the rotor disk to be idealised. But in reality these effects are still there. Therefore a figure of merit (F.M.) was used to compensate. The F.M. chosen was 0.6 and was more on the conservative side, because highly efficient rotors have a F.M. of 0.75 to 0.80. Figure 7.5 below confirms this. In this figure it can be seen that figures of merit beyond 0.8 are impractical and that a figure of merit of 0.5 is easily achievable. Therefore a figure of merit of 0.6 is deemed reasonable for the hover-bike design.

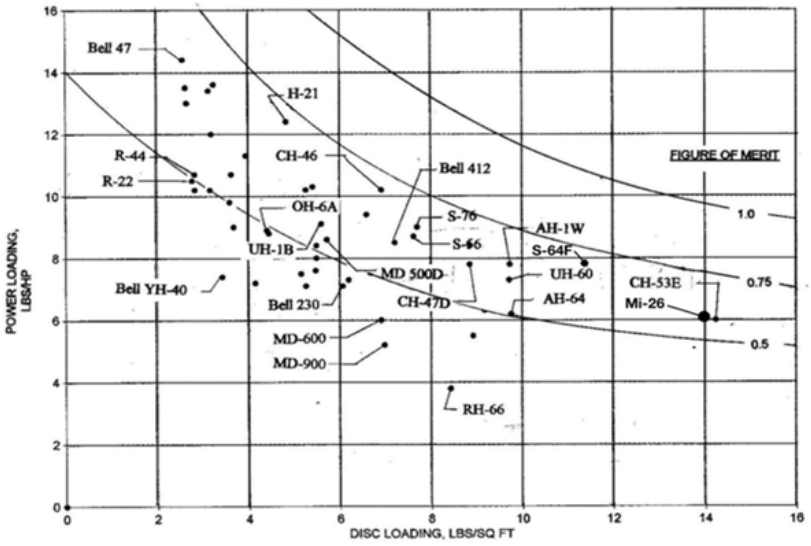

Figure 7.5: Power loading vs disk loading[50]

The method used to estimate the power required for the hover-bike was the disk actuator theory. The disk actuator theory is described extensively in literature for helicopter design. [24]. Helicopters are of different design than the hover-bike, but the hover-bike falls in the same weight category as ultralight helicopters. Therefore the actuator disk theory is tested with the data of a DJI drone. The data is given in Table 7.10. DJI is a manufacturer of high end drones and equipment. Therefore it is assumed that the propellers are engineered to a higher level, giving a higher figure of merit of 0.7 [−] for the rotor disk.

Table 7.10: DJI Inspire 2 data[31][32]

m	3.44 [kg]
g	9.81 [m/s^2]
ρ	1.225 [kg/m^3]
t_{hover}	23 [min]
$E_{battery}$	97.58 [W]
$D_{propeller}$	0.38 [m]
Number of propellers	4 [-]
A	0.454 [m^2]
$F.M.$	0.7 [-]

The thrust that is necessary to hover is given by

$$T_{hover} = m \cdot g = 3.44 \cdot 9.81 = 33.7[N] \tag{7.19}$$

[31] URL:https://www.dji.com/inspire-2/info#specs[cited 24-06-2018]
[32] URL:https://store.dji.com/product/inspire-2-1550t-quick-release-propellers[cited 24-06-2018]

Then the power required to hover can be calculated with Equation 7.11

$$P_{hover} = \sqrt{\frac{T^3}{2 \cdot \rho \cdot A}} \cdot \frac{1}{F.M.}$$
$$P_{hover} = \sqrt{\frac{33.7^3}{2 \cdot 1.225 \cdot 0.454}} \cdot \frac{1}{0.7} = 265.0[W] \tag{7.20}$$

Comparing the outcome with the following power calculation:

$$P_{hover} = \frac{E_{battery}}{t_{hover}} = \frac{97.58}{23/60} = 254.6[W] \tag{7.21}$$

Comparing the different results show that the difference is 265.0/254.6 = 1.04, which means that the results differ only 4% from each other. From these results it can be concluded that the actuator disk theory is not only applicable to helicopters but also to drones and other rotor-craft.

7.4.3. Verification of the battery size

To design the batteries a number of calculations had to be performed. These calculations were done with the use of a Python program. To verify this program a number of inputs were changed.
First the required available energy for the batteries were changed. First this input was increased, which should result in a increase in battery size. The size of the battery should increase by increasing the strings. This was correctly verified. After increasing the energy required, this input was decreased. This should lead to a decrease in battery size till some extend, until the point where the battery size was determined by the power requirement. A comparable procedure was performed with the power requirement.

7.4.4. Validation of the battery size

For validation of the the battery of the hover-bike the results should be compared with real life examples. A good real life example with which the battery pack can be compared is with the battery pack of a *Tesla model S*. The total weight of the battery pack of a *Tesla model S*, with a 85 kWh battery pack, is 540 kg. This results in a energy density of 157 Wh/kg[33]. Comparing this with the energy density of the hover-bike, 245 w/kg, it can be concluded that the real life energy density is lower.
However, the weight used as reference weight includes the weight of the power distribution system and a active cooling system. Therefore, also a comparison is made with a battery pack without the cooling system and the power distribution system. The energy density of a battery pack is 207 Wh/kg[34]. Taking into account that the battery cells used are different it can be concluded that the energy densities are in the same range when looking at package level.

7.5. Requirements compliance

This chapter shortly discusses the range and endurance characteristics of the hover-bike and compares the outcome with the requirements that were established in the baseline report.

7.5.1. Range and Endurance

These performance requirements were established in the baseline report[40].

- HB-FR-ST-02 The hover-bike shall have a minimum range of 100 km while maintaining a 100 km/h speed.
- HB-FR–ST-04 The hover-bike shall be able to fly for at least 1 hour while maintaining a 100 km/h speed.

For endurance and range the flight time is 60.2 minutes at a speed of 29.3 m/s. That means that a distance of 106.2 km will be covered. Then requirement HB-FR-ST-02 is met, because the range is more than 100 km at a speed faster than 100 km/h. The endurance is also met because the hover can fly for more than 1 hour at a speed faster than 100 km/h, therefore requirement HB-FR–ST-04 is met.

7.5.2. Service ceiling

The requirement for the service ceiling is:

- HB-FR-ST-03 The service ceiling will be at least 3000 ft above sea-level.

The service ceiling of the hover-bike is dependent on the density of air at higher altitudes. At higher altitudes the air is thinner resulting into less mass being accelerated by the rotors, which means that more power will be required by the engines. The engines have a very high combined power output of 253.7 kW which means that the hover-bike could potentially fly at very high altitudes. At an altitude of 3000 feet = 914.4 m the air density is 1.121 02 kg/m^3[35]. With an density of 1.121 02 kg/m^3 the flight time is only slightly reduced to 57.3 minutes. That is because the required power only scales with $\sqrt{2}$, when the density is halved. Therefore requirement HB-FR-ST-03 is considered to be met.

[33] URL: `https://en.wikipedia.org/wiki/Tesla_Model_S#Battery` [Cited 20 June 2018]
[34] URL: `https://insideevs.com/tesla-battery-teardown-video/` [Cited 20 June 2018]
[35] URL:`https://www.digitaldutch.com/atmoscalc/` [cited 24-06-2018]

At an altitude of 6000 m the density is 0.6597 kg/m^3, then the flight time for maximum endurance is reduced to 42.5 minutes. Altitude sickness can start to occur in humans at an altitude of 2000 meters[36]. The pilot puts the limit on the service ceiling and not the hover-bike, because the pilot is much more affected due to altitude than the hover-bike. An endurance of 42.5 minutes at an altitude of 6000 meters is within 70.8% of requirement HB-FR–ST-04.

7.6. Sensitivity analysis

In the design of the power and propulsion system a large number of parameters do influence the final design. The main design parameters of the hover-bike that are influenced are the endurance, the performance and the total mass of the hover-bike. Increasing one or more of the parameters will decrease the other parameter. For example, increasing the endurance will increase the mass and reduce the performance of the hover-bike. Therefore, the influence of changing these parameters will be analysed in this section.
Below two lists are given for the input parameters and output parameters.
List of inputs:

- Total hover-bike mass
- Mass budget, heavier components means that there is less space for batteries
- Rotor diameter
- Amount of lift from the wing
- Rotor efficiency, the so-called figure of merit
- The aerodynamic drag
- Energy density of the batteries
- Air density
- Design thrust to weight ratio for the desired performance

List of outputs:

- Endurance in terms of minutes flown
- Range in terms of distance covered
- Required power for maximum thrust

As can be seen, there are quite a lot of inputs to find only a few desired outputs. Each input has it's influence on the design. The governing equation from the momentum theory is the following, which was also derived in subsection 7.1.3:

$$P_{actual} = \sqrt{\frac{T^3}{2 \cdot \rho \cdot A}} \cdot \frac{1}{F.M.} \tag{7.22}$$

The power is directly dependent on the thrust, air density and rotor diameter and figure of merit.
The thrust on it turn is given by the following two equations, depending on the mission profile of the hover-bike.

$$\begin{aligned} T &= \sqrt{Drag^2 + (m \cdot g \cdot (1 - L))^2} \\ T_{max} &= m \cdot g \cdot \frac{T}{W} \end{aligned} \tag{7.23}$$

Here it can be seen that the thrust is dependent on the drag, the mass, thrust to weight ratio and the wing lift. Here the wing lift is a percentage of the mass of the hover-bike. From these three equations a relation can be established as to how much the actual power changes by changing each of these parameters.
The flight time is given by the following equation:

$$\begin{aligned} t_{flight} &= \frac{m_{battery} \cdot u_{batt}}{Power} \\ t_{flight} &= m_{battery} \cdot u_{batt} \cdot F.M. \cdot \sqrt{\frac{2 \cdot \rho \cdot A}{T^3}} \end{aligned} \tag{7.24}$$

By varying the parameters a change in the power consumption and flight time can be deduced. It becomes apparent from Table 7.11 that only a few parameters have a linear relation with the power and flight time. This is also apparent from Figure 7.3 that the flight time does not change linearly. It becomes apparent that the thrust to weight ratio has the largest influence on the output. An increased thrust to weight ratio would mean that the mass would increase by a large margin, pushing the design beyond acceptable limits. The drag and air density have the least influence on the outputs. The drag has less of an impact, because most energy spent by the engines is used to provide upwards thrust. The density has less of an effect, because the density only starts to get low at higher altitudes as 6000 meter.

[36] URL:https://en.wikipedia.org/wiki/Altitude_sickness[cited 24-06-2018]

Table 7.11: Sensitivity of flight time and power

Parameter times 2	Change in Power	Change in flight time
m	2	0.660
$m_{battery}$	1.485	1.557
L	0.481	2.084
$D_{propeller}$	0.500	2
F.M.	0.500	2
D	1.414	0.707
u_{batt}	-	2
ρ	0.707	1.414
$\frac{T}{W}$	2.828	0.356

8
Structure

8.1. Methods

This section will outline the methods that were used in the design and analysis of the Scorpeon structure. The material selection and determination of the centre of gravity and moment of inertia will also be covered.

8.1.1. Geometry constrains and design

The first step to be taken towards sizing the hover-bike is to consider which transportation method is going to be used and how would you operate the hover-bike. In the previous chapter of operations and logistics it was discussed that the hover-bike should be operated by one person and transported using a trailer that only one person with a regular license can tow on normal roads without the need of any special license. Using a normal driving license can tow up to 750 kg without the need of a special license [1].

Moreover, as it is required to transport it on normal roads the width is set to fit in one car lane, which vary between 2.5 m and 3 m with 2.6 m as an average lane width[2]. Moreover, the maximum length was determined by the trailer selection which was 4.2 m in length[3]. In addition for the height there were predetermined maximum height values that can use roads and that was 4m according to the Geneva convention[4].

8.1.2. Material selection

In this section the method of selecting the most suitable material for the hover-bike different components will be discussed. However, as a first step it is required to know the characteristics of the material that is needed by the hover-bike. The material that is required for the main frame of the hover-bike needs to sustain high loads and hence it is required to stiff and strong. Moreover due to cost and mass constrains it is required to be cheap and light.

First, in order to analyse all material possibilities, a tree structure is analysed to assure all materials are presented. The material tree is given in Figure 8.1. The main focus lies on metals and composites only as all other materials do not fulfil the material requirements. In addition, wood is eliminated due to low stiffness and that it can not handle high load manoeuvres. Ceramics were also eliminates as they have brittle features where the material starts shattering apart if loaded in tension. Furthermore, polymers were rejected due to there sensitive behaviour towards heat and there extremely plastic behaviour.

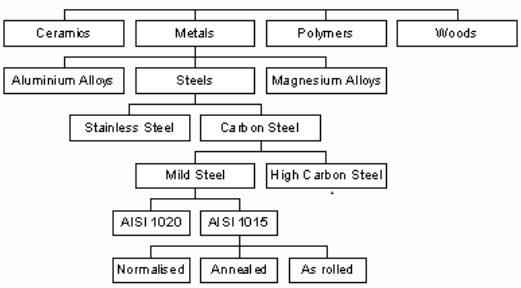

Figure 8.1: Material tree structure [5]

[1] URL: https://www.gov.uk/towing-rules [Cited 23 June 2018]
[2] URL:https://ops.fhwa.dot.gov/FREIGHT/publications/size_regs_final_rpt/size_regs_final_rpt.pdf [Cited 23 June 2018]
[3] URL: http://bigtextrailers.com/70pi-x-tandem-axle-pipe-utility/ [Cited 23 June 2018]
[4] URL: https://tunnels.piarc.org/en/operational-safety-requirements-geometry/vertical-clearance [Cited 23 June 2018]
[5] URL: http://www-materials.eng.cam.ac.uk/mpsite/physics/overview/default.html [Cited 23 June 2018]

The next step after eliminating those materials is to choose which material fits best the requirements profile using Ashby plots. As it can be seen from Figure 8.2a & Figure 8.2b that the best match to the requirements in terms of density, strength, stiffness and price are the metals. This results in elimination of composites due to their high cost and due to their hard joining mechanisms.

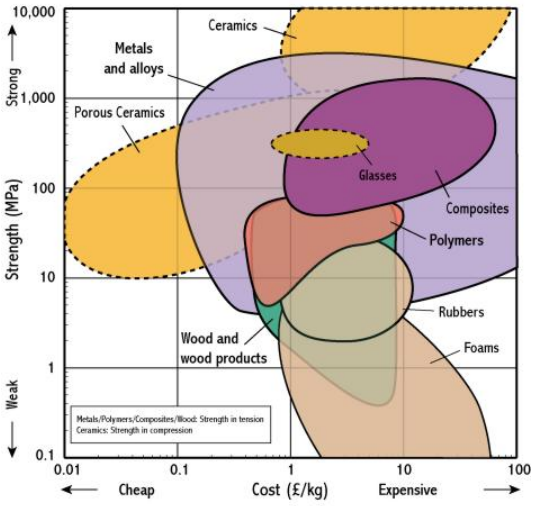

(a) Strength vs Cost Ashby plot [6]

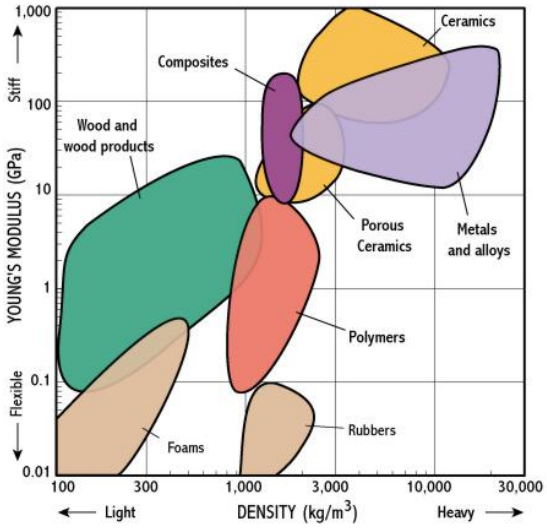

(b) Young modulus vs Density Ashby plot [7]

In addition after selecting that metals are the best match, it was required to analyse which metal is the best, hence a more detailed Ashby plot is generated in Figure 8.3. From this figure it can be seen that aluminium alloys are the best match due to their low density and high stiffness. Eventually, it was decided to select Aluminium T6061-T6[8] over T7075 due to its superior weldablity tendency[9].
Furthermore, for the landing gear the material selected needs to be of a higher stiffness to provide support to the whole structures and to have a crumple zone in case of crashing. After comparing between composites and aluminium T7075 as it has a higher stiffness that T6061-t6 it has been decided to select T7075 due to it being easier to design and manufacture making it the cheaper alternative with comparable performance to composites.

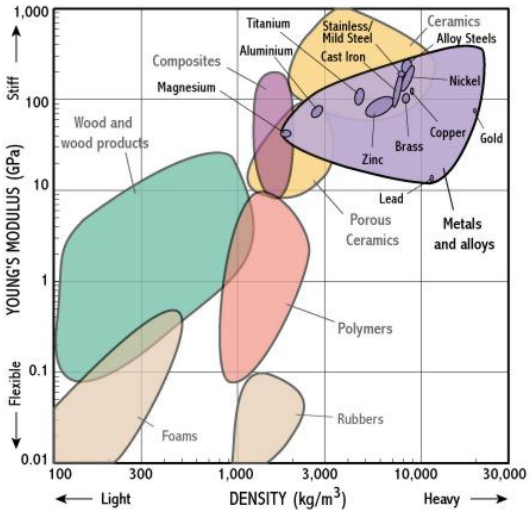

Figure 8.3: Young modulus vs Density Ashby plot [10]

[6] URL: http://www-materials.eng.cam.ac.uk/mpsite/physics/overview/default.html [Cited 23 June 2018]
[7] URL: http://www-materials.eng.cam.ac.uk/mpsite/physics/overview/default.html [Cited 23 June 2018]
[8] URL: https://www.makeitfrom.com/material-properties/6060-T6-Aluminum [Cited 23 June 2018]
[9] URL: http://blog.onlinemetals.com/6061-vs-7075-aluminum-alloy/ [Cited 23 June 2018]

8.1.3. Structural analysis

The structure and the load cases of the hover-bike are very complex. Stress analysis with analytical solutions require dramatic simplifications and idealisations. Because of this, analytical solutions were deemed unfeasible and inaccurate. It was therefore opted to use the finite element method (FEM) for the structural analysis. As an advantage this allows for rapid iterations to the design. High stress concentrations can easily be located and mitigated by increasing beam width or adding more trusses. Similarly, the structural weight can be optimised in the locations were the structure is over-designed.
The assumptions that were taken in the structural analysis are listed below.

- **The structure can be estimated by a finite collection of elements**
  The structure is estimated by a mesh made out of small triangular elements. This allows the use of the finite element method to analyse the structure.
- **The structure can handle all load cases if it can withstand the critical load cases**
  The flight profile consists of multiple varying load cases. In order to analyse this, the structure was analysed for the most critical load cases. It is then assumed that the structure can handle all less critical load cases too.
- **The loads on the structure are modelled by discrete forces**
  All components inside the structure are modelled as forces in a function to their weight. The thrust from the propeller is modelled as forces from the motor attachment point. The lift provided by the wings is modelled as a remote force and moment which is applied on the vertical separator beams.

Following from this last assumption, the critical load cases had to be established. These were determined to be the following.

- **Load case A: Maximum lift in thrill configuration**
  This load case will occur when the hover-bike is in thrill configuration and the rotors are spinning at full power for the maximum thrust-to-weight ratio.
- **Load case B: Maximum lift in range/endurance configuration**
  This load case will occur when the hover-bike wings are producing maximum lift and the rotors are spinning at full power in range/endurance configuration.
- **Load case C: Maximum impact on landing gear at MTOW**
  This load case will occur in the range/endurance configuration when the hover-bike lands with the highest allowable impact.
- **Load case D: Maximum stress on structure during parachute deployment**
  This load case will occur in the range/endurance configuration when the parachute deploys.

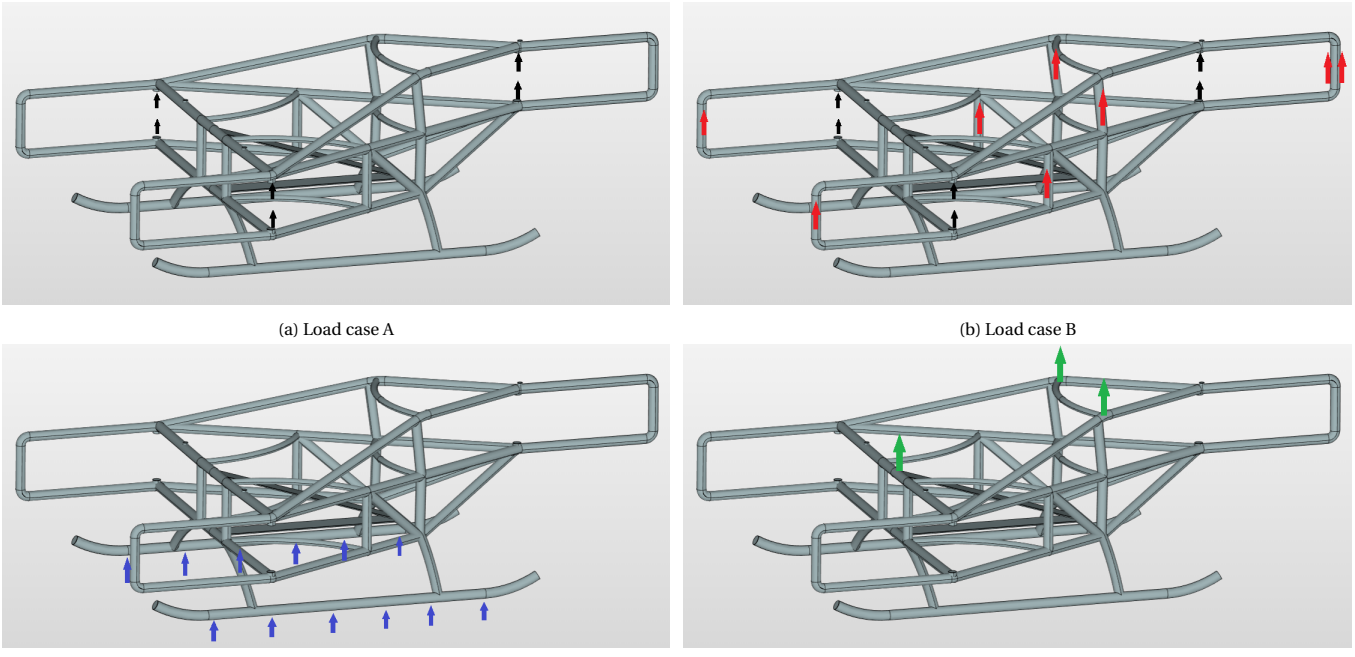

(a) Load case A

(b) Load case B

(c) Load case C

(d) Load case D

Figure 8.4: Critical load cases of the hoverbike

8.1.4. Mass budget

It is important to actively track the weight of the hover-bike during the design phase. Because of this, a mass budget is set up consisting of the heaviest sub-components. These sub-components are as follows.

Table 8.1: Mass budget sub-components

Motors
Propellers
Structure + Landing gear
Safety system
Payload
Ducts + Wings
Battery
Miscellaneous

The weight of lighter subsystems is accounted for collectively in the miscellaneous group.

8.1.5. Moment of inertia and centre of gravity

Centre of gravity

In order to achieve the best possible performance with the hover-bike, it is advisable to have the centre of gravity (CG) exactly in the middle of the vehicle. More specifically this is in the centroid of the triangle defined by the three motor pairs. When this is the case each motor will have to output the same power during hovering.

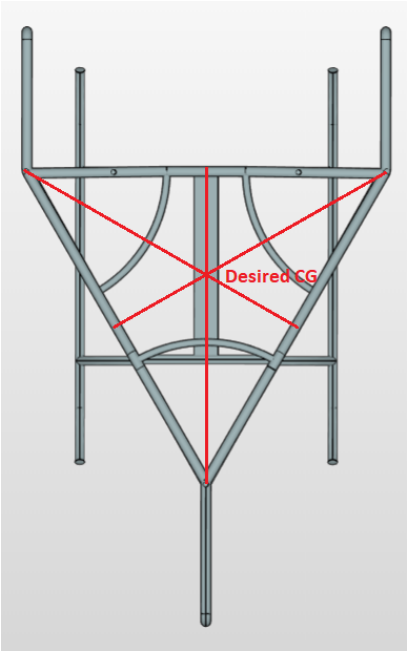

Figure 8.5: Desired CG of the hover-bike

To calculate the centre of gravity, the sub-components in Table 8.1 will be considered. Note that most of these sub-components have a fixed position in the geometry of the structure. The battery and payload can be placed in a range of positions however. Since these components are relatively heavy. They can be positioned as such that the CG is in the middle of the vehicle. The CG is calculated as follows.

$$CG = \frac{1}{M} \sum_{i=1}^{n} m_i \mathbf{r}_i \tag{8.1}$$

Moment of inertia

With the position of all components and the CG known, the moment of inertia of the vehicle can be calculated. The moment of inertia of every separate component in Table 8.1 is calculated. Then the Steiner term is calculated with respect to the CG.

$$I = I_{cm} + md^2 \tag{8.2}$$

Since the structure is complex, its moment of inertia will be calculated in the CAD environment. The moment of inertia of the motors, propellers, safety system and payload is calculated by using an approximate cylinder of the same volume and mass. The battery and wings their moment of inertia is calculated by using an approximate cuboid of the same volume and mass. This can be seen in Figure 8.6

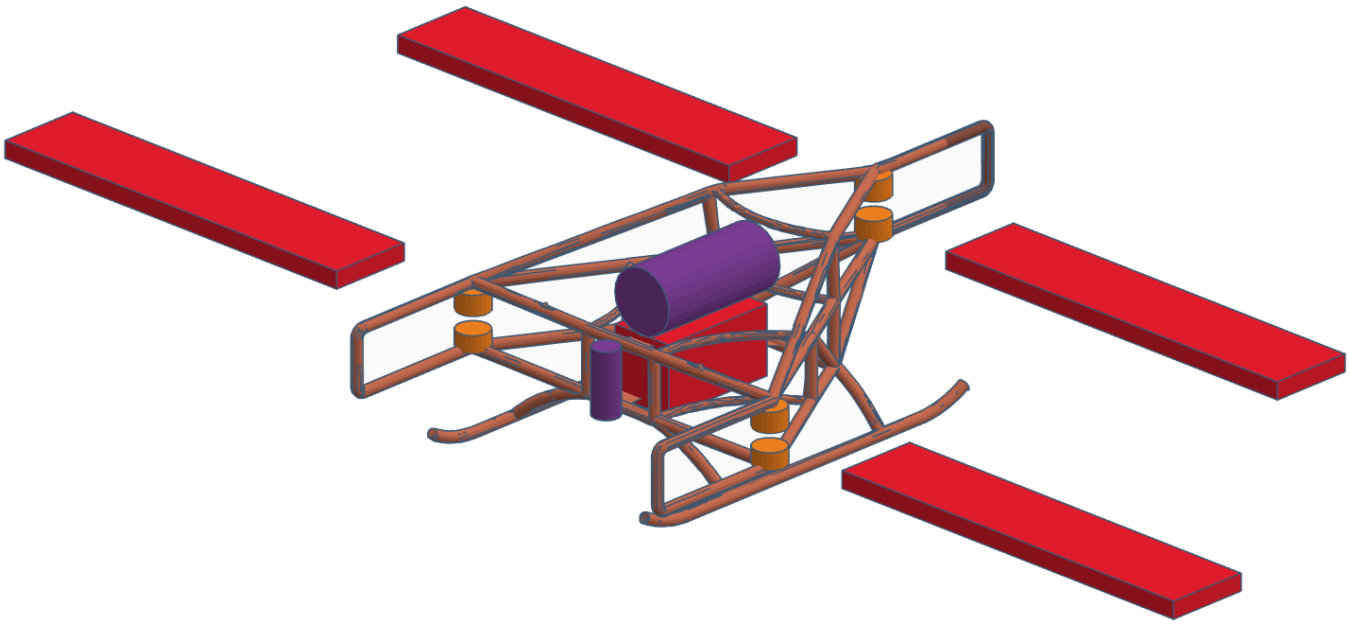

Figure 8.6: Simplification used for the moment of inertia calculations

8.2. Iterations

This section will discuss the iterations and revisions that were made to the structure.

8.2.1. Geometry constraints and design

The geometry constraints did not change during the design phase. Changes to the actual design to optimise the structure were constantly incorporated however. This section will discuss the four major revisions. These revisions are shown in Figure 8.7a, Figure 8.7b, Figure 8.7c and Figure 8.7d respectively. The specific changes in each design are listed below.

Structure revision 1

- Introduction of an upper and lower frame:
  A single frame with one motor on top facing upwards and one rotor on the bottom facing downwards would result in a vertical rotor separation of 38 cm. In order to benefit from the advantage and efficiency gains from contra-rotating rotors, the rotors shall be separated by no more than 20% of the rotor diameter. In our case, this is 32 cm. As a solution an upper and a lower frame was introduced. The separation of the rotor disks can be adjusted by changing the length of the vertical spacers in the design

Structure revision 2

- Positioning of the back rotor:
  The back rotor is positioned in a more upward position. This was done to increase the performance of the vehicle during cruise. The higher position of the rotor allows a cleaner intake of air since there is less interference from the body of the pilot. Furthermore, the vertical separation between the front and back wings is increased. This is because the wings are positioned on the same level as the rotor. As a result there is less interference induced by the front wing on the back wing.

- Use of thinner, hollow beams.
  The structure is made of thinner beams. This was done because the structural analysis pointed out that revision 1 was over designed. The thinner beams bring the weight of the structure down and also make for a less bulky appearance of the hover-bike. Furthermore, hollow beams are used as they are more effective in carrying a bending moment compared to a solid beam of the same weight.

Structure revision 3

- Addition of a landing gear.
  A landing gear is added, inspired by the landing gear of conventional helicopters. The advantage of skids is the light weight and ability to absorb impact.

- Addition of curved rotor guard beams.
  Curved rotor guard beams were added to the structure. These beams are essentially zero force members to the structure and can therefore be made quite thin. However, since it is important to shield the driver from the hazardous spinning rotor blades, these beams are necessary to mount a partial duct to protect the driver.

- Varying inner diameter of the beams.
  Structure revision 2 introduced hollow beams as the main building blocks of the structure. As expected, its structural analysis pointed out that not every member experiences the same forces and stresses. Therefore the inner diameter of the beams was chosen according to the expected stress in the beams.

Structure revision 4

- Making use of bend beams.
  Where possible, the beams in the structure are bend. This relieves the stresses that were previously present in the corner welds.
- making use of corner brackets.
  Since a lot of joints in the structure still require welds, corner plates are introduced. These plates are welded in the corner of a welded beam joint and thereby relief the stress.
- Further optimisation of the beam inner diameter.
  The inner diameter of the beam members is further optimised following from the structural analysis performed in revision 3.

8.2.2. Structural analysis

The structure revisions mentioned in subsection 8.2.1 largely resulted from the structural analysis that was performed. The load cases that each structure revision was subjected to is given in Table 8.2.

Table 8.2: Structural analysis on structure revisions

Structure revision	Applied load case
Revision 1	Load case A
Revision 2	Load case A, B
Revision 3	Load case A, B, C, D
Revision 4	Load case A, B, C, D

8.2.3. Mass budget

The mass of the structure changed through the different structure revisions. The structural mass of the revisions is given in Table 8.3

Table 8.3: Structural mass for the structure revisions

Structure revision	Mass [kg]
Revision 1	182
Revision 2	64
Revision 3	79
Revision 4	58.8

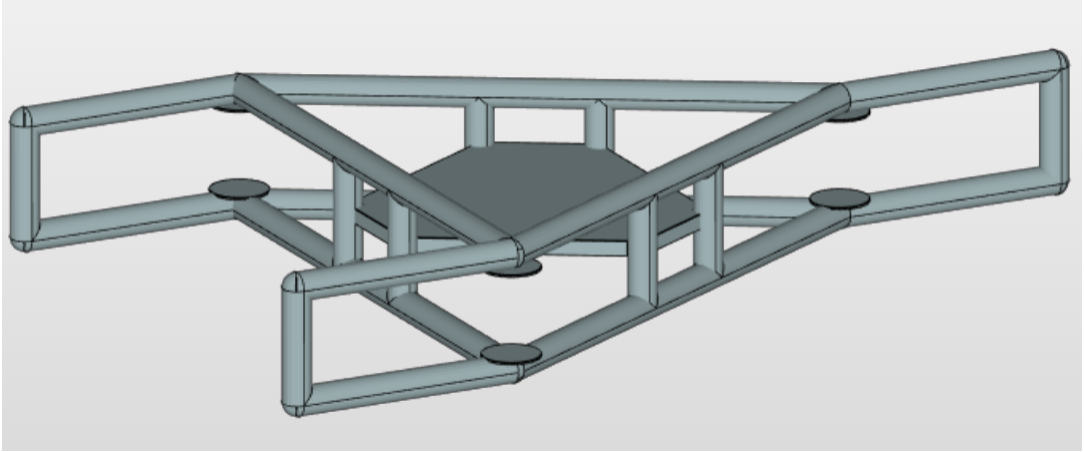

(a) Structure revision 1

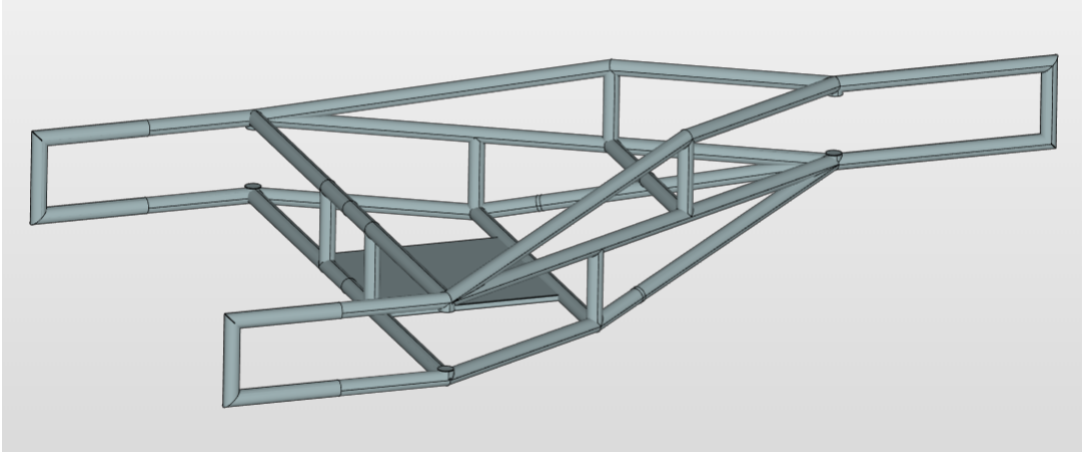

(b) Structure revision 2

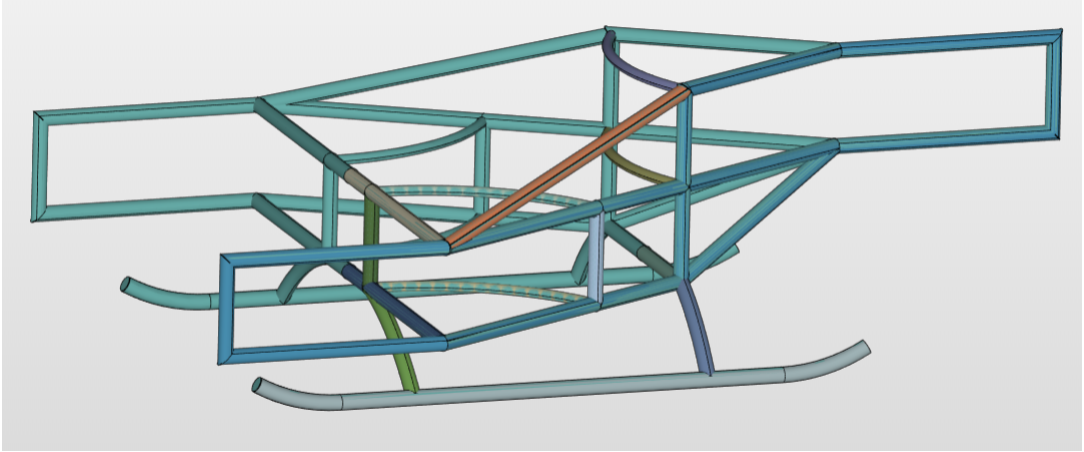

(c) Structure revision 3

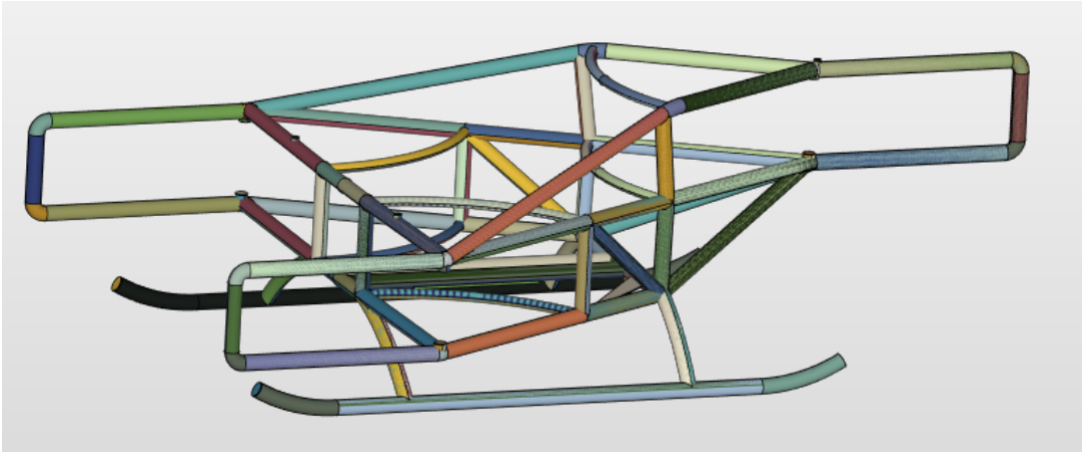

(d) Structure revision 4

Figure 8.7: Structure revisions

8.3. Results

This section will discuss the results of the structure design and analysis. The final dimensions of the Scorpeon will be given and the field of view of the pilot will be discussed. Furthermore the results of the structural analysis are shown. Finally, the determined position of the centre of gravity and the moment of inertia of the vehicle is given.

8.3.1. Geometry constrains and design

The hover-bike is designed as such that it can be easily transported on a trailer. For this the duct/wing assemblies need to be detached from the main frame. Furthermore, the rotors need to be aligned along the longitudinal axis. The final dimensions of the hover-bike during transportation and thrill mode are given in Figure 8.8a and Figure 8.8b.

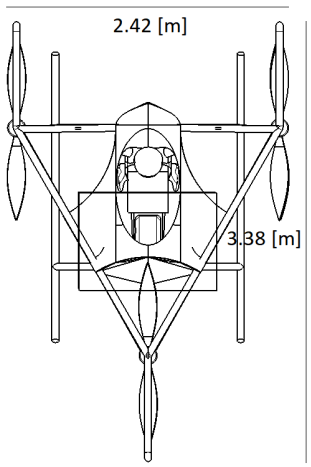

(a) Hover-bike dimensions for transportation

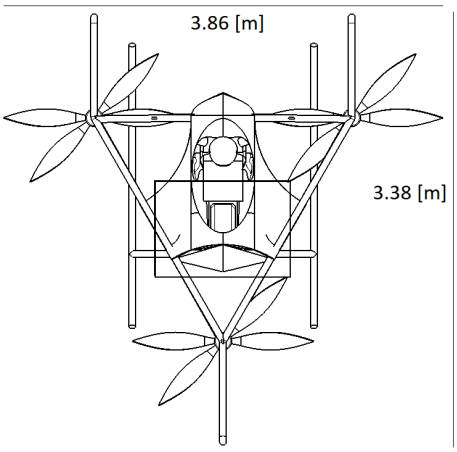

(b) Hover-bike dimensions in thrill mode

The dimensions of the hover-bike in transportation mode can be seen in Figure 8.9.

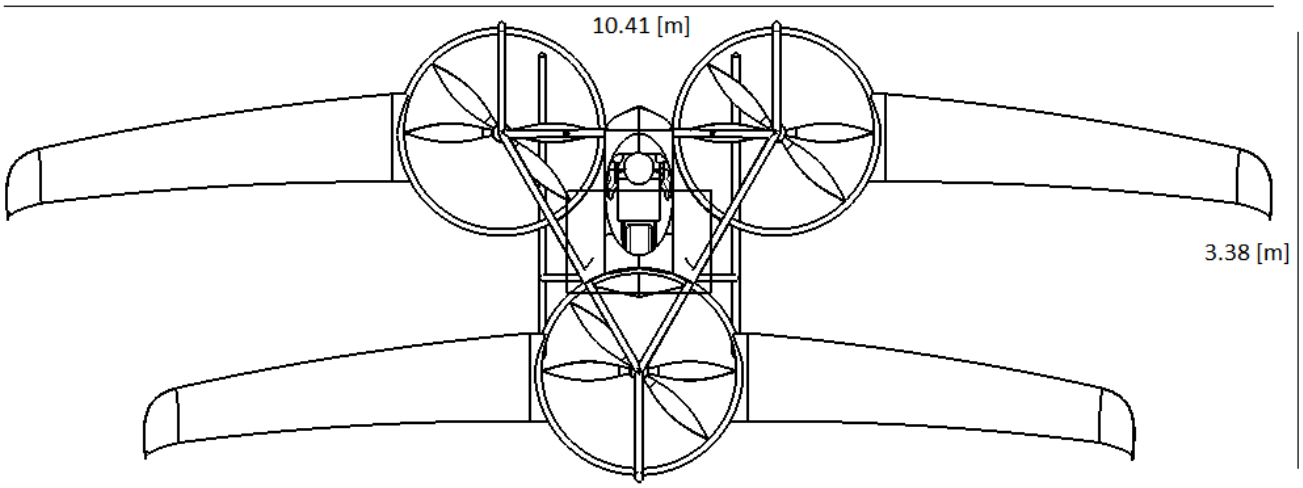

Figure 8.9: Hover-bike dimensions in transportation mode

It is important to note that these dimensions do not equate to the required take-off and land area. This is further explored in 16.2.1.

8.3.2. Field of view

For the hover-bike it is important that the driver is able to see clearly around him. Obstacle and vehicle avoidance are heavily dependent on this aspect. For this reason two requirements on the viewing angles were set in the beginning of the project. Those were HB-CS-ST-04: The hover-bike shall have a front vertical viewing angle of at least 15°, and HB-CS-ST-05: The hover-bike shall have a side vertical viewing angle of at least 45°. Both of these requirements were set to make sure the pilot would have enough vision during flight, while also maintaining the same sense of freedom as on a motorbike.
As can be seen in Figure 8.10 the front viewing angle is mainly restricted by the skin and the windscreen around the pilot. If the pilot is bend down and in the thrill mode position the front viewing angle will be 49°. The view is also slightly blocked by the propellers and ducts to the sides which is visible in the top view of the hover-bike in Figure 8.9. However most will still be possible to see. Requirement HB-CS-ST-04 is therefore met.
Next to the front viewing angle the side viewing angle needs be analysed as well. For this aspect more angles are considered,

since there are several objects obstructing the view. In Figure 8.11 three angles can be seen, these angles are measured with respect to the bend down position of the pilot. When assuming the pilot is still being able to see somewhat through the rotating propellers the field of view is blocked by the panels in front of him, therefore the viewing angle will be 52°. The 26° angle is what the pilot is able to see when he looks a bit backwards and over the skin panels through the front and back propellers. Field of view will be 16° when assumed is that the pilot can not see through the propellers. In Figure 8.12 the viewing angle is obstructed more by the ducts, the viewing angle will be limited to only 11°. In the transportation mode the vehicle will not make any aggressive movements, therefore the movement will be more predictable hence the visibility is less important than in the thrill mode. The side viewing angle is mainly important for landing, when the vehicle is hovering. In this phase the pilot can easily sit upright and have a viewing angle of at least 52°, hence requirement HB-CS-ST-05 is also met.

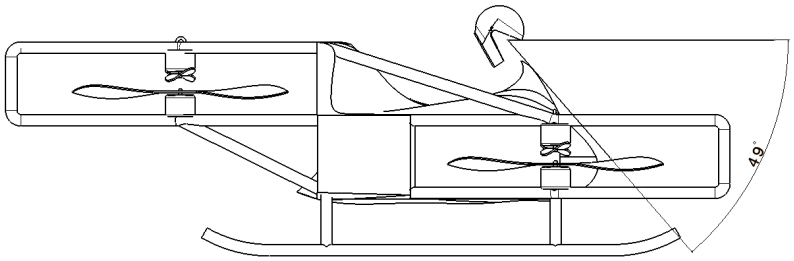

Figure 8.10: Front viewing angle

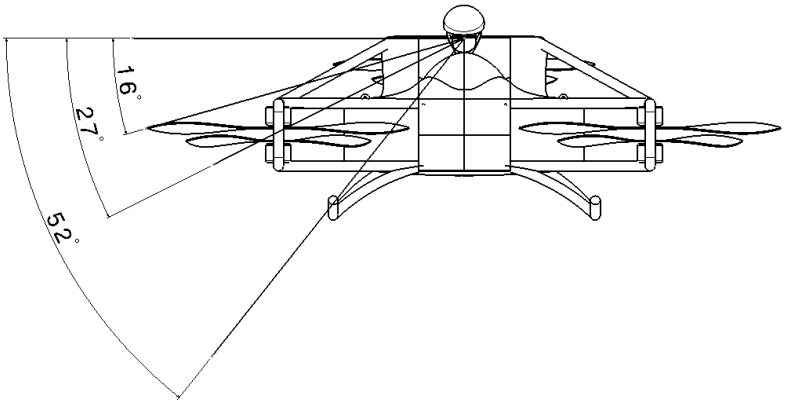

Figure 8.11: Side viewing angle in thrill mode

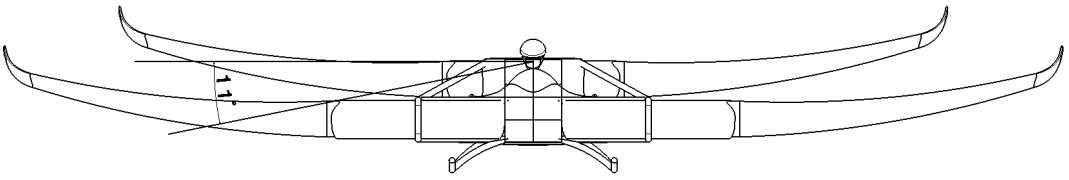

Figure 8.12: Side viewing angle in transportation mode

8.3.3. Material selection

These are the properties of the selected materials of 6061-T6 and 7075 found in Table 8.4.

Table 8.4: Properties of Al 6061-T6 and Al 7075 [11]

Material	Al T6061	Al T7075
Elastic modulus [GPa]	68	70
Ultimate stress [MPa]	220	240 to 590
Yield stress [MPa]	170	120 to 510
Elongation for failure (%)	11	1.8 to 12
Poisson ratio	0.33	0.32
Density [g/cm^3]	2.7	3.0

8.3.4. Structural analysis

In the following section the results from the finite element analysis are shown. The analysis is performed on the fourth design iteration and the scale used is the gradient from blue to red, with red representing a stress of 50 MPa.

Load case A: Maximum lift in thrill configuration

The maximum stress in the structure is 68 MPa.

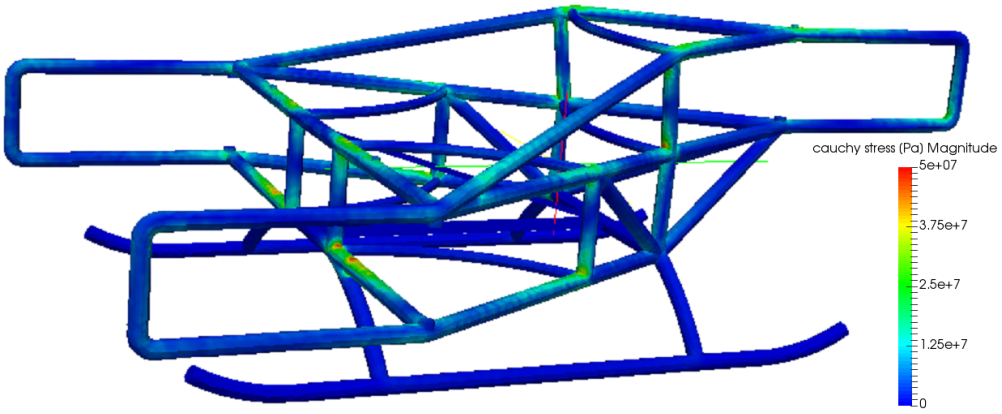

Figure 8.13: Maximum lift in thrill mode

Load case B: Maximum lift in range/endurance configuration

The maximum stress in the structure is 84 MPa.

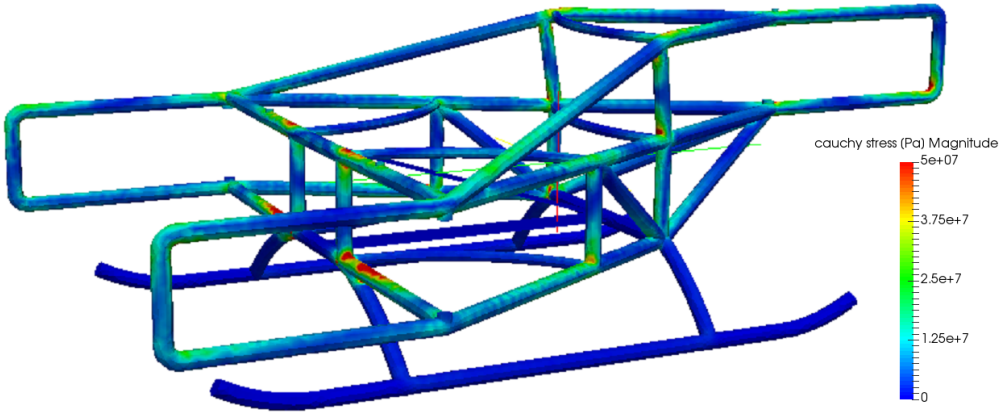

Figure 8.14: Maximum lift in transportation mode

Load case C: Maximum impact on landing gear at MTOW

The maximum stress in the structure is 98 .

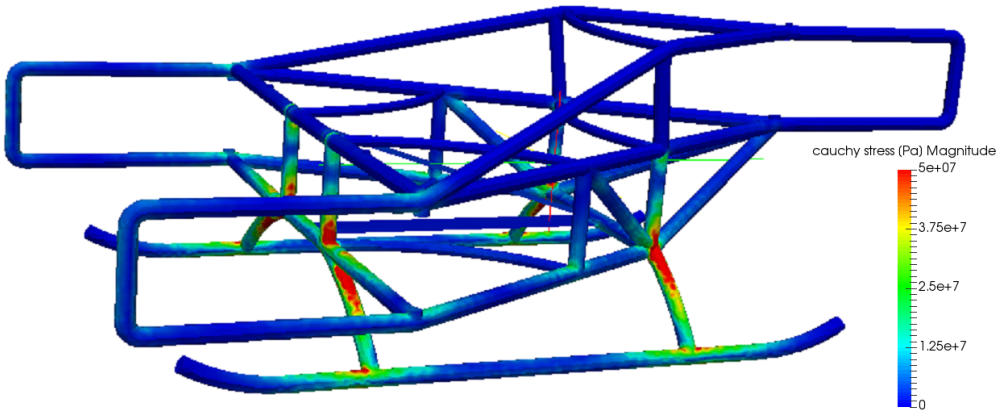

Figure 8.15: Landing gear impact

Load case D: Maximum stress on structure during parachute deployment
The maximum stress in the structure is 133 MPa.

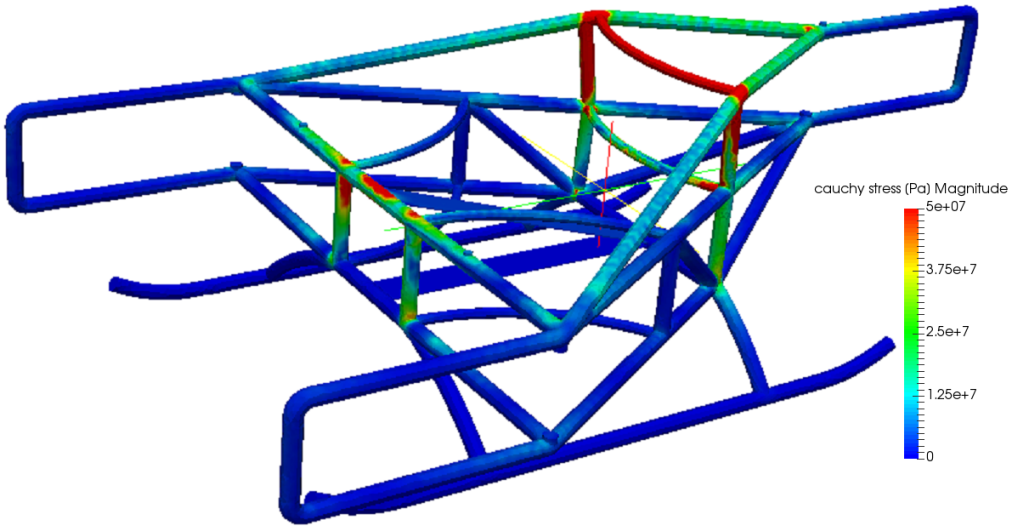

Figure 8.16: Parachute deployment

Impact absorption of the landing gear
The maximum stress is 320 MPa.

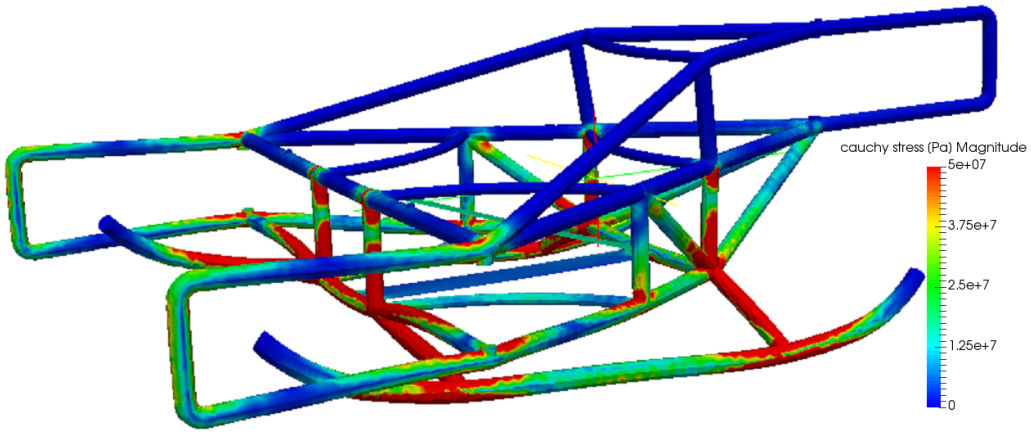

Figure 8.17: Impact absorbtion of the landing gear

Discussion
The factor of safety is defined as the yield stress divided by working stress. In the aerospace industry, a safety factor of 1.5 is considered the minimum [12]. The main structure is made out of Al T6061 with a yield stress of 170 MPa. As can be seen in above figures, the maximum stress does not exceed 84 MPa for load case A and B. Therefore, the factor of safety is 2.0 and no yielding is expected to occur during the operation of the hover-bike. The factor of safety is sufficiently large that high frequency vibrations and fatigue behaviour should also not influence the structural integrity of the main structure. [13]
No yielding or fatigue should occur in the landing gear as shown in Figure 8.15. Al T7075 has a large range of yield stress depending on the exact alloy composition. Considering a minimum safety factor of 1.5, care must be taken that the yield stress of chosen composition is above $1.5 * 98 = 147$ MPa. Considering this it can be concluded that the structure is safe-life. For the stress on the structure during parachute deployment, no failure should occur. Considering the working stress of 133 MPa as seen in Figure 8.16 and an ultimate stress of 220 MPa, this requirement is met with a factor of safety of 1.7. An impact resulting from a free fall 3 m drop or a parachute landing will result in an impact speed of 6 m/s. Large deformations and potential failure in the landing gear is expected. This is beneficial to the pilot because part of the impact will be absorbed in this way.

[12] URL: `https://ntrs.nasa.gov/archive/nasa/casi.ntrs.nasa.gov/20140011147.pdf` [Cited 25 June 2018]
[13] URL: `http://doras.dcu.ie/19502/1/Ping_Hwa_20130725155530.pdf` [Cited 25 June 2018]

8.3.5. Mass budget

In the table below the mass budget is given for the sub-components of the hover-bike. The mass of the structure was estimated to be 58.8 kg according to the material volume in the CAD design. A mass of 60 kg was used however in the mass breakdown. This is to account for the extra material used in the welded joints.

Table 8.5: Mass budget for thrill mode

Sub-component	Mass [kg]
Structure	60
Duct & wings	N.A.
Motors	42.6
Propeller	20
Safety system	13.4
Miscellaneous	24
Battery	185
Payload	100
TOTAL	445

Table 8.6: Mass budget for transportation mode

Subcomponent	Mass [kg]
Structure	60
Duct & wings	55
Motors	42.6
Propeller	20
Safety system	13.4
Miscellaneous	24
Battery	185
Payload	100
TOTAL	500

8.3.6. Moment of inertia and centre of gravity

Centre of gravity

The centre of mass of the battery and the payload were placed 0.71 m behind the front beam, as shown in Figure 8.18.

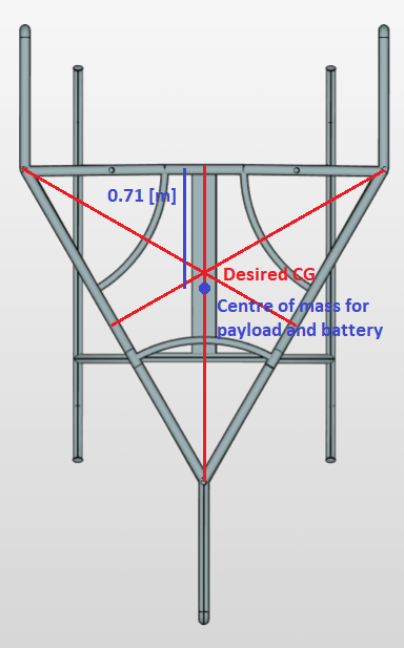

Figure 8.18: Centre of gravity

Like this the CG of the whole vehicle aligns exactly with the desired CG in thrill mode. In transportation mode the CG will shift 0.05 m aft due to the added weight of the wings. This is not expected to affect the performance significantly.

Moment of inertia
Since the position of the CG and all sub-components is now known, the moment of inertia can be calculated. The moment of inertia for both the thrill mode and transportation mode is tabulated in Table 8.7 and Table 8.8

Table 8.7: Moment of inertia in thrill mode

Component	**m [kg]**	**Ixx [kg m^2]**	**Iyy [kg m^2]**	**Izz [kg m^2]**
Structure	60	38.40	44.02	77.27
Motor + propeller (left bottom)	10.43	4.32	13.16	16.13
Motor + propeller (left top)	10.43	3.85	12.69	16.13
Motor + propeller (right bottom)	10.43	4.32	13.16	16.13
Motor + propeller (right top)	10.43	3.85	12.69	16.13
Motor + propeller (back bottom)	10.43	18.44	0.68	18.15
Motor + propeller (back top)	10.43	19.40	1.64	18.15
Safety system	24	6.65	0.55	6.60
Battery	185	10.30	7.41	7.89
Payload	100	14.73	13.17	6.56
Miscellanious	24	2.62	0.81	2.31
Total	**445**	**130.94**	**144.02**	**225.48**

Table 8.8: Moment of inertia in transportation mode

Component	**m [kg]**	**Ixx [kg m^2]**	**Iyy [kg m^2]**	**Izz [kg m^2]**
Structure	60	41.49	44.13	80.25
Motor + propeller (left bottom)	10.43	5.13	13.22	16.88
Motor + propeller (left top)	10.43	4.62	12.70	16.88
Motor + propeller (right bottom)	10.43	5.13	13.22	16.88
Motor + propeller (right top)	10.43	4.62	12.7	16.88
Motor + propeller (back bottom)	10.43	16.82	0.64	16.57
Motor + propeller (back top)	10.43	17.74	1.56	16.57
Safety system	24	7.8	0.57	7.72
Battery	185	8.74	7.94	5.80
Payload	100	12.93	12.49	5.43
Miscellanious	24	3.23	0.85	2.88
Duct+wing front left	13.75	6.43	72.78	77.75
Duct+wing front right	13.75	6.43	72.78	77.75
Duct+wing back left	13.75	23.85	26.64	47.80
Duct+wing back right	13.75	23.85	26.64	47.80
Total	**500**	**188.27**	**318.91**	**453.31**

8.4. Verification and Validation

8.4.1. Validation of finite element software

For the validation of SimScale, we refer to the solid mechanics validation cases in the documentation of the software. [14] Below, the validation for a thick plate under pressure is performed. The simulation in SimScale is compared to the numerical results presented in the National Agency for Finite Element Methods and Standards [NAFEMS]. The geometry of the plate is shown in Figure 8.19a

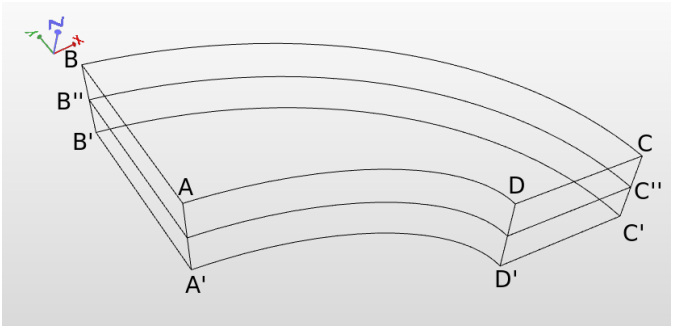

(a) Geometry of the plate

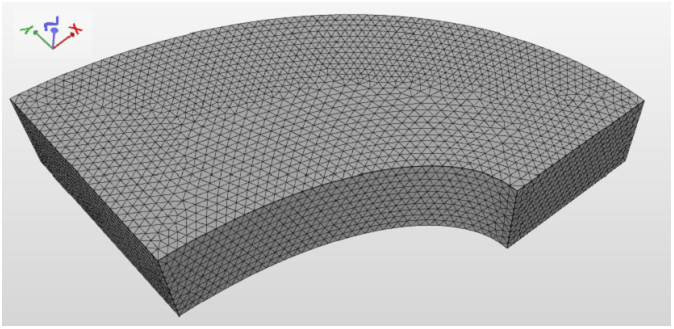

(b) Mesh of the plate

Material:

- Isotropic: E = 210 GPa, v = 0.3

Constraints:

- Face DCD'C' zero y-displacement
- Face ABA'B' zero x-displacement
- Face BCB'C' x and y displacements fixed
- z-displacement fixed along the edge B"C"

Loads:

- Pressure of 1 MPa on Face ABCD

A quadratic tetrahedral mesh comparable to the performed analysis was used. The comparison for the validation case is shown in Table 8.9

Table 8.9: Stress comparison for the validation case

	σ_{YY} at point D [MPa]
[NAFEMS]	5.3800
SimScale	3.3961
Error	0.30 %

8.4.2. Validation of the moment of inertia values and centre of gravity

The position of the CG can be verified by experience and intuition. Heavy components are placed in the middle of the vehicle and other components are placed evenly around it. Therefore it can be expected that the CG is located in the centroid of the triangle defined by 3 motor pairs.

The moment of inertia values are crucial for the control system of the hover-bike. Since the appearance of the hover bike in transportation mode is comparable to light general aviation aircraft, a comparison is made. In the table below the moments of inertia of the Sunburst model 'C'[15] are compared to those of the hover-bike.

Table 8.10: Moment of inertia comparison

	Sunburst model 'c'	**Hover-bike**
Wingspan [m]	11.94	10.41
Ixx [kg m^2]	22.50	188.27
Iyy [kg m^2]	422.74	318.91
Izz [kg m^2]	477.79	453.3

As can be seen Izz is very similar for both vehicles. The reason for the difference in Ixx and Iyy can be explained since the Sunburst model 'C' has most of its mass located along the span of a single wing. The hover-bike has a front and a back wing and therefore the value for Ixx is higher and Iyy is lower.

[14] URL: `https://www.simscale.com/docs/content/validation.html` [Cited 25 June 2018]
[15] URL: `https://ntrs.nasa.gov/archive/nasa/casi.ntrs.nasa.gov/19840008095.pdf` [Cited 25 June 2018]

9
Control & Manoeuvrability

The aim of this chapter is to propose and describe the control design of the Scorpeon hover-bike. This section will start by determining the method and approach for the control and manoeuvrability system design. Following is the reference axes and the primary and secondary assumptions regarding the modelling of the hover-bike. Afterwards the architecture of the control is presented while elaborating on the flight mechanics. After having determined the basic control system and properties the mission profiles are taken into account for the design. Subsequently the performance of the control system is assessed while verifying the requirements. Finally the modelling and simulation tools determining the control properties are verified an validated in the last section.

9.1. Method & Approach

9.1.1. Workflow

After completing the design in the midterm report [42] and computing key stability and manoeuvrability properties, analysis is followed by a final design. Figure 9.1 presents the work flow at this stage leading to a final design which is verified and validated. The first phase includes defining the different stability and manoeuvrability states which the driver can choose. Since these modes will influence the performance of Scorpeon , it is important to identify and specify the modes including the consequences on control and manoeuvrability. After specifying the modes the equations of motions (EOM) are set up. These EOM allow setting up a non-linear control loop. For this loop first the angular control will be created. After structuring the loop, the proportional integral derivative controls are tuned. Afterwards more Scorpeon properties are implemented, such as the aerodynamic coefficients, thrust limits and the response time of the motors. Only after the model is completed, a final PID tuning takes place. Now the control design is complete, the requirements can be validated and disturbances can be tested for.

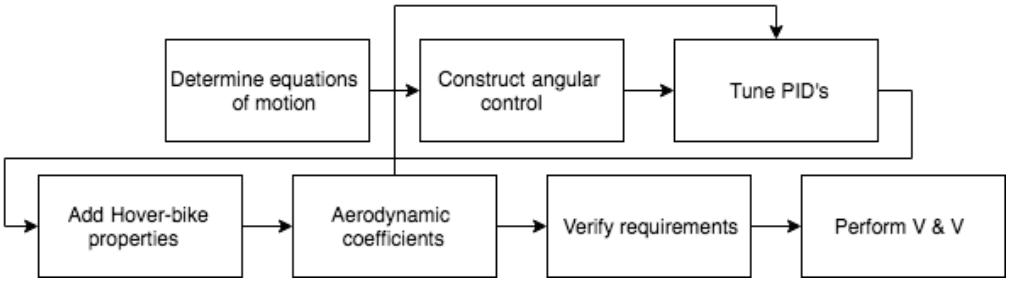

Figure 9.1: Workflow design control

9.1.2. Reference Axis

For designing the control and manoeuvrability properties, the body axis system is used. The origin of the axis system is located at the centre of mass of the hover-bike. The positive x axis is directed in the forward direction of the hover-bike. The positive y axis is located in the right direction when viewing in the direction of the positive x axis. The positive z axis is pointing down in the direction to earth while in normal non inverted flight. The speed in x, y and z direction are labelled u, v and w respectively. The roll, pitch and yaw angle are symbolised by ϕ, θ and ψ respectively. The forces X, Y and Z are the applied forces in x, y and z direction respectively. The model furthermore uses a inertial frame to project the positional dynamics on. Future graphs and explanations on positional parameters will use the inertial frame.

9.1.3. Primary Assumptions

No drag generated due to $\dot{\phi}$, $\dot{\theta}$ and $\dot{\psi}$ For modelling the hover-bike dynamics, the drag created by attitude adjustment rates are not taken into account. The latter expects the drag contribution due to the relatively low absolute speeds to be minimal.

Duct interference not taken into account As explained in 7 the ducts have significant effect on the performance of the rotors. Although the consequences of the duct are considerably high, at this stage of the design the impact is not included

Wing interference not taken into account Not only do ducts interfere the airflow into the propeller, the wings have a contribution too. Especially at high air speeds the interference is significant, however due to time constraints this interference

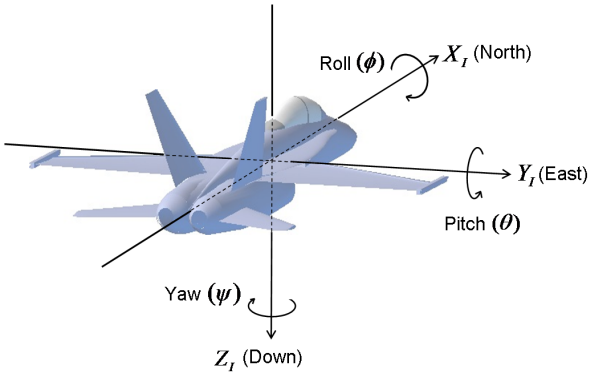

Figure 9.2: Body frame used for calculations and modelling.

is not yet taken into account.

9.1.4. Secondary Assumptions

Rigid body The hover-bike is anticipated not to deform in any flight phase of both modes. Considering the wings, aero-elastic effects are not taken into account. The perfect rigid body assumption is assumed to have negligible effects.

symmetry in xz plane Scorpeon is assumed to be symmetric in the xz plane, resulting in $I_{xy} = 0$. This assumption significantly simplifies the equations of motion.

Mass is constant Although the motors use up electricity during hover and flight, the mass is assumed invariable over time. Additionally weight increase due to water and dirt are as well not taken into consideration.

Earth is flat and non rotating The inertial frame is assumed to be located on a flat and none rotating earth. Although the dynamics at this stage will not be critically influenced by this assumption, it is substantial for elaborate future modelling.

Standard atmosphere at every height The air density as well as the pressure and temperature is assumed to be constant over the altitude simulated for. The hover-bike performance will definitely be influenced by altitude, however such altitudes are not simulated for.

9.2. Control Design

9.2.1. Modelling the hover-bike

Equations of motion First the physical model is discussed where the equations of motions are being used. The physical response as for the mathematical model of the hover-bike changes according to the control inputs in τ_B which consists out of T, τ_ϕ, τ_θ and τ_ψ. The control inputs represent the total thrust and torques around the x, y and z axis. The EOM in the inertial frame, which is rewritten for calculating the accelerations, is given in equation 9.5. The EOM in the body frame including transformations is given in equation 9.1. J^{-1} is a transformation matrix, which converts angular accelerations in the inertial frame to the body frame. As mentioned previously τ_B represents the moment control input as shown in the first term of 9.6. The following matrix **C** signifies the Coriolis term, which contains gyroscopic and centripetal terms as shown in 9.2 and 9.3. The state vector q consists out of two smaller vectors, ξ which consists out of the states x y z for cartesian position coordinates and η which consists out of the states for roll ϕ, pitch θ and yaw ψ. Both vectors are combined in one EOM notation as shown in equation 9.8 with corresponding matrices 9.9,9.10, 9.12 and 9.11, which are needed to translate Lagrange and Newton equations to Euler notation as shown in [52]. Equations 9.12 represent the aerodynamic drag forces in the inertial frame. The blue area in figure 9.3 includes the mathematical model for the dynamics of hover-bike and integrators allowing a feedback control loop for the attitude angles.

$$\ddot{\eta} = \mathbf{J}^{-1}(\tau_B - \mathbf{C}(\eta, \dot{\eta})\dot{\eta}) \tag{9.1}$$

$$C(\eta, \dot{\eta}) = \begin{bmatrix} C_{11} & C_{12} & C_{13} \\ C_{21} & C_{22} & C_{23} \\ C_{31} & C_{32} & C_{33} \end{bmatrix} \tag{9.2}$$

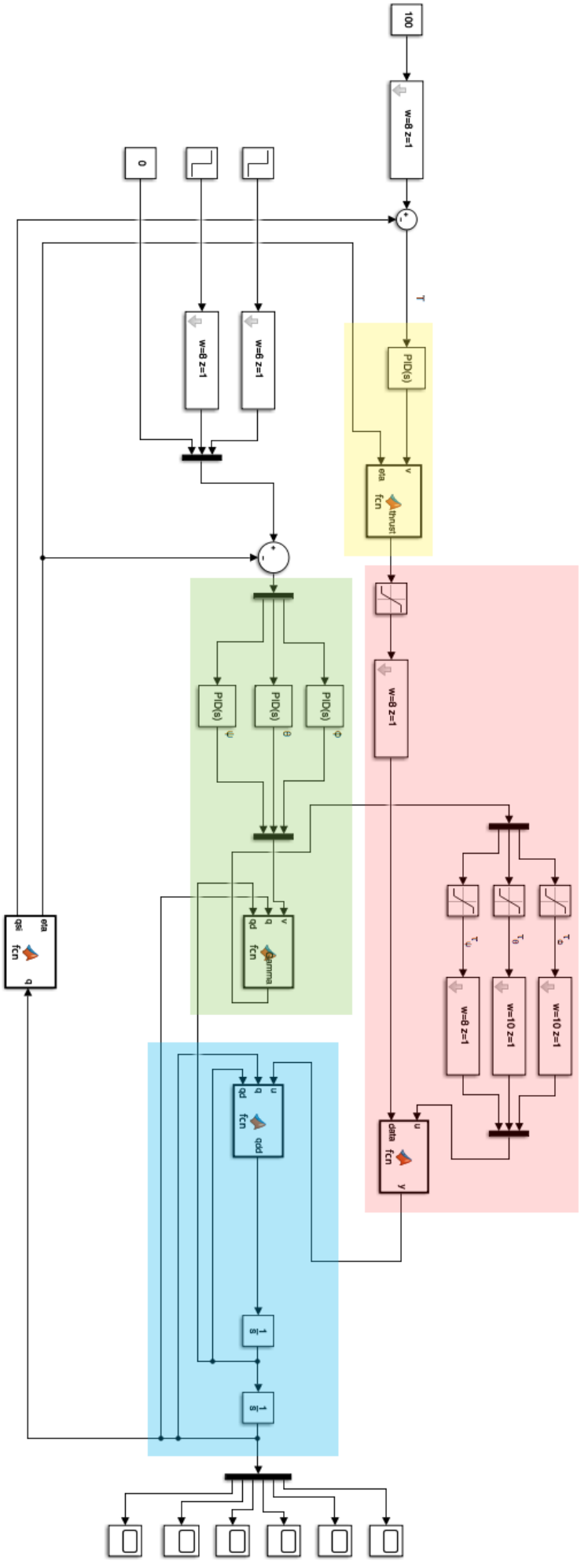

Figure 9.3

Figure 9.4: Control lay-out.

$$
\begin{aligned}
C_{11} &= 0 \\
C_{12} &= (I_{yy} - I_{zz})(\dot{\theta} C_\phi S_\phi + \dot{\psi} S_\phi^2 C_\theta) + (I_{zz} - I_{yy})\dot{\psi} C_\phi^2 C_\theta - I_{xx}\dot{\psi} C_\theta \\
C_{13} &= (I_{zz} - I_{yy})\dot{\psi} C_\phi S_\phi C_\theta^2 \\
C_{21} &= (I_{zz} - I_{yy})(\dot{\theta} C_\phi S_\phi + \dot{\psi} S_\phi C_\theta) + (I_{yy} - I_{zz})\dot{\psi} C_\phi^2 C_\theta - I_{xx}\dot{\psi} C_\theta \\
C_{22} &= (I_{zz} - I_{yy})\dot{\phi} C_\phi S_\phi \\
C_{23} &= -I_{xx}\dot{\psi} S_\theta C_\theta + I_{yy}\dot{\psi} S_\phi^2 S_\theta C_\theta + I_{zz}\dot{\psi} C_\phi^2 S_\theta C_\theta \\
C_{31} &= (I_{yy} - I_{zz})\dot{\psi} C_\theta^2 S_\phi C_\phi - I_{xx}\dot{\theta} C_\theta \\
C_{32} &= (I_{zz} - I_{yy})(\dot{\theta}) C_\phi S_\phi S_\theta + \dot{\phi} S_\phi^2 C_\theta) + (I_{yy} - I_{zz})\dot{\phi} C_\phi^2 C_\theta - I_{xx}\dot{\psi} S_\theta C_\theta - I_{yy}\dot{\psi} S_\phi^2 S_\theta C_\theta - I_{zz}\dot{\psi} C_\phi^2 S_\theta C_\theta \\
C_{33} &= (I_{yy} - I_{zz})\dot{\psi} C_\theta^2 S_\phi C_\phi - I_{yy}\dot{\theta} C_\theta S_\theta S_\phi^2 - I_{zz}\dot{\theta} C_\theta S_\theta C_\phi^2 + I_{xx}\dot{\theta} C_\theta S_\theta
\end{aligned} \tag{9.3}
$$

$$
J(\eta) = \begin{bmatrix} I_{zz} & 0 & -I_{zz} S_\theta \\ 0 & I_{yy} C_\phi^2 + I_{zz} S_\phi^2 & (I_{yy} - I_{zz}) C_\phi S_\phi C_\theta \\ -I_{xx} S_\theta & (I_{yy} - I_{zz}) C_\phi S_\phi C_\theta & I_{xx} S_\theta^2 + I_{yy} S_\phi^2 C_\theta^2 + I_{zz} C_\phi^2 C_\theta^2 \end{bmatrix} \tag{9.4}
$$

$$
\begin{bmatrix} \ddot{x} \\ \ddot{y} \\ \ddot{z} \end{bmatrix} = -g \begin{bmatrix} 0 \\ 0 \\ 1 \end{bmatrix} + \frac{T}{m} \begin{bmatrix} C_\psi S_\theta C_\phi + S_\psi S_\phi \\ S_\psi S_\theta C_\phi + C_\psi S_\phi \\ C_\theta C_\phi \end{bmatrix} - \frac{1}{m} \begin{bmatrix} A_x & 0 & 0 \\ 0 & A_y & 0 \\ 0 & 0 & A_z \end{bmatrix} \begin{bmatrix} \dot{x} \\ \dot{y} \\ \dot{z} \end{bmatrix} \tag{9.5}
$$

$$
\tau_B^T = \begin{bmatrix} \tau_\phi \tau_\theta \tau_\psi \end{bmatrix} \quad \eta^T = \begin{bmatrix} \phi & \theta & \psi \end{bmatrix} \quad \xi^T = \begin{bmatrix} x & y & z \end{bmatrix} \tag{9.6}
$$

$$
\ddot{q}^T = \begin{bmatrix} \ddot{x} & \ddot{y} & \ddot{z} & \ddot{\phi} & \ddot{\theta} & \ddot{\psi} \end{bmatrix} \tag{9.7}
$$

$$
\ddot{q} = M(q)^{-1}(B(q)u - C(q,\dot{q})\dot{q} - A(q,\dot{q})\dot{q} - G) \tag{9.8}
$$

$$
M(q) = \begin{bmatrix} mI_{3x3} & 0_{3x3} \\ 0_{3x3} & J(\eta) \end{bmatrix} \tag{9.9}
$$

$$
C(q,\dot{q}) = \begin{bmatrix} 0_{3x3} & 0_{3x3} \\ 0_{3x3} & C_\eta(q,\dot{q}) \end{bmatrix} \tag{9.10}
$$

$$
G = \begin{bmatrix} mge_3 \\ 0_{3x1} \end{bmatrix} \quad mge_3 = \begin{bmatrix} 0 \\ 0 \\ m * g \end{bmatrix} \tag{9.11}
$$

$$
A(q,\dot{q}) = \begin{bmatrix} A_\eta(q,\dot{q}) \\ 0_{3x1} \end{bmatrix} \quad A_\eta(q,\dot{q}) = \begin{bmatrix} (0.015 + 0.544(sin(\theta)cos(\theta)))(1.3048cos(\theta) + \pi sin(\theta))\frac{1}{2}\rho V_x^2 S \\ (0.015 + 0.544(sin(\theta)cos(\theta))(1.2248cos(\theta) + \pi sin(\theta))\frac{1}{2}\rho V_y^2 S \\ 1.28\frac{1}{2}\rho V_z^2 S \end{bmatrix} \tag{9.12}
$$

9.2.2. Angular control

The angular control part is displayed in green and partly consists out of three proportional integrated derivative (PID) controllers, controlling the attitude angles. The PID loop is a control feedback loop mechanism which restores the actual state to the desired reference state in a optimum manner. The function block within the green area in figure 9.3 contains a linearisation function which computes the amount of torque needed for the angles ϕ, θ and ψ as shown in equations 9.14 9.11 9.16 9.17 9.18. Γ is the vector containing τ_ϕ, τ_θ and τ_ψ. c and u show whether that part is controlled for or not, meaning the dynamics of either ξ, which are not controlled, or η which are controlled are called.

The PID's are tuned using the PID tuner as available in $Matlab$. During tuning the quickest response and shortest transient phase is not initially preferred as this contributes to a too rigid control system in where small errors will lead to a singular system.

$$
M_q = \begin{bmatrix} M_{uu}(q)_{3x3} & M_{uc}(q)_{3x3} \\ M_{cu}(q)_{3x3} & M_{cc}(q)_{3x3} \end{bmatrix} \tag{9.13}
$$

$$
= \begin{bmatrix} m & 0 & 0 & 0 & 0 & 0 \\ 0 & m & 0 & 0 & 0 & 0 \\ 0 & 0 & m & 0 & 0 & 0 \\ 0 & 0 & 0 & I_{xx} & 0 & -I_{xx}sin(\theta) \\ 0 & 0 & 0 & 0 & I_{yy}cos(\phi)^2 + I_{zz}sin(\phi)^2 & (I_{yy} - I_{zz})cos(\phi)sin(\phi)cos(\theta) \\ 0 & 0 & 0 & -I_{xx}sin(\theta) & (I_{yy} - Izz)cos(\phi)sin(\phi)cos(\theta) & I_{xx}sin(\theta)^2 + I_{yy}sin(\phi)^2cos(\theta)^2 + I_{zz}cos(\phi)^2cos(\theta)^2 \end{bmatrix} \tag{9.14}
$$

$$
\Gamma = \beta + \alpha * \nu \tag{9.15}
$$

$$
\Delta = (B_c - M_{cu}M_{uu}^{-1}B_u) \tag{9.16}
$$

$$\alpha = \Delta^{-1}(M_{cc} - M_{cu}M_{uu}^{-1}M_{uc}) \tag{9.17}$$

$$\beta = \Delta^{-1}(-M_{cu}M_{uu}^{-1}h_u + h_c) \tag{9.18}$$

$$h = C(\eta,\dot{\eta})\begin{bmatrix}\dot{x}\\ \dot{y}\\ \dot{z}\\ \dot{\phi}\\ \dot{\theta}\\ \dot{\psi}\end{bmatrix} + G \quad h_u = h[1:3] \quad h_c = h[4:6] \tag{9.19}$$

9.2.3. Altitude control

The altitude control part is shown in yellow which consists out of one PID controller, correcting for vertical position. The adjusted thrust T is calculated using formula 9.20 which includes the current pitch and roll angle. o_z represents a vertical position vector while m and g represent the mass and gravitational acceleration respectively. o_z is the output of the altitude PID controller, which is treated as a vector for the thrust calculation. In order to increase the user-friendliness, it is chosen to include altitude control wherefore the user can focus more on other fun riding aspects such as turns.

$$T = m * \frac{(o_z + g)}{(cos(\phi) * cos(\theta))} \tag{9.20}$$

9.2.4. Input

This section will discuss two types of input, namely the reference input and the control input. In order to perform as many realistic simulations as possible, all reference inputs have been fitted with a second order filter which implements a response time in a delay format for altitude, roll and pitch angle. The control input possesses the same second order filters however with different parameters. Next to the filters, saturation blocks have been added to limit the control inputs to realistic and possible torques and thrust. In the function block in the red part, before the control inputs enter the hover-bike dynamics model the in blue area, a coupling calculation is performed. This computation involves subtracting the thrust needed for the torque from the total thrust needed for attitude control. The latter means that would there be a manoeuvre initiated that proportionally needs more torque than total thrust is available to maintain a certain altitude, the hover-bike will not be able to maintain altitude. The maximum torques are calculated using the hover-bike dimensions and maximum thrust available for every rotor.

9.2.5. Hover-bike properties

After the control design in terms of configuration and modelling has been finalised, the Scorpeon parameters can be added. For the control inputs the limits for torque and thrust are adjusted. The maximum allowable T is 7500 N while the maximum τ_ϕ is 3015 Nm and τ_θ is 1815 Nm. After adjusting propeller related parameters, the weight and MOI's are modified. The corresponding weight and MOI's are found in table 8.8 for transportation mode and 8.7 for thrill mode. The next section will show the performance differences between the used modes.

9.3. Results

An exemplary flight case is given in figure 9.8 which shows data divided over multiple graphs. This particular flight simulation from the beginning starts accelerating to an altitude of 5 m. After 6 seconds the maximum pitch angle is applied resulting in a longitudinal acceleration. The graphs in the first row demonstrate the response delay of the electric motors. The first graph 9.8a demonstrates the real response for total thrust in blue while the second graph indicates the delay in pitch torque. The maximum thrust that is applicable is as previously mentioned 7500 N, which can be observed at about 7.5 s where to thrust is maximised. Another aspect worth noting is the initial decrease in altitude after the pitch angle is maximised. Due to a torque the total thrust generated is not enough to keep the hover-bike at the same altitude resulting in an altitude decrease of a meter. Graph 9.5d shows the pitch angle which is set at 0.78 rad at 6 seconds.

9.3.1. Requirements

HB-FR-S-06 The hover-bike shall be stabilised by a control loop. This requirement is met since a PID feedback control mechanism is implemented. With and without the ducts and wings mounted, the hover-bike is artificially kept stable. The hover-bike configuration including the wings mounted inevitably will result in more power and thrust needed for stability and manoeuvrability purposes.

HB-FR-S-07 The hover-bike shall have a maximum pitch angle of 45° degrees. The hover-bike will not only limit the inputs to 45° degrees, but also restrict the hover-bike in the control system to move beyond 45° degrees by using saturation block located after the hover-bike modelling.

HB-FR-S-09 The longitudinal acceleration shall be at least 8.3 m/s^2. To verify this requirement the maximum pitch angle is applied from the beginning of this simulation. The graphs of speed and acceleration are shown in figure 9.6. As observed the longitudinal acceleration requirement is met.

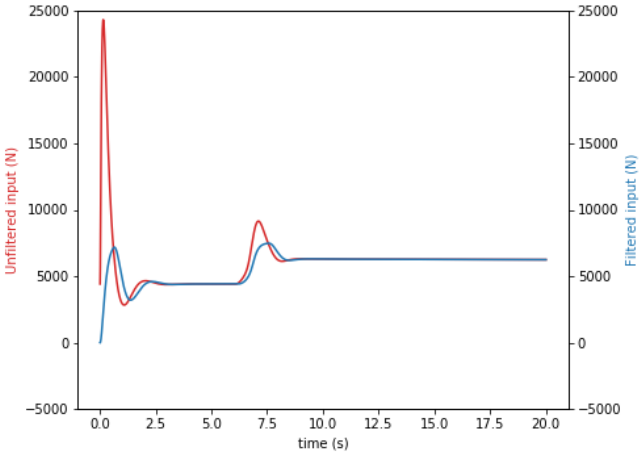

(a) Total thrust.

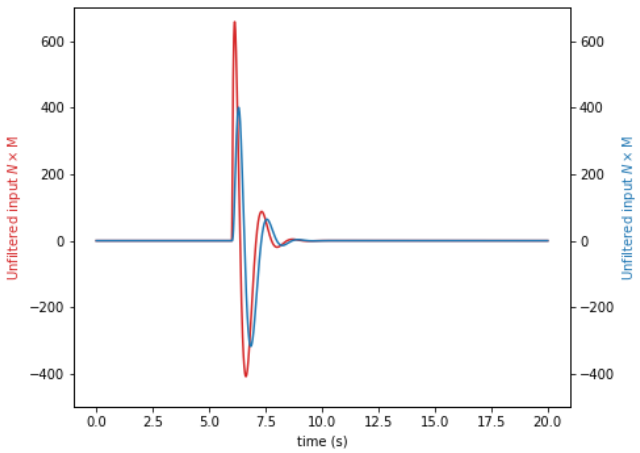

(b) Pitch torque.

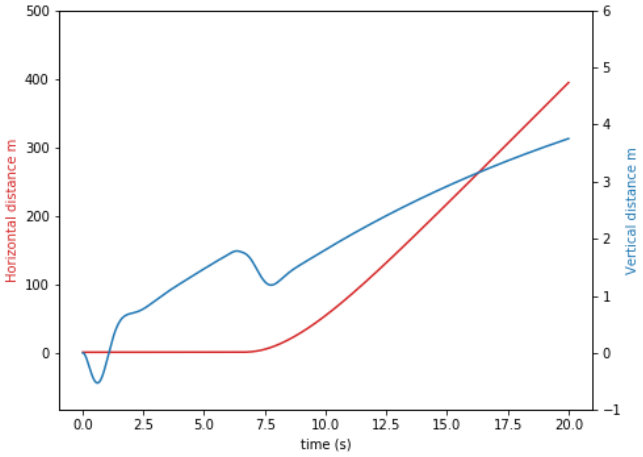

(c) Distance covered for x and z

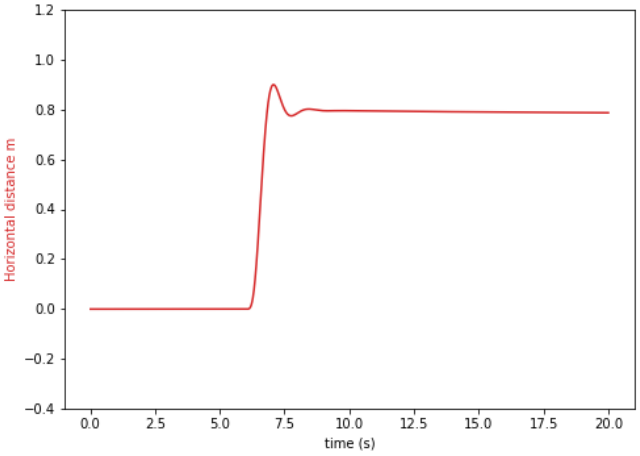

(d) Pitch angle.

Figure 9.5: Sample test simulation

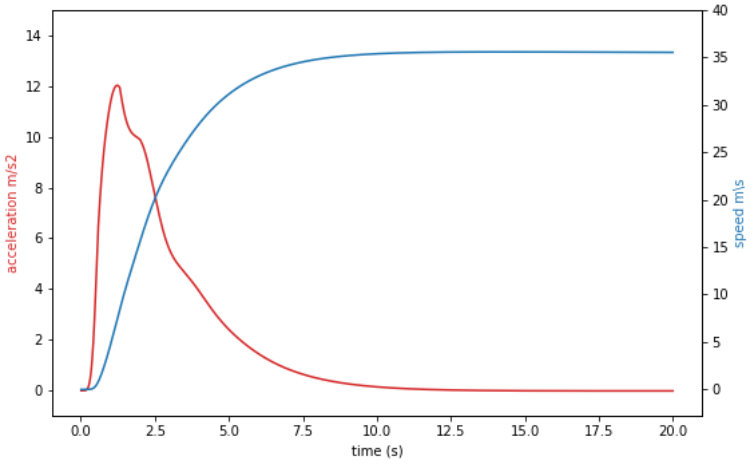

Figure 9.6: Longitudinal acceleration and speed requirement.

HB-FR-S-10 The vertical acceleration shall be at least 4.7 m/s^2. As shown in figure 9.7, the vertical acceleration requirement is met.

HB-FR-S-11 The longitudinal speed shall be at least 150 km/h. As observed in figure 9.6, the maximum longitudinal speed is 36 m/s which translates to approximately 130 km/h. Although this requirement is currently not met, it must be noted that the computed drag used in the model plotted makes use of the first drag approximation wherefore it differs from the maximum speed of 200 km/h. The final drag approximation could not be used in simulations as it resulted in singularity

HB-FR-S-12 The hover-bike shall be able to take turns with at least 1.7 G. Unfortunately this requirement is not met, since the maximum load factor in turns is 1.2 G. Although this experience requirement is not fulfilled, a fun and adventurous ride is still possible.
The simulation starts at -9.81 m/s^2 since thrust at the beginning is 0 N, causing the hover-bike to initially fall. At this stage of the simulations ran, an initial stable state of the hover-bike could not be added in the simulation.

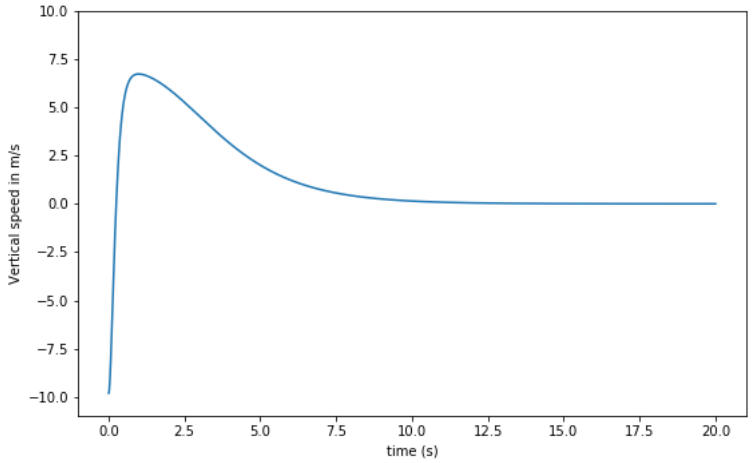

Figure 9.7: Vertical acceleration requirement. The simulation starts at -9.81 m/s^2 since thrust at the beginning is 0 N, causing the hover-bike to initially fall.
Note: the y axis label should read acceleration in stead of speed.

9.3.2. Thrill and Transportation Mode

As mentioned previously, Scorpeon will possess the ability to mount wings and ducts for a thrill and transportation mode. This inevitably will have effect on the manoeuvrability characteristics of the hover-bike, due to the increase in mass and MOI. This increase is such significant, that the control does not have to be adjusted for gains or filters to decrease the load factor during manoeuvring. Figure 9.10 simulates an exemplary flight which starts at a 28.6° degree pitch angle and 28.6° degree roll angle. After 10 seconds the reference roll angle changes to -28.6° degrees as indicated by the blue marker in figure 9.10. As expected the thrill mode is able to turn much tighter corners while receiving the same inputs, contributing to the adventurous and fun ride. Since drag due to changing attitude rates is not taken into account, the difference between the modes will be slightly bigger, as wings will significantly contribute to this rate induced drag.

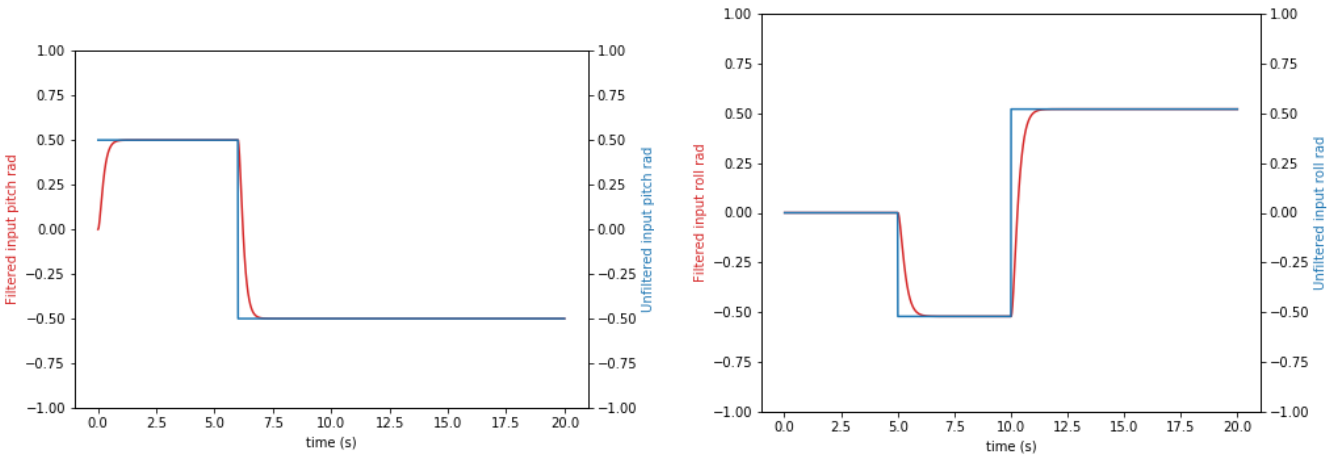

(a) Reference pitch input.

(b) Reference roll input.

Figure 9.8: Trajectory reference inputs.

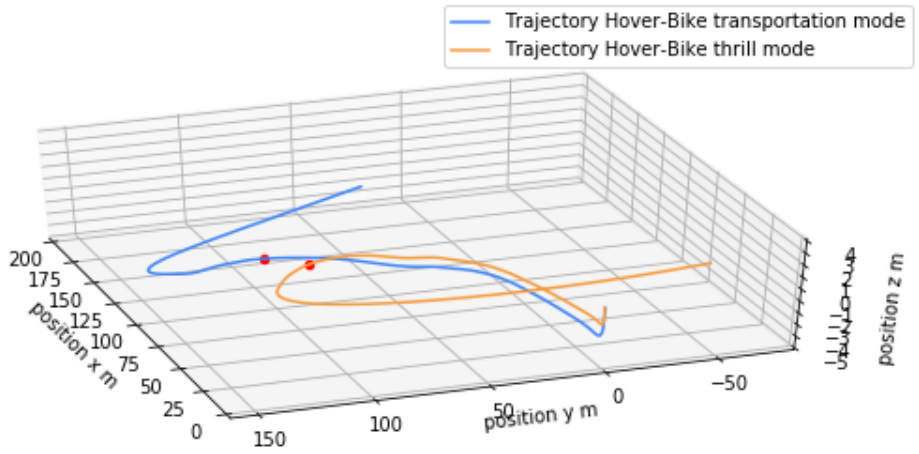

Figure 9.9: Difference in trajectories while receiving equal reference inputs..

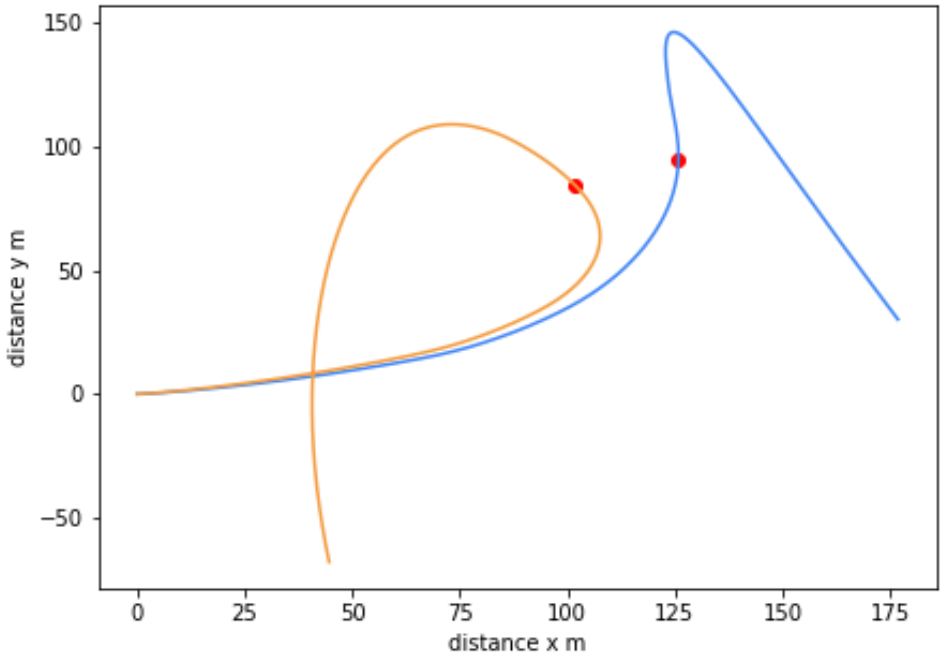

Figure 9.10: Top view of trajectories

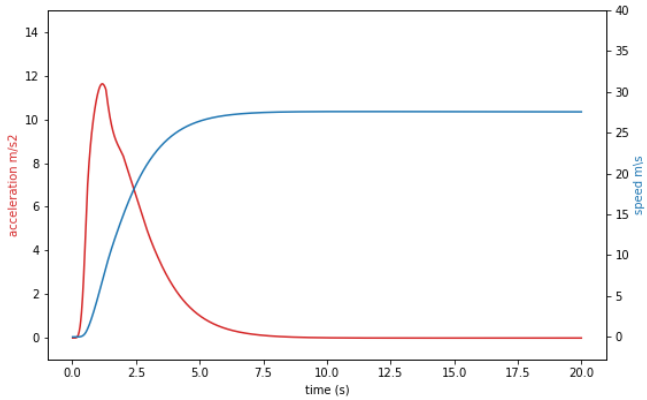

(a) Verification of model, drag multiplied by two.

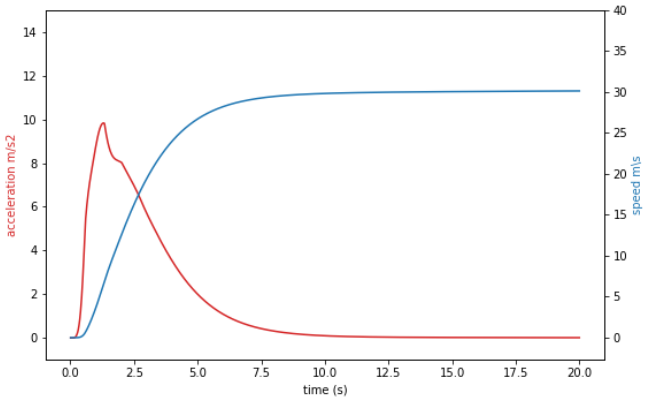

(b) Verification of model, doubled mass and MOI.

9.4. Verification & Validation

Verification Verification for the control and manoeuvrability characteristics means examining the method for assessing and simulating stability and manoeuvrability parameters. For this section it represents to what extent the mathematical, thus simulation, model represents the chosen physical model. In order to accomplish verification of the previous simulations and performance parameters given, designated model variables will be adjusted to analyse whether the output shall change as expected and accordingly. Specifically the correctness of the EOM will be investigated. Therefore to accomplish this analysis drag, mass and MOI will be varied and the result will be compared to the original output. Figure 9.11a increases drag by a factor of two and performs an equal simulation to figure 9.6. As expected and observed, the plot shows a slight decrease in acceleration and a significant decrease in maximum air speed. By doubling the mass and MOI the following graph 9.11b is created which is repeatedly compared to figure 9.6. Due to the increased MOI the acceleration has decreased as expected. Therefore, it can be concluded that the mathematical model used to simulate the dynamics of Scorpeon is correct and verified.

Validation Validation for the control and manoeuvrability characteristics means examining whether the simulation accurately represents the physical manoeuvres. In order to validate the EOM and model a similar multi rotor should be modelled for. However, since there are no comparable vehicles, parameter of a small drone shall be implemented and compared. By completing the same procedures that have been applied for the hover-bike simulations including PID tuning. The same sample reference inputs are given as in figures 9.8. The parameters which have been replaced are found in table 9.1. The validity and validation parameters were used from [52]. Figures 9.12 show similarity with the hover-bike simulations in 9.8. Difference are accountable by the weight and inertia changes of the drones, however the overall response is correct.

Table 9.1: Validation multirotor parameters.

Parameter	Value	Unit
m	0.468	kg
I_{xx}	$4.856 \cdot 10^{-3}$	m^4
I_{yy}	$4.856 \cdot 10^{-3}$	m^4
I_{zz}	$8.801 \cdot 10^{-3}$	m^4
A_{xx}	2.5	N/s
A_{yy}	2.5	N/s
A_{zz}	2.5	N/s

9.5. Sensitivity Analysis

The sensitivity analysis for the control part is slightly different than the sensitivity analyses in other chapters. Most design aspects, such as structures, change loads or dimensions and analyse whether the new design is exceeding a certain limit value. However for control, since control concerns modelling, the responses are the variable factor which possess certain characteristics as settling time and overshoot value. The variables calculated by structures, aerodynamics and propulsion are inputs which can be varied but who truly are not modelling properties. Purely control variables for the hover-bike wherefore a sensitivity analysis is performed, are filters and saturation blocks. Both the analysis have the same reference inputs given as 9.8 for comparing purposes.

Filters Filters in the control design are used to recreate a response delay for the electric motors, so thrust and torques are delayed. Would the delay become too large, the filtered signal will start counteracting the unfiltered input as can be seen in figure 9.13a. Would the delay be higher than 1.2 s the model will become unstable. Value below 1.2 s are feasible however lower values are preferred as the reaction time decreases as well.

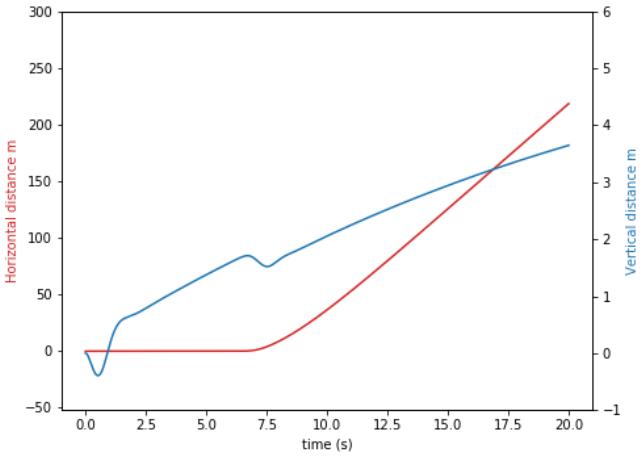

(a) Distance covered for x and z of the reference multi rotor.

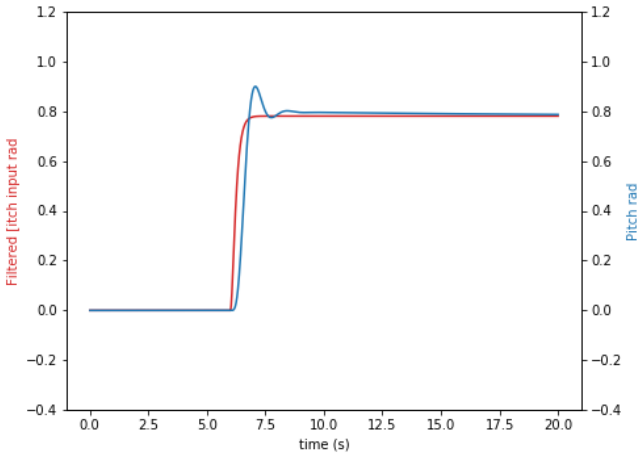

(b) Reference roll input of the reference multi rotor.

Figure 9.12: Validation reference multi rotor.

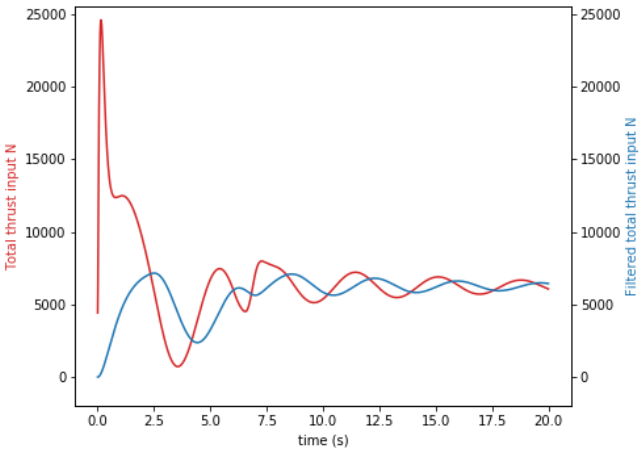

(a) Sensitivity analysis for filters.

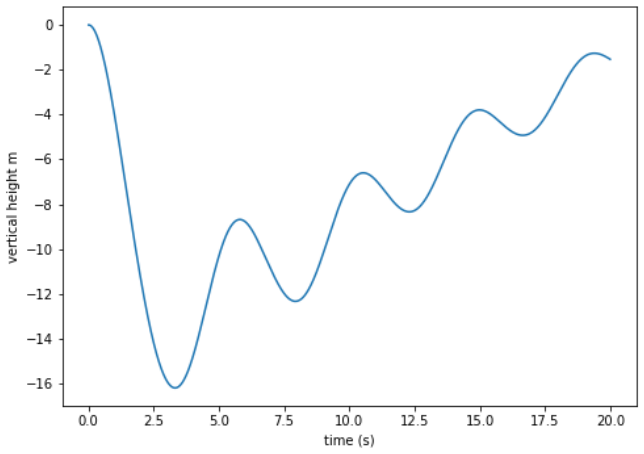

(b) Sensitivity analysis for saturation blocks.

Saturation blocks Saturation blocks limit signal values to a given maximum and minimum value. Saturation blocks are implemented for the control inputs T, τ_ϕ, τ_θ and τ_ψ. However would the band with of allowable values be too narrow, the model may become unstable and singularity is possible. Since T, τ_ϕ, τ_θ and τ_ψ are strongly correlated, adjusting saturation limits may interfere with the stability around other axis. By decreasing the saturation band with by 90 %, the response in figure 9.13b is observed. The latter response is on the edge of becoming unstable, meaning none of the saturation blocks for torque are allowed to decrease more than 90 %.

10
Human-Machine-Interface

To design the human-machine interface, one must first understand what is required of it. The main purpose of the system is to allow the pilot to control the Scorpeon comfortably with all the necessary information he might need to feel in control. It is therefore natural to start by identifying what inputs are needed from the pilot to directly control the hover-bike. These will be called "Fundamental Controls" and are the first things to be designed in section 10.1. It is crucial to provide the user with the necessary information he/she might need in-flight to assure his/her confidence mid-air. This specially includes the battery level or attitude/height of the vehicle. The way in which this information is communicated to the user is therefore the second thing that will be discussed in section 10.2. In addition to the fundamental inputs, there are some functions that the pilot might want to activate easily without scrolling through the interface's options. Such functions include the deployment of the parachute, which must be easily evoked by the pilot. These will be referred to as "secondary controls" and are discussed in section 10.3. The interface through which the user will be able to navigate through the hover-bike's options and optimise it to his/her flying style will finally be treated in section 10.4.

10.1. Fundamental Controls

In this section the fundamental controls will be designed. Before describing the final design, the process that lead to it will be briefly explained. This includes: identifying fundamental inputs, understanding the induced loads on the pilot, different design options, and finally the Final design.

Fundamental inputs

Since variable pitched wings have been discarded, the control of the bike is achieved solely through differential thrust, which means that analogous to a drone there are only four possible forces that can be exerted on the vehicle: τ_x,τ_y, τ_z and Z. Note that the same reference frame is used as in chapter 9 in which τ_x,τ_y, τ_z are angular accelerations around x, y, z respectively and Z is a linear acceleration along z. Through these 4 forces, position, velocity, acceleration and attitude are achieved. Depending on the level of automation and the flight mode that the pilot chooses, different inputs can be chosen to control the machine. For instance, while beginner drone pilots might choose to control roll and pitch angle with self levelling features, advanced pilots prefer to use the "acro" mode in which they control pitch and roll **rates** due to its increased freedom of manoeuvrability. Regardless of the mode chosen, there will always be four inputs needed: pitch control, roll control, yaw control, and thrust control. Note that for example, the pilot might choose to only control height, his intended direction in the two dimensional plane at that height, and his orientation (in that same plane). This option would still need 4 inputs, and it is the flight controller which based on what the pilot requires calculates the necessary reaction forces on the vehicle.

Loads on the pilot

The different loads that the pilot will experience strongly affects the way the human-machine interface is designed as bio-mechanical feed-through should be avoided at all costs. The predicted maximum loads are portrayed in Table 8.9. As we can see, the maximum loads experienced by the pilot are all achieved in the thrill phase. This is due to the higher thrust-to-weight ratio without the added weight of the wings. With the wings, a load lower than 0gs in z could potentially be attainable with a negative angle of attack, but the flight computer will make sure this does not happen. In any case, the pilot will be provided with a seat-belt which secures his hips to the seat but does not fix his upper body, which is only restrained by the core strength of the pilot. Similarly, even-though the machine is capable of inducing lateral accelerations (in y) as strong as longitudinal ones (in x), the Scorpeon is not designed to be driven sideways so lateral support must not be as extensive. Since the handling mechanism is assumed to be at arms length to the pilot's cg, and the seat-belt can be considered to act as a hinge on the pilot, rotational accelerations are assumed to be counteracted by the pilot as linear forces on the handling system. This assumption is better portrayed in Figure 10.1. The magnitude of rotational accelerations, which are achieved by differential thrust between motors are programmable to match the pilot's abilities to counteract it and avoid inducing unwanted inputs. It is now clear that the combination of the pilot's hands must be able to support him/her in x, y, and z.

Table 10.1: My caption

	X	Y	Z	$\mathscr{L}$	$\mathscr{M}$	$\mathscr{N}$
Transportation mode	± 0.67g	± 0.67g	-1.4g-0g	weak	moderate	weak
Thrill mode	± 0.81g	±0.8	-1.7g-0g	moderate	strong	weak

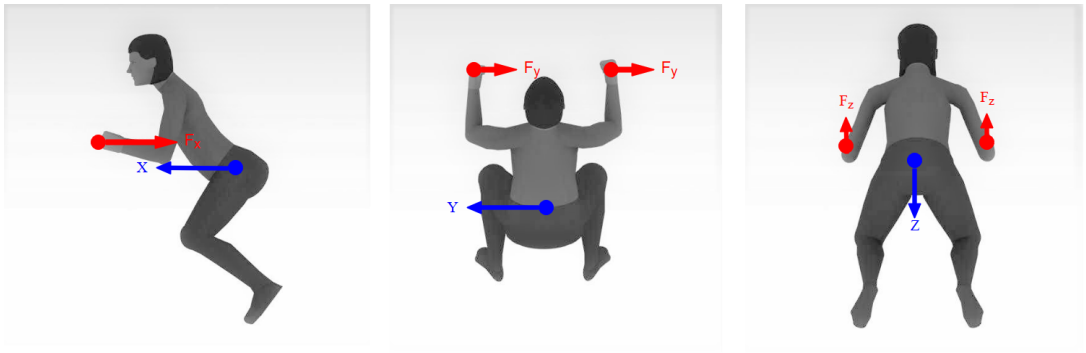

Figure 10.1: Forces on the controls due to hover-bike accelerations

10.1.1. Final design: joybar and pedals

A hover-bike is a unique concept, this is due to the fact that it has the same degrees of freedom as a drone but prefers the control mechanics of an aircraft or motorcycle. A drone is controlled with a joystick which is fine because the person controlling the drone is not feeling the accelerations and movements of the drone itself. When a person moves along with the controlled object, and in this case a hover-bike, a "drone" joystick is not preferred. A handlebar is more "fun" and "intuitive" when controlling a hover-bike and leads to a similar experience and thrill level as that of a motorcycle, except a handlebar has limited control over inputs as there are now 6 degrees of freedom. This is why we chose a unique handlebar design in order to control the hover-bike in all 6 degrees of freedom. The JoyBar is a combination of an aircraft joystick and a motorcycle handlebar. The ends of the handlebar are supported with forearm supports and the hands are placed in a sphere (Joysphere) where it holds a stick as can be seen in Figure 10.2.

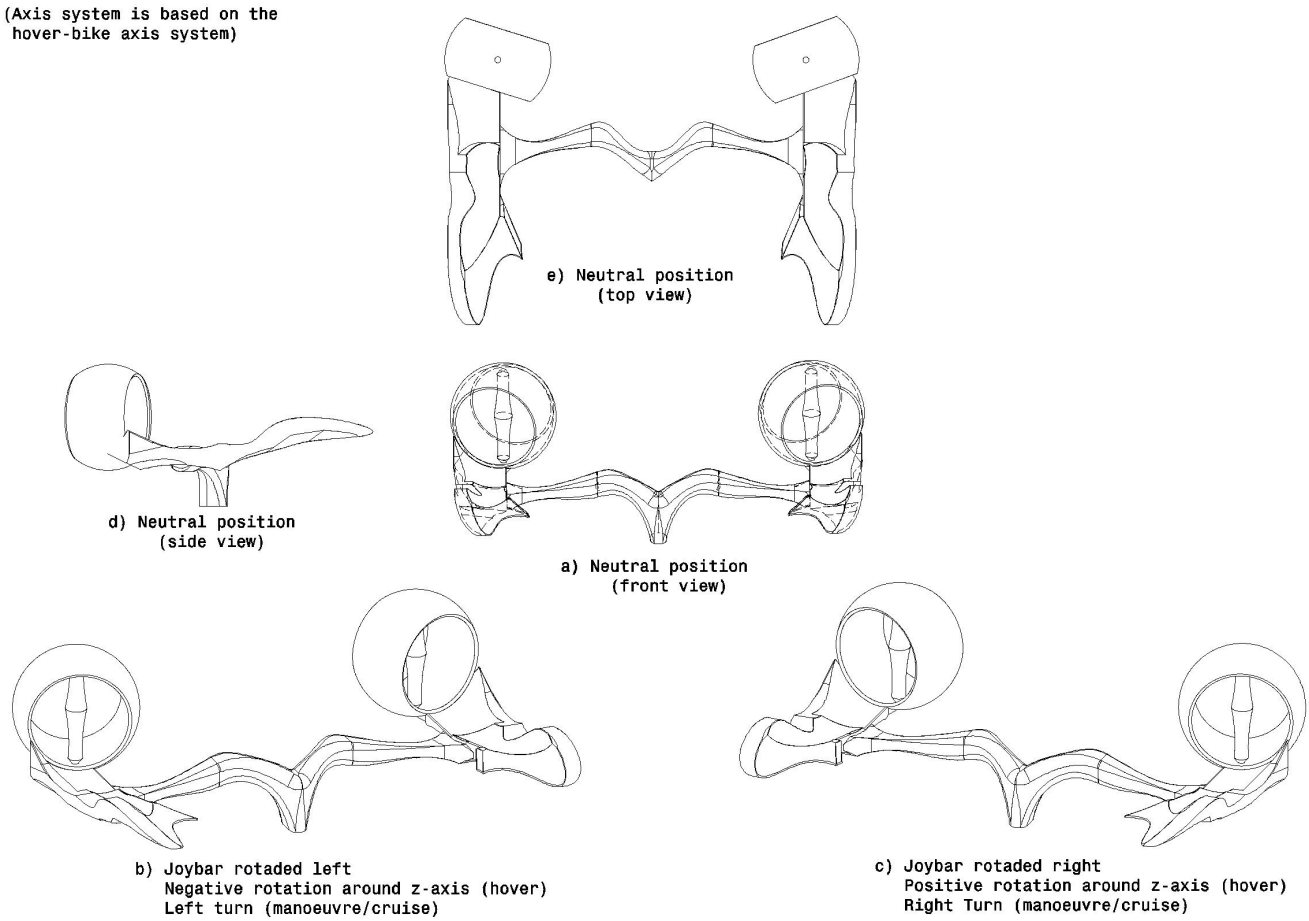

Figure 10.2: The Joybar and its movements

The controls are split into the hover phase and into the manoeuvre/cruise phase. During the hover phase the Joybar is only used to yaw by rotating the Joybar (Figure 10.2 b and c), during cruise rotating the Joybar causes the hover-bike to make left and right turns. For all other controls the Joysphere (Figure 10.3) is used.

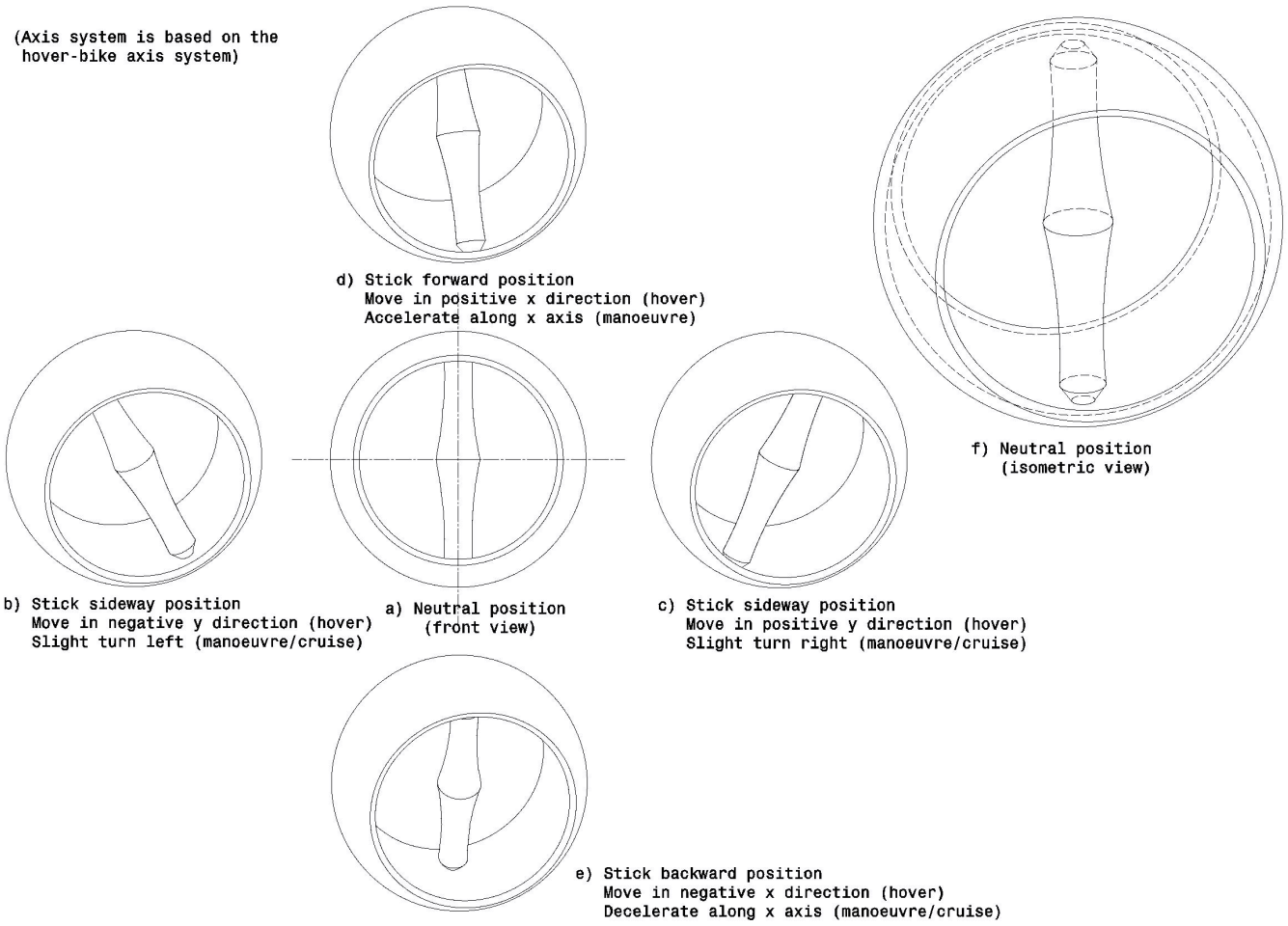

Figure 10.3: The Joysphere and its movements

During hover moving the stick inside the sphere sideways makes the hover-bike roll that induces a sideways movement, and during manoeuvre/cruise the hover-bike makes a slight turn (Figure 10.3 b and c). It is a "slight" turn because in manoeuvre/cruise turns are mainly done by rotating the entire Joybar. The sphere is also used to accelerate forward and to brake (decelerating). This is done by moving the stick forward and backwards, which are shown in Figure 10.3 d and e.
As mentioned before, the Sphere is supported by a forearm support. This is to maximise the support to the pilot arms in order to keep the pilot stable and in order to minimise the "support" force on the stick to keep the pilot at a stable position. This way all the force exerted on the stick are pure for manoeuvring. Finally, with the pedals the height is controlled. The legs of the pilot are supported and the right foot is free to move during each phase and does not require to exert a force to keep the pilot stable on his seat. This way pressing the pedal the front of the right foot makes the hover-bike go up and pressing the pedal with the back of your foot (heel) makes the hover-bike go down. This way during hover, manoeuvring and cruise all 6 degrees of freedom are covered.

10.2. In-flight information

Providing the pilot with flight data makes his flying experience safer and more enjoyable. Due to restricted space in the cockpit however, there must be a compromise in the information that is displayed. The space available to the pilot is first analysed to identify potential locations for information display and secondary controls. Considering the position of the pilot, there are three obvious places to display information: on the handlebars, in front of the handlebars (below the windshield), and on the windshield. In Table 10.2, the information that can be available to the pilot is shown for three regimes: thrill mode, transportation mode, and pre/post-flight. While data that must be displayed is marked with a "yes", parameters with "opti." refer to secondary data that can be displayed according to the user's taste but is not mandatory. The optional information choice will increase in size as the customers report to the Headquarters (through feedback in the website) what they would find usefull. A "no" implies that such information can not be displayed in this regime as it could lead to the pilot getting distracted and cause damage. It is important to keep in mind that there should not be too much information available at once as this can make the display confusing and inefficient. Note that a "*" represents information whose importance mandate its availability even if the display fails. There will therefore be redundancy in the availability of this data.

Table 10.2: Data available to the pilot

Data	Displayed in flight mode?		
	Thrill mode	**Transportation mode**	**Post/pre-flight**
Battery status *	Yes	Yes	Yes
Time/range untill dead battery *	Yes	Yes	Yes
Map and GPS	Opti.	Opti.	Opti.
FLARM	Yes	Yes	Opti.
Flight mode	Yes	Yes	Yes
speed	Yes	Yes	Opti.
altitude *	Yes	Yes	Opti.
maintenance	No	No	Opti.
ESC/motor/ battery temperature	Yes	Yes	Opti.
Warning indicator*	Yes	Yes	Yes
Black-box/ flight log	No	No	Opti.
Attitude	Yes	Yes	Opti.
Audiovisual entertainment	NO	Opti.	Opti.
Weather forecast	Opti.	Opti.	Opti.

Figure 10.4 gives an idea of what the cockpit will look like. Note that this is a top view, so the view of the pilot would be sightly lower. This is why the parachute activation handle seems quite exposed while in real life, it might not even be visible from the top view as it would be hidden by the structural beam. The main flight display is in front of the joybar angled towards the pilot. It is split in 2 sections, the Crucial data is constantly displayed on the left half while optional data is shown on the right side and the pilot can juggle through different optional data. The information that is extremely important is visible on the wing-shield bottom beam so that it is in the pilot's field of vision while operating the vehicle. This includes the FLARM, altitude, battery status and a warning light that warns the operator of a problem which will be displayed more thoroughly in the "optional data" section of the display. The different switches and control knob can be seen behind the joybar.

Figure 10.4: Pilot view of the cockpit

10.3. Secondary controls

Apart from the joy-bar and pedals, which control basic flight, there is a need for other interfaces to interact with the rest of the system. Each of the needed control inputs will be discussed along with their input method. The position of these controls can all be seen in Figure 10.4

Parachute deployment

The parachute deployment system must be easily accessible in order to assure a rapid activation. Given that the parachute is located in the nose of the Scorpeon , a mechanical activation lever is fitted at the far front of the cockpit. To avoid accidental deployment, the lever must be rotated 90 degrees and pulled. The mechanical aspect of this lever makes the parachute deployment completely independent of any other subsystem, which is preferable as it is a failure in other subsystems which cause the need for deployment in the first place.

Self land

A switch that can be activated to make Scorpeon auto-land can be very useful in various occasions. Such instances can range from sudden physical discomfort,hindering his piloting abilities, to a novice who does not feel comfortable to land by himself. To avoid accidental activation, this switch has a cover which must first be lifted to reveal the toggle-switch switch that can then be activated. This is similar to the engine switches in a commercial aircraft cockpit.

Auto-pilot

As soon as the auto-pilot switch is engaged, the flight-computer will use the current heading, speed and altitude/vertical velocity and keep these constant. Simultaneously, the auto-pilot "window" appears on the main display, which shows the different parameters with their current value. The pilot can then use the knob and arrow to change any value he wants. Since thrill mode is all about having fun handling the hover-bike, this feature is mainly intended for the less exciting transportation mode.

customised input

Two extra three-position switches will be used as customised inputs for the pilot. This might be used to change flight characteristics like switching from sport mode to standard mode, changing the input mode from angle to angle rate, or to change more simple display related setting like the optional data to be shown in which screen.

knob, arrows and general input

This is the main controls used to navigate through Scorpeon's interface. It consists of a knob with a button in its centre. The knob can also be moved upwards, sideways, and downwards to navigate through the interface. This is the equivalent of a mouse in a computer. If confused, please refer to the picture.

10.4. Vehicle options interface and customisation

The different settings that can be changed in the hover-bike will now be briefly mentioned. It is important to point out that These setting are unique to the user as Scorpeon remembers what setting were chosen for each key-card, making one shared vehicle customised to several different people. The different settings that can be changed are :

- Joybar input-definition (only in thrill mode as transportation mode is highly automated to be very efficient)
- Joybar sensitivity
- Optional information to be displayed
- Customised switches definition
- Limiting maximum acceleration and angles more than the predefined software
- Flight mode

A new pilot should be able to adequately fly the Scorpeon within six hours of training. This training is done by using a simulator that could be run on a laptop with the joybar. This allows all newbies to have some experience and know what to expect before flying the real thing.

11
RAM

RAM is an acronym that stands for reliability, availability and maintainability which is an analysis that is performed in order to predict failure modes and their consequences on the hover-bike and pilot. Moreover, these analysis are done to check the functionality of the hover-bike under certain conditions.

11.1. Reliability

Reliability is defined as the probability of the hover-bike performing a certain function under given conditions within a specific time. In order to analyse reliability of the hover-bike the reliability of each component is required to be evaluated from mathematical simulations or from reference data. However, due to the early stage of the design accurate reliability values are hard to be achieved, hence references from other vehicles reliability will be used in order to analyse a fist estimate of the hover-bikes reliability.
In order to analyse the reliability it is required to go from bottom to top as seen in Figure 11.1. That allows to see which components can be increased in reliability either by adding redundancy or by getting a higher quality and more expensive component to increase the total reliability of the whole system as reliability is calculated using Equation 11.1 and the total system reliability is the multiplication of each subsystem that builds up this system.

$$R(t) = e^{-\lambda_f t} \tag{11.1}$$

First in order to be able to calculate reliability it is assumed that all the components have an exponential failure rate with time, however this is not an accurate estimate as different components can have different failure modes but it helps building up a first estimate for reliability. Failure rate is the number of times a component can fail with in a determined period of time.
To establish a rough estimate for the hover-bike reliability, the reliability values of small aircraft, around 1000 kg, are used. These values are found in a study done by NASA[12]. Dividing the major hover-bike into four systems, structures & aerodynamics, electrical, propulsion and safety & control, the values from the data sheet can be extrapolated. This generates the reliability values found in Table 11.1.

Table 11.1: Reliability estimates from data sheets for a 6 hour mission [12]

System	**Reliability**
Structures & aerodynamics	0.99940
Electrical	0.99997
Propulsion	0.99986
Safety & control	0.98080
Total Reliability	**0.98004**

The numbers given in Table 11.1 represent the reliability values of aircraft during six hour missions. These, already, have been in the market for so long that their reliability keeps growing in accuracy. However, in the case of the hover-bike, which uses an innovative form of flying, can be affected by risks that might not be accounted for which can lower the reliability of the hover-bike. Moreover, due to lack of information about the reliability of the battery pack, the reliability can also decrease ever further. Meanwhile, having redundancy in ESCs, motors and sensors, the reliability of the hover-bike is increased. Furthermore, since the brushes almost don't have any moving parts compared to regular combustion engines, the hover-bike's reliability is increased even further.

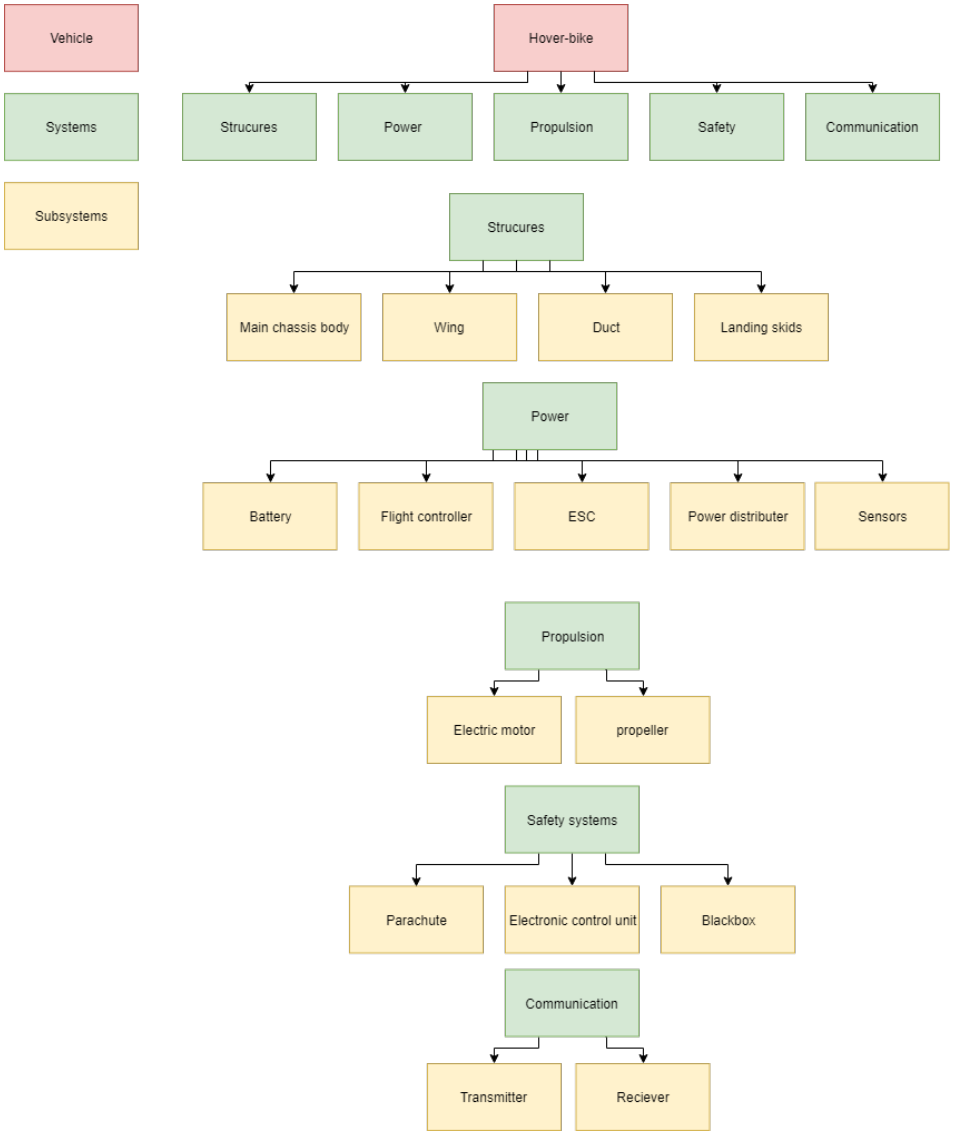

Figure 11.1: Reliability lay-out of the hover-bike

11.1.1. Complex system reliability

The reliability for complex systems can be measured or specified by using mean time between failures (MTBF) given in Equation 11.2[2], where the mean time to failure corresponds to the average time to failure of non-repairable components and the mean time of repair is used to capture the complete break-down and repair cycle. Moreover, another method that can be used is the failure in time (FIT) which is defined as the failure rate per billion hours[2].
Unfortunately, at this stage of the design the reliability calculated is based on references which are not accurately calculated. In order to get more reliable data, in the following design phases tests have to be performed, for example by using the Arrhenius High Temperature Operating Life (HTOL) model [2] which can calculate the reliability of components based on test data.

$$\text{MTBF} = \text{Mean time to failure (MTTF)} + \text{Mean time to repair(MTTR)} \tag{11.2}$$

11.2. Availability

Availability is a measure of how much time the system can be operational assuming optimum performance. In order to assess availability a clear definition of the conditions when the hover-bike is "available" and when is it "unavailable" needs to be assessed. The hover-bike is unavailable during the charging of the battery, which is estimated to take about two hours. Additionally, it is unavailable during transportation of the hover-bike from parking location to the the take-off location which takes around 30 to 60 minutes as a first estimate, as it differs depending on the location of residence of the pilot. Pre-flight checks, preparations and periodic maintenance checks per flight hour takes about fifteen minutes which the hover-bike is considered to be unavailable. All the values given above gives a summation of unavailable time of about three hours taking transportation time about 45 minutes.
Furthermore, the analysis of hover-bike's availability should be done double, as the operating time differs depending on selected mode. Using transportation mode it gives one hour of available time, however, using thrill mode gives an available

time of about 20 minutes.

$$\text{Availability} = \frac{\text{Available time}}{\text{Available + unavailable time}} \tag{11.3}$$

Using the equation mentioned above it can be found that the availability for transportation mode is 0.25 and for thrill mode is 0.1 using transportation time of $45 mins$ as an average value.

11.3. Maintainability

Maintainability of the hover-bike is the measuring method of the ease or complexity of performing a maintenance. A better definition is the probability of restoring a component to its optimal conditions, within a certain period, using limited prescribed tools and resources.
In order to analyse the maintainability of the hover-bike the method of finding the mean time to repair (MTTR) [7] is going to be quantified using equation 11.4 which is used to find the average of the maintenance time in case of failure.
Unfortunately, at this point of designing the hover-bike its challenging to analyse the MTTR due to lack of information about subsystem maintenance and lack of information to simulate the repairing time of the hover-bike subsystems.

$$\text{MTTR} = \frac{\text{Total maintenance time}}{\text{Number of repairs}} \tag{11.4}$$

12
Safety

Even though an excellent safety record may not be the first thing that comes to mind with the concept of a hover-bike, its safety standards are just as high as any other aerial vehicle. This section will discuss the systems that are in place to mitigate hardware failure and human error. Furthermore, safety systems are either active or passive safety measures that will be further discussed and analysed. Moreover, human error is one of the main reasons for accident occurrence in vehicles , hence further analysis to mitigate and limit human errors are going to be discussed.

12.1. Dead-man zone analysis

The hover-bike has 6 propellers, each driven by an electric motor and electronic speed controller. Failure in any one of these would cause a rotor to stop spinning. Furthermore, all of these components are powered by a battery. Three safety systems are set up to mitigate failure in aforementioned components.

12.1.1. Landing gear

Similar to conventional helicopters, the landing skids are designed to absorb impact. Therefore the landing gear is the main safety system for altitudes below 5 meter.

12.1.2. Redundancy

A failure in one of the ESC's, motors or propellers would result in the loss of thrust at only one rotor blade. As long as the forces and moments are still balanced the hover-bike will be able to land safely with the thrust provided from the remaining 5 rotor blades.

Redundancy check: Assume one rotor of a contra-rotating pair fails. The remaining rotor will have to produce a thrust $\frac{1}{3}$ the weight of the vehicle. A thrust to weight ratio of 1.05 is necessary to maintain basic manoeuvrability. The required power of the remaining rotor for both the performance (no duct) and endurance (duct and wing) configuration is calculated below using momentum theory.

Performance configuration

m : $\frac{440}{3} = 147$ [kg]
A : $2.01[m^2]$
F.M. : 0.6
η_{motor} : 0.9
η_{duct} : no duct

$$P = \sqrt{\frac{(mg\frac{T}{W})^3}{2*\rho}}\eta_{motor}\eta_{duct} = 49.0 \text{ [kW]}$$

Endurance configuration

m : $\frac{500}{3} = 166$ [kg]
A : $2.01[m^2]$
F.M. : 0.6
η_{motor} : 0.9
η_{duct} : 1.2

$$P = \sqrt{\frac{(mg\frac{T}{W})^3}{2*\rho}}\eta_{motor}\eta_{duct} = 42.1 \text{ [kW]}$$

Since the maximum power of the hover-bike motors is rated at 50 [kW], it can be concluded that the single rotor will be able to provide a sufficient amount of thrust for both configurations. The torque created by the propellers can be balanced as shown in the figure below.

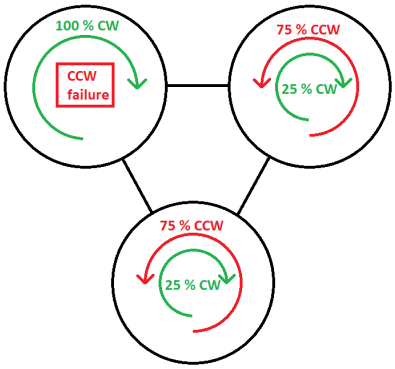

Figure 12.1: Torque balancing during engine failure

Dual rotor failure cannot be mitigated with the redundancy mode. The redundancy mode will be activated automatically by the flight controller in the event of a failure. The pilot will be advised by a warning message to land immediately.

12.1.3. Parachute

The hover-bike is also equipped with a ballistic parachute. The parachute can be activated by a manual system at any time by the pilot. No electrical or automatic deployment systems by the flight controller were considered. This is done such that the parachute can be safely deployed in the event of any electrical or battery failure. It is therefore up to the discretion of the pilot to deploy the parachute manually if the altitude is sufficient and the landing area is safe. The parachute system should be deployed at altitudes above 80 [m] to allow for enough time for the parachute to fall open and the ability to land safely. [1]

12.1.4. Overview

Below a comparison table and the height velocity curve can be seen for the 3 safety systems.

Table 12.1: Safety systems

	Landing gear	**Redundancy**	**Parachute**
Allowed Component Failure	ESC Motor Propeller Battery Electrical	ESC Motor Propeller	ESC Motor Propeller Battery Stucture Electrical
Suitable activation altitude	0 - 5 [m]	5 - 1000 [m]	80 - 1000 [m]
Safety mode	Impact absorbtion	Powered landing	Parachute landing
Activation mode	Always connected to structure	Automatic	Manually by pilot

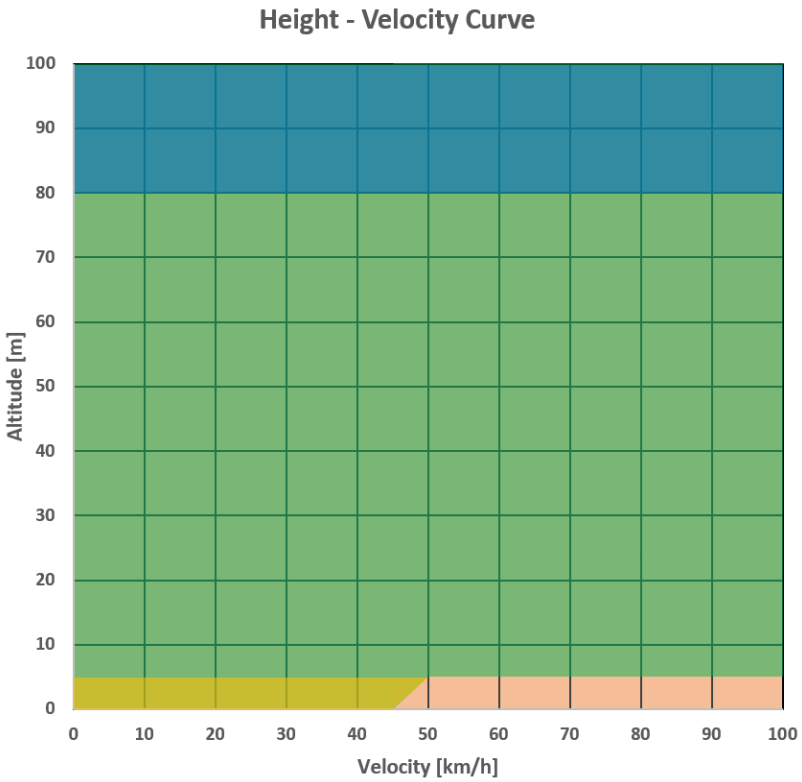

Figure 12.2: Height-velocity curve for all safety systems.
Yellow: Landing gear
Green: Redundancy
Blue: Parachute and Redundancy
Red: Avoid

It is worth noting that the red zone should be avoided since as a result of the high horizontal velocity the impact on the landing gear would be too large. Furthermore, it is advised to ascend to altitudes above 80 [m] quickly. The list of allowed failures is most extensive here and it gives the pilot more time to react to failures.

[1] URL: `https://www.galaxysky.cz/grs-5-560-115m2-p36-en` [Cited 28th June,2018]

12.2. Human error

One of the main cause of accidents for aerial and terrestrial vehicles are caused by a human mistake. This occurs due to many reasons starting from wrong decisions, panicking or even by mishandling the vehicle into extreme conditions it is not designed for. In order to minimise and eliminate the human errors, a few measurements will be taken to overcome these errors.

Firstly, a designated airspace will be booked for the hover-bike recreational manoeuvring which will limit the fear of other aerial vehicles interfering with the hover-bike. Moreover, the hover-bike will be equipped with the FLARM which is a device that keeps the pilot informed of the location of other vehicle in order to avoid a collision before it is too late. As an additional safety layer, general collision avoidance rules will be taught to the pilot in order to avoid vehicles that do not have FLARM or TCAS installed. However, in case of the failure of all above scenarios, then a quick reaction is required from the pilot to make his own decision.

A pilot may misuse Scorpeon by flying in undesignated airspace or pushing the bike beyond it's technical limits. Both of these scenarios will be discussed.

In order to limit the misuse of the hover-bike in terms of controls, some parameters will be limited to certain values that can not be exceeded by the pilot. In case the pilot tries to exceed those limits, a warning message will be shown to him that the inputs are unavailable for safety reasons. The limited parameters will be the pitch, roll, speed, and the number of gs that the pilot can pull. Firstly the pitch will be limited to 45 degrees both in transportation and thrill mode. Moreover, the roll will be limited to 20 degrees for transportation mode and 45 degrees for thrill mode. Furthermore, the speed limit for thrill mode is 200 km/hr, while the speed limit for transportation mode is set to 150km/hr. In addition, the gs that a driver can pull will be about 1.5g for transportation and 1.7 for thrill mode.

Due to high g manoeuvres or in case of a panic attack due to high altitude or dizziness, a few steps should be taken by the pilot. Firstly the pilot should take off his hand from the controls this will allow the hover-bike to stabilise into hovering which gives the pilot a chance to catch his breath and prepare him to perform landing manoeuvre if required.

Humans tend to be curious about what is the surrounding them which increases the risk of pilots going beyond the designated airspace. In order to prevent this situation or to minimise the impact that it can cause a few measures are taken. The hover-bike will have GPS sensor data sent to the air traffic control in order to locate it. In case the pilot goes into restricted airspace, an error message will be first shown on the hover-bike screen and if this message is ignored, the air traffic control will contact the pilot in order to let him know that he is trasspassing into a different undesignated airspace.

12.3. Passive safety

In this section, passive safety measures will be discussed to have a deeper understanding of the safety measures taken by the hover-bike to ensure the pilots safety. First, the battery safety will be discussed, followed by the redundancies to improve the hover-bike reliability and decrease risk.

Firstly, battery safety had to be taken into account as it is one of the most crucial aspects of using electric power supply especially lithium ion batteries. The risk of battery venting due to short circuit or due to overloading the batteries can lead into catastrophic events that might even cause explosion of the battery. The first aspect considered in the design is having two battery packs instead of one as in the worst case scenario, it is easier to contain one battery-pack explosion than two. A battery shell will be designed in order to keep the explosion from the pilot without harming him. Moreover, redundancy has been added to the batteries in such a way that if 4 strings of cells fail, the pilot will be informed allowing him to initiate landing with enough power required. Furthermore, to avoid over heating and pressure building up in case of battery venting an air cooling mechanism will be designed.

Further safety measures were also required for the pilots safety. Due to the manoeuvres the pilot can perform there is a probability of him being imbalanced on the hover-bike , hence a leg harness will be added in order to limit the lower body movement from the hover-bike.

Systems reliability is boosted to increase the safety of the hover-bike. That is done by adding as a first layer of safety redundancy for sensors as their redundancy benefits beats the weight and cost penalty that they can cause. Furthermore, in case of redundancy total failure of some sensors can be compensated by the combined output of other sensors. For instance: if the GPS sensor failed, the accelerometer, pitot-tube and gyroscopes will make an estimation of where the hover-bike location will be.

13
Technical risk assessment

During the previous phases the risks of the hover-bike were assessed. After assessment a mitigation plan was set up [42]. In the final design a more detailed design is created using fault tree analysis. Therefore, a more specific technical risk assessment can be performed.

13.1. Fault tree analysis

A fault tree analysis (FTA) is a top-down approach for analysing reliability from systems level into component level, by organising the component in terms of failure relationships. Moreover, the fault tree is structured by starting on the top cell with the final event that can occur. Then going down the tree the cells will represent system failure that must occur to result into the higher events to occur. The cells are connected by a Boolean AND and OR gates to represent the failure.

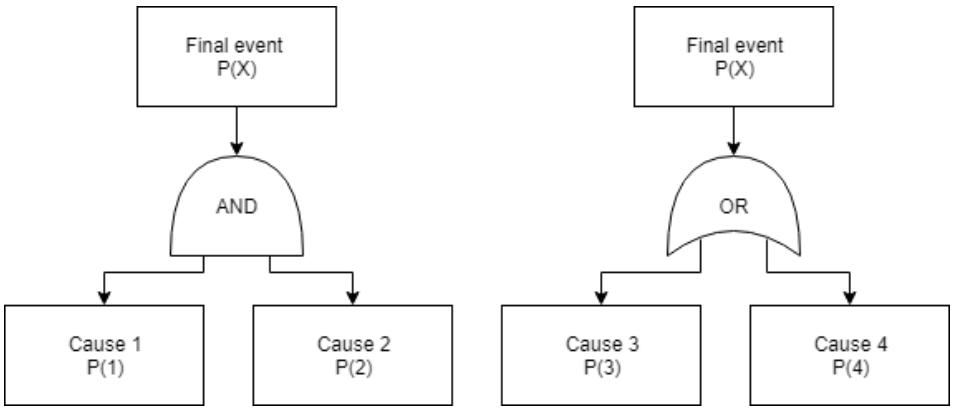

Figure 13.1: Fault tree analysis simplified example

Using Figure 13.1 the probability of event X to occur is caused by 1 and 2 to occur simultaneously giving a probability equation giving in Equation 13.1. Moreover, in case of the failure being caused by cause 3 or cause 4 then the probability of failure is given in Equation 13.2.

$$p_x = p_1 p_2 \tag{13.1}$$

$$p_x = p_3 + p_4 - p_3 p_4 \tag{13.2}$$

13.2. Risk identification, assessment & mitigations

In this section the risks of the hover-bike will be identified and assessed. Next to identification and assessment, the risk of the event will be mitigated. The final events will occur as consequence of lower level events. Therefore, when the lowest level of events are mitigated this automatically result in mitigation of the higher level events. Moreover, the likelihood of each risk to occur is assumed due to the lack of information, because the likelihood of risks are depending on tests and data available. This is done to show in the mitigation if the likelihood or impact was mitigated.

13.2.1. Power system

The following identifications and assessments of the events are based on the FTA of power. The FTA can be seen in figure 13.2.

Battery overheating (1.1.1.a): When too much power is drawn from an individual cell the temperature can increase significantly. This can result into battery venting. Without the safety systems, the likelihood of this event occurring is rated as likely and the impact will be catastrophic. Therefore, safety measures are implemented in the design.

Firstly to reduce the impact of venting of the battery cells venting holes will be placed in the casing of the battery pack. Therefore, no pressure can be build up. Secondly, to reduce the likelihood a battery controller will be added which can cut of string of battery cells in case they are overheating. This reduces the likelihood to unlikely and the impact to critical.

Short circuit (1.1.1.b): A battery short circuit can occur inside the battery pack. This can for example be a result from moisture entering the battery package or an internal connection can get undone and make contact with other parts inside the battery package. The likelihood of this happening is expected to be unlikely. However, the impact can be catastrophic.

To mitigate this, the cells will be arranged in such a way that the chance of an internal short circuit occurring is reduced. Also a the battery controller can cut of strings which will reduce the impact. Resulting in a likelihood of very unlikely and an impact of critical.

Manufacturing error (1.1.2.a): Making mistakes is something that can not be ruled out. This can also happen during manufacturing of the hover-bike. Manufacturing errors can result into connection failure in the power system. Therefore, the impact of the production errors is rated to be critical. The chance of a manufacturing error occurring on a single part of the production is low. However, since the production of the hover-bike needs a great number of actions the likelihood is rated to be possible.

Reducing the work pressure by given the engineers more time during manufacturing will help reducing the likelihood. Secondly, hiring higher skilled people will also help reducing the likelihood. This reduces the likelihood to unlikely.

Extensive vibrations (1.1.2.b): Extensive vibrating of the hover-bike can have big influence on the state of the battery. Especially it can result in loosening of connections. After one connection is loosened, this can result in moving parts inside the battery, which can cause even more connection failures. Therefore, the impact is rated as catastrophic. However, the chance of this happening is relatively low and therefore the likelihood is rated as possible.

To reduce the impact of extensive vibrations a cover will be placed over the cells such that this prevents internal part from moving as much as possible. To reduce the likelihood the battery packs will be placed on dampers. This will dampen some vibration the battery packs receive via the frame. This reduces the likelihood to unlikely and the impact to critical.

Overheating (1.2.1): The overheating of the power distribution can occur when the system is overloaded. This means that the cable can warm up to much which can cause a fire. Therefore, the impact of overheating of the power distributions is rated to be catastrophic. However, the likelihood of this event happening is rated to be unlikely.

To mitigate this event fire resistant cabling will be used on the hover-bike. This will reduce the impact of the overheating. Also, a safety margin will used on the cable thickness. This reduces the impact to critical and the likelihood to very unlikely.

Manufacturing error (1.2.2.a): This event is comparable with the event *Manufacturing error (1.1.2.a)*. Therefore, the likelihood and the impact are comparable. They are rated to be possible and critical, before mitigation. After mitigation they are rated to be unlikely and critical.

Extensive vibration (1.2.2.b): Extensive vibrations will not have great effect on on power distribution system, since most of the power distribution system consist out of flexible cabling and cable connections. Therefore, the impact is rated to be minor. Since most of the vibrations will come from flying the hover-bike the likelihood to occur is likely.

The impact of extensive vibrations can be reduced by strapping the cabling to the frame of the hover-bike. This reduces the impact to insignificant.

Short circuit (1.2.3): Short circuit inside the power distribution system can lead to an overall failure of the hover-bike. A short circuit can can cause an overload of the whole system. This increases the chance of fire. Therefore, the impact of a short circuit is rated to be catastrophic. The likelihood, however, of a short circuit occurring is relatively low. Therefore, the likelihood is rated as possible.

To mitigate this event all the components will be shielded where possible. Also circuit brakes will included into the design. This reduces the likelihood to very unlikely and the impact to critical.

Overloading ESC (1.3.1): During cruise flight the chance of overloading the ESC's is low. However, during intense use of the hoverbike the power use will drastically increase, increasing the likelihood of overloading. Therefore, overloading of the ESC's is rated to be likely. Since the ESC's are crucial for controlling the electric engines the impact will be critical.

To prevent the ESC's form overloading the maximum power from the batteries to the ESC's will be limited by the power distribution board. This will reduce the likelihood to possible.

Manufacturing error (1.3.2.a): This event is comparable with the event *Manufacturing error (1.1.2.a)*. Therefore, the likelihood and the impact are comparable. They are rated to be possible and critical, before mitigation. After mitigation they are rated to be unlikely and critical.

Extensive vibrations (1.3.2.b): Since the ESC's will be placed relatively close to the engine they will likely suffer from extensive vibrations. However, since the ESC's consist out solid part the chance of damage being caused by these vibrations is low. Therefore the impact is estimated to insignificant.

To mitigate the likelihood the ESC's will be placed on dampeners. This reduces the likelihood to possible.

Short circuit (1.3.3): The ESC's mainly consist out of non flexible solid components. Therefore, the chance that components will touch during flight is low. However, should moisture come inside the ESC's the chance of short circuit increases. Therefore, the likelihood is estimated to be unlikely. However, when a short circuit occurs inside the ESC's it will have great influence on the performance of the ESC's, which results the expected impact to critical.

In order to mitigate the likelihood for a short circuit the ESC's will be put sealed in such a way that moisture cannot enter the inside of the ESC's. This reduces the likelihood to very unlikely.

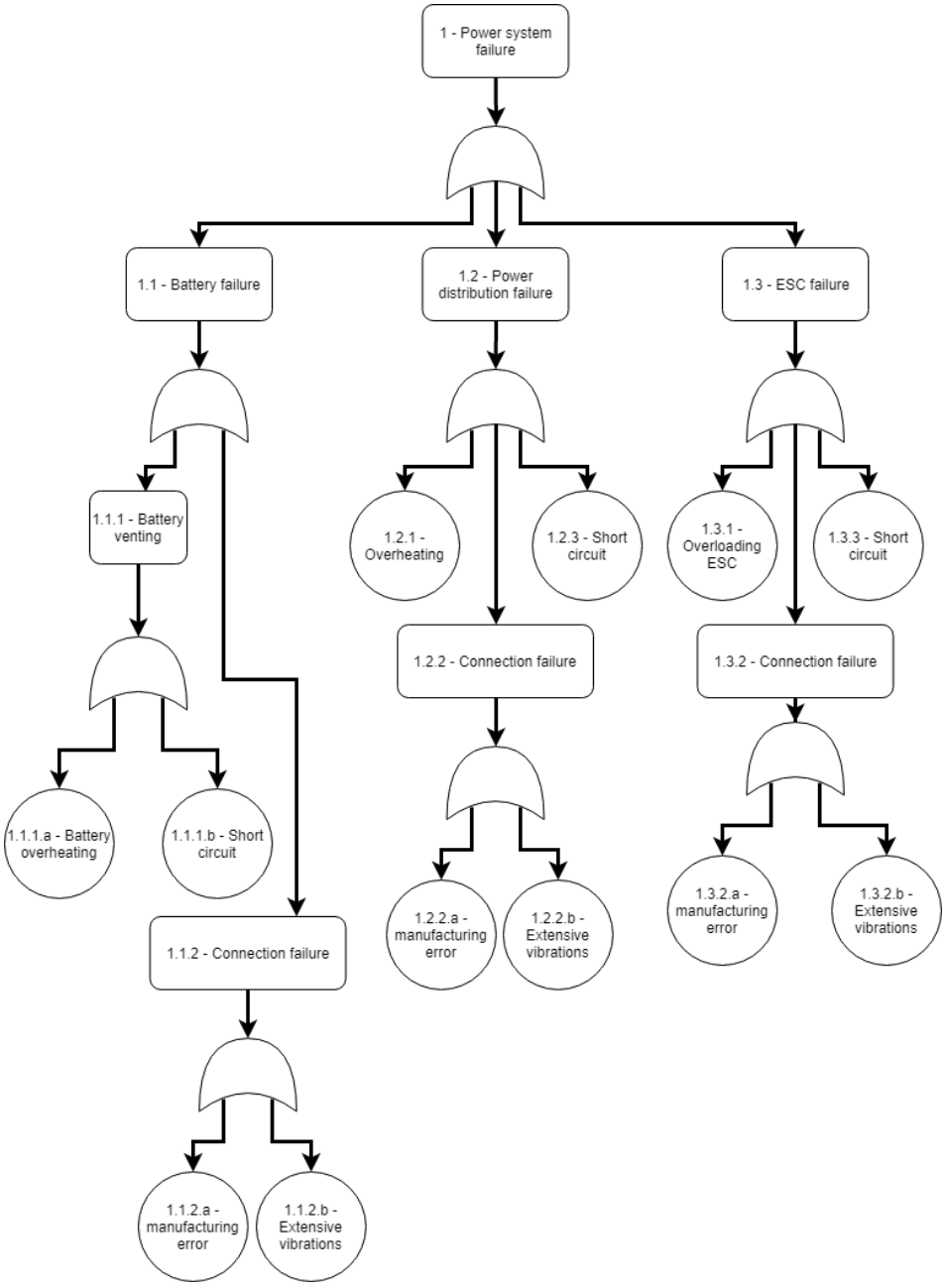

Figure 13.2: The FTA for the power system

13.2.2. Propulsion system

In this section the risk associated with propulsion failure will be discussed with methods that can mitigate these errors. The FTA of the propulsion can be seen in Figure 13.3.

Hit by debris (2.1.1): Due to the airflow during take-off and landing caused by the propellers can cause particles from the ground to circulate over the propellers and harm this propeller. This risk would cause a rough landing in case of a propeller failing from debris impact with a high likelihood of it occurring.

In order to mitigate this risk of getting hit by debris a landing gear with crumple zone is added in order to reduce the landing severity in case of propeller failure. The landing gear would cause the severity and impact to be reduced , however it would not change the likelihood of the risk to occur.

Bird strike (2.1.2): Bird strike is always a risk that should be considered in any flying vehicle as it one of the most critical failure that can occur during flying which leads into a catastrophic failures that have a high likelihood of occurring depending on the location as places with lakes and waterfronts have higher probability of bird strikes to occur.

In order to mitigate this risk some measures could be taken in order to decrease the likelihood of a bird strike to occur, the pilot can limit hovering or flying over lakes which increases the probability of a bird strike [10]. Moreover, bird activity should be known before flying to avoid the likelihood of a strike to occur.

Overheating(2.2.1): Overheating can occur due to overloading by high or low voltage than requires or by continuously turning it on and off the engines can lead into catastrophic failures however the probability of the occurring is unlikely.

In order to mitigate these errors the pilot should be informed in the Manuel how to operate the hover-bike in order to limit the likelihood of this risk to occur. Moreover, including engine redundancy decreases the impact of one engine failing as the hover-bike can still be operational using 5 engines instead of 6.

Shaft fatigue(2.2.2): Due to overloading forces on the propeller or due to a misalignment of the propeller which causes the shaft to get overloaded and sustain higher forces, however the impact of failing shaft is catastrophic but with an unlikely likelihood to occur.
Moreover, in order to mitigate this risk by well lubricating the shaft and by checking them in the maintenance check that will decrease the likelihood of it occurring. On top of that, redundancy in motors lower the impact of the shaft failure occurrence.
Vibrations(2.2.3): Vibrations due to misalignment of the propellers will cause an imbalance of forces which causes vigorous vibrations that can cause deterioration in the structural integrity of the hover-bike, however the impact is catastrophic but its very unlikely to occur as the pilot will feel the vibrations before taking off to a high altitude.
Electrical speed controller (ESC) failure(2.2.4): The ESC's can get fried if it receives to much amps or it fries by overheating, resulting in a motor failure. This would have a catastrophic impact as it would cause the hover-bike motors to shut down, moreover this risk likelihood is possible to occur.
In order to mitigate this risk every engine has its own independent ESC making it have less impact on the hover-bike. In addition, a fuse can be implemented to sense the increase in voltage and cut the circuit to keep the ESC safe.

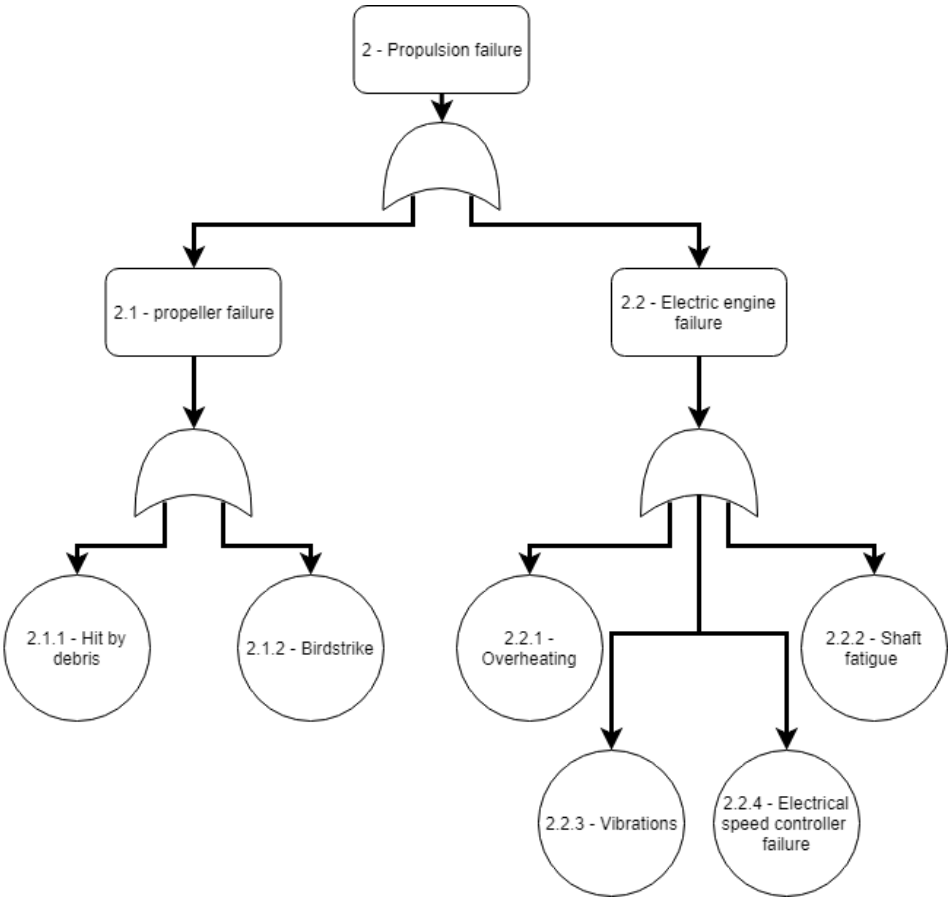

Figure 13.3: The FTA for the propulsion system

13.2.3. Structures

In this section the risk associated with structure failure will be discussed with methods that can mitigate these risks. The FTA of the propulsion can be seen in Figure 13.4.
Bird strike (3.1.1.a): The same risk impact and mitigation plan was discussed in risk number(2.1.2)
Hit by debris (3.1.1.b): The same risk impact and mitigation plan was discussed in risk number(2.1.1)
Moisture (3.2.1): Due to rain or humidity in the atmosphere the structure might corrode which if not treated can weaken the structure, which can have catastrophic impact on the hover-bike during high g manoeuvres.
Moreover, in order to mitigate this problem the aluminium used will be anodised which is a technique to protect bare metal from corrosion. Structural check ups during maintenance for corrosion or dents will lower the likelihood of failure due to corrosion.
Wing damage (3.3.0.a): During transportation mode when the wings are attached the pilot can take a high g manoeuvre that the wing cant sustain its load, which can cause the wing to break or even detach. This will only have a minor impact as it will only lead into a lower performance of the hover-bike.
In order to mitigate this a certain set of g's can not be exceeded during manoeuvres lowering the likelihood of this risk to occur.
Crash landing(3.4.1): In case of crash landing due to an uncontrolled landing or because of a certain failure. This can lead into critical injuries to the pilot with a possible likelihood to occur.
In order to mitigate this risk a crumple zone has been added to the landing gear to lower the impact into a minor impact.

Overloading(3.4.2): The hover-bike is designed to have a payload of 100kg. Any increase to this payload might lower the performance and can even lead into structural failure during high g manoeuvres which can lead into critical impact.
However, in order to mitigate this risk a weight check will be performed by having a comparison between expected acceleration and actual acceleration and if it is lower than expected landing is initiated. That will cause the likelihood and impact to lower as it will be shown before initiating the take-off.

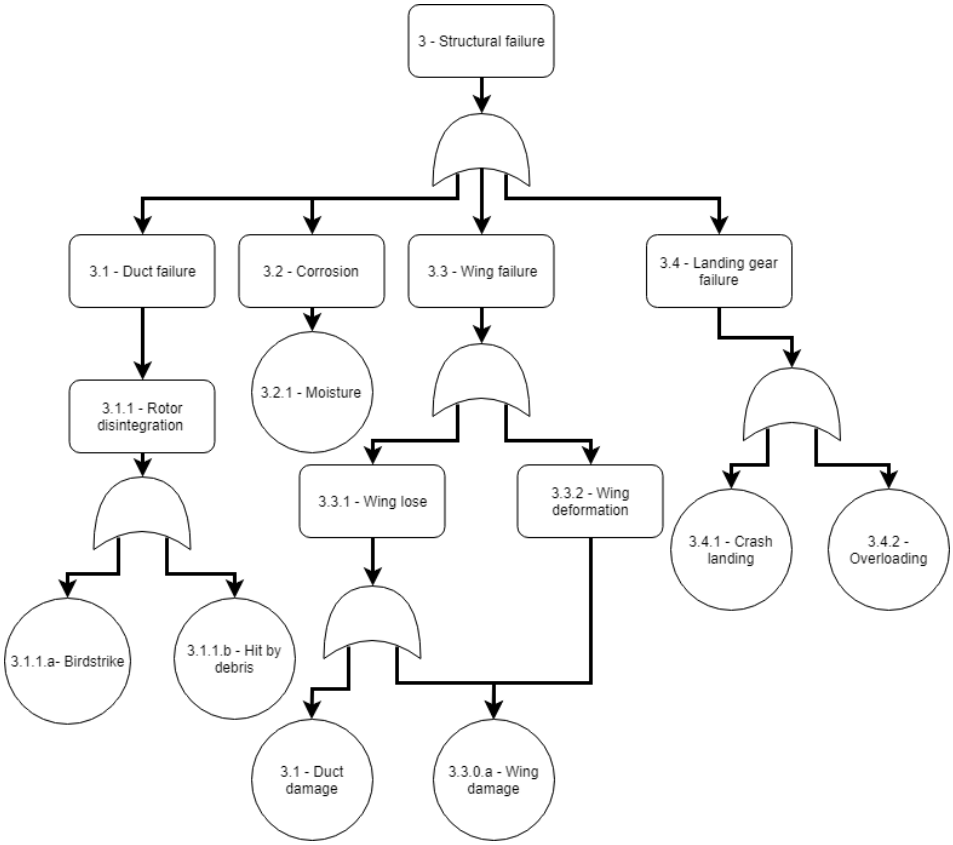

Figure 13.4: The FTA for structures

13.2.4. Human-Machine interface, Machine-Human interface and communication

In this section identifications and assessment on the risk of interface between the pilot and the hover-bike and communications is given.

Communication failure (4.1): Communication failure occurs when the pilot can not communicate with other vehicles or the air traffic control in one or both directions. Therefore, the communication failure can be split up in two parts; receiver failure and transmitter failure.

- **Receiver failure (4.1.1):** Failure of the receiver would mean that the hover-bike will not receive information from other vehicles or air traffic control. If this event occurs the pilot has to trust on his visibility. This will make the impact critical. Since receivers are already flight proven the likelihood for this event to occur is unlikely.
  However, in order to mitigate this risk the pilot will be restricted to only use the hover-bike when weather conditions are good in a low traffic density area. This will reduce the impact to minor. Also a second receiver will be added to the hover-bike. This reduces the likelihood to very unlikely.
- **Transmitter failure (4.1.2):** Failure of the transmitter will mean that there is no communication from the hover-bike to other vehicles or to air traffic control. Comparable to a receiver failure the impact is rated to be critical and the likelihood as unlikely.
  To mitigate this event a second transmitter is added to the hover-bike. Which reduces the likelihood to very unlikely.

Control input failure (4.2): A control input failure can be due to a sensor failure inside the control bar or as consequence from cable connection failure. When this event happens the consequence will catastrophic, since the hover-bike will be uncontrollable. This event is unlikely to occur.
In order to mitigate this event a button, which initiates a auto-land procedure, will be added on the hover-bike. This reduces the impact to critical.

Display failure (4.3): The hover-bike will use a display to show the flight information. Should this display fail the pilot will not receive any information on the status of the hover-bike. This makes the impact of a display failure critical. The likelihood for a display failure to occur is unlikely.
To mitigate this risk two extra small displays will be placed on the control bar which show the current battery charge status. This reduces the impact to minor.

Flight computer failure (4.4): Should the flight computer fail the hover-bike will be completely uncontrollable, this makes the impact catastrophic. However, flight computers are already flight proven and they do not use any moving parts. This

makes the likelihood for the flight computer to fail very unlikely.
The hover-bike's safety system makes use of a parachute which lands the hover-bike as safe as possible. This slightly mitigates the impact, however the impact is still rated as catastrophic.

13.3. Technical risk maps

In this section the technical risk maps can be found. Table 13.1 shows the technical risk map before the risks are mitigated. After mitigation the technical risk map changes to Table 13.2.

Table 13.1: Technical risk map

Likelihood					
	High probability			(3.4.2)	
	Likely	(1.3.2.b)	(1.2.2.b)	(1.3.1)	(1.1.1.a), (2.1.2), (3.1.1.a)
	Possible		(3.3.0.a)	(1.1.2.a), (1.2.2.a), (1.3.2.a), (2.1.1), (3.1.1.b), (3.4.1)	(1.1.2.b), (1.2.3), (3.2.1)
	Unlikely			(4.1.1), (4.1.2), (4.3)	(1.1.1.b), (1.2.1), (2.2.1), (2.2.2), (2.2.4), (4.2)
	Very Unlikely				(2.2.3), (4.4)
		Insignificant	Minor	Critical	Catastrophic
		Impact			

Table 13.2: Mitigated technical risk map

Likelihood					
	High probability				
	Likely	(1.2.2.b)			
	Possible	(1.3.2.b)	(2.1.1), (3.1.1.b)	(1.3.1)	(2.1.2), (3.1.1.a)
	Unlikely		(3.3.0.a), (3.4.1), (3.4.2), (4.3)	(1.1.1.a), (1.1.2.a), (1.1.2.b), (1.2.2.a), (1.3.2.a), (2.2.4), (4.2)	
	Very Unlikely		(4.1.1)	(1.1.1.b), (1.2.1), (1.2.3), (1.3.3), (2.2.1), (2.2.2), (4.1.2)	(2.2.3), (3.2.1), (4.4)
		Insignificant	Minor	Critical	Catastrophic
		Impact			

14
Cost Analysis

In this chapter the cost of the hover-bike will be analysed. The analysis is split up into 3 parts, material cost is explained in section 14.1, manufacturing in section 14.2 and operational cost in section 14.3. Finally an overview of the cost analysis is in section 14.4

14.1. Material cost

The material cost of the hover-bike is determined by the amount of materials used and the price per unit mass. For different aspects of the hover-bike the material price is estimated and summarised below in Table 14.3

Structure cost To estimate the cost of the structure the prices of aluminium tubing is used, together with the dimensions of the structure. The structure weighs 60 kg and uses tubes of 6 cm outer diameter with 0.5 cm wall thickness. Furthermore aluminium 6061T6 was chosen as a material for the structure. Tubes with standard dimensions were used as a reference to find a price per kg. A tube with an outer diameter of 6.35 cm, a wall thickness of 0.635 cm and 2.44 m long weighs 7.54 kg and costs $121.56[1]. This gives a price of around €14.00 per kg for 6061T6 aluminium. When a loss of material is implemented of 10%, then the material cost for the structure will become $60 \cdot 1.10 \cdot$ €14.00 = **€920**.

Propeller cost The same approach that was used in the midterm report [42] is applied here. Using the reference data from Table 14.1 the cost of the propellers can be calculated. The average price is €10.00 per centimetre of propeller diameter. When one propeller has a diameter of 1.6 m and two blades per propeller, then the price of one propeller becomes €10.00 · 1.6 · 100 = €1600.00. Then the total propeller cost for 6 propellers becomes **€9600**.

Table 14.1: Reference propeller prices

Diameter	Price	Price/Diameter (€/cm)
208 [cm] [2]	$2950 = €2,510.00	€12.00
127 [cm] [3]	$899 = €765.00	€6.00
167 [cm] [4]	$2463.00 = €2,096.00	€12.50
165 [cm] [5]	$1550 = €1,319.00	€8.00
183 [cm] [6]	$2500 = €2,132.00	€11.50
	Average:	€10.00

Engine and battery cost The engine chosen for the design of the hover bike, is a 45 [kW] brushless engine[7]. The price of this engine turns out to be $700[8] = €608. Then the total cost of the engines will be €608 · 6 = **€3650**.
In chapter 7 the total weight for the batteries was estimated at 184 kg, and the amount of cells inside the batteries is 2920. The cells chosen were the panasonic B 20700 and their cost is $8.49[9] = €7.32 per cell. Then the total battery cost will become €7.32 · 2920 = **€21400**.

Wing and duct cost The material cost for carbon fibre composites is €85 per kg[10]. The wing duct combination weight was estimated at 55 kg and a 10% loss of material is assumed during production. Therefore the manufacturing cost is estimated at €85 ·1.10· 55 = **€5140**.

[1] URL:https://www.onlinemetals.com/merchant.cfm?pid=7898&step=4&showunits=inches&id=71&top_cat=0 [cited 23-06-2018]
[2] URL:https://whirlwindpropellers.com/aircraft/product/ga200l-stol/ [cited 23-may-2018]
[3] URL:http://mymobilemms.com/OFFTHEGRIDWATER.CA/MultiCopter-Propeller/Carbon-Fiber-Large-Propellers-2-Blades-50-Inches-CW-CCW [cited 23-may-2018]
[4] URL:http://www.aircraftspruce.com/catalog/appages/whirwind05-12614.php [cited 23-may-2018]
[5] URL:https://whirlwindpropellers.com/aircraft/product/propeller-for-jabiru-3300-engines/ [cited 23-may-2018]
[6] URL:https://whirlwindpropellers.com/aircraft/product/ga200cn/ [cited 23-may-2018]
[7] URL:www.reacherbrushless.com/product/45KW-motor.html [cited on 19-06-2018]
[8] URL:https://frchobby.en.alibaba.com/product/60611108725-803193582/45KW_75Nm_sensored_outrunner_brushless_motor_for_electric_boat.html [cited 21-06-2018]
[9] URL:https://www.orbtronic.com/20700-panasonic-sanyo-ncr20700b-battery-rechargeable-li-ion [cited 21-06-2018]
[10] URL:https://www.compositesworld.com/columns/give-us-affordable-carbon-fiber [cited 21-06-2018]

Miscellaneous cost Miscellaneous items are listed below in Table 14.2 and their respective cost. Miscellaneous items consist out the electronic equipment that is on the hover-bike, such as the human machine interface (HMI), lights, radio, etc... Furthermore the cost of safety components such as a parachute system and blackbox are included. The total cost of miscellaneous items is **€10900**.

Table 14.2: Cost of miscellaneous item

Item	Price
2 Joysticks (HMI)[11]	€558
LCD screen[12] (MHI)	€88
Lights[13]	€363
Flight data recorder[14]	$600 = €516
Parachute system[15]	€5160
Flight controller[16]	$179.95 = €155
Radio XCOM VHF[17]	€2920
Cabling+insulations[18]	INR 4886.4 = €62
Seat[19]	€179
FLARM RED[20]	€900
Total	€10900

Material cost overview All costs for material are summarised below in Table 14.3. It becomes immediately clear that the batteries take a huge chunk out of the cost budget of the hover-bike. If the hover-bike would need a larger battery size in the future, then this would have large influences on the total cost. Only miscellaneous costs would stay fairly constant when the size of the hover-bike needs to change. The total material cost is estimated at **€52000**

Table 14.3: Cost Overview

Segment	Cost [€]
Structure	920
Propeller	9600
Engine	3650
Battery	21400
Wing and duct	5140
Miscellaneous	10900
Total	**52000**

14.2. Manufacturing cost

Aircraft manufacturing was used as a reference to estimate the cost of manufacturing the hover-bike. Aircraft are not sold in very large quantities such as cars. Automated production is not economically viable when products are sold in small quantities, therefore labour plays a significant role to produce aircraft parts. Data collected on manufacturing aircraft components confirms this[21]. The collected data is shown in Table 14.4.

[11] URL:https://www.bol.com/nl/p/hotas-warthog-flight-stick/1004004013520875/?suggestionType=typedsearch&bltgh=iCTCyZJGaG5dFd4ucelK5A.1.9.ProductTitle[cited 22-06-2018]

[12] URL:https://www.bol.com/nl/p/raspberry-pi-7inch-touch-display-lcd/9200000062964380/?suggestionType=browse&bltgh=q4-g2BK5fZfH7e5scm1PTw.1.13.ProductTitle[cited 22-06-2018]

[13] URL:http://aviolights.com/sites/default/files/navigator_ultra_360_-_data_sheet.pdfhttp://aviolights.com/navigator-ultra-360.html[cited 22-06-2018]

[14] URL:https://www.ebay.com/itm/15600-501-flight-data-recorder-/292584202206[cited 22-06-2018]

[15] URL:http://www.pipistrel.ca/resources/PDF-pipistrel-price/Taurus-RTF.pdf[cited 22-06-2018]

[16] URL:https://www.uavsystemsinternational.com/product/3d-robotics-pixhawk-flight-controller/[cited 22-06-2018]

[17] URL:http://www.pipistrel.ca/resources/PDF-pipistrel-price/Taurus-RTF.pdf[cited 22-06-2018]

[18] URL:http://www.kmaelectricals.com/fm/1616395/001.pdf[cited 22-06-2018]

[19] URL:https://www.motorcyclespareparts.eu/en/suzuki-parts/2017-sv650aua-motorcycles/optional-seat[cited 22-06-2018]

[20] URL:http://www.pipistrel.ca/resources/PDF-pipistrel-price/Taurus-RTF.pdf[cited 22-06-2018]

[21] URL:https://ocw.mit.edu/courses/aeronautics-and-astronautics/16-885j-aircraft-systems-engineering-fall-2004/lecture-notes/pres_willcox.pdf[cited 23-06-2018]

Table 14.4: Manufacturing cost in dollar per pound

	Labour [$/kg]	Material [$/kg]	Other [$/kg]	Total [$/kg]
Wing	276	93	40	408
Empennage	732	220	106	1057
Fuselage	308	86	44	439
Landing gear	49	44	7	100
Installed Engines	112	41	16	170
Systems	143	41	21	205
Payloads	184	45	27	256
Final Assembly	26	2	1	29

The prospects of the hover-bike are that it will not be mass produced and sold in large quantities, especially during the start up phase. Therefore a lot of labour will be necessary to produce parts and assemble the hover-bike. Most parts of the hover-bike will be bought as of the shelf products, such as propellers, engines, miscellaneous items, cabling, etc.... But the structure, wings and ducts will have to be produced by the hover-bike company itself.
Extracting percentages from Table 14.4 gives an estimate of how much the the manufacturing will cost for the wings, ducts and structure. The landing gear of the hover-bike consists out of skids and are therefore part of the structure. Then manufacturing costs for these parts will become:

Table 14.5: Manufacturing cost hover-bike

	Price fraction of material	Material cost	Manufacturing cost
Wing	93/408	€5140.00	€22500
Structure	86/439	€920.00	€4700

Assembly costs are estimated at $\frac{29}{408+439} \cdot (22550 + 4700) =$ €930. The total manufacturing cost of the hover-bike will become €22500+€4700+€930 = **€28130**.

14.3. Operational cost

The operational cost consist out maintenance costs and charging costs. Maintenance costs are mostly dependent on the labour cost and the cost of replacing parts. Charging costs are dependent on the flying frequency and price per kWh. To determine the operational costs the case of 2 flight hours per week was chosen, which means that there are 104 flight hours per year.

Maintenance For helicopters and general aviation different maintenance checks with their respective intervals are necessary. For the Robinson 22 series there is a 100 flight hour check, a 2200 flight hour check, 4400 flight hour check and a yearly inspection. The prices for each maintenance check is dependent on the amount of labour that is involved. For example a 100 flight hour check requires more labour than a 2200 flight hour check. Table 14.6 gives an impression of how much each maintenance check will cost in terms of labour.

Table 14.6: Price overview of labour[22]

Maintenance check	Price $
Yearly check	900
100 flight hour check	900
2200 flight hour overhaul	15000
4400 flight hour overhaul	16500

The price of labour is estimated by dividing the maintenance cost of each check over the flight hours. This gives an hourly labour cost of $\frac{900}{100} + \frac{15000}{2200} + \frac{16500}{4400} =$ $19.57 In euro's that is €16.94 per flight hour. The yearly check costs $900 which is equal to €790. Then if the hover-bike is flown for 104 hours per year and a yearly check takes place, the labour cost will come down to $16.94 \cdot 104 + 790 =$**€2550**.
The cost of replacement parts is dependent on how fast parts will wear out. The only moving parts of the hover-bike are the propellers and engines. Batteries don't have moving parts, but they do experience a lot of charge/discharge cycles. The electric engine are of the brushless type, which means that there are less engine parts that will wear out. As a result brushless engines will have a long running time. Therefore it is assumed that the only parts that need frequent replacement are the propellers and batteries. It is estimated that the batteries will be able to take 500 charge/discharge cycle before the capacity drops below 70%[23]. If one flight equals one charge/discharge cycle than that would mean that the batteries will have to be replaced after 500 flight hours. Resulting in a cost of €21400/500 = €42.80 per flight hours.

[23] URL: `http://batteryuniversity.com/index.php/learn/article/how_to_prolong_lithium_based_batteries` [cited 21-06-2018]

The propellers will have a running time of 1000 to 2000 flight hours [24]. If the propellers need to be replaced after 1000 flight hours then this would cost €9600/1000 = €9.60 per flight hour. In total replacement parts will cost €42.80 + €9.60 = €52.40 per hour. Then the yearly costs for replacement parts would cost $52.40 \cdot 104$=**€5450**.

Charging costs To estimate the yearly charging costs the following scenario is used. The hover-bike is mainly designed for a thrilling flying experience, but it can also be used for transportation mode. The batteries hold a charge of 45.2 kWh chapter 7. If one flight uses the whole battery charge and two flights per week are performed, than the total energy use for one year becomes $45.2 \cdot 104 = 4700.8$ kWh. The average price for one kWh in Europe costs €0.21[25], therefore the total charging costs per year will be around a **€1000**.

Operational cost overview Adding up all the costs of operating the hover-bike for one year the total cost will come down to €2550 + €5450 + €1000 = **€9000**. This is the yearly cost when the hover-bike is flown for 104 hours. The operational costs exclude any taxes or insurance payments that might be in place.

14.4. Total cost overview

All the analysed costs are summarised below in Table 14.7. Requirements HB-CS-ST-07 was given in section 3.3 that states that the prototype of the hover-bike shall cost less than €100,000. The cost of the prototype consist out of material cost and manufacturing cost and does not include the cost of design and capital cost. Then from Table 14.7 it can be deduced that the cost of a prototype will be around **€80000**, therefore requirement HB-CS-ST-07 is met. The prototype cost does not include value added tax, because this is different for countries around the world. The cost of operating the hover-bike for 1 year, while flying 104 hours per year, costs **€9000**.
Profit margins in the car industry are around 8.7% and 4.5%[26], but cars are mass produce products. For the hover-bike a profit margin of 12.5% was chosen, because the hover-bike will be produced and sold in lower quantities. Then the total selling price will become €80000 · 12.5% = €90000.

Table 14.7: Overview of the cost analysis

	Price
Material cost	€51610
Manufacturing cost	€28180
Selling price	€90000

[24] URL: http://propellerman.com/hours-or-years.html [cited 21-06-2018]
[25] URL:http://appsso.eurostat.ec.europa.eu/nui/show.do?dataset=nrg_pc_204&lang=en [cited 23 May 2018]
[26] URL:https://www.dw.com/en/big-carmakers-big-profits/a-19480709 [cited 28 june 2018]

15
Sustainability development strategy

Sustainability is currently gaining in concern among companies while designing any type of vehicle. The hover-bike might not be the most sustainable transport vehicle but sustainability methods are required to implement for improving its sustainability performance. Sustainability consists of three main themes and aspects: Social, Environmental and Economic sustainability. This chapter will discuss the design approach regarding hover-bike in order to increase sustainability and minimise its impact towards the aspects previously mentioned. This chapter will discuss all the development strategies used through out the whole design phase, which is highly influenced by the midterm report [42].
In this phase of designing, several aspects are considered to make the hover-bike more sustainable. This is done by analysing the use of the hover-bike and anticipating its possible impact on the social, environmental and economic sustainability.

15.1. Social sustainability

The hover-bike was designed to give a new thrilling experience to the customer. However, its impacts and effects on society are of great importance and are to be analysed assuming and predicting certain scenarios that might occur while finding solutions.

Employment rate The hover-bike will open new jobs opportunities for young and experienced engineers, technicians and managers. This will cause the unemployment rate to go down in the Netherlands and other cities depending on the expansion rate of hover-bike. Moreover, it will allow for more versatile opinions for solving problems that will allow more innovative and creative designs for the hover-bike.

Employee satisfaction The company's employees must be well motivated, healthy and enthusiastic in order to perform well under high-pressure circumstances. This can be achieved by creating some motivational and friendly atmosphere in such a way that employee can perform at his/her maximum capabilities. Additionally, leaving some chance for creativity and innovation by hearing and considering design suggestions from staff members can boost the motivation of employees. Since being heard gives great sense of appreciation and belonging towards the company and the team. Through structurally organising short meetings for discussing the contentment towards the employees environment, the previous key features for satisfaction can be achieved

Customer satisfaction Moreover, the hover-bike ease of use will allow the customer to have a shorter time in order to fly and have a license for the hover-bike. This will boost the customer happiness as it won't take a long time to experience the thrills delivered from the hover-bike. Moreover, a wide variety of modes that can be achieved by the hover-bike allows increased user-friendliness and gives more option for controlling the hover-bikes performance. Furthermore, during the design of the hover-bike two aspects were taken into consideration, the hover-bike's thrilling aspect and the functionality aspect. In order to satisfy both aspects, removable wings and duct are added to give more endurance to hover-bike and hence increase transportation capabilities. Adding these capabilities would make the customer more satisfied with the product due to its versatile functionalities. Next to increasing the versatility, a close connection should be kept with the customer. By expanding the involvement of the company in the begin phase of the user-experience, the customer will reach out to the company much sooner will the customer encounter an issue, which will increase the gratitude towards the company.

Legal aspects Furthermore, legal aspects need to be considered since hover-bike can be used to intrude on peoples privacy. This can be avoided by regulating the take-off and landing areas and by setting a minimum altitude of hovering to maintain the privacy of the residence. In addition a set of rules and regulations will consider any operational misuse of the hover-bike as the customer's fault, as the company will not be held accountable for these mistakes. These rules and regulations will be well communicated to the customer in order to protect civilians, customers, and the company's reputation.
In addition, the company has to write down a detailed user manual in order to inform the pilot of the rules, regulations and proper use of hover-bike. Additionally, a disclaimer should be added. In case of a customer failing to follow these rules, the disclaimer will be held responsible of his actions and the company would not be held responsible for not following these rules.

Noise Noise is a big issue when it comes to health concerns, particularly in Europe and in many developed countries [26]. Consequently, the European Union has started implementing new noise regulations to limit noise caused by vehicles[4], especially at night time as it was observed to affect humans sleep cycle and health[22]. In order to avoid discomfort to

people in urban areas, hover-bikes will only be allowed to take-off and land in rural areas to maintain a low level of noise to civilians. Moreover, after taking off it is allowed to hover above cities but at a minimum height to avoid causing noise and affecting people. Due to those effects, the flying of hover-bike is prohibited during night time due to noise effects and lack of visual area making it unsafe for the customer.
As a first estimate of noise, it is assumed that the hover-bike has a similar noise level to Bell J-2A helicopter [1] generating 100 db at 30m. Using Equation 15.1 a minimum attitude of 300m can be estimated to lower the decibels to 80 db making it more comfortable and less ear damaging to pedestrians. Moreover, for the safety and well being of the pilot a noise cancelling earphones will be one of the protective gear-like ones used for fighter jets pilots.

$$L_2 = L_1 - \left| 20 \cdot log \frac{r_1}{r_2} \right| \tag{15.1}$$

Maintenance Maintenance is a crucial part of any vehicle, such that a good and fast maintenance service is always preferred. In order to achieve a good maintenance service, highly experienced employees are going to be employed as supervisors on the maintenance procedure to reassure high quality and fast maintenance. Moreover, the hover-bike should also be more accessible in order to make the maintenance checks faster, which makes customers more satisfied and lowers the complexity of the maintenance job.

15.2. Environmental sustainability

When it comes to environmental sustainability, EU targets are set relatively high. In order to maintain these high expectations, a strategy needs to be developed. This strategy is critical as to minimise the production of greenhouse gases, help to save the planet from climate change.

Recyclability The hover-bike uses 184 kg of battery mass. Most of this mass comes from the Lithium-ion battery cells. The recycling process of lithium-ion batteries is not yet profitable. Therefore, battery cells are not yet completely recycled. In the future it is expected that lithium-ion batteries will be fully recyclable[2]. Secondly the frame of the hover-bike is made out of aluminium and weights 60 kg. Aluminium can be melted and used again for new purposes. In other words, aluminium is recyclable.
The battery mass and the mass of the structure combined will be 244 kg. This means that the requirement **HB-CS-ST-20**, which states that at least 50% of the hover-bike should be recyclable, can be met in future.

Production pollution The production process cause pollution and a waste of materials that can harm the environment. In order to prevent air pollution caused by production a cleaner way with less greenhouse gases are emitted to limit air pollution caused by the hover-bike production. Moreover, for minimising the wasted materials a lean manufacturing production is used in order to decrease the amount of wasted materials introduced in the environment which might cause pollution.

Carbon footprint Operational pollution is required to be analysed in order to maintain a low carbon footprint after the end of life of the vehicle. The carbon footprint and emission of batteries are comparably less than gasoline as it can be seen in Figure 15.1 from a study performed comparing between cars [3]. However, there is a penalty for manufacturing batteries in term of CO_2 emission but it is more environmental friendly on the long run.

Noise pollution Noise pollution is another source of pollution as it disturbs wildlife and disturbs the peace for civilians. In order to minimise noise production for the hover-bike a minimum attitude have been set to limit noise pollution reaching humans and terrestrial wildlife. Moreover a designated flying zones will be assigned in rural areas at least 700 m from building and civilians in order to be able to take-off and land without disturbing the civilians.

15.3. Economical sustainability

Economical sustainability is crucial to ensure a longer lifespan for the company's survival in the market as only 50 percent of the companies will survive for 5 years since they opened up. Therefore, if economical sustainability is not planned for, the company might go bankrupt causing people to lose their jobs and income and moreover it will affect the development of the hover-bike due to insufficient funds.

Investors In order to achieve a good appeal to the customers a group of experienced marketing and design consultants will be hired in order to give feedback about the design and how to improve it in order to meet customers satisfaction. Moreover, that will cause the company to have a better overview of market need, hence company's investors and shareholder are satisfied with the work performed allowing more money flow to the company's capital.

[1] URL: http://www.industrialnoisecontrol.com/comparative-noise-examples.htm [Cited 25 June 2018]
[2] URL: http://batteryuniversity.com/index.php/learn/article/recycling_batteries [Cited 16 June 2018]
[3] URL:https://thecorrespondent.com/7056/why-electric-cars-are-always-green-and-how-they-could-get-greener/741917761200-afaa6e5d [Cited 23 June 2018]

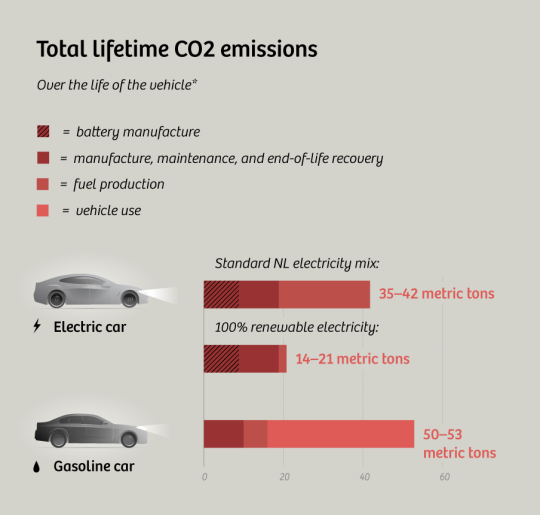

Figure 15.1: Gasoline vs Electric vehicle emission

Lean manufacturing Lean manufacturing is the production process in which material waste is minimised as it has an impact on the environment and also affecting economical sustainability too. That is because every wasted material is considered as wasted money as it won't be used in production, however, it was paid for. Hence, lean manufacturing is used for both saving the planet and to saving money to the company.

Maintenance Maintenance of hover-bike takes huge amounts of money to perform and run given in section 16.2.2. In order to minimise these costs, several aspects can be seen to affect the maintenance cost in section 16.2.2, which is because different systems require different amount of money to maintain. Moreover, selecting critical systems with high reliability would cause a decrease in the rate of maintenance in such that more millage or hours can be covered by the hover-bike before the periodic checks, hence lowering the budget for maintenance.

End of life disposal To support the sustainability of this hover-bike, it must be disposed in a sustainable manner at the end of its life. The process planned to properly dispose the product can be seen in Figure 15.2. The first step in the disposal of the vehicle is evaluating its condition. If the owner just wants to sell the product that is still in good shape, then it will simply be given through maintenance and sold again in a second-hand store. If the bike is not functional, then it is either classified as "total loss" or "partial loss". A partial loss means the hover-bike can still be salvaged and its components are all checked. The salvageable components are sent to the refurbishing plant where they are used to make refurbished bikes and then sold in a second-hand store. Note that all above can be done by 3rd parties. The components that were not salvageable along with the bikes that suffered total loss are dismantled and then sent to the "scrap material sorting" where they are then either recycled or sent to the toxic waste disposal. The recycled material is then used to make new parts for the assembly line.

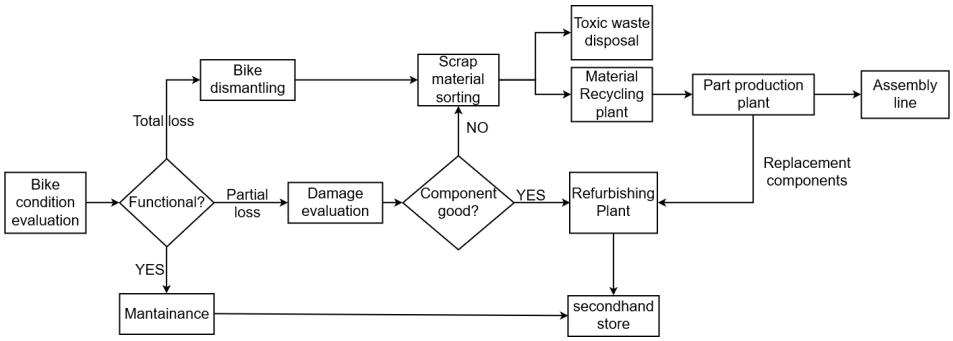

Figure 15.2: steps for a sustainable disposal of the hover-bike

16
Scorpeon design outline

As all the preliminary analysis has been covered, all technical aspects of the Scorpeon can be summarised to obtain a complete overview, which is given in section 16.1. Along with this summary, the hover-bike logistics are outlined in section 16.2. Then, the production plan of the Scorpeon is provided in section 16.3. The compliance matrix, which shows which requirements have and which ones have not been met, is given in section 16.4 and lastly, an overview of some recommendations for the final design is given in section 16.5.

16.1. Scorpeon characteristics

The characteristics of the hover-bike are split into four parts. First, the complete layout of the vehicle is provided in subsection 16.1.1. Secondly, the structural details of the Scorpeon subsystems are shown in subsection 16.1.2. The breakdown of the cost, mass and power of the vehicle are summarised in subsection 16.1.3.

16.1.1. Vehicle layout

The electrical layout can be seen in Figure 16.1. The figure shows how the power cables will be routed from the batteries to the motors. The two electric motors are at the same location laterally and longitudinally, because one is above the other motor. Therefore the electric motors are denoted as 2*M. Subsystem like communication, machine human interface, flight controller, black box, FLARM, subsystem power distribution board and subsystem battery are contained in the front of the hover-bike under "Subsystems and sub-battery". The parachute is located in the front of the hover-bike as well. Furthermore, the external layout for both transportation and thrill mode can be seen in Figure 16.2

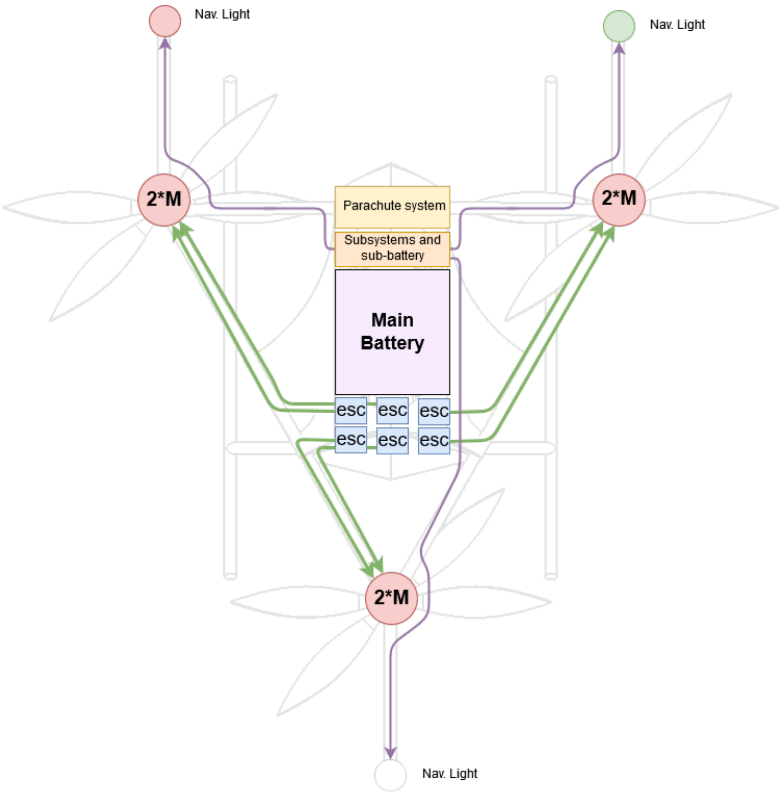

Figure 16.1: Electrical layout of the hover-bike (Green line = power from esc to electric motors, purple line = power from subsystem-battery to lights)

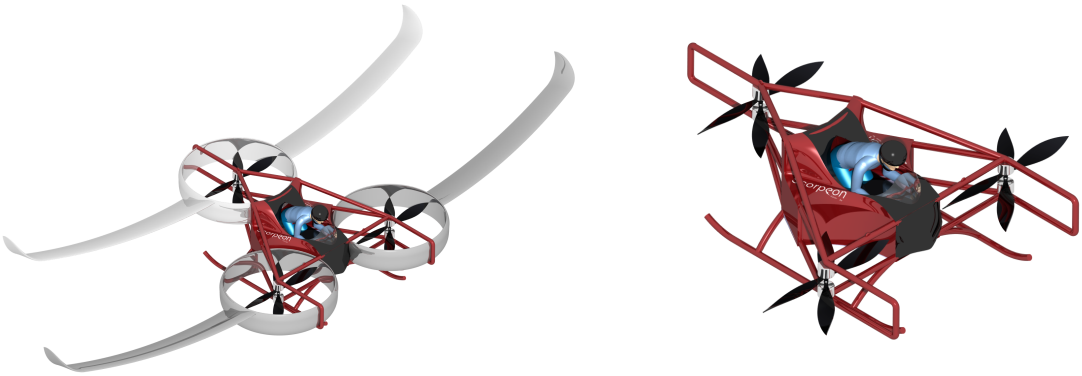

(a) (b)

Figure 16.2: Isometric view of the exterior of the Scorpeon in (a) transportation mode and (b) thrill mode.

16.1.2. Subsystem details

The subsystem aspects have been mentioned throughout the entire report, yet it is good to have a concise overview. Therefore, all subsystem details regarding the dimensions of the subsystems are shown in Table 16.1. This includes the dimensions and power consumption.

Table 16.1: Overview of subsystem details of the hover-bike concept.

Subsystem	Aspect	Value	Subsystem	Aspect	Value
Wing	Half wing span	3.2 m	Rotor	Diameter	1.6 m
	Aspect ratio	10.4		Contra-rotor gap	0.16 m
	Total surface area	8.7 m^2		Airfoil distribution (root-to-chord)	MH126-MH112-MH114-MH120
	Quarter chord sweep	0°	Power	Number of engines	6
	Taper ratio	0.45		Maximum power output	300 kW
	Root-tip twist	28° (washin)		Battery voltage	148 V
	Geometric angle	37°	Body structure	Width	2.4 m
	Airfoil	Selig S4061		Length	3.4 m
				Height	0.6 m

16.1.3. Budget resource allocation

Furthermore, the power, mass and cost has been distributed over the vehicle and its subsystems. The cost and mass distribution of the Scorpeon is visualised in the pie charts in Figure 16.3 in SI units. The power distribution is not shown in a pie chart, as most of the power is distributed to the batteries and, as such, the pie chart would not be clear. Therefore, this distribution is shown in Figure 16.3

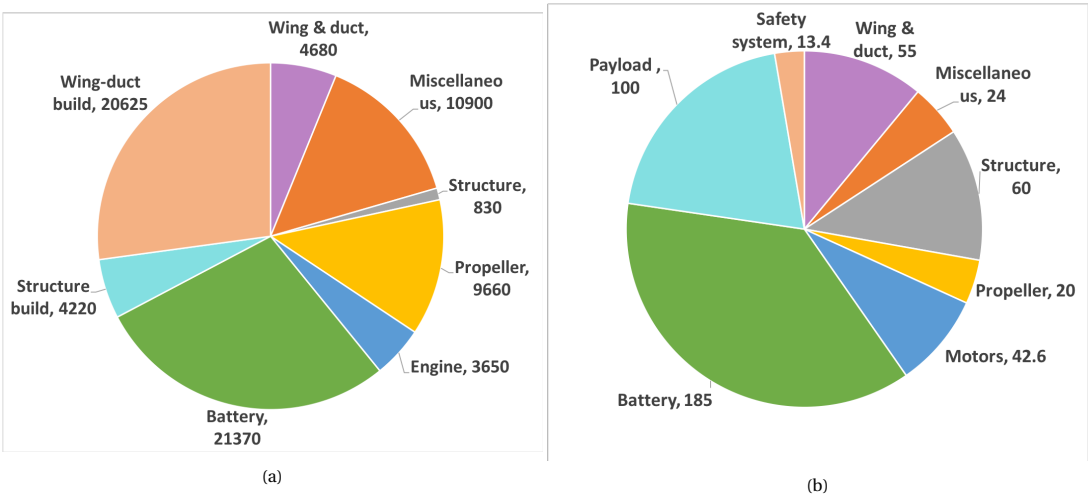

(a) (b)

Figure 16.3: Pie charts displaying (a) the cost distribution in euros and (b) the mass distribution in kilograms. In both charts, the value of each component is given in the brackets after the component name.

Table 16.2: Vehicle power distribution.

Subsystem	LCD screen	Lights	Black box	Safety ECU	FLARM	Joybar	Flight controller	Transmitter/ Receiver	Motors
Power (W)	4.5	35	5	5	8	5.9	35	15	250×10^3

16.1.4. Performance characteristics

This section will summarise the performance characteristics of Scorpeon in both the transportation configuration and thrill configuration. The analyses are done in Equation 7.1.1, chapter 7 and chapter 9.

Aspect	Value
Speed	29.7 m/s
Acceleration	8 m/s^2
Range	105 km
Endurance	60 min

Table 16.3: Performance characteristics transportation mode

Aspect	Value
Speed	55 m/s
Acceleration	12 m/s^2
Range	32 km
Endurance	9.8 min

Table 16.4: Performance characteristics thrill mode

16.2. Operations and Logistics

This section describes the operations associated to owning a Scorpeon . This consists of the flight operations in subsection 16.2.1, the description of the maintenance plan is provided in subsection 16.2.2, while the definition of the headquarters is provided in subsection 16.3.5.

16.2.1. Flight operations

The flight-operations of the hover-bike mainly concerns with how the vehicle is expected to be treated before, during and after flight. An operations diagram was already created during the mid-term, yet since the design is known in more detail now, the organisations diagram has also become more in depth as shown in Figure 16.4. The vehicle needs to be properly checked before it can actually be flown. The first check is a general visual one. The pilot shall see if the hover-bike does not have any obvious damage, such as dents and cracks. The second check is denoted as a "pre-operational checklist". This is comparable to a pre-check before driving a car. The pilot will check if there are any warning lights/signs active, if there is enough power left and if the sensors are working properly[1]. If there are any issues that the driver can not fix by him/herself, he/she is directed to the maintenance section, which is outlined in subsection 16.2.2. After the pre-flight checks are done and everything is indeed working properly, the hover-bike is ready to take-off from a helipad, but first the desired flight profile needs to be determined, which determines which flight configuration should be used, further explained below. During the flight, the system shall continuously check for a critical failure of the hover-bike. Finally, the pilot shall perform a small post-flight check to determine any issues that may have occurred during flight, similar to the pre-flight checklist.

[1] As an example, when the hover-bike gets activated, the dials should all move left and right such that the driver can check if these are indeed operational

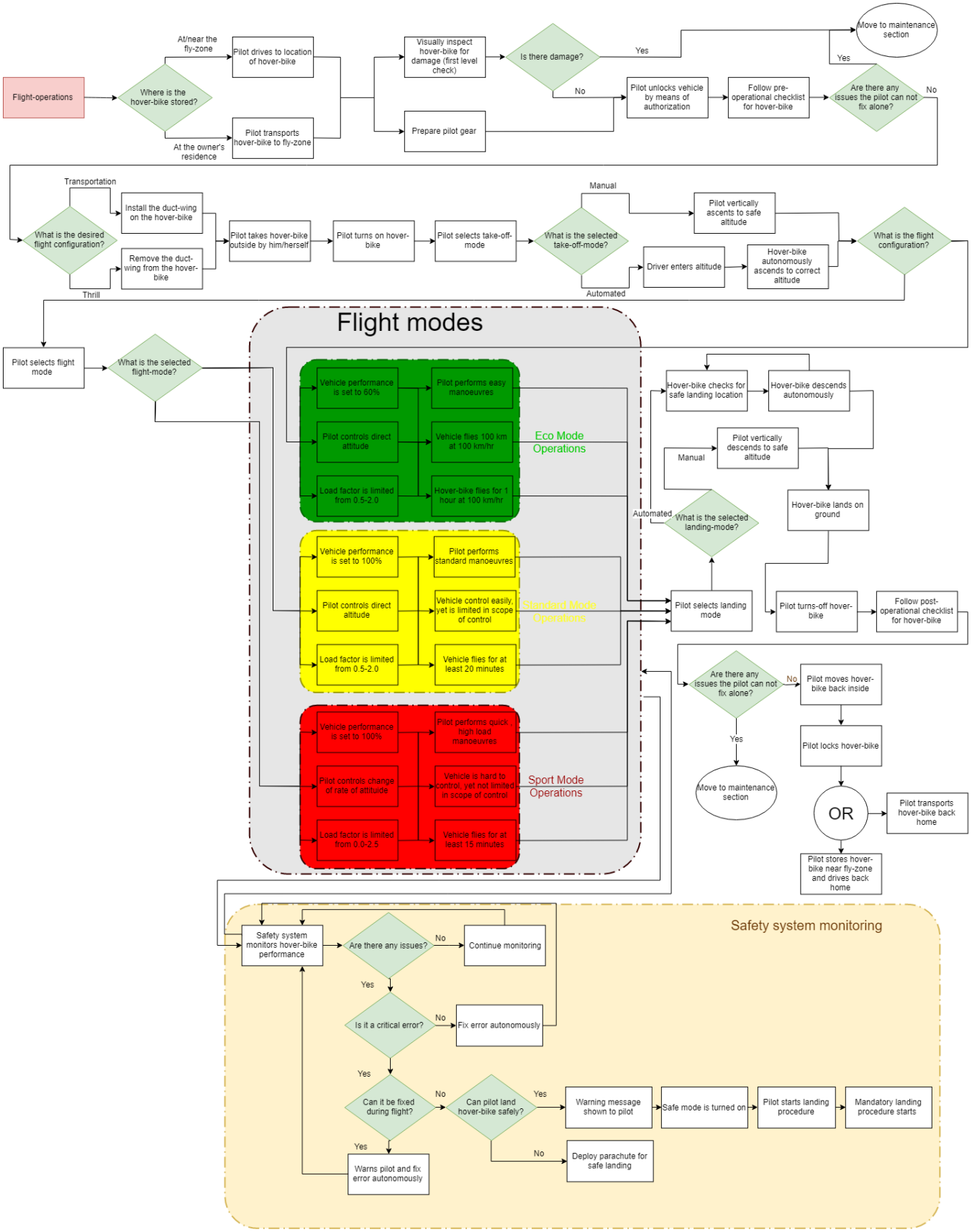

Figure 16.4: Flowchart showing the steps in the flight-operation phase.

16.2.2. Maintenance plan

Maintenance is a crucial phase in the process of operating the hover-bike. This phase is responsible of making the hover-bike operate in its optimum prime condition at all time and allow for early detection of any deterioration that might occur in the hover-bike components.

The maintenance starts when the customer calls the maintenance centre to describe what problems he is facing. The maintenance centre will try to assist the customer if the problem can be fixed without the need of professional help. However, in case of a critical failure or a problem that needs to be checked by a professional, the customer will have to transport the

hover-bike to the maintenance centre to perform the maintenance procedures.
Moreover, the maintenance can vary from daily maintenance performed by the customer during pre-flight checks or by the maintenance centre if the service mileage is reached or in case of unplanned failure. The steps taken during periodic and non periodic maintenance are illustrated in Figure 16.5. The service mileage checkup is a systematic checkup done for quality assurance purpose so that the hover-bike keeps performing in the ideal condition that usually takes a couple of hours to be performed in the centre. During that, the maintenance centre check up the fluids and mechanical parts are checked for their performance and in case of any faulty components it will either be repaired or replaced depending on their state.
Moreover, in case of a sudden failure or accident the maintenance centre will perform a first estimate check in order to estimate the hover-bike maintenance time. After estimating the time required for repairs, the customer will be informed of the time and given two options, whether he would like the hover-bike to be delivered to him after repairs for extra fees or that he can personally come pick it up himself after repairs.

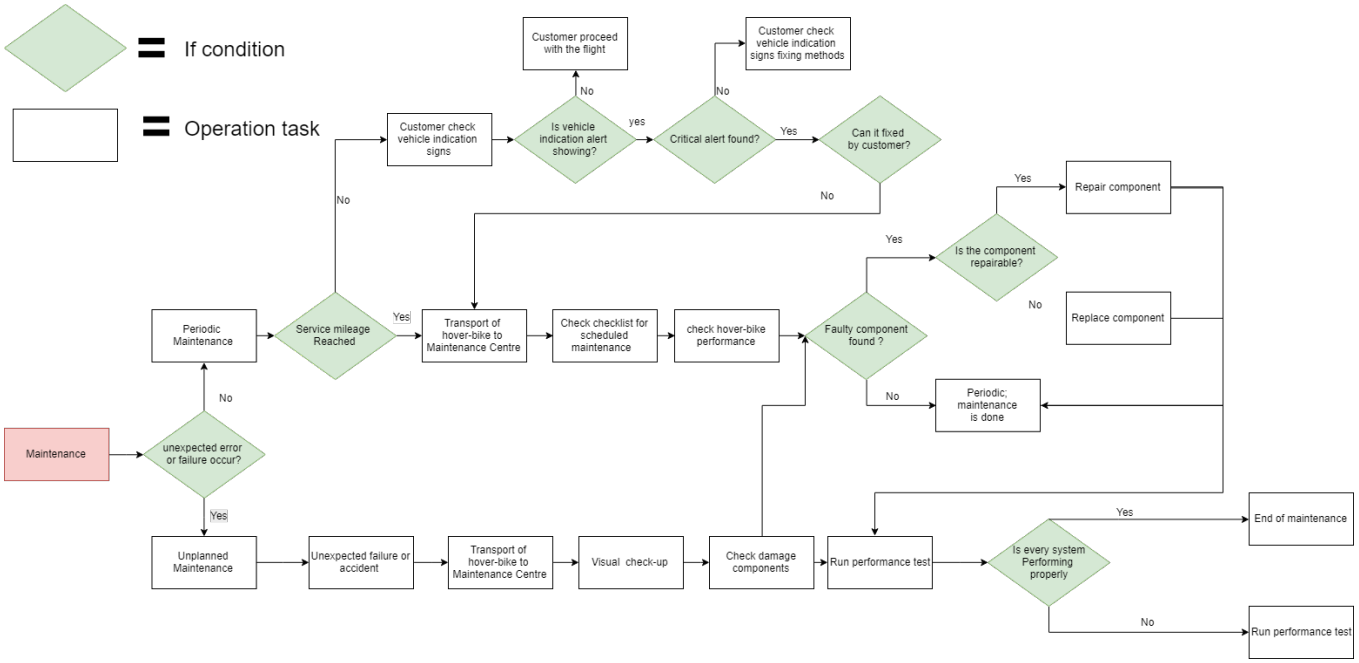

Figure 16.5: Maintenance plan for the hover-bike

16.3. Production plan

Production planning is about setting up a plan of how the final product is going to be produced and which methods are to be chosen in terms of manufacturing and assembly to deliver a product with the required specification and tolerances. Moreover, a detailed production planning can only be achieved after the design of the final design and knowing the specifications and tolerances as seen in Figure 16.6. Due to the lack of information about tolerances at this stage of the design manufacturing techniques will be selected without taking tolerance into consideration.

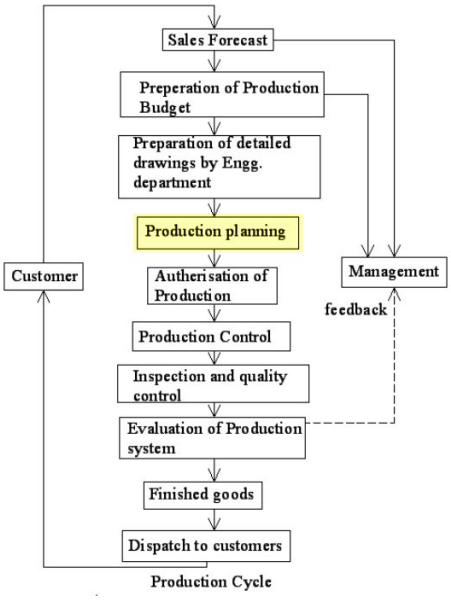

Figure 16.6: Production cycle

In addition, there are many types of production to select from like single item manufacturing, mass manufacturing or batch manufacturing. These types of manufacturing all depends on the purpose of the product and how will it be used. For the prototype of the hover-bike a single item manufacturing process will be used and then after certification and quality control acceptance a mass manufacturing process will be initiated.

16.3.1. Production

In this section the material manufacturing and joining mechanisms will be discussed in order to have a better overview of the production process taken to produce the hover-bike structure. Moreover, the assembly methodology selected in order to increase job performance and to increase productivity.

Manufacturing process

For manufacturing of the structural tubes the drawn tube process is used. The drawing process is better illustrated in Figure 16.7. One of the shown process of tube drawing shown in Figure 16.7 will be selected in order to form metal tubes from aluminium T6061 metal rods. Aluminium T6061 can be manufactured using the mentioned due to its high formability property.

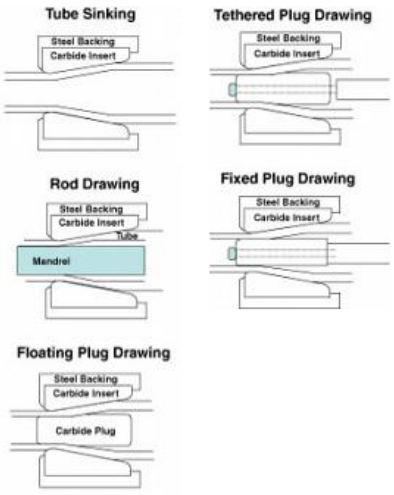

Figure 16.7: The differences among tube drawing methods include the presence or absence of a rod or plug, whether and how the plug is fixed in position, and the die angle.[2].

Duct and wing manufacturing

For the duct and wing assembly given in Figure 16.8, composite materials were chosen. The reason for this is the high strength to weight ratio for these materials. This allows the wing and duct assembly to be made very light weight. Since the wings are located relatively far away from the centre of gravity of the hover-bike, the added moment of inertia to the vehicle is significant and is proportional to the mass of the assembly. Furthermore, light wings and duct allow for easy handling by the pilot when attaching and detaching from the main frame.

Figure 16.8: Duct-wing structure

For the production process of the ducts and wings, the hand lay up technique was chosen. Hand lay up allows for the manufacturing of complex shapes and curves with higher dimensions. Moreover,the direction of the fibres can be chosen and maximum strength can be obtained in the desired direction.A schematic showing the procedure of this manufacturing technique is given in Figure 16.9.

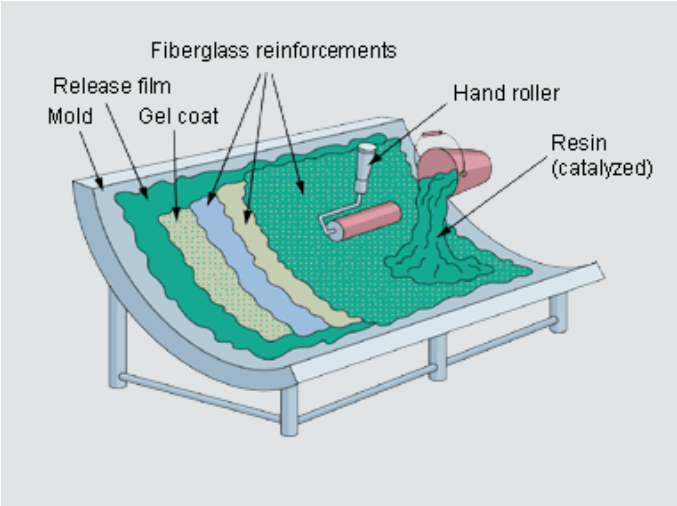

Figure 16.9: An illustration for the hand-lay-up procedure.[3].

Joining
In order to join the structural design into a sub assembly it is decided to use gas metal-arc welding shown in Figure 16.10 in order to weld the structural tubes together to form the body frame sub assembly. Moreover,gas metal-arc welding is used welding process as the tube thickness is below 6mm which is maximum allowable thickness for this process. Moreover, the material being welded is shielded using argon gases to prevent aluminium tubes from oxidation.
Furthermore, due to welding heat affected zones might start appearing causing irregularities in the material properties. To overcome this dilemma aluminium T6061 is capable of heat treatment to improve the affected parts from welding.

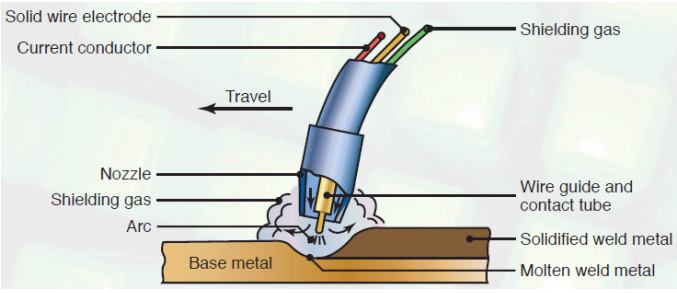

Figure 16.10: Arc welding illustration [4]

16.3.2. Assembly

The assembly will be analysed during the mass production phase as at that time is were assembly is the most crucial. During mass production the components and parts that form sub assemblies are produced in batches to avoid overflow of

components or unorganised assemblies.
Moreover, a system is required to be implemented in order to join the sub assemblies into the main assembly and then into a final product. In order to find the ideal solution a comparison between dock-like system and line assembly is performed. After analysing the solution it was found that line production is more optimum due to its benefits like: simple planning, minimal transport, good progress indicator as delays would be clear in the line and lastly maximum routine work per crew. Line assembly can be visualised using Figure 16.11 in which each stations performs a certain sub assembly. Each assembly line consist of many stations in which the same crew is continuously working on the same routine work with same time allocated to each station to perform their tasks , when the time is passed the hover-bike moves to the next station at the same time. Moreover, having the same crew, performing same tasks is beneficial for the production rate as it reduces cost due to faster production. The number of hours spent on production of one hover-bike decrease by time due to the crews learning curve. A hover-bike assembly line illustration shown in Figure 16.12.

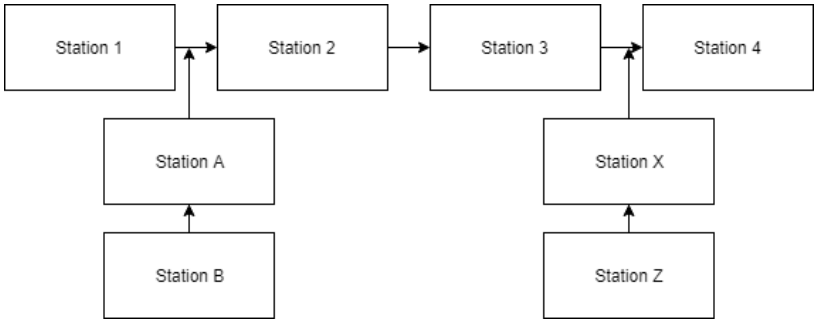

Figure 16.11: Assembly line illustration with 2 sub assembly lines

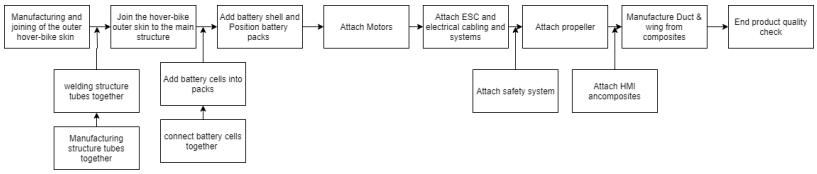

Figure 16.12: Assembly line for the hover-bike

16.3.3. Quality control and assurance

Quality control and assurance is a main step and measure that needs to be considered as the team is thriving to produce a high quality vehicle for the customer to proudly own. Process focused quality assurance has been selected as a quality assurance method, the method is illustrated in details in Figure 16.13. During this process, every part is checked before and after each stage to make sure that every part is within the high standards and expectations set by the company. However, this process is considered time consuming as every part needs to be checked but it is necessary for the manufacturing crew to develop well and learn how to deliver high quality products with the supervision of experts.
In addition, for quality control every hover-bike presented well be tested for performance and tested for critical situations. If the hover-bike passes the performance test it will be quality checked and sold to distributors and customers. In case of failure to pass the test, the hover-bike will be marked and returned to the factory to perform further analysis on it in order to prevent the same error of ever occurring again. An example of quality inspection for the structural body is shown in Figure 16.14.

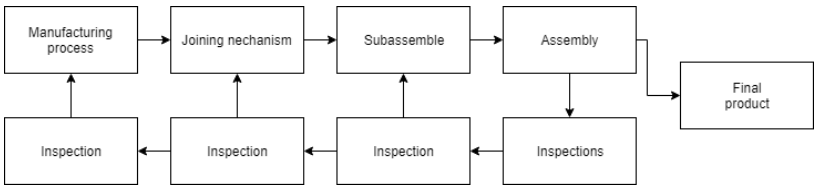

Figure 16.13: Process focused quality assurance

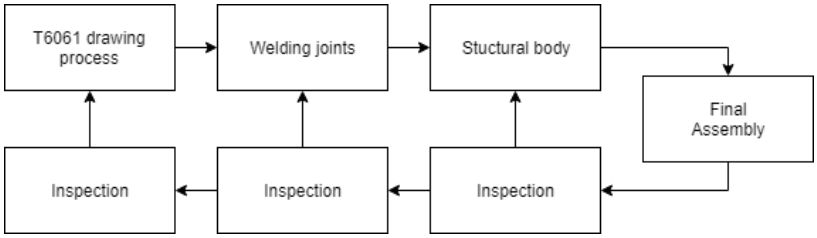

Figure 16.14: Process focused quality assurance for structural assembly

16.3.4. Headquarters

The headquarters is defined as the group of 10 engineers that designed the hover-bike. Headquarters also has a hover-bike license providing facility and secretary. After the hover-bike is launched and is available on the market, the team of engineers will continue improving and innovating the hover-bike. If necessary, customers can contact the headquarters through e-mail. For more direct contact costumers can contact licensed aviation service centres for all the repairs and maintenance via phone or e-mail. The aspects that are provided by the headquarters:

- Software updates to hover-bikes.
- Training for aviation service centres in order to become licensed hover-bike mechanics.
- Manuals to the aviation service centre.
- Training to get the the hover-bike licence. This is done by a weekend training in which the basics will be taught to operate the hover-bike.
- Warranty of 1000 flight hours or 5 years (which one expires first).

Furthermore, hover-bikes must undergo a yearly mandatory check, similar to cars. This check comes at the cost of the owner and will be done at an aviation service centres. These will also be sending regular feedback to the headquarters, as the mechanics working there have a front row view regarding reoccurring problems of the Scorpeon. Especially after the first hover-bikes are sold, it is expected to get a lot of feedback from these service centres, which will also perform maintenance and repairs. Lastly, there will be training provided from the headquarters, as mentioned above, however, this is done by a weekend training to understand the basics of controlling the hover-bike.

16.3.5. Regulations

To actually make sure that the hover-bike pilots have an understanding of the air traffic regulations, it was decided that an RPL is a mandatory permit that the pilot must have, before riding the hover-bike. Officially the Scorpeon does not fall under the RPL licence. This is because the maximum take-off weight of the Scorpeon in transportation mode is more than 450kg and also because the Scorpeon has multiple engines. Hoverever, it is expected that due to the due to the Scorpeon 's simplicity and it's unfriendliness it will get an exception and thereby will fall under the RPL regulation. Furthermore it is expected that the regulations concerning hover-bike's will change soon in the future due to the upcoming hover-bike market, and the hover-bike will get its own set law and regulations.

16.4. Requirement compliancy

This section shows the requirements which where set at the beginning the hover-bike design accompanied with the compliance of our design to these requirements. Furthermore, it is given in which specific section the current requirement is met or not met. For the requirements which were not met a brief comment a given why the requirement is not met. The requirements compliance matrix are shown in Table 16.5 and Table 16.6.

Table 16.5: Requirements compliance matrix part 1

ID	Requirement	Compliance	Section	Comment
HB-FR-ST-01	The hover-bike shall be movable in 6 degrees of freedom.	✓	9.2	-
HB-FR-ST-02	The hover-bike shall have a minimum range of 100 km while maintaining a 100 km/h speed.	✓	7.5	-
HB-FR-ST-03	The service ceiling shall be at least 3000 ft above sea-level.	✓	7.5	-
HB-FR-ST-04	The hover-bike shall be able to fly for at least 1 hour while maintaining a 100 km/h speed.	✓	7.5	-
HB-FR-ST-05	The hover-bike shall be able to vertically take-off and land.	✓	7.5	-
HB-FR-S-06	The hover-bike shall be statically stable and dynamically damped.	✓	9.3	-
HB-FR-S-07	The hover-bike shall have a maximum pitch angle of 45 degrees.	✓	9.3	-
HB-FR-S-08	The hover-bike shall be able to operate in an atmospheric temperature range of 0 to 40 degrees Celsius.	✓	7.3.5	-
HB-FR-S-09	The longitudinal acceleration shall be at least 8.3 m/s2.	✓	9.3	-
HB-FR-S-10	The vertical acceleration shall be at least 1.7 m/s2.	✓	9.3	-
HB-FR-S-11	The longitudinal speed shall be at least 150 m/s.	✓	9.3	-
HB-FR-S-12	The Hover-bike shall be able to take turns with at least 1.7 G.	✓	9.3	-
HB-FR-ST-13	The hover-bike shall be able to safely bring down the pilot from FL030 in case of emergency.	✓	12.1	-
HB-FR-ST-14	The hover-bike shall transmit its position with a transponder.	✓	5.2.1	-
HB-FR-ST-15	The hover-bike shall be able to be handled by a single person at any time.	✓	16.2.1	-
HB-FR-ST-16	The hover-bike shall possess a radio for communication.	✓	7.3.4	-
HB-FR-ST-17	The hover-bike shall be equipped with a system that monitors the operational state of the hover-bike.	✓	5.2.1	-
HB-FR-ST-18	Handling qualities shall be such that 6 hours of training is sufficient to safely operate the hover-bike.	✓	10.4	-
HB-FR-ST-19	The hover-bike shall be equipped with instruments showing the operational state of the hover-bike.	✓	10.2	-
HB-FR-ST-20	The turn around time of the hover-bike shall be less than 30 hours.	✓	7.3.5	-
HB-FR-ST-21	The start-up procedure of the hover-bike shall take less than 3 minutes.	X	11.2	Adding the time of unloading to the start-up procedure will take more than 3 min (approx 15 min).

Table 16.6: Requirements compliance matrix part 2

ID	Requirement	Compliance	Section	Comment
HB-CS-ST-01	The maximum take-off weight of the hover-bike shall be 500 kg.	✓	8.3.5	-
HB-CS-ST-02	The maximum payload weight of the hover-bike shall be 100 kg.	✓	8.3.5	-
HB-CS-ST-03a	The hover-bike shall fit in a trailer of width 2.6 m.	✓	8.3.1	-
HB-CS-ST-03b	The hover-bike shall fit in a trailer of height 4 m.	✓	8.3.1	-
HB-CS-ST-03c	The hover-bike shall have a front vertical viewing angle of at least 15 degrees.	✓	8.3.1	-
HB-CS-ST-04	The hover-bike shall have a front vertical viewing angle of at least 15 degrees.	✓	8.3.2	-
HB-CS-ST-05	The hover-bike shall have a side vertical viewing angle of at least 45 degrees.	✓	8.3.2	-
HB-CS-ST-06	The hover-bike shall be able to take off from a site with diameter or length and width of 12 m[6].	✓	16.2.1	-
HB-CS-ST-07	The production costs of a prototype shall be at most€100,000.	✓	14.4	-
HB-CS-ST-08	The pilot has should have a Recreational Pilot License.	✓	16.3.5	-
HB-CS-S-09a	The hover-bike shall be able to withstand bird strikes.	X	13.2.2	The design is not able to take into account this requirement.
HB-CS-S-09b	The pilot shall be shielded against hazardous components.	✓	8.2.1	-
HB-CS-S-10	The hover-bike shall have a safety rate of at most 1 fatality for every 200.000 flight hours.	X	-	Currently jot feasable to justify due to the lack of data on the reliability of the components.
HB-CS-S-11	Vital components of the hover-bike shall be "safe-life" for the operational life of the vehicle.	✓	8.3.4	-
HB-CS-S-12	The hover-bike shall be equipped with a black-box.	✓	5.2.1	-
HB-CS-ST-13	The pilot shall have a clear 360 degrees view.	✓	8.3.2	-
HB-CS-ST-14	The hover-bike shall be equipped with navigation lights.	✓	5.2.1	-
HB-CS-ST-15	The pilot shall be warned when approaching restricted airspace.	✓	5.2.1	-
HB-CS-ST-16	The pilot shall be able to safely exit the hover-bike in case of emergency.	✓	12.1	-
HB-CS-ST-17	The first prototype of the hover-bike shall be build before 2022.	✓	17	-
HB-CS-ST-18	The design phase of the hover-bike shall be finished before 2020.	✓	17	-
HB-CS-ST-19	At least 50% of the materials used for the production of the hover-bike shall be recyclable.	✓	15.3	
HB-CS-ST-20	At the end of life 50% of the operative empty mass of the hover-bike shall be ableto be disassembled, disposed off and recycled.	✓	15.3	
HB-CS-ST-21	The hover-bike shall have a minimum operational life of 3000 flight cycles.	X	15.2	Mora analysis on the reliability and testing the hover-bike is necessary to justify the requirement.

16.5. Recommendations

Recommendations for further research are given to improve on the design of the hover-bike. Further research is necessary to improve current models and to investigate the overlapping areas between the structure, control, aerodynamics and power and propulsion. Together they are responsible for the performance of the hover-bike. All components of the hover-bike have to work together to turn the hover-bike into a successful product. Items that need further research are:

- The aerodynamic group and power and propulsion group found different results for the estimation of the power for the propellers. The aerodynamic group used blade element method to estimate the power of the propellers and the propulsion group used the actuator disk theory to determine the required propeller power. There is a still a large gap between both estimations and up until now an explanation for the difference has not been found.
- Reiterate the propellers size with improved models for the structure weight, wing weight, duct weight and battery weight. At the beginning of the detailed design phase the propeller size was estimated with simpler tools. From that point on the propeller size was fixed to give a starting point of the design of the hover-bike. Reiterating the propeller size will improve the performance and endurance of the hover-bike.
- Investigate the transitional phase between vertical take-off and lift and regular flight. The transitional phase is non-linear and it is harder to predict the behaviour of the hover-bike in this phase. Further research is necessary to find out what kind of effect this has on the design of the hover-bike.
- Investigate the effects of gusts and wind. The power and propulsion analysis does not include the effect of gust and wind on the power consumption. Most probably the effects of gust will reduce the flight time. If the flight time is reduced larger batteries or wings may be necessary to be able to meet the range and endurance requirements.
- Further reliability studies are necessary, because a broader spectrum of reference vehicles will improve the accuracy of the reliability analysis performed during the detailed design.
- Cooling of the electrical equipment such as engines, batteries and control units has not been taken into account. These systems should not overheat, as that could cause damage these systems. When cooling becomes a problem then these systems should either be reconfigured or redesigned.
- The ageing effect of batteries has to be studied in the post DSE activities. An ageing battery will lose capacity and this will reduce the range and endurance. If ageing of the batteries is significant then the batteries have to accommodate for that.
- The pilot sits on top of the hover-bike and therefore interacts with the airflow around the hover-bike. Which means that the pilot is actually part of the aerodynamic shape of the hover-bike. Therefore the aerodynamic interference of pilot of the rest with the hover-bike should be analysed.
- There is quite a bit of interference between the wings, propellers and ducts and further research is necessary to improve the model that analyses these interference's. When there is too much interference between these components then their location or their shape should be reconsidered.
- Structural analysis of ducts and wings needs to be performed, because of the aerodynamic forces acting on these components. The structure of these components should be able to withstand the aerodynamics forces and they should be rigid enough to prevent warping of the wing.
- The aerodynamic effects of the wings and ducts have to be taken into account of the control analysis, because of the aerodynamic damping of these components. Too much aerodynamic damping could hamper the manoeuvrability of the hover-bike. If this is the case then this could lead to design reconsiderations.
- Contra rotating propellers produce a lot more noise than conventional propellers. One of the reasons why ducts are added is because of the noise. The hover-bike could potentially produce too much noise, when the ducts are removed for the thrill mode. If the hover-bike makes too much noise then this could pose constraints on where the hover-bike can be flown. Thrill mode is described in section 3.1.
- The effect of bird strike has not been taken into account yet into the design of the hover-bike. Bird strike could have large consequences and as such the likelihood and effect of bird strike has to be investigated.

17
Post DSE activities

This chapter explains the activities that will take place after the DSE is finished. The post DSE activities are presented in two figures. Both figures contain the same content, but they give a different view on the activities after the DSE.

Logic Diagram The purpose of the logic diagram of the the post DSE activities is to give an overview of all the tasks that have to be performed when the DSE is Done. Important emphasis has to be given to the funding and certification. The best performing hover-bike on paper will never be built if the funding is not sufficient and if certification does not allow the hover-bike fly. Therefore a market plan, getting funding, contacting suppliers and certification authorities are crucial steps in the post DSE activities.

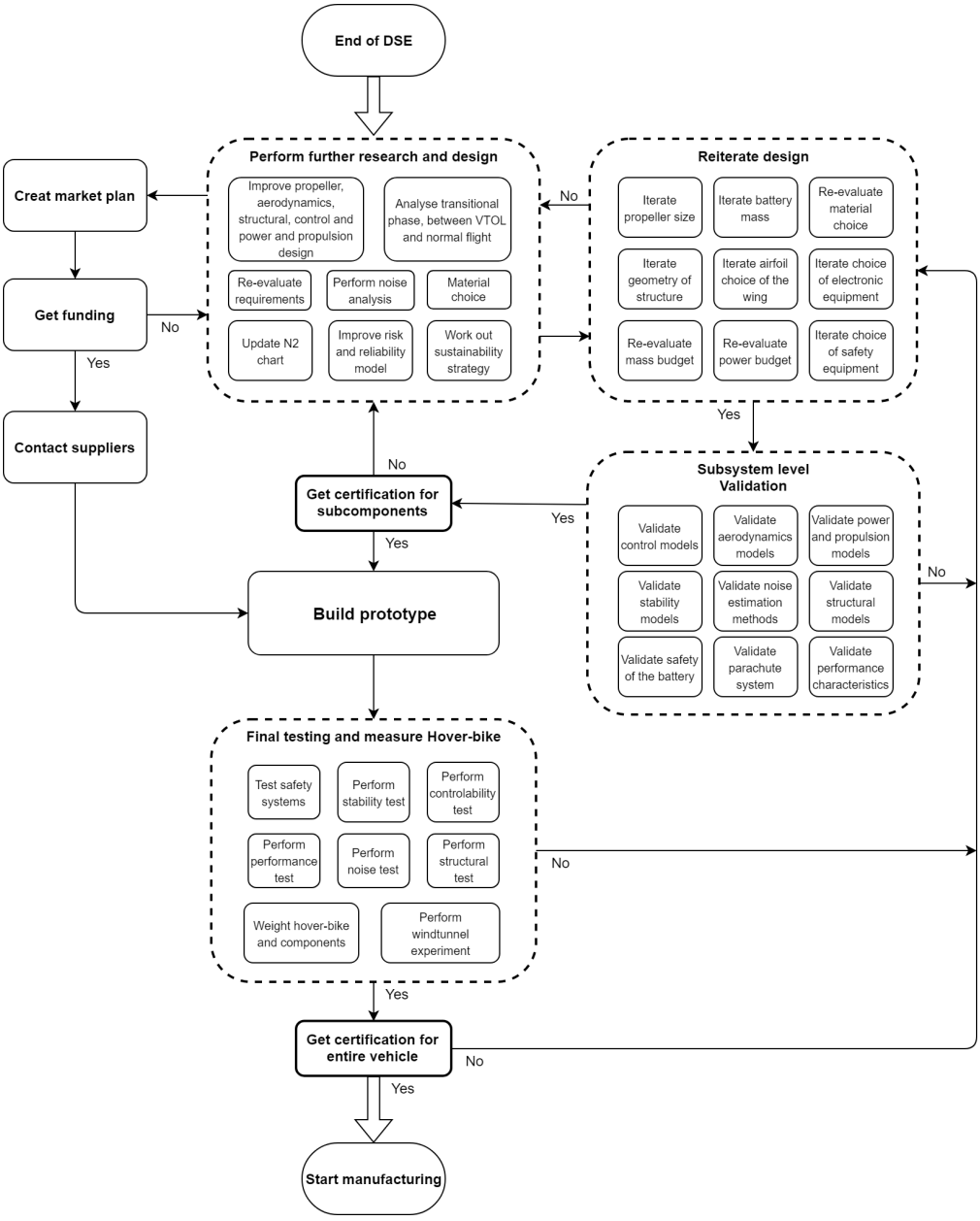

Figure 17.1: Post DSE logic diagram.

Gantt Chart The gantt chart has the same content as the logic diagram, but in this case the activities are ordered in a time schedule. In the near future the different activities are separated only by a short period of time lasting a few months. Further

in the future the periods become longer and last a few months. The designing phase will be finished by 2018 and the first prototype will be built in 2019. [42]

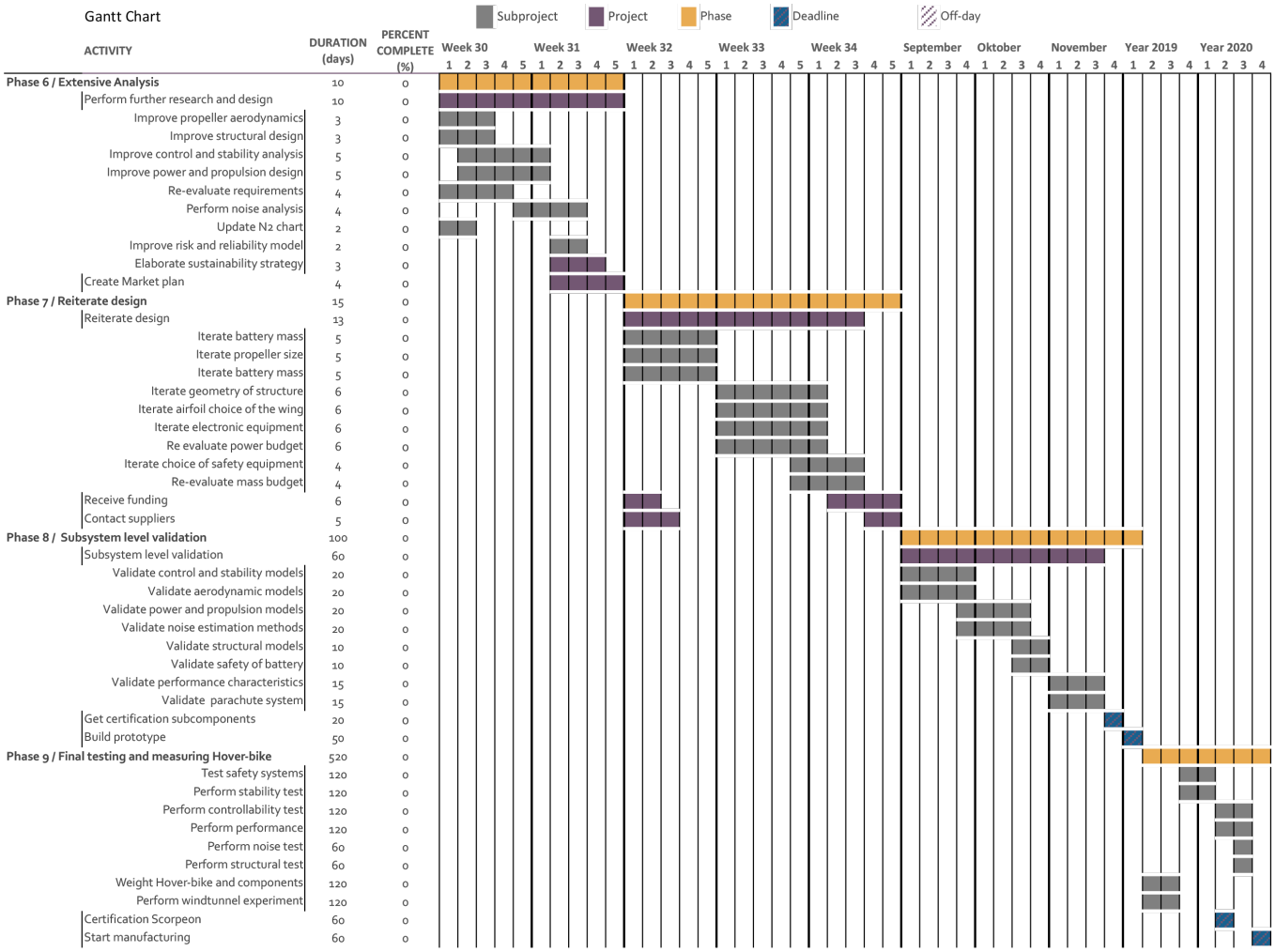

Figure 17.2: Post DSE Gantt chart

Bibliography

Periodicals

[1] J.R. Dieffenbach, P.D. Palmer, and Mascarin A.E. “Making the PNGV Super Car a Reality with Carbon Fiber: Pragmatic Goal or Pipe Dream?” In: *SAE Paper* 960243 (1996).

[2] Paul Ellerman. “Calculating Reliability using FIT & MTTF: Arrhenius HTOL Model”. In: *microsemi, Tech. Rep.* (2012).

[3] Martin R Fink. “Airframe noise prediction method”. In: (1977).

[4] Raquel Girvin. “Aircraft noise-abatement and mitigation strategies”. In: *Journal of Air Transport Management* 15.1 (2009), pp. 14–22.

[5] Dennis L Huff, Brenda S Henderson, and Edmane Envia. “A First Look at Electric Motor Noise For Future Propulsion Systems”. In: (2016).

[6] DW Kurtz and JE Marte. “A review of aerodynamic noise from propellers, rotors, and lift fans”. In: (1970).

[7] Jim Modrouvanos. “EPD 0009 RELIABILITY AVAILABILITY AND MAINTAINABILITY (RAM)”. In: 2 (Mar. 2010).

[8] United Nations. “Guiding Principles on Business and Human Rights”. In: (2011).

[9] Roger Nicholson, William S Reed, and Safety Pilot. “RIAC Automated Databook”. In: *Aero Quarterly* 43 (2011), pp. 17–24.

[10] Roger Nicholson, William S Reed, and Safety Pilot. “Strategies for Prevention of bird-Strike events”. In: *Aero Quarterly* 43 (2011), pp. 17–24.

[11] Kate Palmer et al. “Total cost of ownership and market share for hybrid and electric vehicles in the UK, US and Japan”. In: *Applied energy* 209 (2018), pp. 117–118.

[12] Duane Pettit, Andrew Turnbull, and Henk A Roelant. “General aviation aircraft reliability study”. In: (2001).

[13] Jarosław Stanisławski. “Prediction of helicopter HV zone and cueing the emergency maneuver after power loss”. In: *Archive of Mechanical Engineering* 57.1 (2010), pp. 21–44.

[14] Yin Yin et al. “Reliability Analysis of Landing Gear Retraction System Influenced by Multifactors”. In: 53 (Mar. 2016), pp. 1–12.

Books

[15] Federal Aviation Administration. “Rotorcraft Flying Handbook”. In: U.S. Government Printing Office, Washington D.C., 2000.

[16] Federal Aviations Administration. *Advisory Circular, Heliport Design*. U.S. Depratment of Transportation, 2012, p. 112.

[17] James A. Crabtree. “WEIGHT ESTIMATION for HELICOPTER DESIGN ANALYSIS”. In: Society of Aerospace Weight Engineers, 2011.

[18] Dr J.W.McCroskey D.H.Peckham. *Technical Status Review on Drag Prediction and Analysis from Computational Fluid Dynamics: State of the Art*. AGARD, Advisory Group for Aerospace Research & Development, 1989, pp. 8–6.

[19] Matthias Finkbeiner et al. “Towards Life Cycle Sustainability Assessment”. In: Technische Universität Berlin, 2010.

[20] Jay Gundlach. “Designing Unmanned Aircraft Systems - A Comprehensive Approach”. In: American Institute of Aeronautics and Astronautics, 2012, pp. 317–326.

[21] Dewey H. Hodges and G. Alvin Pierce. *Introduction to Structural Dynamics and Aeroelasticity*. 2nd ed. Cambridge Aerospace Series. Cambridge University Press, 2011. DOI: 10.1017/CBO9780511997112.

[22] Charlotte Hurtley. “Night noise guidelines for Europe”. In: WHO Regional Office Europe, 2009.

[23] D.J. Inman. “Engineering Vibration”. In: Pearson Education, Inc., 2008, pp. 6–8.

[24] W. Johnson. “Helicopter Theory”. In: Dover Publications Inc, 1994, pp. 35–36.

[25] John D. Anderson Jr. and Professor Emeritus. “Introduction to Flight”. In: McGraw Hill, 2012, pp. 888–889.

[26] Rokho Kim et al. “Burden of disease from environmental noise”. In: 2007.

[27] Walter Klöpffer. “Life Cycle Assessment”. In: Wiley-VCH, 1997, pp. 223–228.

[28] Dubravko Miljković, Mladen Maletić, and M Obad. “Comparative investigation of aircraft interior noise properties”. In: 2007.

[29] GS. Nusholtz et al. “Air bag effectiveness as function of impact speed”. In: Traffic Inj Prevention, 2003, pp. 128–135.

[30] Daniel P. Raymer. *Aircraft Design: a Conceptual Approach*. American Institute of Aeronautics and Astronautics, 2012.

[31] J. Seddon. *Basic Helicopter Aerodynamics*. BSP Professional Books, 1990, p. 9.

[32] XFLR5. “Analysis of foils and wings operating at low Reynolds numbers”. In: *Guidelines for QFLR5 v0.03* (2009).

[33] Xiao-Su Yi, Shanyi Du, and Litong Zhang. *Composite Materials Engineering*. 1st ed. Vol. 2. Springer Singapore, 2018. DOI: 10.1007/978-981-10-5690-1.

[34] X. Zhao. “Aircraft Life Cycle Cost Analysis and Design Integration: A Knowledge Based Engineering Approach”. In: Technical University of Delft, 2017, pp. 28–30.

Proceedings

[35] Mark Drela. “XFOIL: An Analysis and Design System for Low Reynolds Number Airfoils”. In: *Low Reynolds Number Aerodynamics*. Ed. by Thomas J. Mueller. Berlin, Heidelberg: Springer Berlin Heidelberg, 1989, pp. 1–12. ISBN: 978-3-642-84010-4.

[36] Mark W. Mueller and Rafaello D’Andrea. “Stability and control of a quadrocopter despite the complete loss of one, two, or three propellers”. In: International Conference on Robotics & Automation, 2014. URL: http://flyingmachinearena.org/wp-content/publications/2014/mueIEEE14.pdf.

[37] Paul Pounds and Robert Mahony. “Design Principles of Large Quadrotors for Practical Applications”. In: IEEE International Conference on Robotics and Automation, 2009. URL: %5Curl%7Bhttps://ieeexplore.ieee.org/stamp/stamp.jsp?tp=&arnumber=5152390&tag=1%7D.

[38] H. Twardy. “On a variable-thrust hydrogen-oxygen rocket engine”. In: vol. 2. 7. 1975, pp. 627–647. DOI: https://doi.org/10.1016/0094-5765(75)90006-5. URL: http://www.sciencedirect.com/science/article/pii/0094576575900065.

Reports, Theses, and Individual Papers

[39] AIAA. “Mass Properties Control for Space Systems”. In: (2015). URL: https://www.aiaa.org/uploadedFiles/Publications/Standards/S-120A_SEC_Public_Review_andCo_ballot_Draft.pdf.

[40] Yuze Chen et al. “Hover-bike Baseline Report - Version 1.1”. In: (2018).

[41] Yuze Chen et al. “Hover-bike Project plan - Version 1.1”. In: (2018).

[42] Yuze Chen et al. “Mid-TermReport - Version 1.1”. In: (2018).

[43] Mark Cutler et al. “Comparison of Fixed and Variable Pitch Actuators for Agile Quadrotors”. In: ().

[44] Mark Cutler et al. “Comparison of Fixed and Variable Pitch Actuators for Agile Quadrotors”. In: (2015), p. 17. URL: http://acl.mit.edu/papers/GNC11_Cutler_uber.pdf.

[45] Elena Dubrova. “A review on the key issues for lithium-ion battery management in electric vehicles”. In: *Journal of Power Sources* 226 (2013), pp. 272–288.

[46] Elena Dubrova. “Mission design activities "The green book"”. In: (2008), p. 147. URL: https://pld.ttu.ee/IAF0530/draft.pdf.

[47] NASA EMC. “Fault tolerant design: An introduction”. In: (1991), p. 27. URL: https://http://spacecraft.ssl.umd.edu/design_lib/Greenbook_master.pdf.

[48] Andrew Gibiansky. “Quadcopter Dynamics and Simulation”. In: (2012). URL: http://andrew.gibiansky.com/blog/physics/quadcopter-dynamics/.

[49] Leo Victor Lazauskas. “Hydrodynamics of Advanced High-Speed Sealift Vessels”. In: (2005).

[50] J. Gordon Leishman. “Rotorcraft Aerodynamics”. In: (2010). URL: https://onlinelibrary.wiley.com/doi/10.1002/9780470686652.eae018/figures#eae018-fig-0003.

[51] Teppo Luukkonen. “Modelling and control of quadcopter”. In: (2011).

[52] Teppo Luukkonen. “Modelling and control quadcopter”. In: (2011). URL: %5Curl%7Bhttp://sal.aalto.fi/publications/pdf-files/eluu11_public.pdf%7D.

[53] K.W. Mangler and H.B. Squire. “The induced velocity field of a rotor”. In: (1953).

[54] Jacob Markish. “Valuation Techniques for Commercial Aircraft Program Design”. In: (2002).

[55] Osgar John Ohanian. “Ducted Fan Aerodynamics and Modeling, with Applications of Steady and Synthetic Jet Flow Control”. In: (2011). URL: https://vtechworks.lib.vt.edu/bitstream/handle/10919/27687/Ohanian_OJ_D_2011.pdf.

[56] Hesham Rakha and Ivana Lucic. “Variable Power Vehicle Dynamics Model for Estimating Truck Accelerations”. In: *Journal of transportation engineering* (2002), pp. 412–419.

[57] Michael S. Selig, John F. Donovan, and David B. Fraser. *Airfoils at Low Speeds*. 1989.

[58] Thomas W. Sheehy and David R. Clark. “A METHOD FOR PREDICTING HELICOPTER HUB DRAG”. In: (1976).

[59] Herbert W. Talking. “CHARTS FOR HELICOPTER PERFORMANCE ESTIMATION”. In: *Wartime Report*. National Advisory Comittee for Aeronautics, 1945.

[60] W Timmer. *An Overview of NACA 6-Digit Airfoil Series Characteristics with Reference to Airfoils for Large Wind Turbine Blades*. Jan. 2009.

[61] J. S. Vanderover and K. D. Visser. “Analysis of a Contra-Rotating Propeller Driven Transport Aircraft”. In: (2009). ISSN: 13699-5725. URL: https://www.rcgroups.com/forums/showatt.php?attachmentid=2815700.

[62] Miao Wang. “Driving an autonomous car with eye tracking”. In: (2010), p. 4. URL: http://www.mi.fu-berlin.de/inf/research/publications/techreports/tr2010/B-10-03/B-10-03.pdf.

[63] James L. Webre et al. “AIRWORTHINESS AND FLIGHT CHARACTERISTICS EVALUATION OF THE MCDONNELL DOUGLAS HELICOPTER CORPORATION (MDHC) 530FF HELICOPTER”. In: (1990).

[64] Bogumila ZWIERCHANOWSKA Wojciech KANIA Wienczyslaw STALEWSKI. “Design of The Modern Family of Helicopter Airfoils”. In: (2007). URL: http://ilot.edu.pl/prace_ilot/public/PDF/spis_zeszytow/191_2007/05_Kania_Stalewski_Zwierchanowska.pdf.

[65] Dong-Wan Yoo et al. “Dynamic modeling and control system design for tri-rotor UAV”. In: (2010).

[66] David Walter Zingg. *An approach to the design of airfoils with high lift to drag ratios*. University of Toronto Institute for Aerospace Studies, Tech. Note 245, 1983.

Electronic Publications

[67] A. Deperrios. *About XFLR5 calculations and experimental measurements*. 2009.

[68] Prof. Dr. Gill E. *AE3211-I Verification and Validation for the Attitude and Orbit Control System*. 2018.

[69] Martin Hepperle. *JAVAPROP - Users Guide*. 2017. URL: https://www.mh-aerotools.de/airfoils/java/JavaProp%5C%20Users%5C%20Guide.pdf.

[70] Th. van Holten and J.A. Melkert. *AE4-213 Helicopter Performance, Stability and Control*. 2002.

[71] Grant Ingram. “Wind Turbine Blade Analysis using the Blade Element Momentum Method”. In: (2011). URL: http://community.dur.ac.uk/g.l.ingram/download/wind_turbine_design.pdf.

[72] Prof. Q.H. Nagpurwala. *Ducted fans and propellers*.

[73] Dr. Ganesh Rajagopalan. *Notes for V/STOL Aerodynamics and Performance (AER E 442)*. 2002. URL: http://www.public.iastate.edu/~aero442/unit3.pdf.

A

Reference data propeller sizing

Table A.1: Reference propeller data

Propeller	Diameter [m]	Mass [kg]
GA200L-STOL[1] PROPELLER	2.08	8.16
WHIRLWIND ULTRALIGHT 350[2]	1.68	5.90
GA-J2B[3]	1.65	3.63
GA-200CN[4]	1.83	5.44
Wood-Maple - 24x12 Propeller[5]	0.61	0.14
Classic - 20x10 Propeller[6]	0.51	0.17
Turnigy Type D Light Wood Propeller[7]	0.51	0.13
Turnigy 3D Gas Propeller[8]	0.51	0.11
GA-UL260[9]	1.68	3.63
GA-RW3B[10]	1.78	5.44

Table A.2: Reference engines data

Electric motor	Power output [W]	Mass [kg]
Hobbyking X-Car 4976[11]	6000	0,425
Turnigy RotoMax[12]	7992	2.074
Turnigy AquaStar[13] T20 3T	5280	0.971
NT-12kW[14]	12000	4.1
NT-15kW[15]	15000	5.4
Nova 15[16]	15000	2.5
Nova 30[17]	30000	6.5
4535 ASTRO[18]	15000	5.44
Reacher paraglider motor[19]	45000	5.9

[1] URL:https://whirlwindpropellers.com/aircraft/product/ga200l-stol/ [cited 06-06-2018]
[2] URL:http://www.aircraftspruce.com/catalog/appages/whirwind05-12614.php [cited 06-06-2018]
[3] URL:https://whirlwindpropellers.com/aircraft/product/propeller-for-jabiru-3300-engines/ [cited 06-06-2018]
[4] URL:https://whirlwindpropellers.com/aircraft/product/ga200cn/ [cited 06-06-2018]
[5] URL:https://www.masterairscrew.com/collections/wood-series/products/wood-maple-24x12-propeller [cited 06-06-2018]
[6] URL:https://www.masterairscrew.com/collections/classic-series/products/classic-20x10-propeller [cited 06-06-2018]
[7] URL:https://hobbyking.com/en_us/turnigy-type-d-light-wood-propeller-20x6-1pc.html [cited 06-06-2018]
[8] URL:https://hobbyking.com/en_us/turnigy-3d-gas-propeller-20x6-1pc.html [cited 06-06-2018]
[9] URL:https://whirlwindpropellers.com/aircraft/product/propellers-for-ul260350-engines/ [cited 06-06-2018]
[10] URL:https://whirlwindpropellers.com/aircraft/product/lsa-s-t-o-l-propellers-ga-rw3b-3-blade/ [cited 06-06-2018]
[11] URL:https://hobbyking.com/en_us/hobbyking-x-car-4976-1740kv-sensorless-brushless-motor.html?___store=en_us [cited 27-may-2018]
[12] URL:https://hobbyking.com/en_us/turnigy-rotomax-100cc-size-brushless-outrunner-motor.html?___store=en_us [cited 27-may-2018]
[13] URL:https://hobbyking.com/en_us/turnigy-aquastar-t20-3t-730kv-1280kv-water-cooled-brushless-motor.html?___store=en_us [cited 27-may-2018]
[14] URL:http://nt-power.eu/doc/nt-power-datasheet-motor-12kw.pdf [cited 06-06-2018]
[15] URL:http://nt-power.eu/doc/nt-power-datasheet-motor-15kw.pdf [cited 06-06-2018]
[16] URL:https://plettenberg-motoren.net/en/products/motor-solutions/motors [cited 06-06-2018]
[17] URL:https://plettenberg-motoren.net/en/products/motor-solutions/motors [cited 06-06-2018]
[18] URL:http://www.astroflight.com/4535 [cited 06-06-2018]
[19] URL:http://www.reacherbrushless.com/product/45KW-motor.html [cited 06-06-2018]